THEORY AND RESEARCH IN ENGINEERING

EDITOR:
PROF.DR.ADNAN HAYALOĞLU

gece kitaplığı

İmtiyaz Sahibi / Publisher • Yaşar Hız
Genel Yayın Yönetmeni / Editor in Chief • Eda Altunel
Editörler / Editors • Prof. Dr. Adnan Hayaloğlu
Kapak & İç Tasarım / Cover & Interior Design • Gece Kitaplığı

Birinci Basım / First Edition • © Eylül 2020
ISBN • 978-625-7243-79-7

Gece Kitaplığı / Gece Publishing
Türkiye Adres / Turkey Address: Kızılay Mah. Fevzi Çakmak 1. Sokak Ümit Apt. No: 22/A Çankaya / Ankara / TR
Telefon / Phone: +90 312 384 80 40
web: www.gecekitapligi.com
e-mail: gecekitapligi@gmail.com

Baskı & Cilt / Printing & Volume
Sertifika / Certificate No: 47083

Theory and Research in Engineering

EDITOR

Prof. Dr. Adnan Hayaloğlu

gece kitaplığı

CONTENTS

Chapter 1

DETERMINATION OF THE SUITABLE AREAS FOR SOLAR POWER PLANTS (SPP) USING ANALYTIC HIERARCHY PROCESS (AHP) AND GEOGRAPHIC INFORMATION SYSTEMS (GIS) IN THE EASTERN MEDITERRANEAN BASIN, TURKEY

Ozan ARTUN[1]

1 Dr., Cukurova University, Vocational School of Karaisali, Department of Architecture and City Planning, 01770 Karaisali, Adana, TURKEY.

INTRODUCTION

The increasing need for energy in today's world and the understanding of clean environment in this context have increased the need of human beings for new and renewable energy sources. The need for energy and the importance of energy production is one of the leading issues in every period of human history. With the struggle for colonialism and the industrial revolution afterwards, the importance of energy has increased and caused various treaties, alliances between countries and even wars between countries on energy resources. Countries' policies and strategies are concentrated on energy. With the increasing industry and technology since the 20th century, energy resources and diversity have increased due to energy needs and production (Yılmaz & Duhan, 2017).

At the present time An important part of the energy supply in the world is produced from fossil fuels. It shows that the use of fossil fuels has a major impact on the world ecology and global climate and world economy. The price of oil and other fossil fuels has been increasing rapidly in recent years. Due to the fact that, the majority of the countries of the world want to reduce energy costs and pollution effect, new policies are developed in this regard. Also, concerns about climate, energy security, and increasing fuel prices have enhanced interest in fossil fuels (Sehan et al., 2011; Traube et al., 2013).

The sun has the largest energy source among renewable energy sources. Solar energy, which was neglected in the past years, came to the fore with the increase in the population, the increasing need of energy and the development of technology. When environmental effects are taken into consideration, the sun ranks first among the most harmless energy sources. The most important benefits of using solar energy compared to other types of energy are as follows. The sun is an inexhaustible source of energy and the energy obtained from the sun is clean energy. Its technology is not complicated, it does not depend on foreign, its operating costs are low and it is suitable for local applications. In addition to this, the disadvantages of this energy are that it requires storage as sunlight is not continuous, large areas are required for installation, high initial installation cost, and being affected by the difference of summer-winter, day-night. Considering all these situations, the importance of the location becomes evident in the establishment of the Solar Power Plant (SPP). Renewable energy has expanded rapidly in the last decade in our country. Solar energy is the most dominant type of energy contributing to renewable energy production with wind energy.

Although the sun is an inexhaustible source of energy, it does not reach everywhere with a constant value. In this case, certain conditions must be met in order to establish a power plant. In Turkey, the appropriate place for SPP installation, Solar Energy Potential Atlas gives a certain idea. This atlas uses values based on sunshine time and radiation intensity. But for detailed and more realistic studies, factors such as slope of the land, properties of the land, soil condition and geology of the land, proximity to distribution networks are required (Ayday et al., 2016).

In our country, many studies have been carried out in the establishment of the Solar Power Plant (SPP), which has a great potential, and in determining the location of this power plant. Due to the high cost of installation and the fact that many variables are effective in the SPP site selection, obtaining and interpreting spatial data in site selection studies is possible by using Geographic Information Systems (GIS) (Yalçın & Yüce, 2020).

In recent years, Geographical Information System (GIS) and multi criteria evaluation (MCE) methods have become an increasingly popular method for different site selection studies (Saltuk & Artun, 2019; Artun & Saltuk, 2018; Akinci et al, 2013). For assisting in decision-making, Multi criteria evaluation methods were developed in the 1960s. In literature studies, it is seen that MCE is a widely used concept in many fields. It is known that the combination of GIS and MCE techniques is increasingly used as a very important spatial decision support system (SDSS) to identify suitable siting locations (Malczewski, J., 1999). Using the combination of GIS and MCE techniques validated research on the site selection of solar farms is very rare.

In Turkey, Uyan (2013) determined the appropriate SPP areas in Karapinar (Konya) by evaluating the AHP multi-criteria decision making method, in the GIS environment. Ayday et al., (2106) has determined suitable areas for SPP site selection in Eskişehir with criteria such as land slope, aspect characteristics of the land, soil condition and geology of the land, proximity to distribution networks. Uyan (2017) determined the appropriate SPP areas in Çumra (Konya) by evaluating the AHP method, in the GIS environment. Yalçın and Yüce (2020) have determined the areas for the Investment of SPP in Burdur via GIS based AHP Method.

In the study, it is tried to determine suitable areas for SPP investment in the Eastern Mediterranean Basin by using many variables. The study was carried out in the Eastern Mediterranean basin. It covers 4 provinces (Adana, Osmaniye, Hatay and Kahramanmaraş) in this basin.Turkey Solar Energy Potential Atlas of the Turkey General Directorate of Renewable Energy (GDRE) may give you an idea for the investments can be made in the study area, but it was aimed to create a more comprehensive Land Suitability Index Map in GIS environment. The different variables obtained for SPP investment fields and Analytic Hierarchy Process (AHP) method are used for this purpose (Saaty, 1980; Wind & Saaty, 1980).

For SPP site selection, a Geographic Information System (GIS) -based Multi-criteria evaluation for were applied in Adana, Osmaniye, Hatay and Kahramamaraş provinces. For being guide to investors and researchers hereafter, the suitable areas, alternative areas and unsuitable areas for WEP siting in the study area were determined in terms of GIS.

MATERIALS AND METHODS

Study Area

The Eastern Mediterranean region is located in the eastern part of the Mediterranean Region, named after the sea in the south. (Figure 1). The Eastern Mediterranean region covers Adana, Hatay, Kahramanmaraş and Osmaniye provinces. (Fig.1). This study was carried out in the Eastern Mediterranean basin of the Mediterranean Region of Turkey. Adana is located at the northeastern edge of the Mediterranean, where it serves as the gateway to the Cilicia plain. This large stretch of flat, fertile land lies southeast of the Taurus mountains. Hatay is traversed by the north-easterly line of equal latitude and longitude. 46% of the land is mountain, 33% plain and 20% plateau and hillside. The most prominent feature is the north-south leading Nur Mountains. Kahramanmaras is a city in the Mediterranean Region of Turkey. The city lies on a plain at the foot of the Ahir Mountain. Located on the eastern edge of the Cukurova plain in the foothills of the Nur Mountains, the gateway between Anatolia and the Middle East (Anonymous, 2020a).

In this study, initially, the criteria that are capable to describe different restrictions related to solar power plant site selection is tried to identify. Due to each constraint, the individual map layers were created then. The study area was divided into 30 m. - 30 m. grid cells. Thus each grid cell represented an alternative place for an SPP site. The factors accepted to be effective in the selection of SPP areas were determined according to the criteria specified in the related literature (Table 1.).

In the study, the elevation data were collected from ASTER Global Dem V.3 with a resolution of 30 m. Slope and aspect data were derived from ASTER Global Dem V.3 and resampled to 30 m. resolution (NASA, 2019). Distance, Roads and Transmission data were derived from OpenStreetMap and resampled to 30 m. resolution (Anonymous, 2020b).

Figure 1. *Map of Turkey and the Study Area*

Table 1. *The data set chosen for MCDA modelling. (Anonymous, 2020b), (NASA, 2019),*

Criteria Name	Description	Source
Distance	Distance from Residential areas (m)	Derived from OpenStreetMap
Slope	Slope in degrees obtained from altitude (%)	Derived from ASTER/ ASTGTM.003
Aspect	Aspect in degrees obtained from altitude (Direction)	Derived from ASTER/ ASTGTM.003
Roads	Distance from Roads (m)	Derived from OpenStreetMap
Transmission	Distance from Transmission Lines (m)	Derived from OpenStreetMap

Analytic Hierarchy Process

In this study, the AHP technique, a frequently used multi-criteria decision-making technique in the literature, will be used for the determination of suitable places for Solar Power Plants. The selected criteria will be weighted according to this method. AHP technique is a structural technique used to analyze interrelated criteria in solving complex problems. In this model, the binary comparisons matrix is obtained based on the binary comparisons between the criteria.After that, the weights of the criteria are determined.

Table 2. *AHP evaluation scale (Saaty, 1980).*

Numerical value of Pij	Definition
1	Equal importance of i and j
3	Moderate importance of i over j
5	Strong importance of i over j
7	Very strong importance of i over j
9	Extreme importance of i over j)
2,4,6,8	Intermediate values

The AHP, is a mathematical method. This method is developed by Saaty in 1977. The main aim of this method is to analyzie complex decisions involving many criteria (Table 2). AHP method, is one of the most effective methods used in spatial planning in recent years (Ayday et al., 2014; Uyan, 2017). In this method, the criteria are weighted between 1 and 9, taking into account the scale of importance (Saaty, 1990). The weight of the criteria is important in obtaining the result in AHP method and the weights can be different, depending on the decision makers' preferences.

In this study, the five criteria (Distance from Residential Areas, Slope, aspect, Distance from Roads and Distance from Transmission Lines) determined for AHP analysis were evaluated in the AHP analysis software. This software is prepared by Goepel (2018) and it is provided on the internet. In this context, a binary comparison was made primarily for AHP priorities. Depending on the importance of the criteria, selections were made in the range of 1-9 on the AHP scale and were calculated automatically (Anonymous, 2020c).

Criteria

For this study the following factors were considered in the determination of the suitable areas for solar power plants: Distance from Residential Areas, Slope, Aspect, Distance from Roads and Distance from Transmission Lines.

Each criteria are explained below.

Distance from Residential Areas

The proximity to residential areas of solar power plants can be taken as an economic factor.

In the study, for residential areas, with a <1000 m. buffer zone was scored as 1, 1000-2000 buffer zone was scored as 2, 2000-5000 m. buffer zone was scored as 3 and > 5000 m. buffer zone was scored as 4 (Figure 2.).

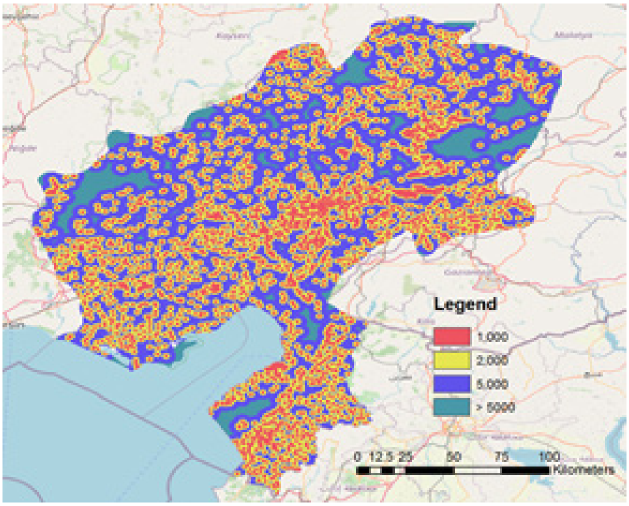

Figure 2. *Suitibility Index Map of the Distance from Residential Areas of the Study Area*

Slope

The slope must less than 3% for all aspects for the SPP site (Uyan, 2017). The slope was divided into four parts in the study. 1% buffer zone is given as 1, 1–2% buffer zone is given as 2, 2–3% buffer zone is given as 3 and >3% buffer zone is given as 4 (Figure 3.).

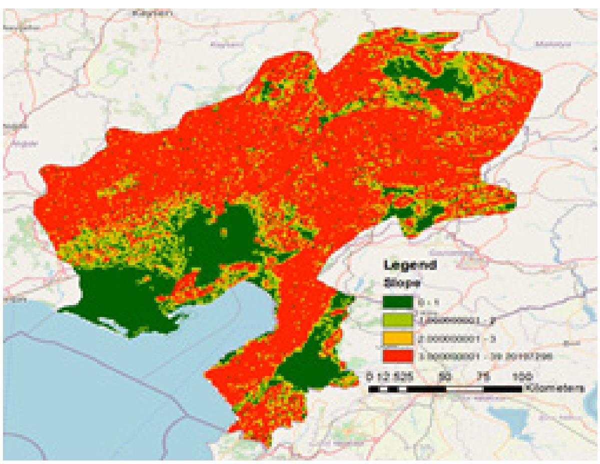

Figure 3. *Suitibility Index Map of Slope of the Study Area*

Aspect

The aspect is a very important criterion for SPP installation. For the status of the aspect, the north and south directions of the study area are determined. Southern directional lands benefit more from sunlight, so it is important to identify these lands.

In the study, the south direction is given as 1, flat areas is given as 0, southeast direction is given as 1, southwest direction is given as 2, east direction is given as 2, west direction is given as 3, northeast direction is given as 3, northwest direction is given as 4 and east direction is given as 4 (Figure 4).

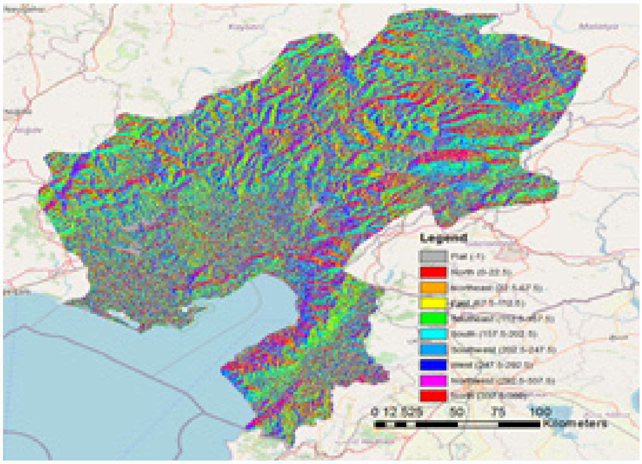

Figure 4. *Suitibility Index Map of Aspect of the Study Area*

Distance from Roads

Roads are an important criterion for an economical and efficient site selection. The cost may decrease in the infrastructure works that carried out in areas close to the main roads (Uyan, 2017; Yalçın & Yüce, 2020). In this study, roads and railways were evaluated together.

In the study, <1000 m buffer zone is given as 1, 1000–2000 m buffer zone is given as 2,000– 5000 m buffer zone is given as 3, >5000 m buffer zone is given as 4 (Figure 5).

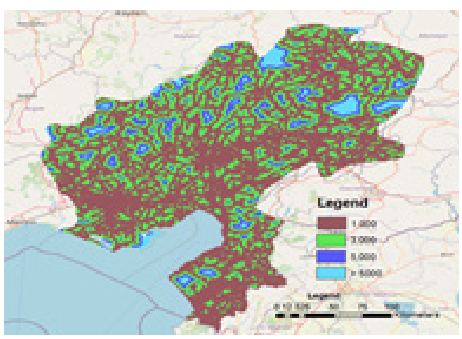

Figure 5. *Suitibility Index Map of Distance from Roads of the Study Area*

Distance from Transmission Lines.

Proximity to existing electrical transmission lines are important economically (Uyan, 2017).

In the study, <1000 m buffer zone is given as 1,1000–3000 m buffer zone is given as 2, 3000–5000 m buffer zone is given as 3, 5000–10000 m buffer zone is given as 4 and >10,000 m buffer zone is given as 5 (Figure 6).

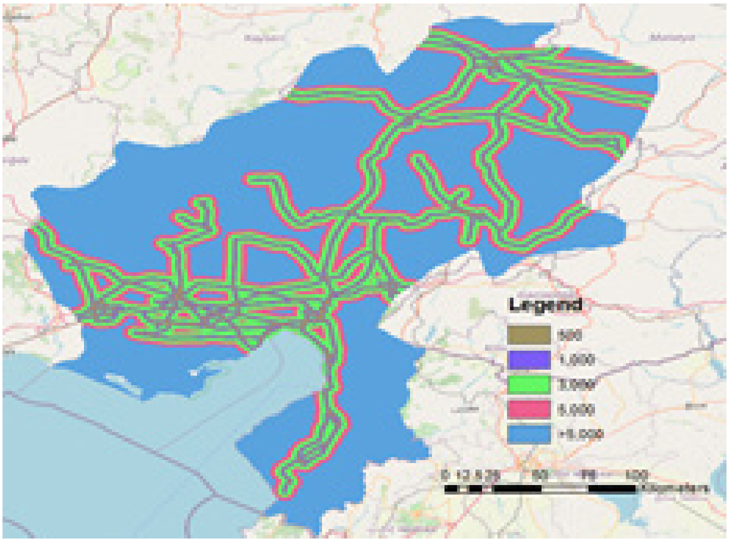

Figure 6. *Suitibility Index Map of Distance from Transmission Lines of the Study Area*

The obtained factors were evaluated in a GIS environment and all the raster data resampled to 30 m. resolution. The Weighted Sum analysis of the Spatial Analyst Tool in the ArcGIS program is used for creating the Land Suitability Index Map for SPP siting by using the AHP method (Figure 8.).

RESULTS AND DISCUSSION

AHP method is an important multi-criteria decision making method. It is one of the most effective methods used in spatial planning in recent years. In the AHP method, users are enable to determine the weights of the parameters in the solution of a multi-criteria problem. In the AHP method, a hierarchical model is used for every problem, consisting of objectives, criteria, sub-criteria and alternatives (Saaty, 1990). In this study, it was focused on the use of GIS together with MCE methods for site selection of solar power plants. The weights of the criteria, that used in the site selection process are determined separately by binary comparisons with the AHP. Determination of the weights with the AHP method gives quite positive results. In this method, the criteria are weighted between

1 and 9 considering the scale of importance. After the problem is set in a hierarchical structure, the weights of the criteria forming the hierarchy are calculated (Öztürk & Batuk, 2010).

In the study, scoring is made with the utilization of the preference scale suggested by Saaty (1980), for evaluating the criteria included in a level compared with other criteria included in the next hierarchy level (Table 2). A pairwise comparison matrix is then created (Saaty, 1980, Saaty, 1990). The pairwise comparison matrix consists of $n(n-1)/2$ comparisons, for n number of elements (Malczewski, 2010, Öztürk & Batuk, 2010).

In this study, five criteria (distance from residential areas, slope, aspect, distance from roads, distance from transmission lines) determined for AHP analysis are evaluated in the free online software (Anonymous, 2020c), prepared for making AHP analysis by Goepel (2018).

Initially, a double comparison was made for AHP priorities (Figure 7). Depending on the importance of the criteria, 1-9 selections were made in the AHP scale and calculated automatically. As a result of the calculation, the Consistency Ratio was determined as 8.20% and the weights of the criteria were determined as a result of the double comparison (Table 3). It is considered that the judgments exhibit a sufficient degree of consistency and that the assessment can be continued, in the case where the consistency ratio calculated for the judgments is below 0.10 (Öztürk & Batuk, 2007; Akıncı et al., 2013).

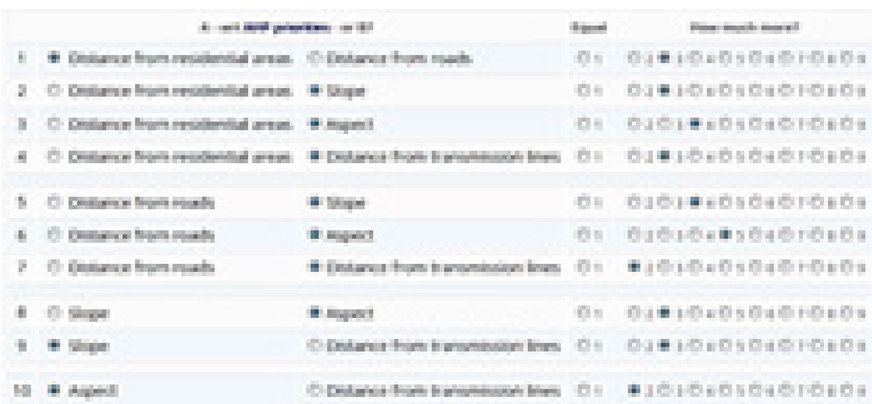

Figure 7. *The pairwise comparison module in the software (Anonymous, 2020c); AHP Evaluation Scale: 1- Equal importance, 3- Moderate importance, 5- Strong importance, 7- Very strong importance, 9- Extreme importance, 2,4,6,8- Intermediate values*

Table 3. *Resulting weights for the criteria based on pairwise comparison*

CATEGORY	PRIORITY	RANK
Aspect	% 41.50	1
Slope	% 26.50	2
Distance from Transmission Lines	% 16.20	3
Distance from Residential Areas	% 9.80	4
Distance from Roads	% 6.00	5

In the study, selected criteria weights are calculated with AHP method. Resulting weights for the criteria based on pairwise comparison was calculated as 41.5% for Aspect, 26.5% for Slope, 16.2% for Distance from Transmission Lines, 9.6% for Distance from Residential Areas and 6% for Distance from Roads (Table 3). The obtained weights factors were evaluated in GIS. For creating the land suitability index maps for the SPP siting, the Weighted Sum analysis of the Spatial Analyst Tool in the ArcGIS program is used (Figure 8.). With the locations of the present SPP sites in the study area, the validity of the created map was checked.

The criteria selected according to the general characteristics of the study area were combined with ArcGIS software using the weight values obtained with AHP and suitable areas for the SPP installation were determined. The land suitability index map is divided into three categories: "unsuitable areas", "alternative areas" and "suitable areas". According to the results obtained, 3.29% of the working area are suitable for the establishment of a solar power plant. 65.93% of the study area are in an alternative suitability. 30.78% of the study area is not suitable for building a solar power plant.

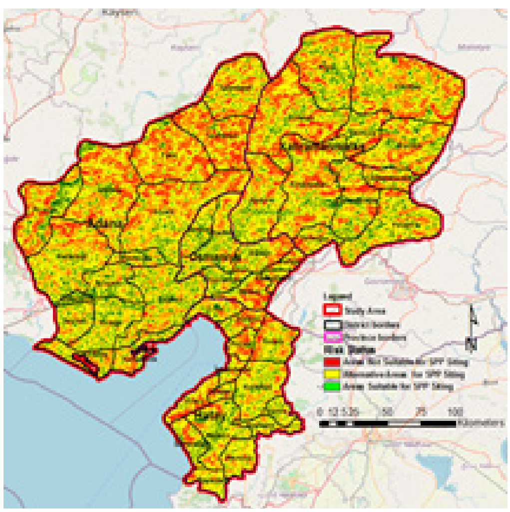

Figure 8. *Land suitability index map in the study area.*

The SPP facilities in the Adana province are mostly located in Yuregir and Ceyhan districts. This confirms the created land suitability index map. In addition to Yuregir and Ceyhan districts, some parts of Saricam and Karaisali districts have suitable or alternative areas for SPP siting. According to the land suitability index map, in the study area, Aladağ, Feke and Saimbeyli districts are less suitable for SPP than other districts.

The SPP facilities in the Osmaniye province are mostly located in Kadirli and Duzici districts. This also confirms the created land suitability index map. In addition to Kadirli and Duzici districts, some parts of Toprakkale and Sumbas districts have suitable or alternative areas for SPP siting. It was determined in the study area, Merkez district is less suitable for SPP than other districts.

Kahramanmaras has 12 SPP power plants, especially in Ekinözü, Afşin and Pazarcık districts. According to the land suitability index map, in addition to Ekinözü, Afşin and Pazarcık districts, some parts of Andirin, Elbistan and Dulkadioglu districts have suitable or alternative areas for SPP siting. In the study area, Goksun and Onikisubat districts are less suitable for SPP than other districts.

Hatay has 3 SPP power plants, especially in Merkez district. According to the land suitability index map, in addition to Merkez districts, some parts of Erzin, and Hassa districts have suitable or alternative areas for SPP siting. These results also support the results of the MCE study conducted in Hatay without using AHP method by Geçen (2019).

CONCLUSION

In Turkey, the solar energy potential of the Mediterranean, Southeast Anatolian and Central Anatolian regions are high. It is observed that the provinces in the Mediterranean region are provinces with high solar energy potential due to their geographical location in the study area.

Solar power plants (SPP) investments are becoming widespread in the Eastern Mediterranean Region. In Turkey, for integration of the solar energy into the economy, government supports made to investors has been increasing since 2013. This increases the interest in SPP investments.

In this article, a site selection study for SPP investment in the Eastern Mediterranean region with GIS based AHP method, based on five different criteria is conducted. It has been determined that the areas suitable for SPP determined in this study are largely compatible with the current SPP locations. This shows that the criteria used in the study are generally sufficient for evaluations. The conformity obtained GES conformity map can be used in preliminary evaluations for investors. By increasing the criteria, investment areas can be determined much more precisely. This can contribute to feasibility studies.

In Turkey, the years 2015 -2016 has been a key year for solar energy investments. Solar energy investments are expected to progress more quickly after the spring of 2020. Especially, the fact that the energy costs are rising very much and the costs of the panels in the solar energy systems decrease to almost one-third level, makes the investment appetite of the people about solar energy. Five years ago, while the depreciation of a solar power system was about 9-10 years, today this period has decreased to 4 years. For this reason, this study is important for the people who will invest in solar energy in the future.

Fossil fuels both pollute the environment and increase their economic values day by day have led people to new and renewable energy sources. According to the forecast of the international energy agency (IEA), solar energy will be the cheapest source of electricity generation in many countries by 2040. At the same time, the Ministry of Agriculture and Forestry in our country provides support for solar energy in agricultural irrigation. This is one of the strengths of our country in energy.

Our country offers attractive investment opportunities for domestic and foreign investors, especially in the fields of wind and solar energy. In terms of solar energy Turkey is among the countries with a high potential, due to the its surface area, size and long duration of sunshine. With the development and improvement of investment environment, providing energy reforms, it will become an increasingly attractive market for investors in Turkey in the coming period. For this reason, this study is important for the investors, who will invest in the Eastern Mediterranean Region.

Solar energy should not be seen only as an electricity generation tool. In addition to generating electricity, solar energy also has widespread uses in areas such as hot water production, cooking and heating and cooling of residences and workplaces. Solar powered hybrid heat pumps and electric combi boilers are now used in residential and commercial establishments. While regional heating systems are installed with various hybrid sources all over the world, solar technologies and products have an important place in these systems.

Roof and heat pump applications are the personal or small-scale individual use of solar energy investments. Investors are also supported for these. This study is also important for the small scale investors who will make such investments.

Unfortunately, investments in solar energy did not reach the desired level in our country. For this reason, public institutions, universities and non-governmental organizations should be in unity to use domestic and renewable energy sources and increase investments. Therefore, similar studies should be done in the future.

REFERENCES

Akıncı H., Ozalp A. Y, Turgut B., (2013) Agricultural land use suitability analysis using GIS and AHP technique , Computers and Electronics in Agriculture 97; 71–82

Anonymous, (2020a). Mediterranean Region Online Access Date:04.01.2020 web site: https://tr.wikipedia.org/wiki/Akdeniz_B%C3%B6lgesi(In Turkish)

Anonymous, (2020b). OpenStreet Map Online Access Date:03.01.2020 web site:, https://www.openstreetmap.org/#map =7/39.031/35.252

Anonymous, (2020c). AHP Priority Calculator Access Date:15.01.2020 web site: https://bpmsg.com/academic/ahp_calc.php,.

Artun O., Saltuk B., (2018), Geographic Information System (GIS)-Based Mult-Critera Evaluation For Greenhouse Site Selection: Tigris Basin Case Study. Fresenius Environmental Bulletin Volume 27- No.12A pages9019-9025.

Ayday C, Yaman N, Sabah L, Höke O. Site Selection Of Solar Power Plant By Usıng Open Source GIS For Eskişehir Province.(2016) 6. Uzaktan Algılama-CBS Sempozyumu (UZAL-CBS 2016), 5-7 Ekim 2016, Adana (In Turkish)

Geçen R. (2019) Determining The Potential Of Solar Power And Suitable Area For Constructing Solar Power Plant In Hatay Province. Turkish Studies Social Sciences. Volume 14 Issue 6, 2019, p. 3031-3054 (In Turkish)

Goepel, K.D., (2018). Implementation of an online software tool for the analytic hierarchy process (AHP-OS). International Journal of the Analytic Hierarchy Process, Vol. 10 Issue 3 2018, pp 469-487.

Malczewski, J.,1999 GIS and Multicriteria Decision Analysis, John Wiley & Sons, Inc., New York.

Jacek Malczewski (2006) GIS based multicriteria decision analysis: a survey of the literature, International Journal of Geographical Information Science, 20:7, 703-726, DOI: 10.1080/13658810600661508

NASA/METI/AIST/Japan Spacesystems, and U.S./Japan ASTER Science Team (2019). ASTER Global Digital Elevation Model V003 [Data set]. NASA EOSDIS Land Processes DAAC. Accessed 2020-01-05 from https://doi.org/10.5067/ASTER/ASTGTM.003

Ozturk, D., Batuk, F., 2007. Criterion Weights in Decision Making with Multiple Criteria. Yıldız Technical University Sigma Engineering and Science Journal 25 (1),86–98. (In Turkish)

11. Ozturk, D., Batuk, F., 2010 Using Analytical Hierarchy Method In Spatial Decision Problems. Sigma Engineering Science Journal Volume 28, Pages 124-137. (In Turkish)

Saaty, T. L., (1980). The Analytic Hierarchy Process: Planning, Priority Setting, Resource Allocation, ISBN 0- 07-054371-2, McGraw-Hill

Saaty T.L. (1990). How To Make A Decision: The Analytic Hierarchy Process. European Journal of Operational Research, 48(1), 9-26.

Saltuk, B., Artun O., (2019). Multi-Criteria Decision System For Greenhouse Site Selection In Gediz Basin, Turkey Using Geographic Information Systems (GIS). Fresenius Environmental Bulletin Volume 28 –No. 8/2019 pages 6358-6365

Shen YC, Chou CJ, Lin GTR., (2011). The portfolio of Renewable Energy Sources For Achieving The Three E Policy Goals. Energy ;36:2589–98.

Traube J, Lu F, Maksimovic D, Mossoba J, Kromer M, Faill P, et al., (2013) Mitigation of Solar Irradiance Intermittency In Photovoltaic Power Systems With Integrated Electric-Vehicle Charging Functionality. IEEE Transactions on Power Electronics. 2013;28(6):3058–67.

Uyan M., (2017) GIS-Supported mapping of solar power plant sites using AHP method . Pamukkale Univ Muh Bilim Derg, 23(4), 343-351, (In Turkish)

Wind, Y., Saaty, T. L., (1980). Marketing application of the analytic hierarchy process. Management Science, 26 (7): p. 641-658.

Yalçın, C , Yüce, M., (2020) Determination of Areas Suitable for Solar Power Plant (SPP) Investment in Burdur by GIS Method. Geomatik , 5 (1) , 36-46 . DOI: 10.29128/geomatik.561962 (In Turkish)

Yılmaz, S. , Duhan, D.K., (2017). Energy Security Concept: A Discussion in the Light of the Oil Crisis of 1973. International Journal of Crisis and Political Research, 2017, 1 (3), Pg. 169-199, Ankara (In Turkish)

Chapter 2

A TUTORIAL FOR CREATING A RECOMMENDATION SYSTEM FOR ARTICLES BY USING PYTHON TOOLS

Mustafa AL-ASADI[1]
Sakir TASDEMIR[2]
Ilker Ali OZKAN[3]

1 Selcuk University, Department of Computer Engineering, Konya, Turkey, masadi@lisansustu.selcuk.edu.tr
2 Selcuk University, Department of Computer Engineering, Konya, Turkey, stasdemir@selcuk.edu.tr
3 Selcuk University, Department of Computer Engineering, Konya, Turkey, ilkerozkan@selcuk.edu.tr

INTRODUCTION

Recommendation systems mainly produce a list of recommendations in any field, using one of two methods - via Collaborative Filtering or Content-Based Filtering (Jafarkarimi, Sim, & Saadatdoost, 2012). Collaborative filtering depends on the behaviour of the previous user, such as products that he or she previously purchased or previous assessments, in line with similar decisions made by other users, so that the first user's wishes can be expected based on the decisions of other users (Melville & Sindhwani, 2010). Content-based filtering is based on bringing similar products with their characteristics to the purchased product (Mooney & Roy, 2000). These methods are often used simultaneously to form a single system called Hybrid Recommender Systems (Balabanović & Shoham, 1997).

The difference between the collaborative approach and the content-based method can be illustrated by comparing two known music recommender systems - Last.fm and Pandora Radio.

Last.fm makes a list of recommended songs by observing the bands and sections that are regularly heard by the user, and comparing them with similar lists for other users. And then tells the fm to run sections that do not appear in the current user list, but the sections that are heard by users who have listed similar to the current user list, it is an example of a collaborative filtering method.

Pandora uses specific features of the musical composition or artist - a set of 400 properties - to feed the playlist of users that are similar to the heard tracks, it is an example of a Content-Based Filtering (Freire, 2008).

For both systems, there are strengths and weaknesses, in the first example, for the Last.fm, the system requires a large amount of information per user to get accurate recommendations. This is an example of the so-called cold-start problem, which is common in the Collaborative Filtering systems (Elahi, Ricci, & Rubens, 2016; Rubens, Elahi, Sugiyama, & Kaplan, 2015; Schein, Popescul, Ungar, & Pennock, 2002). Whereas Pandora requires little information to start, but it is far more limited in scope (e.g., it can only make recommendations that are comparable to the original kernel).

Recommendation systems are a good alternative to search algorithms because they help users discover items they may not find. Where recommendation systems are often implemented using search engines to index non-traditional data (Vyas, 2018). Recommendation systems were first mentioned in a working paper entitled "digital bookshelf" in 1990 by Jussi Karlgren at The Royal Institute of Technology and Stockholm University (Karlgren, 1990).

Due to the increasing number of articles published on the web every day. So, the search for resources can be great, especially for beginners. Therefore, the articles recommendation system will be useful because of its ability to provide a customized platform for the articles proposed (Bancu et al., 2012).

The recommendation systems and their application have been searched in different areas, like music ((Bu et al., 2010), (Van den Oord, Dieleman, & Schrauwen, 2013), (X. Wang & Wang, 2014)), videos (Davidson et al., 2010), people (Badenes et al., 2014), jobs ((Bastian et al., 2014), (Kenthapadi, Le, & Venkataraman, 2017), (Mishra & Reddy, 2016)), and research papers ((C. Wang & Blei, 2011), (Joeran et al., 2013), (Beel, Langer, Genzmehr, & Nürnberger, 2013)), and others.

This chapter is a tutorial to creating a recommendation system for articles that match user interests and predicts which articles the user has not read by using python tools. This chapter addresses the following topics: Data Set, Evaluate the Performance of Algorithms, Implement Collaborative Filtering, Testing the Model, Results, Conclusion

DATASET

In this section, we used the Deskdrop dataset (Moreira, 2017), which contains a sample of one year (from Mar. 2016 - to Feb. 2017) from DeskDrop (CI&T's Internal Communication platform). Deskdrop is an internal communications platform, that developed by CI&T, Deskdrop is focused in companies that using Google G Suite. The main features of this platform are allowing for companies' employees to share articles with their peers, and collaborate between them.

DeskDrop dataset contains 73k logged users' interactions on more than 3k public articles that shared in the DeskDrop platform. DeskDrop is consist of two CSV files, are shared_articles.csv, and users_interactions.csv.

Shared Articles

It contains details about the articles that shared in the DeskDrop platform. Each article contains its date of sharing (timestamp), title, the original URL, content in plain text, article language (pt: Portuguese or en: English) and details about the user that shared the article (author). In a given timestamp, there are two possible event types:

CONTENT SHARED: The article has been shared in the platform and is available to users.

CONTENT REMOVED: The article has been removed from the platform.

To simplify matters, we used only "CONTENT SHARED" as event type, assuming that all articles were available during the whole year, then we upload data as Table 1.

Users Interactions

Contains records of user interactions in shared articles (Table 2). The eventType values contain:

VIEW: The users have opened the article only.

LIKE: The users have liked the article.

COMMENT CREATED: The users created a comment in the article.

FOLLOW: The users want to be notified on any new comment in the article.

BOOKMARK: Users added a bookmark to easily retrieve the article in the future

Table 1. Loading Shared_articles data for the first two rows and first four columns.

n	Timestamp	URL	Title	Lang.
1	1459193988	http://www.nytimes.com/2016/03/28/business/dea...	Ethereum, a Virtual Currency, Enables Transact...	en
2	1459194146	http://cointelegraph.com/news/bitcoin-future-w...	Bitcoin Future: When GBPcoin of Branson Wins O...	en

Table 2. Loading users_interactions data for the first two rows and first four columns

n	timestamp	eventType	sessionId	userAgent
1	1465413032	VIEW	1.2642E+18	NaN
2	1465412560	VIEW	3.62174E+18	Mozilla/5.0 (Macintosh; Intel Mac OS X 10_11_2...

Dataset Analysis

After loading the dataset and import the main libraries of python like pandas and NumPy, we are going to take a look at and explore the data by a few different ways:

- Dimensions of Dataset
- Statistical Summary
- Missing Data

Dimensions of Dataset

We can get a quick idea of how many instances (rows and columns) in the dataset by using "shape" property. From Figure 1 and 2, we have 3047 instances and 13 attributes in the dataset of Shared Articles, and 72312 instances and 8 attributes in the dataset of Users Interactions.

```
# shape
print(articles_df.shape)

(3047, 13)
```

Figure 1. Use shape command in python code for Shared Articles dataset.

```
# shape
print(interactions_df.shape)

(72312, 8)
```

Figure 2. Use shape command in python code for Users Interactions dataset.

Statistical Summary

We can take a look at a summary for each numerical attribute by use "describe" property. This includes count, mean, the min and max values and percentiles (Figure 3, 4).

	timestamp	contentId	authorPersonId	authorSessionId
count	3.047000e+03	3.047000e+03	3.047000e+03	3.047000e+03
mean	1.468865e+09	1.969568e+16	4.198685e+17	1.694961e+17
std	7.573604e+06	5.376353e+18	4.390382e+18	5.391587e+18
min	1.459194e+09	-9.222795e+18	-9.120686e+18	-9.212055e+18
25%	1.462401e+09	-4.673420e+18	-1.570135e+18	-4.656768e+18
50%	1.467176e+09	3.455744e+16	-7.092877e+17	3.910429e+17
75%	1.473944e+09	4.716572e+18	3.609194e+18	4.821078e+18
max	1.488308e+09	9.222265e+18	9.210531e+18	9.221043e+18

Figure 3. Use describe command in python code for Shared Articles dataset.

	timestamp	contentId	personId	sessionId
count	7.231200e+04	7.231200e+04	7.231200e+04	7.231200e+04
mean	1.470103e+09	-3.033423e+16	1.252026e+16	3.421273e+16
std	7.258130e+06	5.344755e+18	5.022333e+18	5.344355e+18
min	1.457964e+09	-9.222795e+18	-9.223122e+18	-9.222505e+18
25%	1.464876e+09	-4.726309e+18	-3.596627e+18	-4.613476e+18
50%	1.468343e+09	1.893099e+16	-1.088422e+17	5.029492e+16
75%	1.474461e+09	4.441012e+18	3.766319e+18	4.667962e+18
max	1.488310e+09	9.222265e+18	9.210531e+18	9.223314e+18

Figure 4. Use describe command in python code for Users Interactions dataset.

Missing Data

We can explore any missing values in the data set (NaN value) and length of data by using "info" property. In Figure 5 and 6, it seems no missing value in the dataset.

```
Data columns (total 13 columns):
timestamp          3047 non-null int64
eventType          3047 non-null object
contentId          3047 non-null int64
authorPersonId     3047 non-null int64
authorSessionId    3047 non-null int64
authorUserAgent    669 non-null object
authorRegion       669 non-null object
authorCountry      669 non-null object
contentType        3047 non-null object
url                3047 non-null object
title              3047 non-null object
text               3047 non-null object
lang               3047 non-null object
dtypes: int64(4), object(9)
memory usage: 333.3+ KB
```

Figure 5. Test missing data use describe command in python for Shared Articles dataset.

```
Data columns (total 8 columns):
timestamp      72312 non-null int64
eventType      72312 non-null object
contentId      72312 non-null int64
personId       72312 non-null int64
sessionId      72312 non-null int64
userAgent      56918 non-null object
userRegion     56907 non-null object
userCountry    56918 non-null object
dtypes: int64(4), object(4)
memory usage: 4.4+ MB
```

Figure 6. Test missing data use describe command in python for Users Interactions dataset.

Data wrangling

Data wrangling, sometimes referred to as Data munging, is the process of transforming data from one "raw" into other formats with to make it more appropriate to make analytics (Ramesh, 2015). More specifically, the munging process consists of a number of operations that are applied to an initial data set to be converted to a different but related data set. These operations will be located in several categories: recognition, analysis, filtering, and transformation (Cross, 2001). Furthermore, munging can mean processing raw data to achieve a final form. It can mean analyzing or filtering data, or any of the steps required to identify the data (Kroger, 2016).

In this work, due to there are different interactions types in articles, therefore we associate them with a weight, for example, a comment in an article indicates (4.0) a higher interest of the user on the item than a view (1.0), or than a simple like (2.0) as in Figure 7.

```
event_type_strength = {
    'VIEW': 1.0,
    'LIKE': 2.0,
    'BOOKMARK': 2.5,
    'FOLLOW': 3.0,
    'COMMENT CREATED': 4.0,
}
```

Figure 7. Data munging

User cold-start

Cold-start is a potential problem when you build a recommender system (Schein et al., 2002). When a new user uses the system, the system often does not know anything about that user so that he can build the appropriate suggestions for it. There are several suggested solutions to eliminate the cold start problem. Content-based filtering approaches is one of the most effective solutions to this problem (Lika, Kolomvatsos, & Hadjiefthymiades, 2014). Therefore, we are kept only users that have at least 5 interactions in the dataset as in Figure 8.

```
users_interactions_count_df = interactions_df.groupby
(['personId', 'contentId']).size().groupby('personId').size()
print('# users: %d' % len(users_interactions_count_df))
```

Figure 8. Solve the problem of cold start

Deskdrop allows users to view the article several times and interact with it in different ways (e.g. comment or follow). Therefore, to smooth the distribution and to model the user interest on a given article, we gathering all user interactions in an item by collecting the weight of the force type of the interaction and applying the log transformation to smooth the distribution as in Figure 9. It is worth mentioning that a log transformation can help make a relationship clear and describe the relationship between logs and the geometric mean. Furthermore, the log transformation can be used to make highly skewed distributions less skewed (Log, 2012).

```
def smooth_user_preference(x):
    return math.log(1+x, 2)

interactions_full_df = interactions_from_selected_users_df \
                    .groupby(['personId', 'contentId'])['eventStrength'].sum() \
                    .apply(smooth_user_preference).reset_index()
print('# of unique user/item interactions: %d' % len(interactions_full_df))
interactions_full_df.head(10)
```

```
# of unique user/item interactions: 39106
```

	personId	contentId	eventStrength
0	-9223121837663643404	-8949113594875411859	1.000000
1	-9223121837663643404	-8377626164558006982	1.000000
2	-9223121837663643404	-8208801367848627943	1.000000
3	-9223121837663643404	-8187220755213888616	1.000000
4	-9223121837663643404	-7423191370472335463	3.169925
5	-9223121837663643404	-7331393944609614247	1.000000
6	-9223121837663643404	-6872546942144599345	1.000000
7	-9223121837663643404	-6728844082024523434	1.000000
8	-9223121837663643404	-6590819806697898649	1.000000
9	-9223121837663643404	-6558712014192834002	1.584963

Figure 9. Basic code for log transformation function

EVALUATE THE PERFORMANCE of ALGORITHMS

Data split

Resampling methods are the best statistical techniques to evaluate the performance of an algorithm. Where it permits to make accurate estimates of how the algorithm performs on new data (Brownlee, 2016).

The common types of resampling techniques are Hold-out (Train and Test Split), Cross-Validation (CV), and Repeated Random Hold-out. In this work, we are using Repeated Random Hold-out, in this method we seek to create a random split of the dataset as a hold-out method but repeat the process of dividing (split) and evaluating the algorithm for several times, like K-fold cross-validation. we use, splits the data into an 80% train, 20% test split and repeats the process 42 times (Figure 10).

```
interactions_train_df, interactions_test_df = train_test_split(interactions_full_df,
                                   stratify=interactions_full_df['personId'],
                                   test_size=0.20,
                                   random_state=42)

print('# interactions on Train set: %d' % len(interactions_train_df))
print('# interactions on Test set: %d' % len(interactions_test_df))
```

Figure 10. Basic code for Data split.

Evaluation Methods

In recommender systems, there are several metrics used for evaluation. In this work, we chose Top-N accuracy metrics, which seeks to evaluate the accuracy of the better recommendations provided to a user, comparing with the items the user has interacted in test data (Ziegler, McNee, Konstan, & Lausen, 2005).

We choose Recall@N to determine the Top-N accuracy metric. In this work, Recall@N evaluates whether the interacted item is between the top N items in the ranked list of recommendations for a user (Cremonesi, Koren, & Turrin, 2010) (Figure 11).

```
#Top-N accuracy metrics consts
EVAL_RANDOM_SAMPLE_NON_INTERACTED_ITEMS = 100

class ModelEvaluator:


    def get_not_interacted_items_sample(self, person_id, sample_size, seed=42):
        interacted_items = get_items_interacted(person_id, interactions_full_indexed_df)
        all_items = set(articles_df['contentId'])
        non_interacted_items = all_items - interacted_items

        random.seed(seed)
        non_interacted_items_sample = random.sample(non_interacted_items, sample_size)
        return set(non_interacted_items_sample)

    def _verify_hit_top_n(self, item_id, recommended_items, topn):
            try:
                index = next(i for i, c in enumerate(recommended_items) if c == item_id)
            except:
                index = -1
            hit = int(index in range(0, topn))
            return hit, index
```

Figure 11. Calculate Top-N accuracy

IMPLEMENT COLLABORATIVE FILTERING

Collaborative filtering technique works through building a database (user-item matrix) of the preferences for items by users. It then matches users with pertinent interest and preferences by calculating similarities between their profiles to make recommendations (Herlocker, Konstan, Terveen, & Riedl, 2004). These users build a group called a neighborhood. A user gets recommendations to all those elements (items) that he has not rated before but that were already positively rated by users in his neighborhood. Recommendations that are produced by Collaborative Filtering can be of either prediction or recommendation. Prediction is a numerical value, Rij, expressing the predicted score of item j for the user i (Figure 12), while Recommendation is a list of top N items that the user will like the most as shown in Figure 13. The technique of collaborative filtering (CF) has two main strategies for implementation, memory-based and model-based (Bobadilla, Ortega, Hernando, & Gutiérrez, 2013; Breese, Heckerman, & Kadie, 1998).

Memory-based

This method uses previous memory for user interactions to calculate the similarity between users based on the items they interact with (user-based approach) or calculate the similarity between items based on the users they interacted with (item-based approach). The most commonly used example of this method is User Neighbourhood-based CF, in which the top-N similar users (Which are calculated by Pearson correlation) for a user are selected and used to recommend elements those similar users liked, but the existing user has not interacted till now.

Model-based

This method, models are developed by using different machine learning algorithms (ML) to recommend elements to users (Sarwar, Karypis, Konstan, & Riedl, 2001). There are many types of model-based CF algorithms, like Bayesian networks, neural networks, and latent factor models like as Singular Value Decomposition (SVD).

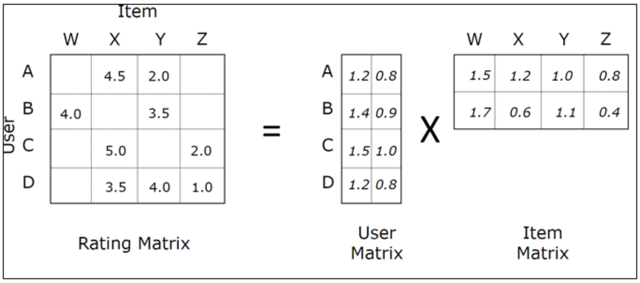

Figure 12. Recommendation by Matrix Factorization (Seo, 2018).

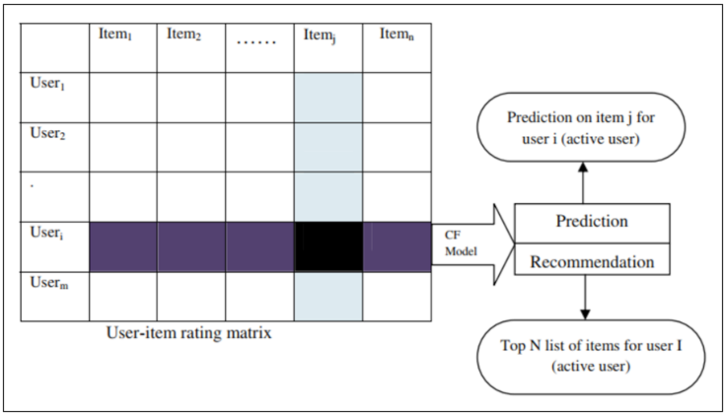

Figure 13. Block diagram for process of collaborative filtering in the model

Matrix Factorization

Latent factor models used Matrix Factorization to represent items and users in a lower-dimensional latent space (Ma, Zhou, Liu, Lyu, & King, 2011). One of the main advantages of this method is that instead of having a high-dimensional matrix that contains a large number of missing values, a smaller matrix will be dealt with a smaller matrix in lower-dimensional space. In this work, we use the common latent factor model called Singular Value Decomposition (SVD). Table 3 shown the initial matrix which consists of 10 rows × 2926 columns.

Table 3. Calculate Top-N accuracy

	personId	contentId	eventStrength
0	9223121837663643404	8949113594875411859	1.000000

An important decision in SVD is the number of factors to factor the user-element matrix. The greater the number of factors, the more precise is the factorization in the original matrix rebuilding (Golub & Reinsch, 1970). Therefore, decrease the number of factors leads to increases the model generalization (Figure 12, 14).

```
In [15]: #The number of factors to factor the user-item matrix.
         NUMBER_OF_FACTORS_MF = 15
         #Performs matrix factorization of the original user item matrix
         U, sigma, Vt = svds(users_items_pivot_matrix, k = NUMBER_OF_FACTORS_MF)

In [16]: U.shape

Out[16]: (1140, 15)

In [17]: Vt.shape

Out[17]: (15, 2926)

In [18]: sigma = np.diag(sigma)
         sigma.shape

Out[18]: (15, 15)
```

Figure 14. The number of factors to factor the user-element matrix

After the factorization, we try to reconstruct the original matrix by multiplying its factors. After factorization of the matrix, we tried to reconstruct the original matrix via multiplying its factors. The new matrix is not sparser. Predictions have been created for elements that the user has not till now interacted with and we will use them for recommendations.

TESTING THE MODEL

For testing the model, we selected one user (for example -1479311724257856983). In Figure 15., the model displays the first 20 articles suggested for the user which match to its interactions in Deskdrop from a train set. It can be seen that among the main user interests are Artificial Intelligence, Machine Learning, Deep Learning and the Google Cloud Platform.

```
In [38]:
inspect_interactions(-1479311724257856983, test_set=False).head(20)

Out[38]:
```

	eventStrength	contentId	title	url	lang
115	4.285402	7342707578347442862	At eBay, Machine Learning is Driving Innovativ...	https://www.ebayinc.com/stories/news/at-ebay-m...	en
38	4.129283	621816023396605502	AI Is Here to Help You Write Emails People Wil...	http://www.wired.com/2016/08/boomerang-using-a...	en
8	4.044394	-4460374799273064357	Deep Learning for Chatbots, Part 1 - Introduction	http://www.wildml.com/2016/04/deep-learning-fo...	en
116	3.954196	-7959318068735027467	Auto-scaling scikit-learn with Spark	https://databricks.com/blog/2016/02/08/auto-sc...	en
10	3.906891	2589533162305407436	6 reasons why I like KeystoneML	http://radar.oreilly.com/2015/07/6-reasons-why...	en

Figure 15. Testing model

RESULTS

Collaborative filtering has been referred to as the similar learning pattern in machine learning, which is used for predicting recommendations based on learning similarity amongst users (Resnick, Iacovou, Suchak, Bergstrom, & Riedl, 1994). The chapter reviews some state-of-the-art recommendation systems applied in the past. In addition, we conducted some analytical operations on the data for the purpose of understanding, representing and converting them into easy-to-use formats. Finally, our proposed system seeks to actively recommend the contents of articles relevant to the reader based on its current history of preferences.

This section from chapter focuses on the results obtained for the Collaborative Recommendation part of the system. When evaluating the Collaborative Filtering model (SVD matrix factorization), we observe that we obtain Recall@10 (46%) and Recall@5 (33%) values as in Figure 16.

```
print('Evaluating Collaborative Filtering (SVD Matrix Factorization) model...')
cf_global_metrics, cf_detailed_results_df = model_evaluator.evaluate_model(cf_recommender_model)
print('\nGlobal metrics:\n%s' % cf_global_metrics)
cf_detailed_results_df.head(10)

Evaluating Collaborative Filtering (SVD Matrix Factorization) model...
1139 users processed

Global metrics:
{'modelName': 'Collaborative Filtering', 'recall@5': 0.33405778573254924, 'recall@10': 0.46816670928151366}
```

Figure 16. Testing model

CONCLUSION

Designing and developing RecSys is a multi-disciplinary effort that has benefited from results obtained in various computer science fields especially machine learning and data mining. And this clear in this tutorial chapter and the results presented above. Many RecSys are centred around the use of various machine learning and data mining algorithms to predict user evaluations for items, or for learning how to correctly rank items for a user. in this tutorial chapter, we created a recommendation system for articles that match user interests and predicts which articles the user has not read by using python tools and using CI&T Deskdrop dataset. Overall, we have noted that the proposed approach works well via traditional matrix factorization methods that are called Singular Value Decomposition (SVD), and predicts well for articles that are not read by the user. in this tutorial, we used these traditional techniques for didactic purposes although there are more advanced techniques in recommendation systems research community, like neural networks and deep learning models.

REFERENCES

Badenes, H., Bengualid, M. N., Chen, J., Gou, L., Haber, E., Mahmud, J., Smith, B. A. (2014). *System U: automatically deriving personality traits from social media for people recommendation.* Paper presented at the Proceedings of the 8th ACM Conference on Recommender systems.

Balabanović, M., & Shoham, Y. (1997). Fab: content-based, collaborative recommendation. *Communications of the ACM, 40*(3), 66-72.

Bancu, C., Dagadita, M., Dascalu, M., Dobre, C., Trausan-Matu, S., & Florea, A. M. (2012). *ARSYS--Article Recommender System.* Paper presented at the Symbolic and Numeric Algorithms for Scientific Computing (SYNASC), 2012 14th International Symposium on.

Bastian, M., Hayes, M., Vaughan, W., Shah, S., Skomoroch, P., Kim, H., . . . Lloyd, C. (2014). *LinkedIn skills: large-scale topic extraction and inference.* Paper presented at the Proceedings of the 8th ACM Conference on Recommender systems.

Beel, J., Langer, S., Genzmehr, M., & Nürnberger, A. (2013). *Introducing Docear's research paper recommender system.* Paper presented at the Proceedings of the 13th ACM/IEEE-CS joint conference on Digital libraries.

Bobadilla, J., Ortega, F., Hernando, A., & Gutiérrez, A. (2013). Recommender systems survey. *Knowledge-based systems, 46*, 109-132.

Breese, J. S., Heckerman, D., & Kadie, C. (1998). *Empirical analysis of predictive algorithms for collaborative filtering.* Paper presented at the Proceedings of the Fourteenth conference on Uncertainty in artificial intelligence.

Brownlee, J. (2016). Machine Learning Mastery with Python. *Machine Learning Mastery Pty Ltd*, 100-120.

Bu, J., Tan, S., Chen, C., Wang, C., Wu, H., Zhang, L., & He, X. (2010). *Music recommendation by unified hypergraph: combining social media information and music content.* Paper presented at the Proceedings of the 18th ACM international conference on Multimedia.

Cremonesi, P., Koren, Y., & Turrin, R. (2010). *Performance of recommender algorithms on top-n recommendation tasks.* Paper presented at the Proceedings of the fourth ACM conference on Recommender systems.

Davidson, J., Liebald, B., Liu, J., Nandy, P., Van Vleet, T., Gargi, U., . . . Livingston, B. (2010). *The YouTube video recommendation system.* Paper presented at the Proceedings of the fourth ACM conference on Recommender systems.

Elahi, M., Ricci, F., & Rubens, N. (2016). A survey of active learning in collaborative filtering recommender systems. *Computer Science Review, 20*, 29-50.

Freire, A. M. (2008). Remediating radio: Audio streaming, music recommendation and the discourse of radioness. *Radio Journal: International Studies in Broadcast & Audio Media, 5*(2-3), 97-112.

Golub, G. H., & Reinsch, C. (1970). Singular value decomposition and least squares solutions. *Numerische mathematik, 14*(5), 403-420.

Herlocker, J. L., Konstan, J. A., Terveen, L. G., & Riedl, J. T. (2004). Evaluating collaborative filtering recommender systems. *ACM Transactions on Information Systems (TOIS), 22*(1), 5-53.

Jafarkarimi, H., Sim, A. T. H., & Saadatdoost, R. (2012). A naive recommendation model for large databases. *International Journal of Information and Education Technology, 2*(3), 216.

Joeran, B., Langer, S., Genzmehr, M., Gipp, B., Breitinger, C., & Nürnberger, A. (2013). *Research paper recommender system evaluation: A quantitative literature survey.* Paper presented at the Workshop on Reproducibility and Replication in Recommender Systems Evaluation (RepSys) at the ACM Recommender System Conference (RecSys' 13). ACM, Hong Kong, China.

Karlgren, J. (1990). *An Algebra for Recommendations*. Retrieved from

Kenthapadi, K., Le, B., & Venkataraman, G. (2017). *Personalized job recommendation system at linkedin: Practical challenges and lessons learned.* Paper presented at the Proceedings of the Eleventh ACM Conference on Recommender Systems.

Lika, B., Kolomvatsos, K., & Hadjiefthymiades, S. (2014). Facing the cold start problem in recommender systems. *Expert Systems with Applications, 41*(4), 2065-2073.

Log, A. (2012). 16. Transformations. *Brain, 3000*, 4000.

Ma, H., Zhou, D., Liu, C., Lyu, M. R., & King, I. (2011). *Recommender systems with social regularization.* Paper presented at the Proceedings of the fourth ACM international conference on Web search and data mining.

Melville, P., & Sindhwani, V. (2010). Encyclopedia of machine learning: Springer-Verlag, chapter Recommender systems.

Mishra, S. K., & Reddy, M. (2016). *A bottom-up approach to job recommendation system.* Paper presented at the Proceedings of the Recommender Systems Challenge.

Mooney, R. J., & Roy, L. (2000). *Content-based book recommending using learning for text categorization.* Paper presented at the Proceedings of the fifth ACM conference on Digital libraries.

Moreira, G. (2017). Articles sharing and reading from CI&T DeskDrop. Retrieved from https://www.kaggle.com/gspmoreira/articles-sharing-reading-from-cit-deskdrop

Resnick, P., Iacovou, N., Suchak, M., Bergstrom, P., & Riedl, J. (1994). *GroupLens: an open architecture for collaborative filtering of netnews.* Paper presented at the Proceedings of the 1994 ACM conference on Computer supported cooperative work.

Rubens, N., Elahi, M., Sugiyama, M., & Kaplan, D. (2015). Active learning in recommender systems *Recommender systems handbook* (pp. 809-846): Springer.

Sarwar, B., Karypis, G., Konstan, J., & Riedl, J. (2001). *Item-based collaborative filtering recommendation algorithms.* Paper presented at the Proceedings of the 10th international conference on World Wide Web.

Schein, A. I., Popescul, A., Ungar, L. H., & Pennock, D. M. (2002). *Methods and metrics for cold-start recommendations.* Paper presented at the Proceedings of the 25th annual international ACM SIGIR conference on Research and development in information retrieval.

Seo, J. D. (2018). Matrix Factorization Techniques for Recommender Systems. Retrieved from https://towardsdatascience.com/paper-summary-matrix-factorization-techniques-for-recommender-systems-82d1a7ace74

Van den Oord, A., Dieleman, S., & Schrauwen, B. (2013). *Deep content-based music recommendation.* Paper presented at the Advances in neural information processing systems.

Vyas, M. (2018). Recommendation Systems. Retrieved from https://blogs.oracle.com/meena/recommendation-systems

Wang, C., & Blei, D. M. (2011). *Collaborative topic modeling for recommending scientific articles.* Paper presented at the Proceedings of the 17th ACM SIGKDD international conference on Knowledge discovery and data mining.

Wang, X., & Wang, Y. (2014). *Improving content-based and hybrid music recommendation using deep learning.* Paper presented at the Proceedings of the 22nd ACM international conference on Multimedia.

Ziegler, C.-N., McNee, S. M., Konstan, J. A., & Lausen, G. (2005). *Improving recommendation lists through topic diversification.* Paper presented at the Proceedings of the 14th international conference on World Wide Web.

Chapter 3

CALENDERING OF PAPER AND ITS EFFECTS ON PRINTABILITY

Öznur ÖZDEN[1]

Sinan SÖNMEZ[2]

1 Asst. Prof. Dr., Istanbul University-Cerrahpasa, Faculty of Forest, Forest Products Chemistry and Technology, Istanbul, Turkey.

2 Prof. Dr., *Corresponding author*, Marmara University, School of Applied Sciences, Department of Printing Technologies, Istanbul, Turkey.

INTRODUCTION

Calendering is one of the final processes that affect the paper properties in the production of many types of paper. In the calendering process, the paper sheet is passed between two or more cylinders with a certain temperature and pressure.

The main purpose of calendering is to modify the surface structure or to bring the thickness of the paper to the desired level with the following process. In case of printing on paper or cardboard, the main calendering goal is to reduce surface roughness and tighten the holes to achieve a good print (Gullichsen and Paulapuro, 1999).

Various coated paper and cardboard products are calendered with an extended soft nip, a conventional soft nip (polymer (steel) nip or hard (steel / steel) nip calender at different line load. The calendered paper surface improves and its gloss increases. Calendering is an essential process to obtain the best printing papers (Wikstrom et al., 1997).

With the development of printing methods, expectations from paper, the material under pressure, have also increased. The most important of these is the demand regarding the smoothness of the paper surface. For this reason, calendering processes have been developed which help smooth the surface to make the paper surface suitable for printing. Accordingly, calender varieties increased over time.

In this chapter, we will give information about the principles of calendering, one of the last stages of paper production, the factors affecting calendering and calender types.

CALENDERING

After leaving the paper drying party in a paper production or coated paper production mill, another series of operations that we call finishing operations must take place. These;

- Calendaring
- Wrap
- Sizing
- Storage
- Delivery

steps are. The most important part of these finishing processes is calendering (URL1).

Calendering is the final step of the paper production process that affects the paper and cardboard properties after drying. Calenders are also used as pre-calenders before coating or size application. The main purpose of calendering is to improve the surface properties of the paper and check the thickness profile. It provides the roughness, brightness and the compression of the structure of the paper, which is one of the most important surface features of the paper surface. Calendering is a process involving three basic mechanical processes: pressure, temperature and plastic flow. The calendering response of pigment coated paper is measured with the level of coated and raw materials (Casey, 1980; Lehtinen and Yhdistys, 2000).

In coated papers, the main purpose of calendering is to increase the brightness and smoothness of the coated paper. To achieve this, the web must be sufficiently plastic to be smooth without crushing the inside of the paper under the pressure of the calender rolls. Unless the plastic is sufficiently plastic, it cannot give a smooth surface and as a result, the gloss will be low. In a study, it was concluded that the pigment-glue and adhesive-glue bonds were broken and the free surface area of the coating increased during super calendering (Casey, 1960).

CALENDERING TYPES

Traditional calendering, which is shown in Figure 1 below, has been used for many years.

Source: *URL2*

Figure 1: *Traditional calender*

Methods of calendering also include their types. Although traditional calendering is still used, new methods and calenders are used in terms of performance and efficiency. Later, there were many developments and different calenders started to be used. Nowadays, calenders have developed as seen in the list below.

Machine calendering (hard rollers, MF)

Brush calendering (old method for cartons)

Soft calendering i.e. one nip per soft cylinder

- Soft calendering on the machine or bright calendering with hard / soft rollers
- Matt calendering with soft / soft rollers on the machine

Multi-nip calendering with medium soft roller (s)

- Off-machine (super calender)
- Off-machine (Janus, OptiLoadetc.)

Large nip shoe calendaring

Hot metal belt calendering (URL3)

In Figure 2, there is an example of calendering on the machine.

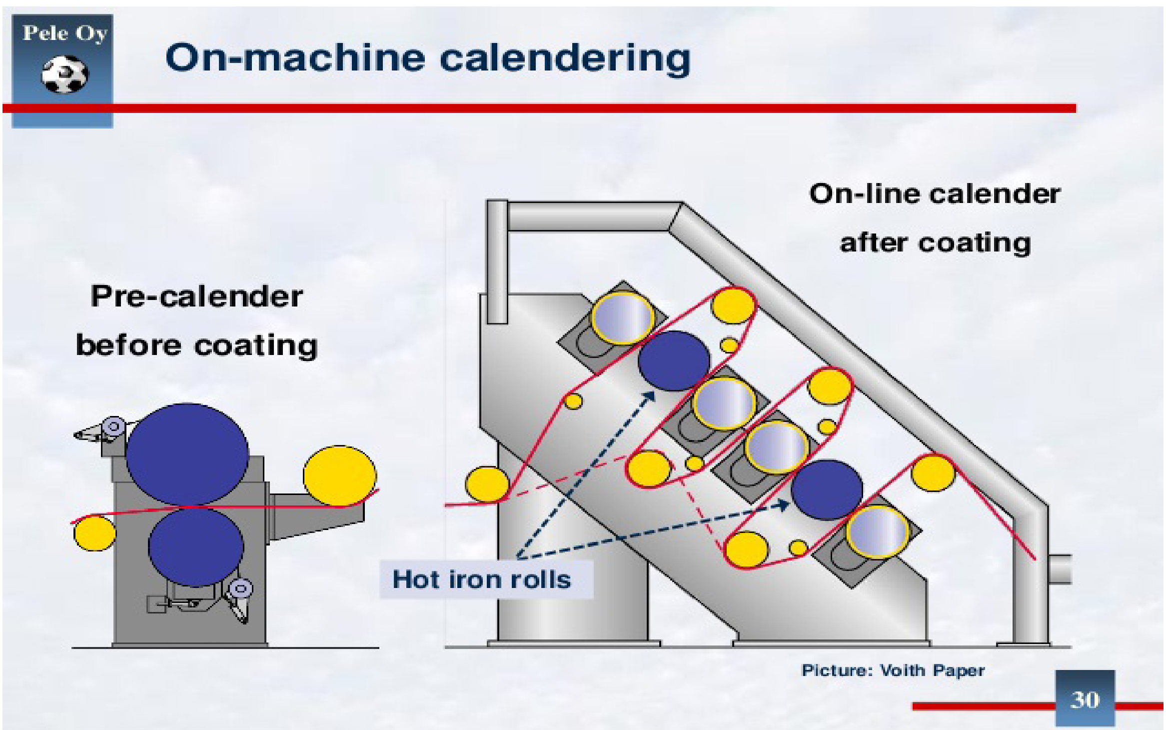

Source: *URL2*

Figure 2: *Example of Calendering on the Machine*

When we make a classification for calenders developed on and off the machine;

Traditional calender

Hard nip calender

Soft nip calender

Super calender

Multi nip calender

- Janus calender
- Prosoft calender
- OptiLoad calender

Specialty calenders

- Wet stack
- Breaker stack
- Friction calender
- Brush finishing
- Long nip calender
- Embossing calender

We can make a classification in the for (Gullichsen and Paulapuro, 1999). Due to these calender types, paper surface properties are further improved by using methods.

HARD NIP CALENDER

Hard nip calenders are used for types of paper and cardboard classes. In this calendering process, the sheet is pressed between two or more cylinders. Hard nip calenders are used in two basic classes.

- Two-cylinder hard nip calenders
- Multi-cylinder hard nip calenders

Two-cylinder calenders were used primarily used for phases that do not require extensive calendering; for pre-calendering pre-coated and finishing of wood-free papers produced with uncoated chemical cellulose. Multi-cylinder calenders are most commonly four or six cylinders. Newsprint is used for smooth wood free papers and specialty papers (Gullichsen and Paulapuro, 1999).

In a hard nip calender process, the nip pressure between the rollers affects the sheet. The control parameters are the linear pressure between the rollers and the roller surface temperature. In addition, the number of nips can be used as control parameters.

SOFT NIP CALENDER

At least one of the rollers in a soft nip calender is a coated soft roller. Most common, one of the two cylinders is the soft roller and the other is the heated hard roller, similar to the heated rollers in the hard nip calender. For matte paper variants, the rollers have two variants, both soft.

An important difference from hard nip calendering in a soft calendering process is that the nip support roller has a soft surface. This difference changes the nature of the whole process. In soft calendering process, process variables;

- Linear pressure
- Working speed
- Hot cylinder surface temperature
- Soft roller coating material
- Steaming
- Soft roller position (against top or bottom edge of draft)

The main difference in the nip behavior of soft calendering is that the sheet and coated cylinder are both compressed, resulting in significantly lower actual pressure compared to the nip pressure in the hard nip calender. The nip is longer, followed by deformation of the calendered sheet after more heat transfer.

Soft calendering provides many gains compared to hard nip calendering. Due to the smoother density, the absorption characteristics of the sheet and the printing results are more uniform. Since the local high spots are not compressed too hard, less bright spots appear on the printed image. The low maximum pressure allows the draft to be calendered for better smoothness without the danger of tarnishing. Compared to the hard nip calender (Figure 3), the resistance properties of the draft can also be maintained better (Gullichsen and Paulapuro, 1999).

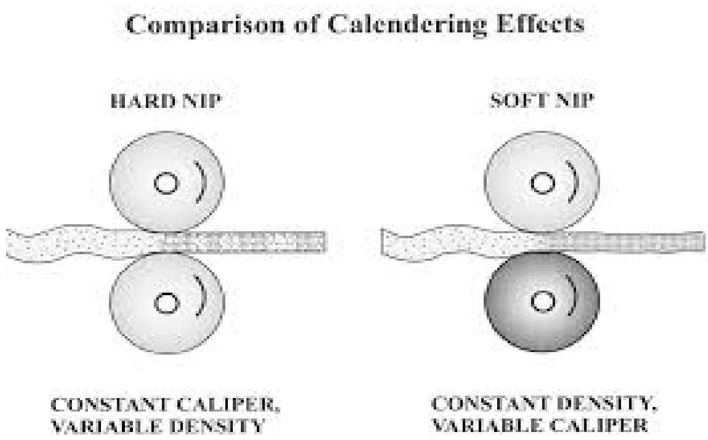

Source: *Gullichsen and Paulapuro, 1999*
Figure 3: *Hard and soft nip calendering*

As with all calender types, new improvements are made in hard nip and soft nip calenders in order to improve them in addition to their basic features. As an example, we can give the hard nip and soft nip calenders in Figures 4 and 5.

The hard nip type calender in Figure 4 has the feature of increasing the total paper production line efficiency.

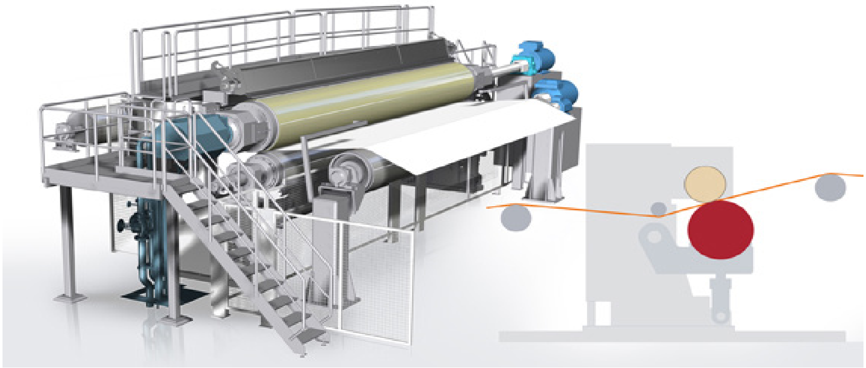

Source: *URL3*

Figure 4: *Hard Nip Calender example*

The soft nip type calender in Figure 5 has a high product quality feature.

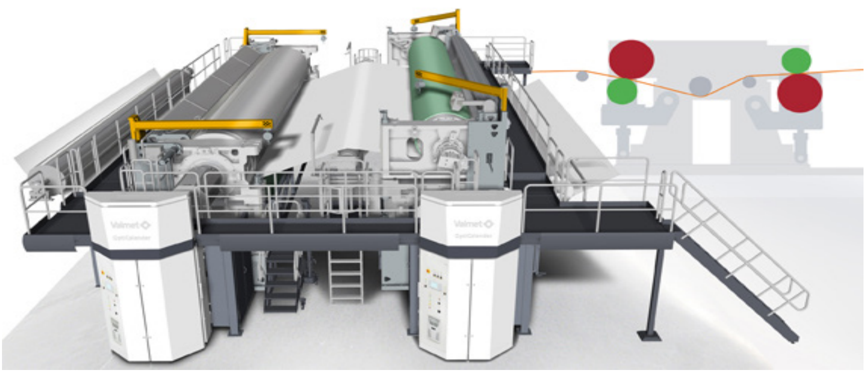

Source: *URL3*

Figure 5: *Soft Nip Kalender*

New type hard nip and soft nip calenders are well suited for the final calendering of different types of cardboard, newsprint and thin paper. Another application area is the pre-calendering of coated paper and cardboard. The hard calender can be applied to both new lines and at all levels of the required precision of profile control, without limitation in width or speed.

What both types of calenders gain;

- Provides high level product quality
- Easy to maintain
- Provides reliable work
- It is a safe investment

Other types of calenders, which are developed according to their properties and the properties they give to the paper, besides the well-known soft nip and hard nip calenders; Opti Calender

Compact (Figure 6).

Source: *URL3*

Figure 6: *Opti Calender Compact - hard and soft nip calendering*

OptiCalender Compact is designed for maximum availability with minimum operating costs. It provides quality calendering, but its structure is largely designed compared to average calenders. Simple, integrated structure makes it extremely easy to commission, daily field operations and maintenance. Naturally, this reduces the initial investment and operating costs required. Figure 7 shows the development from the conventional calender to the optiCalender Compact.

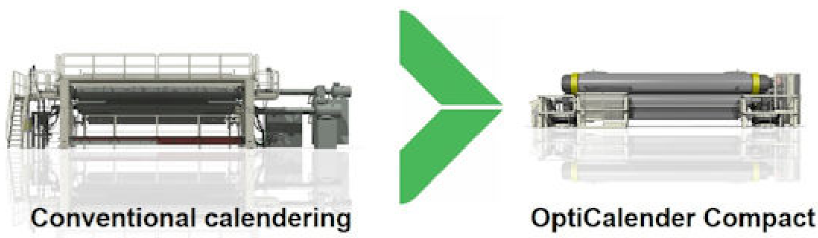

Source: *URL3*

Figure 7: *Comparison of Conventional and OptiCalenders*

Another type of calender metal belt calender (Fig. 8), which is suitable for saving, has a long-finger calendering technique that provides cardboard manufacturers with a great increase in quality and efficiency. The possibilities to increase profit with very high surface quality and to decrease the raw material cost with increasing mass are evident.

Source: *URL3*

Figure 8: *Metal Belt Calender*

Surface quality of the cardboard using Metal Belt Calender

- Excellent macro scale smoothness
- Even topography after coating
- Better optical properties
- It acquires excellent macro-scale topography with the same or better hardness.

MULTI-NIP CALENDER

Until mid-1990, almost all calenders were predefined basic calendering types, hard nip calenders, soft nip calenders and super calenders. Each of these has its advantages and disadvantages. There are rapid developments that affect the paper properties positively in soft calendering. It is clear that the surface properties will not deteriorate due to the technology limit. The multi-nip super calender still creates power for the most demanding calenders (Gullichsen and Paulapuro, 1999).

An opti-nip super calender is shown in Figure 9.

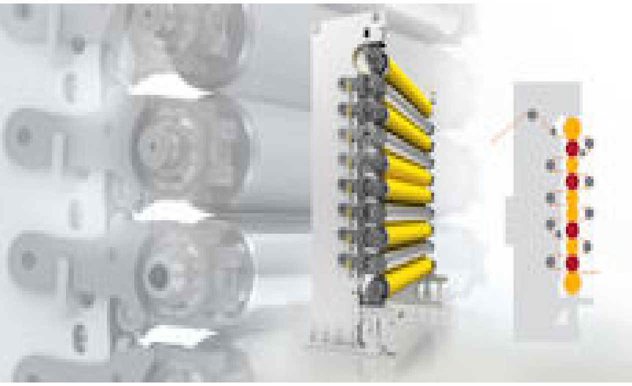

Source: *URL3*

Figure 9: *Example of Opti-nip calender*

New multinip calender is used in both offline and online applications. The OptiCalender Multinip loading principle makes it possible to load all the nipples with the same linear load, so that the first nips can be efficiently plasticized in the paper. Profiling performance is affected by the number of control zones in the upper and lower rollers with deflection compensation. This type of calender;

- Provides high level product quality
- Easy to maintain
- Provides reliable work
- It is a safe investment

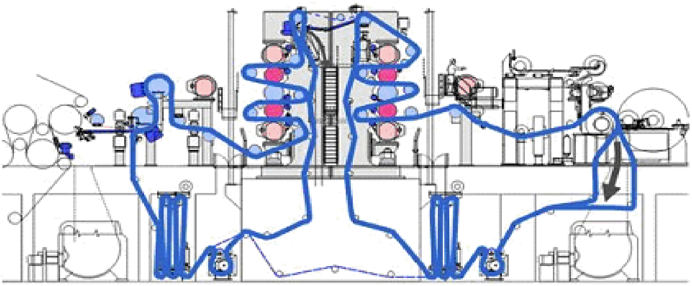

Source: *URL3*

Figure 10: *Multi-nip calender on the machine*

CALENDERING AND FINISHING OF PIGMENT COATED PAPERS

The term calendering is a process that smoothness or polishes the surface of paper and cardboard. Two processes are mentioned in calendering. These are Calender (hard calender and soft calender) and super calender. In addition, there are various types of modifications, but they are all in the final processes (Casey, 1980).

Calendering consists of three mechanical processes: pressure, temperature and plastic flow. Most paper and board types are calendered to create a surface suitable for printing. The term calendering results from a number of different processes where one or more rollers press the sheet with nip pressure to improve surface properties. Calendering reduces Print mottling (Lepoutre et. al., 1979; Preston and Gate, 2005). Calendering can be done online on the paper machine or later offline (Ek et al., 2009). Table 1 contains the features of a calendering process.

Table 1: *Properties of the Calendering Process*

Paper Specifications	Increasing number of nip	Increased load on the calender	Increase of roll diameter	Increased speed of calender	Increase of the temperature of the rolls	Increase of sheet moisture
Thickness	Decreases	Decreases	Increases	Increases	Decreases	Decreases
Smoothness (Regularity)	Increases	Increases	Decreases	Decreases	Increases	Increases
Polishing (Brightness)	Increases	Increases	Decreases	Decreases	Increases	Increases
Stretching MD	Decreases	Decreases	Decreases	No change	Increases	No change
Stretching CD	Decreases	Decreases	Decreases	No change	Increases	No change
Tearing (Rupture) MD	Decreases	Decreases	Decreases	No change	Increases	No change
Tearing (Rupture) MD	Decreases	Decreases	Decreases	No change	Increases	No change
Stretch (Extension) MD	Decreases	Decreases	Decreases	No change	Increases	No change
Stretch (Extension) MD	Increases	Increases	Increases	No change	Increases	No change
Bursting	Decreases	Decreases	Decreases	No change	Increases	No change

Source: *Dean, 1997*

As can be seen in Table 1, increasing the nip number, load on calender, sheet moisture and cylinder temperature during calendering increases the surface smoothness. This increases the printability.

PRINCIPLES OF CALENDERING

Calenders are formed by the combination of many pressurized cylinders to ensure that the surfaces of materials such as paper or plastic film are smooth and shiny. Important variables of the calender; Original paper properties and paper surface and contact areas of the calender rollers.

Effect of calendering on paper properties; As seen in Figure 11, the paper is compressed, Cylinder surface pattern reproduction, Particle distribution and Coating flow.

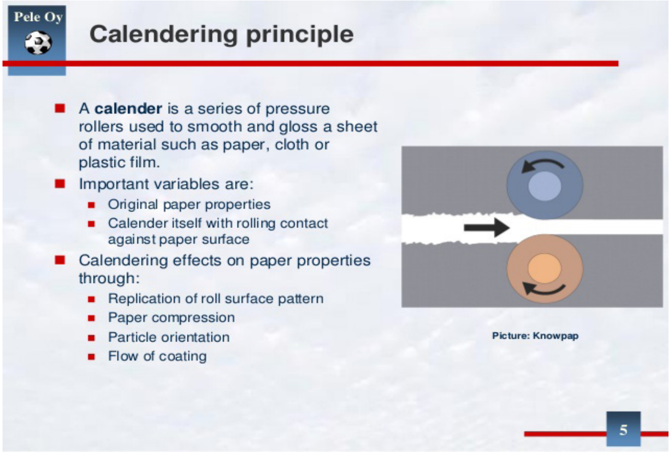

Source: *URL1*

Figure 11: *Principle of calendaring*

When we evaluate calendering in terms of quality, we can see that it is easier to make a paper with glossy surface and it is more difficult to make paper with a dull but smooth surface. As seen in Table 2.

Table 2: *Calendering combinations*

Combinations	Surface smoothness	Brightness
Uncalendered, matt	Low	Low
Polished with brushes	Low	High
Special, silk finish	High	Low
Glossy finish	High	High

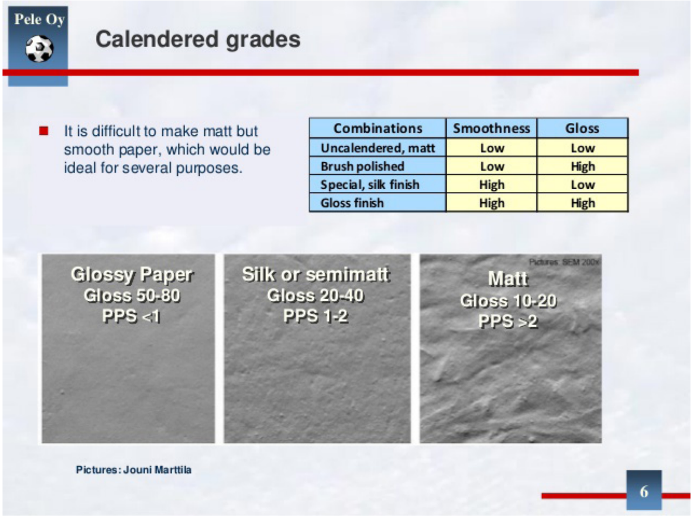

Source: *URL2*

Figure 12: *The effect of calendering*

Coated-paper Surface and Calendering

Coated paper during calendering ıt is compressed between two rolls and this reduces the roughness of the surface. One or both of the rolls can be heated, and a higher temperature or a higher line load increases the compression (Browne et. al., 1995; Rättö, 2002; Larsson et. al., 2007).

When we evaluate the calendering results according to the brightness relationship of the surface smoothness, as seen in Figure 13, the PPS value decreases as the Hunter gloss value increases. In their studies, Beland et al. showed that surface topography is important. Print density and print gloss is much affected by the surface topography of coated paper (Beland and Mattson, 1997) Matt surface is the roughest surface. The calender used here is also soft calender and has 1 nip pressure. The brightest surface was obtained with multiple calenders.

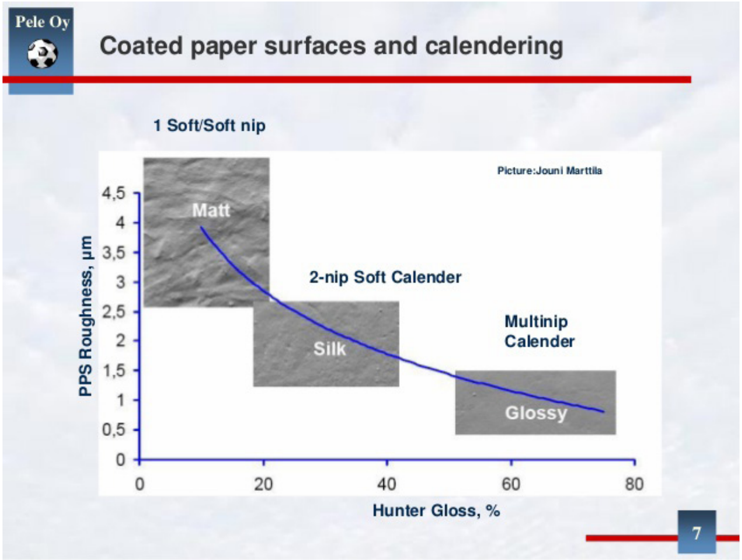

Source: *URL2*

Figure 13: Brightness surface flatness relation in calendaring

The Importance of Roller Surface Smoothness

- Basic polishing and surface smoothness effect is repeated on the opposite side of the hot iron rollers

- The surface smoothness of the flexible rollers also has an effect on the surface of the opposite side of coated paper quality. In this example, when the rough roller is in the lower position compared to the top position, the brightness is 8% lower (No 2 and No 7 roller).

If the new rollers are rough, they should be placed in the top position (Figure 14).

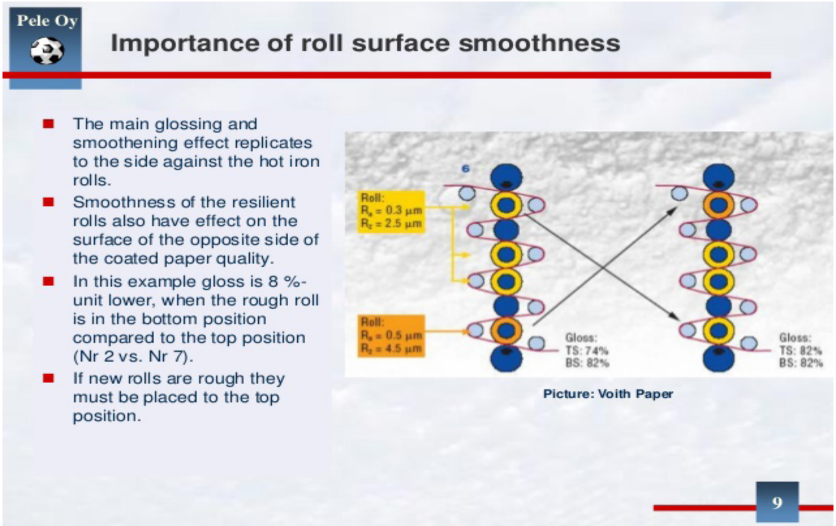

Source: *Zimmermann, 2003*

Figure 14: *Effect of soft roll surface roughness on calendering results*

The Importance of Fiber Wall Thickness

It is important to have several layers of fiber to achieve good formation, surface smoothness, opacity and gloss in a thin paper. It is also important to have thin fiber walls to reduce roughness in offset printing (Figure 14).

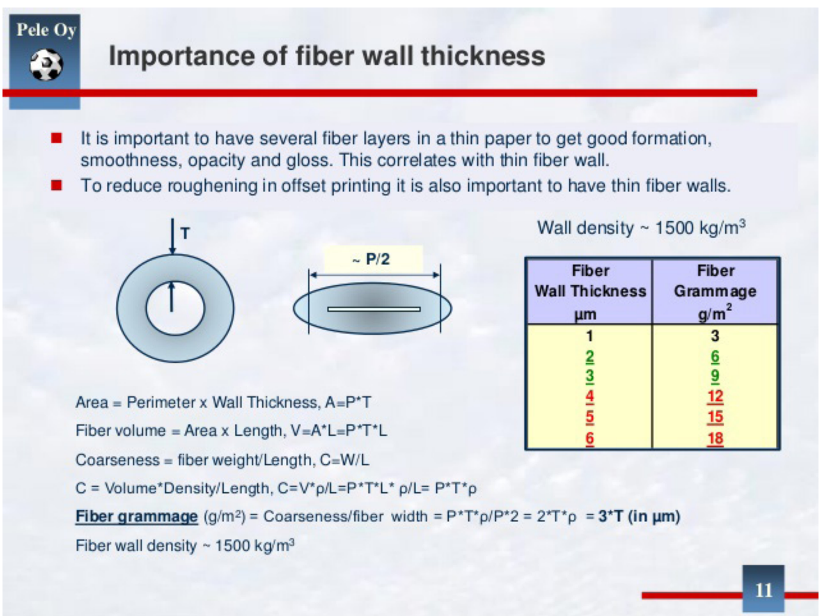

Source: *URL2*

Figure 14: *Fiber wall thickness effect*

EFFECT OF CALENDERING ON PAPER FEATURES

Positive Effects

Surface flatness ↑ (rotogravure)

Gloss ↑ (coated papers)

Absorption and porosity ↓ (SC paper, separable paper, cardboard)

Mohair tendency ↓ (offset)

Thickness control (special papers)

Checking hypocrisy (printing papers)

Negative Effects

Roughness and stiffness ↓

Resistance properties ↓

Light distribution ↓

Opacity and brightness ↓

Blackening, mottling ↑

Wrinkles and calender cuts ↑

Workability ↓

Costs ↑

Special Effects

Expansion of the sheet <0.5%

Drying of paper 1-10% unit

SUPER CALENDER OF COATED PAPER

Most coated papers are super-calendered. Super calendering of coated paper is similar to super calendering of uncoated paper. However, for coated paper, softer cotton filled rolls are used instead of cotton or paper filled rolls used in uncoated paper. A medium level of glazing is given to the paper machine calenders on the papers coated on the machine. However, in order to obtain high gloss, these must also be passed through super calender. The papers coated on the machine are generally 10-12 rolls with high linear pressure and normal coated papers are super-calendered with low linear pressure.

The main purpose of calendering is to increase the brightness and smoothness of the coating. To achieve this, the web must be sufficiently plastic to smooth out without crushing the inside of the paper under the pressure of the calender rolls. If the coated is not sufficiently plastic, it does not give a smooth surface and as a result, the gloss is low.

If the coated is excessive plastic, blackening (lead formation) occurs on the paper. Blackening is an event that results in excessive loss of whiteness and whitening of the reflecting pigment faces.

The results obtained in calendering depend on the type of pigment, the type of glue, the glue-to-pigment ratio, the moisture content of the coating and the availability of the components used in the surface coating. The most important single feature in calendering is the moisture content of the coating. The higher the moisture content, the better the smoothness, but the moisture content of kaolin coated papers should not exceed 4-5% during calendering to avoid the risk of tarnishing.

Some pigments create a much higher gloss than other pigments due to their structure. Some types of kaolin have high gloss. Some types of kaolin are a highly absorbent pigment. Calcium carbonate is generally classified as a matte images pigment, but some types of calcium carbonate can be prepared which will give a fairly high gloss. The porous structure of the pigments also plays a role in this (Gane and Ridgway, 2009). Since the plate-shaped particles settle in a flat state, kaolin gives a characteristic brightness. Since the crystal planes slip more under the load in calendering, kaolin with water in its structure gives a higher gloss than kaolin with less structural water. Calcined kaolin, which has no hydration property and possibly without crystal and cleaved planes, gives coating of relatively low gloss. Some pigments darken more easily than others by calendering. Most of the kaolins tarnish when the moisture content of the coating is above 4% or when very high pressure is used. Kaolin with water in their structure are particularly bad in this regard. Some studies have suggested that kaolin be used in conjunction with calcium carbonate, which has a lower tendency to darken. In the calcium carbonates of the matt image type, the moisture content can be as high as 7-8% during calendering, without the risk of tarnishing.

The particle size of the pigment is the most important factor affecting calendering properties. Generally, the smaller the particle size, the higher the gloss after calendering. In calendering, the whiteness loss of fine kaolin is higher than that of the large kaolin. However, as the first whiteness of fine kaolin is higher than the first whiteness of coarse kaolin, higher whiteness coatings are obtained with thin kaolin as a net result. When measured with the Dennison Wax pick-up test, it has been reported that the strength of coatings made with fine particle size kaolin increases with calendering, the strength of coatings made with large particle size kaolin decreases, and when measured with a resistance pressure test, the opposite is observed.

Another factor affecting the calendering process is the amount of binder in the coating The higher the ratio of the binder to the pigment, the lower the tier of the coating after calendering. The type of binder is also important; Because, as a rule, starch coated papers do not give a high gloss by calendering. Part of this is generally the use of higher binders in starch coated papers.

Generally, calendering reduces the strength of the coating a little. However, if calendering is done properly, the strength should not fall more than a candle number in the Dennison series. A serious decrease in strength as a result of calendering indicates that there is no plasticity in the coating. In such a case, it may be helpful to add plasticizing agents to the coated mixture or to increase the moisture content.

Papers coated on high speed roller machines cause problems in calendering in terms of removing veins and surface shapes in the coating. There are no surface shapes on the papers coated with the tracer knife machine; and they are more easily calendered as a smaller loss in whiteness with opacity. These machines provide a very smooth but low gloss finish that requires minimal calendering or requires no calendering.

Some coatings tend to be pollinated when calendered, that is, very fine coated particles accumulate in the calender rolls. Since coarse pigments tend to break under the pressure of the calender rolls, coatings containing coarse pigments often lead to more dust than fine pigments. Insufficient use of adhesive in coated recipe also causes dusting. Dusting occurs almost always in low strength coated papers. However, as indicated by the wax pick-up test, dusting sometimes occurs on high strength glossy papers. In this case, the reason for dusting may be due to the excessive penetration of the adhesive downward from the top layer of the coating, leaving a surface layer with low glue and hence a tendency to dust, or absence of plasticity in the coating. If the paper is too wet during super calender, fine dust may accumulate on the rolls and lead to vials or grinding. The dusting may be due to the improper preparation of the glossy mixture and the pigment pellets not being bonded securely with the adhesive. Normally, starchy coated papers are dustier than other binders. However, this does not mean that coated papers containing non-starch binders do not cause any dusting difficulties. Papers containing a high proportion of thermoplastic resin adhesive (resin emulsion), when calendered, are coated in a smooth and high gloss finish. Dusting starchy coated papers can sometimes be avoided by adding suitable plasticizing agents, such as fatty acid soaps, wax emulsions, synthetic resin emulsions, and dispersions of insoluble metallic soaps in water. Pollination is one of the problems that occur or disappear from time to time without a specific reason (Casey, 1960).

SPECIAL CALENDERING PROCESSES APPLIED ON COATED PAPER

Paper is always the most important material for printing and printed promotion. Another type is cardboard. In addition, metal and plastic films, textile products and semiconductor materials are also important as substrates.

The performance of the paper in the print depends on its runnability, printability and promotional capacity. Another important feature is the availability of the product and customer satisfaction.

The term printing papers is like a kind of paper. Basic criteria used in printing papers; fiber distribution of base paper, coated, surface finishing and end use. Among these criteria, surface finishing includes calendering (Gullichsen, and Paulapuro, 1998).

There is a strong relationship between the surface texture of coated paper and the effect of calendering properties on print quality (Wanske et al., 2007; Kapoor et. al., 1995).

When the calendering processes described above are performed after the coated process, which is important in increasing the printing feature, the quality of the printing paper increases more. Print gloss is important in printing paper. Print gloss is more influenced by macro-roughness than micro-roughness (Ström (2005). For this, there are various types of special glossing machines used to achieve special effects on coated papers. One of the most important is the friction calender and a paper or cotton-filled roller and one or two steam-heated and water-cooled high gloss cold cast iron valves. Coated surface of paper is passed through the rollers with the iron facing. It rotates at 1.5 times the circumferential speed of the iron roller filled roller and has a polishing effect on this coated. An extremely high gloss can be achieved with the friction calender. However, due to its high cost, this process is limited to box coating papers and a few special types of coated paper used for other decorative purposes. (Casey, 1960).

The different mixtures used during the coating give the paper different properties. Calendering a coated paper, even partially, allows the holes on the paper surface to be reduced further (Chinga et al., 2002; Xiang and Bousfield, 2000).

Porosity and topology of pores, chemistry of surface together with surface tension and viscosity of liquids are playing an important role in paper saturation and calendering (Tollenaar and Ernst, 1985).

As a result, most paper and board types are calendered to produce a surface suitable for printing. The calendering of the printing papers improves their printability by improving their surface properties. The term calendering results from a number of different processes where one or more rollers press the sheet with nip pressure to improve surface properties. The effect of calendering and printability on gloss properties related to this subject has been studied by many researchers. Also researchers have shown that rough paper has high ink demand than smooth paper (Chakrabarti, 2005; Toivakka, 2001; Xiang and Bousfield, 2000; Yamazaki et.al., 1993).

Several techniques are used in the calendering of coated paper and board, and with the growing demands for better quality and high production resulted in the development of new techniques (Wanske et.al., 2006a; Wanske et. al., 2006b)

REFERENCES

Beland, M. C. and Mattsson, L. (1997). Optical print quality of coated papers, *Journal of Pulp and Paper Science*, 23(10): 493-498.

Browne, T. C., Crotogino, R. H., Douglas, W. J. M. (1995). Effect of paper structure on behaviour in a calender nip, *Journal of Pulp and Paper Science*, 21(10): 343-347.

Casey, J. P. (1980). *Pulp and paper chemistry and chemical technology*, Third Edition, vol. IV, John Wiley and Sons, Inc, New York, 2317-2318.

Casey, J. P. (1960). *Paper testing and converting to the final product*, In Pulp and Paper Chemistry and Chemical Technology, vol. III, John Wiley and Sons, Inc, New York, 1493.

Chakrabarti, S. K. (2005). *Understanding the surface characteristics and surface chemistry for printing properties of paper in emerging applications of surface science*, In proceedings of seminar conducted at Chemical Engineering Department, IIT Delhi, 209-215.

Chinga, G., Helle, T. and Forseth, T. (2002). Quantification of structure details of LWC paper coating layers, *Nordic Pulp and Paper Research Journal*, 17(3): 313-318.

Dean, T. W. R. (1997). *The essential guide to aqueous coating of paper and board*, The Pita Coating Working Group, Paper Industry Technical Assocation, ISBN 0-9530227-0-6, Leatherhead, United Kingdom, 303-310.

Ek, M., Gellerstedt, G. and Henriksson, G. (2009*). Pulp and paper chemistry and technology*, in Paper chemistry and technology, vol. 3, ISBN 978-3-11-021343-0, Printing and binding: Hubert & Co. GmbH & Co. KG, Göttingen, Germany, 319-340.

Gane, P. A. C. and Ridgway, C. J. (2009). *Interactions between flexographic ink and porous coating structures*. In TAPPI 2nd Annual PaperCon'09 Conference - Solutions for a Changing World, St. Louis, MO, United States: TAPPI Press.

Gullichsen, J. and Paulapuro, H. (1999). *Papermaking science and technology*, Papermaking Part 3, Finishing, Book 10, Chapter 1, Eds. Juha Ehrola, Ari Hernesniemi, Harri Kuosa, Markku Kyytsönen, Pekka Linnonmaa, Tapio Maenpaa, reijo Pietikainen, Rob Stapels, Mikko Tani and Hannu Vuorikari, ISBN 952-5216-00-4 (the series), ISBN 952-5216-10-1 (book 10), Published by Fapet Oy, Helsinki, Finland, 14-140.

Gullichsen, J. and Paulapuro, H. (1998). *Papermaking science and technology*, Printing, Book 13, Chapter 1, Eds. Prikko Oittinen and Hannu Saarelma, ISBN 952-5216-00-4 (the series), ISBN 952-5216-13-6 (book 13), Published by Fapet Oy, Helsinki, Finland, 12-25.

Kapoor, S. K, Sood, Y. V., Pande, P. C. and Mohta, D. C. (1995). Effect of paper properties on printability in view of latest developments in printing technology, *IPPTA*, 7(2), 48-55.

Larsson, M., Engström, G., Vidal, D. and Zou, X. (2007). Impact of calendering on coating structures, *Nordic Pulp and Paper Research Journal*, 22 (2):267-274.

Lehtinen, E. and Yhdistys, S. P. (2000). *Pigment coating and surface sizing of paper*, In Papermaking Science and Technology, Ed. Esa Lehtinen, ISBN 952-5216-11-X Fapet Oy, Helsinki, 810.

Lepoutre, P. Degrace, J. H. and Mangin, P. J. (1979). Printability of coated papers, *Tappi J.*, 62(5), 33-36.

Preston, J. S. and Gate, L. F. (2005). The influence of colour and surface topography on the measurement of effective refractive index of offset printed coated papers, *Colloids Surf.,* 252 (2-3): 9-104.

Rättö, P. (2002). Description and analysis of paper deformation in a calender nip - Effects of high roll temperatures and thickness variations, *Nordic Pulp and Paper Research Journal,* 17(2): 130-138.

Ström, G. (2005). *Interaction between offset ink and coated paper - A review of the present understanding*, Proc. Advances in Paper Science and Technology, 13th Fundamental Research Symposium, Cambridge, UK, 1101-1112.

Toivakka, M. (2001). A simulation model to predict coating coverage, *Paperi Ja Puu- Paper and Timber*, 83(1): 34-41.

Tollenaar, D. and Ernst, P. A. H. (1985). *Optical density and ink layer thickness*, IGT report, Stichting Instituat voor Grafische Techniek TNO, Amesterdam.

Wanske, M., Klein, R., and Großmann, H. (2007). *Measuring and evaluating the surface quality of gravure papers*, PITA Coating Conference, Cambridge, UK, March, 27-28.

Wanske, M., Klein, R., and Großmann, H. (2006a). *Assessing the surface structure of printing papers under pressure*, TAGA 58th Annual Technical Conference, Vancouver, British Columbia, Canada, 303-312.

Wanske, M., Klein, R., and Großmann, H. (2006b). *Measuring and evaluating the surface quality of gravure papers*, IARIGAI 33rd International Research Conference, Leipzig, Germany, 78-85.

Wikstrom, M., Nylund, T. and Rigdahl, M. (1997). Calendering of coated paper and board in an extended soft nip, *Nordic Pulp and Paper Research Journal*, 12(4): 289-298.

Xiang, Y. and Bousfield, D. W. (2000). Influence of coating structure on ink tack dynamics, *Journal of Pulp and Paper Science*, 6(6): 221-227.

URL1:http://www.knowpap.com/www_demo/english/paper_technology/general/6_finishing/frame.htm (Accessed date – 07.05.2020)

URL2: https://www.slideshare.net/Peeke/calendering-slideshare-3-march (Accessed date 07.05.2020)

URL3:https://www.valmet.com/board-and-paper/board-and-paper-machines/calendering/ (Accessed date – 07.05.2020)

Yamazaki, K., Toshiyasu, N., Yashihiko, H. and Kazuyo, F. (1993). Print mottle effect of binder migration and latex film formation during coating consolidation, *Tappi Journal*, 76(5): 79-84.

Zimmermann, L., (2003). Roll cover and coating effects on calendering quality, *Paper Technology Journal Twogether*, Ed. Dr. Wolfgang Möhle, Special Issue: Systems for Finishing, Published by Voith Paper Holding GmbH & Co. KG, Corporate Marketing, 37-40.

Chapter 4

FOOD-BASED NANOGEL PRODUCTION

Nil ACARALI[1]

1 Yildiz Technical University, Davutpasa Campus, Department of Chemical Engineering, Esenler/Istanbul

1. GEL PRODUCTION

Since animal tissues are treated with acid or alkaline solutions in gelatin production, H bonds and cross-links in collagen structure are partially degraded and molecules can be broken down. In other words, as long amino acid chains become shorter by breaking down, the bonds between them are weakened and water molecules can easily enter the fibrils (Figure 1). Thus, a new structure is formed that can be dissolved even in warm water, and this resulting soluble structure is called gelatin. Enzymes can also sometimes be used with or as an alternative to these chemicals. However, only some special enzymes are used here; because many enzymes that can hydrolyze the protein cannot break down the collagen. Only highly specific collagenase enzymes can break down natural collagen. In this way, the process of treating collagen using chemical or biochemical denaturation (hydrolysis) methods is called "conditioning" in the gelatin industry. Products obtained by this method are also called gelatin hydrolysates, and such products are also used in many areas of the food industry [1].

Figure 1. Schematic view of collagen and gel [1]

Gelatin is obtained by hydrolyzing collagen. There are many types of gelatin. These varieties depend on the composition collagen source and the hydrolytic method used. The main raw material used in gelatin production is bovine bone and skin. Alternative sources such as chicken and fish are available. A number of physical and chemical treatments are applied to get rid of the unwanted substances contained in the raw material. In this way, the oils in the skin and / or minerals in the bones are removed and pure collagen is obtained. The raw material passing through these stages is then hydrolyzed to form hot water-soluble gelatin. Comparison of gelatin with other thickeners in terms of their properties was given in Table 1 [2].

Table 1. Comparison of gelatin with other thickeners in terms of their properties [2]

Gelatin	Other thickeners
It is multifunctional. It can be used as a gelling agent, thickener, emulsifier, antifoam, and a film-forming agent.	Other thickeners cannot perform the functions performed by gelatin alone, it is necessary to use thickeners for each function separately.
Gelatin is not considered as a food additive in many countries including our country, so its use is free and safe.	Other thickeners usually have an E number and are considered a food additive.
Gelatin forms a thermally reversible gel and its most important feature is that it melts at body temperature. Therefore, it is preferred in the food industry.	Other thickeners have higher melting temperatures and even if they form a reversible gel, there is a big difference between melting and gelling temperatures.
Gelatin can be produced in different gel strength and shapes depending on the degree of hydrolysis of collagen.	In order to obtain different gel strength with other thickeners, ingredients such as sugar and salt are used.
Gelatin can be digested completely and easily.	Other thickeners can reduce the absorption of some minerals.
Gelatin can function at normal pH values of foods.	It may be necessary to add salt, sugar and food acids to gell other builders.

2. NANOGEL USAGE AREAS

Based on prior years of increasing production and use of gelatin, Turkey is considered as a natural food in many countries, including, therefore, consumption is not limited. Nanogels have some properties as high stability, biologic consistence, good permeation capability etc. and can be tender to environmental stimuli [3]. Examples of the usage areas of gels were given in Figure 2.

Figure 2. Examples of the usage areas of gels [4]

3. STUDIES IN LITERATURE FOR FOOD-BASED NANOGEL PRODUCTION

It can also be obtained from gelatin fiber plants obtained from the skins, connective tissues and bones of animals. Although there are many literature studies for the production of gelatin of animal origin, there is a small number of gelatin production of vegetable origin. In addition, there are not many studies on the production of nanogels in the food field.

The investigators evaluated the physicochemical structure, current use and future of gelatin in the study. Gelatin is a structurally irreversible pure protein obtained by hydrolysis of collagen extracted from tissues and bones of animals. Skin and bones, which are cleaned from non-collagen materials before production, are heat treated in aqueous medium after acid or alkali treatment, and are purified by extracting from the environment in which they are located. Approximately 60% of the proteins in the animal body are collagen, and the composition of the gelatin produced does not undergo any major changes. In the production process, although the polypeptide length is shortened, amino acid strings are largely preserved. Due to its technological features, gelatin has found wide use in food, cosmetics, photography, medicine and pharmacy. Recently, studies have been made on the production of some antimicrobial, antioxidant and antihypertensive bioactive peptides from collagen or gelatin by enzymatic hydrolysis. Being a natural protein and having technologically important properties, it is considered as an indication that the production and consumption of gelatin will continue to increase in the coming years. However, for consumers with special preferences and sensitivities, it is very important to make gelatin production under controlled conditions and to follow the source meticulously [1].

Researchers examined the properties of various gelatin films consisting of solutions containing different gelatin concentrations. Fourier Transform Infrared Spectroscopy was used to evaluate the composition of various gelatin sources and thus calculate the differences between these compositions. Highly concentrated gelatin films have especially improved mechanical properties such as tensile and puncture strength. Gelatin films obtained by fish skin have the lowest water vapor permeability for each concentration used. All gelatin films have a good barrier against oxygen and oil. Films made of pork skin are the lowest water-soluble species compared to other species. Fourier Transform Infrared Spectroscopy spectra show that plasticizers and gelatins mix and interact well. The use of high concentration gelatins affects the increase in the number of waves of Amid-A, as there is a better interaction between the gelatin functional groups [5].

The other researchers studied the differentiation of bovine and pork gelatin in products processed with Sodium Sulfate Dodecyl-Polyacrylamide Gel Electrophoresis and principal component analysis techniques. Gelatin is widely used in food and pharmaceutical products. In the study, it was aimed to detect and distinguish the source of additional gelatin in processed foods by Sodium sulfate dodecyl polyacrylamide gel electrophoresis combination method and principal component analysis. The yield of gelatin separated from foods by different methods was evaluated. Separated from foods treated with cold acetone and deionized water, gelatin has the same polypeptide pattern. The study showed that removing gelatin from foods with different analysis methods provided strong information about the type of gelatin [6].

A study aimed to compare the physicochemical properties of gelatin obtained by extraction method from chicken skin with beef gelatin. It was found to be more flexible and viscous at different concentrations and frequencies. When the thermal properties are examined, chicken gelatin has a higher melting temperature than beef gelatin according to the results obtained from differential scanning calorimetry. According to the results obtained, chicken gelatin has a more stable structure because the glycine, proline and alanine amino acids in its structure are dominant [7].

In literature, the researchers studied the structure of fish gelatin, their gel specifications and their interaction with egg white proteins. Gelatin was obtained from the northern sea horse mackerel skin by filtration and deionization methods using sodium hydrogen carbonate, sodium hydroxide, sulfuric acid, citric acid and distilled water. Compared to commercial gelatins, ash showed close properties in terms of moisture, color and average molecular weight. The amino acid profile in gelatin extracted from horse mackerel was found to be more similar to sea bream compared to cod fish. Their combinations with egg white proteins have been investigated in terms of their rheological and thermodynamic properties. The gelling properties and compatibility with egg proteins make horse mackerel a potential that can be used in desserts and bakeries [8].

A study was examined on the characteristic and functional specifications of gels obtained from zebra skin. Gelatin was first obtained from the zebra skin sample. Polypeptide models, gel strength, viscosity, tissue parameters and functional properties of gelatin obtained from zebra skin were examined. Amino acid analysis showed that zebra skin gelatin contains almost all of the essential amino acids, the most dominant being glycine. Fourier transform infrared spectroscopy spectra have shown helical arrangements in the structure. These resolutions and functional specifications depend on concentration. Zebra skin gelatin has been shown to have strong refining ability, especially for apple juice, without affecting nutritional values [9].

Some researchers studied the characterization of gelatin obtained by extraction from Atlantic salmon skin in their study. Atlantic salmon and Atlantic cod were extracted from the skin according to the gelatin acid washing process. After filtering and ion exchange processes, extracts are colorless and odorless. Average yields of gelatin from salmon and cod skins in three separate experiments were 39.7% (± 2.2%) and 44.8% (±0.2%) on a dry matter basis, respectively. Gelatin from salmon has been shown to contain slightly more hydroxyproline and proline (15.4% versus 16.6%) than cod, while its cool content is lower (4.6% versus 4.6%). Salmon gelatin was expressed with higher gelling temperature and higher starting gel strength than cod gelatin. During storage at 10°C, gel resistance increased and gelatin produced from cod was more than gelatin produced from salmon. Therefore, gelatin and salmon gelatins made from cod were extracted at 56°C and had the same durability after 7 days of storage. The gels extracted at higher temperature had poorer strength [10].

In an investigation, shark gelatin and pork gelatin were compared in terms of their physical properties. The physical specifications of shark gelatin were investigated by comparing them with pork gelatin after gel formation and gelling. The transition temperature of sol-gel and gel-left is quite low compared to pork gelatin for shark. As a result, shark gelatin has different specifications compared to other gelatin types, not only characteristic but also solution properties have been different [11].

The researchers investigated gelatin alternatives, new developments, challenges and possibilities. Gelatin is considered a special and unique hydrocolloid. They have described the specific features of gelatin, the reasons for improving gelatin alternatives, developments to date in developing gelatin alternatives, possible approaches for developing gelatin alternatives, and future guidelines [12].

The investigators obtained the gelatinization and retrogradation of natural corn starch and the effect of stearic acid on retrogradation. The gelatinization properties of starch were studied by examining swelling and solubility behaviors and by using the 'Differential Scanning Calorimetry' method. In addition, the degree of gelatinization was determined using spectrophotometric method as a function of temperature (50-95ºC). Swelling and solubility curves were determined in the range of 50-95ºC and it was determined that it showed a two-step change with temperature. Since the degree of gelatinization of starch changes with a profile similar to temperature, it was interpreted as events controlling swelling and solubility gelatinization. Differential scanning calorimetry was used to investigate gelatinization in samples with different moisture content [13].

In a study, gelatin, its structure, properties, production, use and quality as a food additive were examined. Gelatin is an additive used in foods as a thickening agent. The transparent, colorless, odorless and easily melting gel structure formed by gelatin cannot be provided by other thickeners. Compared with carbohydrate-induced thickeners, gelatin has some advantages and is preferred. However, it can be supplied cheap because of its easy production and no raw material problem. In recent years, the production of gelatin from animal sources other than pork has been the subject of many scientific studies [2].

Another researchers studied the properties of bio nanocomposite films of gelatin obtained from freshwater sea bream skin combined with hydrophilic and hydrophobic nanoclays. X-ray deflection and microscopic analysis showed a flaky structure combined with scanning electron hydrophilic and hydrophobic nanoclays, nano-compound gelatin-based films. As the result obtained from the scanning electron microscope demonstrated, homogeneity and smoothness of the film surface decreased with nanoclays additives [14].

4. ALTERNATIVE MATERIALS TO THE RAW MATERIAL SOURCE OF NANOGELS

Gelatin is used to start the turbid and unwanted flavors in clear fruit juices. Although these substances are separated from the fruit juice by filtration, they can remain in a small amount. It is not obligatory to write the expression that the juice has been rinsed with gelatin on the label. For this reason, it can be only learned the names of fruit juices that use gelatin in the production [15].

Mass production, which has increased with the consumption rate, has made consumers doubt that the gelatine produced from animal origin is halal and this situation has led to the presence of thickeners as an alternative to gelatin. Gelatin is a 100% animal substance and not vegetative. However, there are thickeners that are produced from herbal materials such as gluten, agar, carrageenan, xanthan gum etc., which will show gel function, and they have thickening agents [16].

Agar (E406), a natural polysaccharide, is produced in the USA and Japan by different seaweeds called 'rhodophyceae'. It is used for thickening milk and dairy products, confectionery and ice cream. In addition, it is used in the manufacture of capsules and ointments used in the cosmetics industry, in the pharmaceutical industry, in the production of dental molds and meat preserves.

Gluten is a type of protein that is often found in cereals such as wheat. It is a remaining substance as a result of cleansing gluten grain grains from starches and has a sticking feature. It has a better taste and smell than gelatin. It is more easily digested by the body, but not suitable for the use of celiac patients [2].

In another study conducted in the literature, fish gel was used as a stabilizer in yoghurt production [17].

Pectin is a polysaccharide found in the cell wall of high plants such as cellulose and hemicellulose. The structure of the pectin includes polygalacturonic acid, ramnogalacturonic acid, galactans and arabinogalactans. Pectins give flexibility and mechanical strength to the plant thanks to its interaction with other cell wall elements. Pectins are involved in controlling cell wall specifications in many physiological processes in cell growth or in plant defense against phytopathogens (disease-causing organisms) [18].

The walls of neighboring cells in the plant are connected to each other with pectin, and this layer consisting of pectin is called middle lamella layer. The amount of pectin is most commonly found in the lamella layer and decreases as it progresses from the cell wall to the plasma membrane.

Fast growing and high moisture soft plant tissues contain high amounts of pectin. The pectin image in the 3D plant cell wall structure is shown in Figure 3 [19].

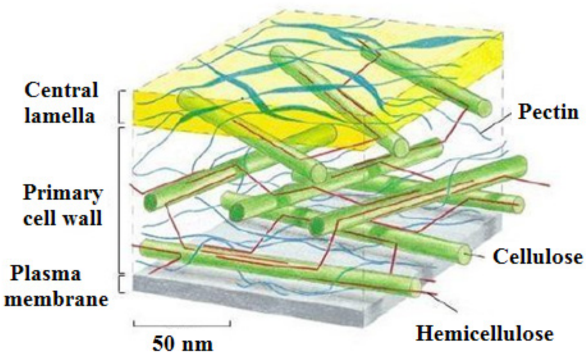

Figure 3. Three dimensional plant cell wall structure [19]

Pectin was formed by the binding of galacturonic acid units partially esterified with methyl alcohol by the α-D-1,4 bonds, and in this linear chain there may be α-L-1,2 linked rhamnose units [18].

The use of pectin in dairy products prevents the agglomeration of proteins, thereby preventing phase separation in the product, for example yogurt, and serum separation at low pH values. In addition, pectin texture added to dairy products improves and prevents syneresis [20].

REFERENCES

[1] Yetim H., (2011), Gelatin Production, Properties and Usage, 1. National Halal and Healthy Food Congress, Ankara.

[2] Boran G., (2011), Gelatin as a food additive: structure, properties, production, use and quality, Yüzüncü Yıl University, Institute of Science, Van.

[3] Naeem, A., Khan K.U., Fahad, M., (2019), Nanogels as drug-delivery systems: a comprehensive overview, Therapeutic Delivery, 10(11), 697-717.

[4] https://www.teknolojitransferi.gov.tr/teknolojitransferplatformu/resources/temp/f2a93303-ae2e-4f35-b007-3f9a28ae4647.pdf. Accessed date: 23.07.2020.

[5] Hanani N. Z.A, Roos Y.H., Kerry P. J., (2012), Use of beef, pork and fish gelatin sources in the manufacture of films and assessment of their composition and mechanical properties, School of Food & Nutritional Sciences, National University of Ireland, Ireland.

[6] Azira N., Amin, Man C., (2012), Differentiation of bovine and porcine gelatins in processed products via Sodium Dodecyl Sulphate-Polyacrylamide Gel Electrophoresis (SDS-PAGE) and principal component analysis (PCA) techniques, International Food Research Journal, Laboratory of Halal Science Research, Halal Products Research Institute, Universiti Putra Malaysia,

[7] Sarbon M. N., Badii F., Howell K. N., (2012), Preparation and characterization of chicken skin gelatin as an alternative to mammalian gelatin, Faculty of Health and Medical Sciences, University of Surrey, Guildford.

[8] Badii F., Howell K. N., (2005), Fish gelatin: Structure, gelling properties and interaction with egg albumen proteins, School of Biomedical and Molecular Sciences, University of Surrey, Guildford.

[9] Ktari N., Jridi M., Nasri R., Lassoued I., Ayed BH, Barkia A., Nasri M., (2014), Characteristics and functional properties of gelatin from zebra blenny (Salaria basilisca) skin, Laboratory of Enzyme Engineering and Microbiology, University of Sfax, Tunisia.

[10] Arnesen A.J., Gildberg A., (2005), Extraction and characterization of gelatine from Atlantic salmon (Salmo salar) skin, Norwegian Institute of Fisheries and Aquaculture Ltd., Norway.

[11] Yoshimura K., Terashima M., Hozan D., Ebato T., Nomura Y., Ishii Y., Shirai K. (2000), Physical Properties of Shark Gelatin Compared with Pig Gelatin, Tokyo University of Agriculture and Technology, Japan.

[12] Karim A.A., Bhat R., (2008), Gelatin alternatives for the food industry: recent developments, challenges and prospects Food Biopolymer Research Group, Food Technology Division, School of Industrial Technology, Universiti Sains Malaysia.

[13] Arık A.E., (2004), Investigation of the effect of stearic acid on retrogradation by gelatinization and retrogradation of natural corn starch, Hacettepe University, Institute of Science, Ankara.

[14] Nagarajan M., Benjakul S., Prodpran T., Songtipya P., (2014), Characteristics of bio-nanocomposite films from tilapia skin gelatin incorporated with hydrophilic and hydrophobic nanoclays, Journal of Food Engineering, Prince of Songkla University, Faculty of Agro -Industry, Thailand.

[15] Batumi, A., (2012), "Halal in Turkey and Halal Food Certification System", Electronic Journal of Food Technology, 1: 51-61.

[16] Çakmakçı, S. and Çelik, M. (1998), Food Additives, Master Thesis, Atatürk University, Erzurum.

[17] Pancar D.E., (2013), The Use of Fish Gelatin as a Stabilizer in Yogurt Production, Yüzüncü Yıl University, Institute of Science and Technology, Van.

[18] Oğuz, M., (2015), Optimization of Pectin Hand with Chemical and Enzymatic Method from Limon Pulp, Master Thesis, Institute of Science, Çukurova University, Adana.

[19] Syeitkhajy, A., (2017), Modified Pectin and Pectin Extraction from Citrus Peels, Master Thesis, Institute of Science, Istanbul University, Istanbul.

[20] Şimşek, S., (2013), Characteristics and Environmental Effects of Pectin and Modified Pectins Obtained from Carrot Mash and Pulp, Master Thesis, Institute of Science, Süleyman Demirel University, Isparta.

Chapter 5

PROCESSING, MICROSTRUCTURE AND PROPERTIES OF SIALON CERAMICS FOR THE USE OF HIGH TEMPERATURE APPLICATIONS

Nurcan CALIS ACIKBAS[1]

Gokhan ACIKBAS[2]

1 Prof. Dr., Nurcan ÇALIŞ AÇIKBAŞ, Bilecik Şeyh Edebali University, Engineering Faculty, Metallurgical and Materials Engineering Department, Bilecik, Turkey, ncalis@gmail.com

2 Assoc. Prof. Dr., Gökhan AÇIKBAŞ, Bilecik Şeyh Edebali University, Vocational School, Mechanical and Metal Technologies Department, Bilecik, Turkey, samgokhanacikbas@gmail.com

INTRODUCTION

Silicon nitride (Si_3N_4) based ceramics have a continuous interest in structural high-tech ceramics since 1955 due to their high temperature mechanical, chemical and thermal properties [1]. The driving force in the development of silicon nitride ceramics was the use of ceramic instead of metal to increase the performance of turbines and piston engines operating at high temperatures. Although the development of the ceramic engine has not fully achieved its goal, today silicon nitride ceramics are used in industrial applications such as engine parts, bearings and inserts that require a range of high temperature resistances. Silicon nitride exhibits much better high temperature properties than most metals due to its high strength at high temperatures and fairly well creep resistance and oxidation resistance. In addition, due to the low thermal expansion coefficient, thermal shock resistance is very good compared to many ceramic materials [2].

It is difficult to produce pure silicon nitride product as a completely dense since the nature of strong covalent bonding between silicon and nitrogen atoms. Therefore it is necessary using sintering aids like Y_2O_3 for the development of dense structures. At the beginning, Si_3N_4 ceramics were produced only by reaction bonding sintering technique and completely dense material could not be produced [3]. In order to benefit from the properties of Si_3N_4, it was necessary to produce completely dense material. High density materials were first produced in 1960s using hot pressing (HP) method with the addition of small amount of sintering aids [4]. However, this technique only allowed the production of simple parts. In the early 1970s, work was focused on the use of Si_3N_4 as a gas turbine. In this scope, pressure-less sintering [5] and gas pressure sintering technique [6] were used for production. These techniques have enabled the production of complex shaped and completely dense materials. When examining the sintering behavior of Si_3N_4, some oxides (Al_2O_3 and BeO) were found to dissolve in Si_3N_4 crystal structure [7,8]. These materials are called “silicon nitride based ceramics”. Since BeO is toxic, its practical use is not available.

SiAlON ceramics are solid solution between Si_3N_4 and Al_2O_3 emerged in the early 1970s. Partial displacement of Si and N atoms with Al and O occur in SiAlON crystal structure. Since SiAlON ceramics are solid solutions and contain less grain boundary phases than Si_3N_4, they have higher creep, corrosion and oxidation resistance [9]. Because of the need for less sintering aids for the production of fully dense SiAlON ceramics, SiAlONs are a good alternative to Si_3N_4 ceramics for high-temperature applications. In addition, the hard phase alpha and tough phase beta are thermodynamically stable at the same time, allowing both hard and tough materials to be obtained. Compared to Si_3N_4, SiAlONs have the advantages of wide composition design and hence obtaining different thermo-mechanical properties [10,11].

The following methods are used to improve the high temperature properties of SiAlON ceramics:

1. Reduction of sintering additive amount

2. Selection of proper sintering aids to ensure refractory grain boundary phase formation

3. Sintering with hot isostatic pressing (HIP), gas pressure sintering (GPS) or spark plasma sintering (SPS)

4. Crystallization of grain boundary phase

5. Vacuum heat treatment

SiAlON ceramics are now used in many niche applications such as space shuttles, cutting tools, piston engine components, turbochargers, bearings, agitators, nozzles etc. requiring high temperature strength, tribological behavior, fracture toughness, oxidation and creep resistance, thermal shock resistance and low density [12,13]. On the other hand, the commercial use of SiAlON ceramics is limited due to the high cost of starting powders, the necessity of sintering under high temperatures and gas pressures and the cost of investment of such sintering systems [14]. Therefore, in order to increase the widen application areas of such materials, studies are needed to reduce production costs without reducing their performance of materials.

The final properties of SiAlON ceramics depend on their structures. Structures can be controlled by processing. Especially microstructure evolution (grain size, aspect ratio of grains, pores, intergranular phase content, chemistry of intergranular phase, impurities etc.) has very pronounced effect on properties. Compositional design is the first parameter that can influence crystal structure, microstructure and hence final properties. The second one is powder processing and the third one is sintering.

In this chapter, processing, microstructure and properties of SiAlON ceramics for the use of high temperature applications and methods to improve the high temperature properties will be discussed.

BACKGROUND

One of the most widely studied engineering ceramics is Si_3N_4 since it provides good combination of mechanical and chemical properties, suitable for structural high temperature applications. SiAlON is a material built on Si_3N_4 crystal structure. The best-known alpha (α) and beta (β) polymorphs of Si_3N_4 are referred to by the same name in SiAlON ceramics (α^1 and β^1, respectively). The general formula of β^1-SiAlON is following:

$$Si_{6-z}Al_zO_zN_{8-z} \quad (1)$$

Where, z represents the displacement amounts of Al and O (the amount of dissolution in the Si_3N_4 structure). The z value ranges from 0 and 4.2. Al^{3+} replaces Si^{4+}, and O^{2-} replaces N^{3-} to achieve charge balance in the Si_3N_4 crystal structure. Since Al-O and Si-N bond lengths are similar (0.175 and 0.174 Å), high dissolution is possible. Very little lattice deformation occurs after displacement and consequently the unit cell size is slightly expanded [9].

α^1-SiAlON is expressed by the following formula:

$$Me_xSi_{12-(m+n)}Al_{m+n}O_nN_{16-n} \quad (2)$$

In α^1-SiAlON, the charge imbalance caused by the introduction of Al^{3+} instead of Si^{4+} can be achieved in two ways since there are two intermediate voids in the unit cell. The first one is as in β^1-SiAlON, N^{3-} is replaced by O^{2-} and the second one is metal cations enter into interstitial sites. Me, can be Li, Na, Mg, Ca, Sr, Y or a lanthanide ion, which should ensure the charge balance as well as stabilize the α^1-SiAlON crystal structure. The size of these holes is 0.13 nm and hence limits the cations to stabilize the structure. Therefore, the size of the ion that can enter the crystal structure is also important. The first ions that can enter the α^1-SiAlON structure are Li^{1+} and Mg^{2+}. Then, Na^{1+}, Ca^{2+} and Y^{3+} were tried and most of the lanthanides ($Z \geq 60$) were found to be able to enter the lattice. In the general formula m is replacement of (Si-N) and (Al-N) and n is replacement of (Si-N) and (Al-O). Lattice distortion carried out due to Al-N bond length (0.187 Å) is longer than Si-N (0.174 Å) and Al-O (0.175 Å). When the metal cations enter the intermediate voids, it strengthen the $3Me(N\text{-}O)_3$ bonds and forms strong $Me(N\text{-}O)_2$ bonds, thereby providing the necessary structural stability. Thus, the unit cell expands more than the β^1-SiAlON structure [9].

Unlike the type and size of the cation, the amount of metal cation that can enter the crystal structure is also important. To stabilize the α^1-SiAlON structure sufficiently, the minimum amount of cations is x = 1 for Me^{1+} and x = 0.5 for Me^{2+}, x = 0.33 for Me^{3+}. The upper dissolution limit is theoretically x = 2. However, since the production of oxygen-free α^1-SiAlON, in which the intermediate voids are completely filled, x = 2 has not been observed until now. When oxygen is in structure, it provides partial charge balance and thus reduces the amount of interstitial metal cations required. The maximum number of entering interstitial atoms was found to be 1.6 for Ca^{2+} and $Yb^{3+.}$ [9]

SiAlON ceramics are generally expressed in quaternary phase diagram. Si_3N_4-4AlN-2Al_2O_3-3SiO_2 is located at the corners (Fig.1). The stability area of β'-SiAlON is seen as a line. β'-SiAlON is formed on the Si3N4-AlN:Al2O3 line, Al and O amount is quite high.The phase relationships in αı-SiAlON are somewhat more complex since introducing the sintering additions and can be explained by the Jänecke Prism (Fig. 2). The base plane in the prism is the section in Figure 2, where β'-SiAlON is described. Since alpha and beta SiAlON phases are thermodynamically stable, it is possible to obtain optimum microstructure and mechanical properties by combining both phases [9].

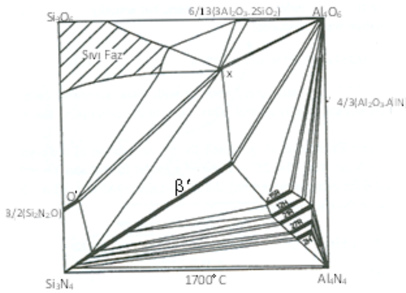

Figure 1. *The phase diagram of Si_3N_4-AlN-SiO_2-Al_2O_3 system at 1700°C [9]*

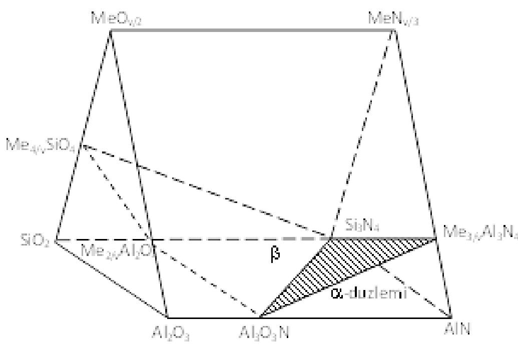

Figure 2. *Jänecke Prism showing the Me-Si-Al-O-N system [9]*

Processing of SiAlON Ceramics

Although SiAlON based materials are potential for many industrial applications, they were not widely used commercially for a long time. The main reason for this is the inability to produce SiAlON ceramics in aqueous media. In order to produce SiAlON ceramics, non-oxide starting powder such as AlN is used in addition to the main raw material Si_3N_4. Non-oxide powders tend to react with water. Bowen et al. observed that AlN reacted with distilled water at room temperature to form an amorphous layer on the surface close to the composition of AlOOH. This layer is converted to $Al(OH)_3$ according to the following reactions [15]:

$$AlN + 2H_2O \rightarrow AlOOH_{\text{amorphous}} + NH_3 \quad (3)$$

$$NH_3 + H_2O \rightarrow NH_4 + OH^- \quad (4)$$

$$AlOOH + H_2O \rightarrow Al(OH)_3 \quad (5)$$

Similar reactions are observed in the interaction of Si3N4 with water, but the effects are not very strong. Therefore Si3N4 can be prepared easily in aqueous environments [15]:

$$Si_3N_4 + 6H_2O \rightarrow 3SiO_{2\ \text{amorphous}} + 4NH_3 \quad (6)$$

Ammonia from reaction 3 and 4 increases the pH of the slurry rapidly and leads to flocculation. Flocculation is not desirable when preparing stable slurry as the particles settle down as a result of flocculation. Reaction 5 enriches the chemical composition of the system in terms of oxide, causing deviations from the targeted SiAlON composition. As a result of these reactions, compositional deviations are likely to lead to undesirable changes in the microstructure and phase content. Therefore, in order to achieve the targeted phase content, the interaction of the powders with water must be minimized.

Today, AlN free Si_3N_4 ceramics can be produced in aqueous media without any problems. However, the above-mentioned reactions cannot be avoided due to the necessity of using AlN to produce SiAlON ceramics. AlN powders coated with various "water-resistant" carboxylic acid groups can be used to prevent the reaction of the AlN powder with water [16-19]. However, in the production method there should be no milling step, only the powders should be dispersed in water by some mechanical methods such as propeller. This is resulted from damage of the protective surface layers after milling.

In the production of SiAlON ceramics, since several different powders are mixed, the milling process is mandatory for this mixture to be homogeneous and to break up the present agglomerates in these powders. Therefore, surface-coated AlN powders make it possible to produce pure AlN ceramics in aqueous environments. However it is difficult to use AlN powder in aqueous environments if milling process is necessary. The possibility of milling AlN with Si_3N_4 and Re_2O_3 mixtures in aqueous medium without flocculation has been investigated by our group. As a result of the mixing and milling studies, it was found that Si_3N_4 and AlN powders can be milled together for maximum 15 minutes without any problem [20]. In other words, flocculation problem was not observed in this process. When the grinding time exceeds 15 minutes, the slurry temperature increases to 58°C and the sludge is flocculated. When opened in these mills, a heavy smell of ammonia is emitted. This is an indication that reactions 3 and 4 are taking place. These reactions enrich the composition with oxygen, leading to deviation from the designed α-β phase composition and further formation of β-SiAlON phase will be carried out. As a result of the studies, it was found out that the way of AlN powder addition and the milling conditions (milling speed, amount of ball, addition sequence of starting powders, milling time) were very important. It has been found that under suitable milling conditions Si_3N_4-AlN mixtures can be milled without hydrolysis and stable slurries can be prepared.

Factors affecting SiAlON microstructure development are: i) raw material properties, ii) process conditions, iii) final material composition (desired phase content). The production method and compositions of the raw materials or starting powders, determine the final material properties. The different starting powders have different particle size, particle size distribution, particle shape and surface area, degree of agglomeration, powder flow, green density and reactivity. Powder characteristics are one of the factors determining the degree of densification. For example, if the particle size distribution provides optimum packaging, high green density and low shrinkage are observed. Similarly, the powders with high surface area are more reactive and easy densify. The α:β phase ratio of the initial silicon nitride powders also has a significant effect on microstructure development and affects densification and grain growth Another important starting material property is the chemistry of the powders used. Impurities are calculated as extra raw materials in the composition design and have effects on the final microstructure and composition [21, 22].

In our previous study, the SiAlON ceramics were produced from low cost refractory grade, impure, less sinter active and hence hard process able β-Si_3N_4 powder. The processing challenges and its solution methods of β-Si_3N_4 powder to produce SiAlON ceramics were explained [14]. We found that unwanted iron and silicon impurities in the initial silicon nitride powder can be removed by magnet and then sieved. By this way desired SiAlON phase composition was achieved and prevented the formation of undesirable intergranular phases which influence the high temperature properties. On the other hand, the powder milling time was found to be effective on silica formation on initial β-Si_3N_4 powder. The silica content on the silicon nitride powder affects the SiAlON phase evolution or α^1:β^1-SiAlON phase ratios. When the oxygen content was 7.8%, aimed α^1:β^1 phase ratio could not be reached and the composition was shifted to the β^1-SiAlON rich region. β-Si_3N_4 powder particle size has a significant effect on microstructural development of SiAlON ceramics. If the β-Si_3N_4 particle size was greater than 0.5 µm, low aspect ratio grains developed [23]. Besides, the availability of SiAlON ceramics with the same properties starting with β-Si_3N_4 powder was also evaluated statistically [24].

In our study, different starting Si_3N_4 powders which were produced by diimide, direct nitridation and combustion synthesis, in as received state, and after milling in different liquid media (aqueous or alcohol), for various milling durations were used to produce SiAlON ceramics. In the study the influence of initial Si_3N_4 powders characteristics (surface chemistry, particle size, particle size distribution, impurities etc.) on SiAlON phase development, sintering, microstructural evolution and mechanical properties were clarified. It has been found that a change in processing conditions such as milling medium (water or isopropyl alcohol) and milling time can have a significant effect on particle surface groups and thus on the microstructure of sintered SiAlON samples [22].

High Temperature Properties

A definition of high temperature is little bit confusing. In materials science and technology, temperatures generally equal to or greater than two-thirds of the melting point of a solid is defined as high temperatures. High temperature properties can be examined under two headings as mechanical and chemical properties. The strength, hot hardness, elastic modulus, fracture toughness, thermal shock resistance are among the mechanical properties. Oxidation and corrosion are chemical properties. Creep resistance is in the class of both chemical and mechanical property [25].

Any stress limit that causes permanent change or break in the internal structure of the material is defined as strength. Factors affecting strength; grain size, interaction of grain boundaries and porosity, distance between porosities and distance to surface, shape and size of impurities. The resistance of the material to crack propagation is called fracture toughness. Fracture toughness depends on microstructure (grain shape, size, surface morphology, grain boundary phase, and strength) and is a material constant. The fracture toughness can be improved by microstructure designs that activate the toughening mechanisms. Grain size, grain surface morphology, grain boundary phase and strength, interface bond strength, are the key microstructural properties which govern the fracture toughness. When the grain size is sufficiently large, the crack more likely to change direction, resulting in increased fracture toughness. If the interfacial bond strength between the grains is sufficiently low, when the crack formed in the material reaches the grain, by changing direction towards the interface, the fracture will be delayed as the energy required for crack propagation will decrease. The main toughening mechanisms are bridging, crack deflection, microcracks and fiber-pull out. While Si_3N_4 ceramics with high interfacial strength shows transgranular fracture, Si_3N_4 ceramic with low interfacial strength have intergranular fracture. The fracture mods are controlled by mainly sintering additives [26-28].

Resistance to plastic deformation is defined as hardness. The hardness of the SiAlON ceramics varies according to the production methods. The hardness of the SiAlON ceramics depends on the α^{1}:β^{1} SiAlON phase composition and microstructure (grain size, distribution, secondary phase, porosity, intergranular phase chemistry etc.) [29]. In dense, poly-crystalline, single-phase beta SiAlON ceramics which do not contain grain boundary phase, the hardness at room temperature decreases with increasing z value in the formula ($Si_{6-z}Al_zO_zN_{8-z}$). The reason for this is that the grain size is 5 or 10 times higher in high z-value SiAlONs than in low z-value SiAlONs. In other words, as z value increases, grain size increases and hardness decreases. The hardness of the α^{1}-SiAlON ceramics prepared by hot pressing was determined as 18-19 GPa (HV10). This value is approximately constant if x in the formula $M_xSi_{3-(3x+n)}Al_{3x+n}O_nN_{4-n}$ has a value in the range of 0.08≤x 0.25. α^{1}-SiAlON ceramics have higher hardness than β^{1}-SiAlONs. This is because the cations used as the addition of sintering aids enter the voids in the α^{1}-SiAlON crystal structure and form solid solution. Therefore, the formation of the glassy phase may be little or no and results in increasing hardness. Hot hardness is affected by grain boundary phases [30,31].

As a function of time and temperature, the deformation that occurs in the material under constant tension is defined as creep. Since creep is important for high temperature applications, it is very important to understand creep behavior, especially in energy conversion systems. Parameters affecting creep are temperature, stress, crystal structure, microstructure, viscosity and composition of grain boundary phase, stoichiometry and the environment. Diffusion and dislocation movement decreases as the covalence of the crystal structure increases. Therefore, the creep resistance of pure carbide and nitride materials is quite high. However, the intergranular phase of the materials increases the creep rate. The main mechanism of creep is the sliding of grain boundaries with temperature rise. The dominating mechanism for diffusion is solution-precipitation through the viscous phase and rearrangement by viscous flow, formation of cavities or cracks accompanied by grain boundary sliding and redistribution of the grain boundary phase in cavitated multigrain junctions. Viscous flow is the most important mechanism affecting the creep rate. The thickness and chemistry of the grain boundary film govern the viscous flow. This can be controlled by sintering aids (cation type, content, cation molar ratio). The affecting parameters of the creep resistance of SiAlON ceramics are amount, composition, distribution, viscosity, type of intergranular phase, porosity content, grain size, grain shape, temperature, stress, production method and oxidation resistance [32-34].

Corrosion and oxidation resistance are the chemical properties of the material. Corrosion occurs as a result of direct interaction with reactive liquid or the interaction of impurities in the ceramic with the surrounding gases or liquid medium. The types of interaction are called active, passive, local, hot. Figure 3a shows the schematic representation of the corrosion interaction regions of silicon nitride Active 1 and passive corrosion occur when there is interaction with hot gases. The oxygen content of the atmosphere is very important. Passive mode is observed when there is enough oxygen in the environment. Active 2 mode is observed when the corrosion reaction results in gas release. The corrosion behavior of SiAlON ceramics are controlled by mainly intergranular phase since they are weak regions compared to grains [35]. Carbide and nitrides are not stable in the oxidizing atmosphere. However, if oxygen partial pressure is above 1 mm Hg, solid, protective SiO_2 layer is formed on the surface. This phenomenon is known as passive oxidation. With passive oxidation, SiAlON ceramics have excellent oxidation resistance. Initially, the formation of SiO_2 is quite rapid, but as the layer thickness increases, silica formation rate decreases. In the case of active oxidation, when oxygen partial pressure is less than 1 mm Hg, there is not enough O_2 to form the protective SiO_2 layer. Therefore, instead of SiO_2, SiO gas is formed (Fig. 3b). Such oxidation is continuous and linear. It can completely consume the material. Oxidation resistance depends on composition and impurities. SiAlON reacts with oxygen in the atmosphere to form a SiO_2 layer on the sample surface. The intergranular phase formed after sintering reacts with the silica layer formed on the surface to form a silicate liquid with a lower melting temperature and lower viscosity than pure SiO_2. As a result, the oxidation resistance decreases due to the chemical corrosion of SiAlON. In order to increase the oxidation resistance, the formation of thermodynamically stable crystal phases in the structure should be ensured and the driving force for diffusion of the sintering additive to the surface should be minimized. If the grain boundary phase is amorphous, it softens at high temperatures, reacting with the solid SiO_2 layer and worsening the oxidation resistance. Therefore, high refractory and low quantity sintering additions should be used to obtain oxidation resistant materials [36-37].

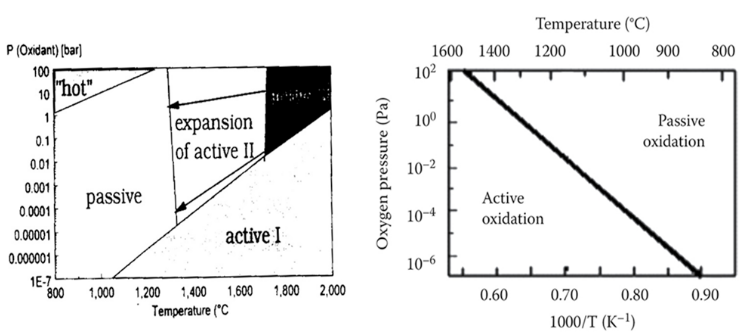

Figure 3. *(a) Schematic representation of the main corrosion interaction sites of Si_3N_4, (b) active and passive oxidation regions depending on temperature and oxygen partial pressure [35]*

Methods for Improving the High Temperature Properties

Due to strong covalent bonding of Si_3N_4 ceramics, they (Si_3N_4 grains) keep their properties up to 1600°C. Their higher covalent bonding energy provides low thermal expansion, high elastic modulus and decomposition temperature, oxidation resistance [38]. However intergranular phases begin to soften less temperature depending on the chemistry of intergranular phase. *Therefore the high temperature properties of SiAlON ceramics are controlled by the nature (crystal or amorphous), composition and amount of* intergranular *phases***.** At high temperature creep, oxidation, corrosion, diffusion, slow crack growth determines the failure behavior and limits the performance/life time of the SiAlON ceramics. Which mechanism will worsen the high temperature property depends on the viscosity and softening temperature of the grain boundary phase.

All processing stages govern the high temperature properties of SiAlON ceramics. Purity of starting powders, designed/aimed phase composition ($100\alpha^{I}\rightarrow100\beta^{I}$- SiAlON), used rare earths for sintering (e.g. the type, molar content and refractoriness of cation/sintering additives), shaping and sintering method/technique etc. Particularly sintering technique is the most important parameter determining high temperature properties.

Si_3N_4 is a highly covalently bonded compound (~ 70%) with a very low diffusion coefficient of nitrogen atoms (diffusion coefficient of 6.8x10-10m^2/s at 1400°C) and silicon atoms (diffusion coefficient of 0.5x10-19m^2/s at 1400°C) [39]. Low mobility of ions in covalently bonded materials reduces the rate of diffusion. Although the movements of ions increase at high temperatures, Si_3N_4 decomposes at 1877°C under nitrogen pressure of approximately 1 atmosphere. It is almost impossible to densification of Si_3N_4 without the use of sintering aids. Therefore, liquid phase sintering is needed. The sintering additives used in liquid phase sintering solidify during cooling to form amorphous or crystalline intergranular phase depending on the cooling regime and the composition of the liquid. The amount of grain boundary phase, chemistry, type and viscosity determine the high temperature properties. There are some ways are possible improve the high temperature properties of SiAlON ceramics. These were explained following sections.

Reduction of Sintering Additive Amount

The most common method to improve high temperature properties is the use of sintering aids, which have high solidus temperatures and form liquids with high viscosity. The high temperature properties of SiAlON ceramics are controlled by intergranular phases. As the content of amorphous intergranular phase increases, the desired high temperature and chemical resistance properties of the materials will deteriorate.

As an approach to improve the high temperature strength, hardness, creep and oxidation resistance is reduction of sintering additive content and sintering with GPS or HIP to obtain full dense structures. SiAlON ceramics are sintered with transient liquid phase sintering, whereby constituents of the initial liquid phase forming agent subsequently dissolve in silicon nitride grains by solid solution, resulting in a decrease in the amount of residual glassy phase at grain boundaries. Therefore the liquid phase must be enough for fully densification and should be minimum to obtain good high temperature properties as well as provides crystallization of glassy phase. It is important to select the right amount and the correct sintering additives in order to obtain both completely dense material and to crystallize the intergranular phase. The limitation of decreasing liquid phase content is elongated grain formation. So the liquid phase content must judiously optimized.

Butler et all. added controlled amounts of Al and N containing polytype phases to control the composition, nitrogen content and the volume fraction of intergranular phases and also the substitution level of the β-SiAlON. The beneficial effect of increasing the nitrogen content and crystallizing the intergranular phase resulted in improvements in strength, creep and slow crack propagation resistance at high temperatures [40].

In our previous study, in order to see the effect of sintering aids amount on the crystallization and coalescence behavior of intergranular phase, SiAlON compositions was produced containing 2.5, 2 and 1.5 mol% sintering aid. And also the effect of cation types on the intergranular phase crystallization was investigated. For this purpose 90Y:5Sm:5Ca, 90Yb:5Sm:5Ca and 90Er:5Sm:5Ca cation system were studied at a constant z value (0.7) [41]. The crystallization of intergranular phase was prevented with the diminishing sintering aids amount. For Y doped SiAlONs, amorphous intergranular phase evolution was detected when the intergranular phase (IGP) was 1.5 and 2 mol%. By increasing sintering aid content to 2.5 mol%, a trace amount of crystal phase (melilite) was observed (see Fig. 4). 4.5Y:4.5Sm:2Ca cation system doped and containing higher amount of sintering aid content (3.3. mol%) and highest Sm cation mole ratio SiAlON showed higher crystallization tendency of IGP with high z value (0.8) SiAlON (see Fig. 5).

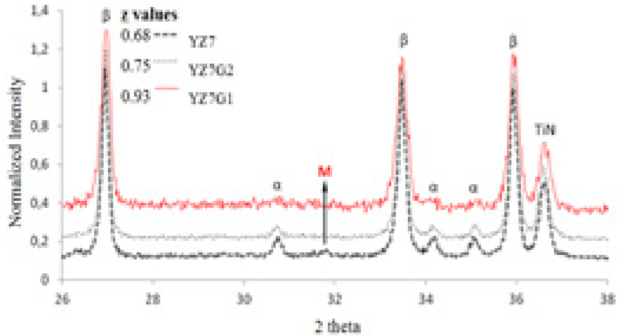

Figure 4. *XRD pattern of 9Y:0.5Sm:0.5Ca containing SiAlON–TiN compositions (z:0.7) which have different amounts of intergranular phase (β:beta SiAlON phase, α:alpha SiAlON phase, M: melilite phase ($Ln_2Si_{3-x}Al_xO_{3+x}N_{4-x}$)) [41]*

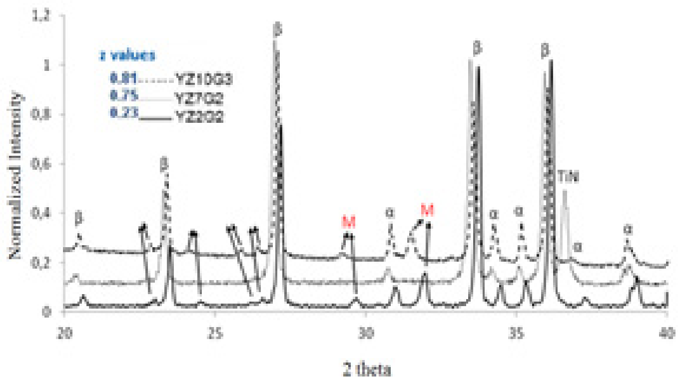

Figure 5. *Comparison of the crystallinity in Y:Sm:Ca containing system with different cation molar ratios and intergranular phase contents (β: beta SiAlON phase, α: alpha SiAlON phase, and M: melilite phase ($Ln_2Si_{3-x}Al_xO_{3+x}N_{4-x}$)) [41]*

The crystallization propencity of Y cation system is lower than the that of Yb and Er cation systems. Forexample when the sintering aid content was 2.5 mol%, melilite and silicate cystal phases were observed for Er and Yb doped SiAlONs, respectively (see Fig. 6). On the other hand 1.5 mol% sintering aids containing Er and Yb doped ceramics had amorphous IGP (see Fig. 7 and 8). As a result, it can be say that intergranular phase crystallization could be controlled by the cation system and cation mole ratios besides sintering aid amount. Besides, solid solution level (z value) has effect on IGP crystallization. SiAlON with 0.25 z value showed melilite phase crystallization while amorphous IGP chemistry was obtained with 0.7 z value. The strong melilite phase crystallization was obtained when z value of 0.8, 3.3 mol% sintering aid content and Sm rich cation system (%45 Sm) [41].

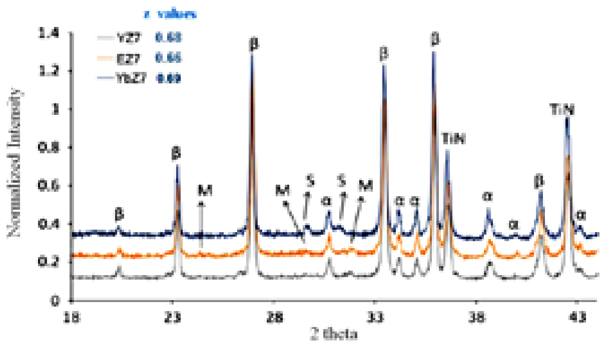

Figure 6. *Comparison of the crystallinity in 9Y/Yb/Er:0.5Sm:0.5Ca containing systems (z:0.7) with 2.5 mol% intergranular phase content (β: beta SiAlON phase, α: alpha SiAlON phase, M: melilite phase ($Ln_2Si_{3-x}Al_xO_{3+x}N_{4-x}$) and S: silicate phase ($Yb_2Si_2O_7$)) [41]*

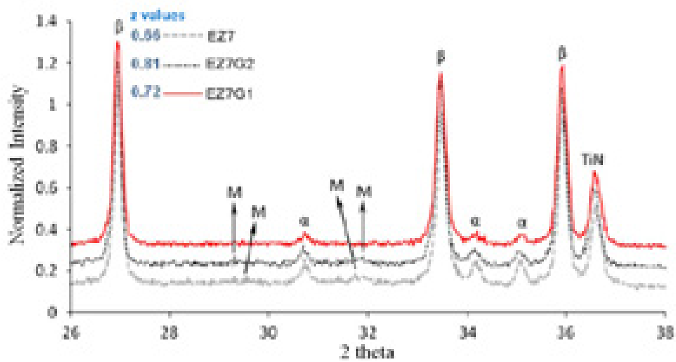

Figure 7. *XRD pattern of 9Er:0.5Sm:0.5Ca containing SiAlON–TiN com positions (z:0.7) which have different amounts of intergranular phase (β: beta SiAlON phase, α: alpha SiAlON phase, M: melilite phase ($Ln_2Si_{3-x}Al_xO_{3+x}N_{4-x}$)) [41]*

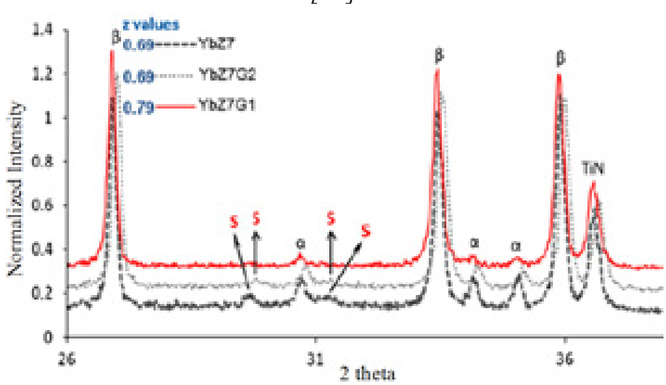

Figure 8. *XRD pattern of 9Yb:0.5Sm:0.5Ca containing SiAlON–TiN compositions (z:0.7) which have different amounts of intergranular phase contents (β: beta SiAlON phase, α: alpha SiAlON phase, M: melilite phase ($Ln_2Si_{3-x}Al_xO_{3+x}N_{4-x}$)) [41]*

As intergranular phase content reduced, the bulk densities decreased since the sintering aid content was lowered. Open porosities increased with the decrease in the sintering additive content since reduced amount of transient liquid phase during sintering led to impaired densification. Sintering studies revealed that Yb doped SiAlONs had the best densification behavior among the studied cation systems. Regarding phase relationships of SiAlONs with the different amount of intergranular phase, by decreasing the amount of sintering aids aimed α'-SiAlON phase content was not achieved in all cation systems. This can be resulted from inadequate amount of cation for stabilizing α'-SiAlON crystal structure [41].

Another study is conducted by Calis Acikbas and Kara, to evaluate the effect of z value on the crystallization of IGP and coalescence. For this purpose SiAlONs were produced in 9Yb:0.5Sm:0.5Ca cation system, 2 mol% sintering aid content and with different z value (0.3, 0.5, 0.7, 0.9 and 1.1) [30]. Z value was found to be an effective parameter in intergranular phase chemistry and crystallization. The Jss phase is stable when z value is in the range of 0.3-0.4. When the z value exceeds 0.74, the grain boundary phase has a reduced tendency to crystallize. When the z value increased above 0.80, the YbAG phase became stable (see Fig. 9). SiAlON samples which has a 0.3, 0.9 and 1.1 z value showed large coalesced pocket size. On the other hand, intergranular phase in Z05 and Z07 samples are generally distributed around the SiAlON grains. For SiAlON samples with a 0.5 and 0.7 z value, intergranular phase distributed around the SiAlON grains. The coalescence of the intergranular phase could be influenced by crystallization (Z03) and/or chemistry of the intergranular phase (Z05, Z07, Z09 and Z11).

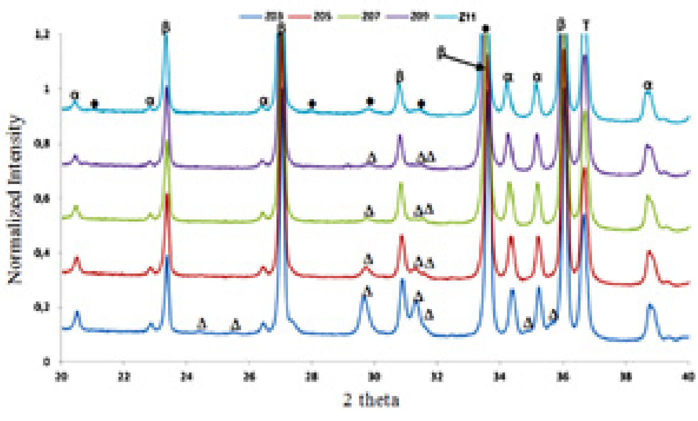

Figure 9. *XRD pattern of assintered SiAlON-TiN composites which have different z values (β: beta SiAlON phase, α: alpha SiAlON phase, T:TiN; Δ:Jss-$Yb_4Si_{2-x}Al_xO_{7+x}N_{2-x}$; ♦:$Yb_3Al_5O_{12}$). [30]*

Selection of Proper Sintering Aids to Ensure Refractory Intergranular Phase Formation

As SiAlON ceramics are produced by liquid phase sintering, this liquid phase usually remains in the microstructure after sintering as the secondary intergranular phase. The type and nature (whether its crystalline or not) of the intergranular phase, its melting temperature, viscosity and oxidation behavior are all important factors as these govern the high temperature properties of the SiAlONs. It is known that crystallisation of the intergranular phase enhances the high temperature properties of liquid phase sintered ceramics. Therefore, one of the main aspects in designing SiAlONs with improved high temperature properties would be to select additives that would provide a good liquid phase sintering behavior and at the same time would crystallize well to refractory phases after sintering. As stated above, there are a number of crystalline phases, either oxygen or nitrogen rich, that can be obtained in the system. Fig. 10 shows XRD spectra of α':β'/SiAlON composite (25% α'-SiAlON) that were prepared with the same amount of additives using a multi cationic mixtures but different cation combinations. Although the general microstructural features (Fig. 11) and mechanical properties are similar for the different dopant combinations, it can be seen in Fig. 10 that various types of crystalline (wollastonite, melilite, silicates, aluminates etc.) or amorphous phases can be formed depending on the dopant types and sintering conditions. It has been found that the extent of crystallization of the intergranular phase seems to vary depending on the type of dopants used. Fig. 12a and 12b illustrate triple junctions crystallized partially and almost fully, respectively, in two α:β/SiAlON composites with the same amount of α:β ratio and intergranular phase content. As the extent of crystallization affects especially the high temperature properties, the application properties of SiAlONs can be improved by careful adjustments of intergranular phase chemistry so as to obtain maximum crystallization. This is demonstrated for cutting tool applications in Fig. 13a which shows cutting performance of the SiAlONs in Fig. 12 on gray cast iron turning. It is clear that substantial improvements in cutting performance can be realized with the SiAlON having better intergranular phase crystallization. In Fig.13b, machining performance of cutting tools which have different crystalline phase chemistry and hence produced from different cation system/systems was given. It has been found that the insert having strong melilite phase crystallization performs better. The second best performing insert has strong silicate phase crystallization. The machining performance decreases as crystallization tendency decreases.

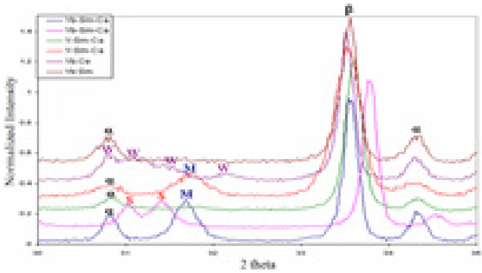

Figure 10. *Phase evolution with different multi cation doped α:β/SiAlON composites containing 25% α-SiAlON (α:alpha SiAlON, β:beta SiAlON, S:Silicate, M:Melilite, W: wollastonite phases) [43]*

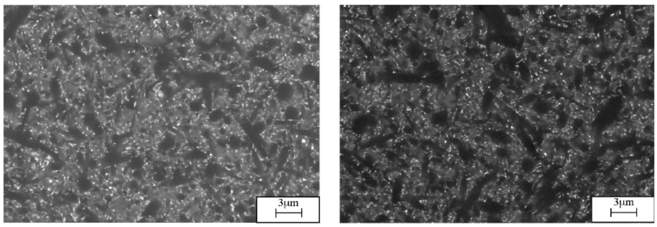

(a) (b)

Figure 11. *Back scattered SEM images of α:β/SiAlON composites containing 25% α-SiAlON (a) crystalline and (b) amorphous intergranular phase, showing similar microstructures.[43]*

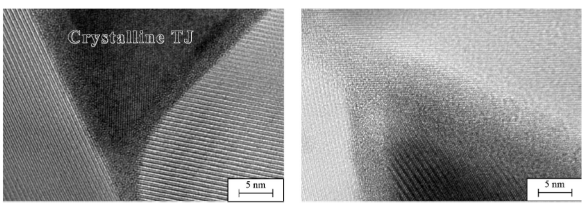

Figure 12. *TEM images of SiAlON with the same amount of doping with different dopants showing (a) better triple junction crystallinity and (b) worse triple junction crystallinity. [43]*

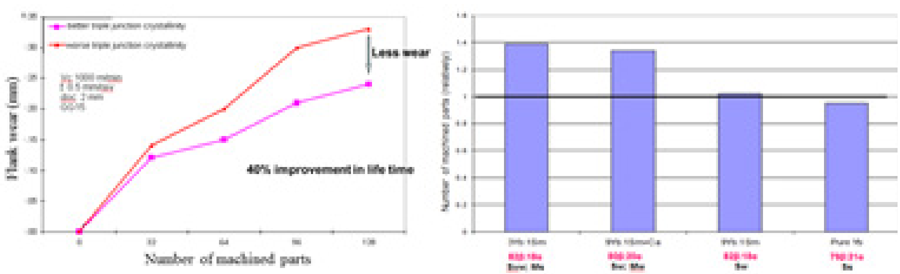

Figure 13. *The effect of (a) crystallinity and (b) dopants on cutting performance of gray cast iron [43]*

The creep resistance is also affected by intergranular film (IGF) composition, chemistry and viscosity. The glass transition temperature

(Tg) decreases as the O/N ratio increases with the introduction of large diameter cations into the IGF. This reduction in Tg worsens creep resistance and limits use at high temperatures. Therefore, the sintering additives used have great effects on creep resistance [44]. To improve these properties, some methods to crystallize the intergranular phases are applied. Although it is possible to crystallize the amorphous phases in the triple junctions, it is quite difficult to crystallize the phases between the two grain boundaries.

Crystallization of Intergranular Phases

Liquid phase sintering/transient liquid phase sintering is a technique commonly used in the production of SiAlON ceramics. Although a liquid phase facilitates easy densification at sintering temperatures, it remains as a residual amorphous phase at SiAlON grain boundaries after cooling. The glassy phase softens above the glass transition temperature, leading to grain boundary sliding under applied stress, which is to a large extent responsible for the degradation of mechanical properties of the sintered material, especially at elevated temperatures. Devitrification of the grain-boundary glass is a well-established technique for improving the high-temperature properties of SiAlON ceramics. But, devitrification in this system is not straightforward [45,46]. The eutectic temperature of the SiAlON systems is generally in the range of 1350°C to 1450°C. For most SiAlON ceramics conventional grain boundary devitrification usually takes place between 1200 and 1400°C, i.e. below the eutectic temperature (BET). This process is essentially a glass-ceramic technique and, in most cases, results in a phase transformation from a low density glass to high density crystalline phase or phases. There is in general no liquid phase appearing in the process to activate the phase transformation, and thus generating flaws at interfaces as a result of volume reduction after devitrification [45].

Another problem is the fact that crystalline grain boundary phase must be in equilibrium with the SiAlON matrix during heat treatment and after cooling; the phase(s) should be refractory and oxidation resistant at elevated temperatures. Because of these critical demands, there is a limited availability of suitable crystalline phases, which can be selected for SiAlON materials. Although various crystalline grain boundary phases have already been studied, there has not been any phase that satisfies demand in both refractoriness and chemical and environmental stability. Among different varieties, YAG ($Y_3Al_5O_{12}$) has been one of the best viable alternatives and so far has widely accepted as an intergranular phase for commercial β- and α-β SiAlONs. On the other hand, such a phase does not contain nitrogen, causing nitrogen rich glassy phase remaining at grain boundaries. In addition, there is always remnant glassy phase when the glass devitrifies [45].

For α-SiAlONs, there are further restrictions: α-SiAlONs have a much smaller solubility for aluminium and in general a higher nitrogen concentration than β-SiAlONs. In SiAlON phase diagrams, α-SiAlON is separated by β-SiAlON from most oxygen-rich crystalline phases and thus the β-SiAlON solid solution intersects most tie lines between the α-SiAlON region and other crystalline phases. As a result, many crystalline phases in equilibrium with β-SiAlON are incompatible with α-SiAlON [45].

There has been another technique is crystallization of the grain boundary phase above eutectic temperature (AET). In this case, as the name implies, crystallisation takes place above the eutectic temperature and the phase transformation involves a liquid phase, and therefore it is a solution and precipitation (or crystallisation) process. There are some unique characteristics of the AET technique. In a conventional glass-ceramic process, the devitrified phase(s) must be that either the compositions or the tie lines are covered within the original glass region. When a liquid phase appears at grain boundaries, however, reactions between the liquid and SiAlON matrix are activated and new equilibrium phase(s) outside the glass-forming range can be crystallised [47]. It is realised that the extended long hour post-sintering heat treatment (e.g. 24 hours) may not be necessary for the AET process, as opposed to BET, because phase transformation takes place in a much rapid manner when temperature is high and a liquid phase is involved. This is an important point as far as industrial applicability of the technique is concerned [45,47]. Shematic representation of AET and BET processes are given in Fig. 14.

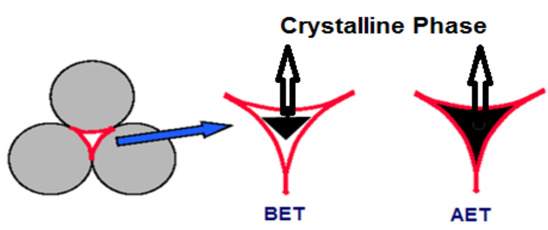

Figure 14. *Schematic representation of BET and AET heat treatments*

The purpose of heat treatment of silicon nitride ceramics is to minimize the amount of intergranular glassy phase or converting them into crystal oxynitride phases to improve high temperature properties. Whether complete crystallization is possible or not depends on the overall glass composition in relation to the stable crystalline oxynitiride phases(s) which can be produced in the particular M-Si-O-N or M-Si-Al-O-N system. The optimum requirements for heat treatment are given below [45].

a) The liquid phase should lie on the binary tie-line between the matrix phase and grain boundary phase composition if only one grain boundary phase is to result from this process; this is illustrated in Fig. 15 where X is the starting composition, M is the matrix phase, G is the composition of the glass formed from the liquid phase L and GB is the devitrified grain boundary phase.

b) If the liquid phase composition at the sintering temperature does not cross the tie-line between the matrix and grain boundary phase(s) then during cooling M+G+GB plus some residual grain boundary phase G2 (depending on cooling rate) will result from sintering and during heat treatment another (more oxygen rich crystalline phase), G1, will devitrify from the glass. This possibility is illustrated in Fig. 16.)

c) If the liquid phase composition comfortably crosses the matrix-grain boundary phase join at the sintering temperature then it will result a high proportion of residual glass and on devitrification a large amount of secondary crystalline phase will devitrify which may adversely effect mechanical properties depending on microstructural mismatch, grain growth, etc. (Fig. 17).

d) If the liquid phase region does not cross the matrix-grain boundary phase join and there is no alternative grain boundary phase other than GB, some undevitrified glass will remain which will degrade the mechanical properties above the glass softening temperature.

e) If the matrix-grain boundary phase join lies considerably below the liquid phase region at the sintering temperature then the resulting product will contain M+GB without significant densification.

f) If there is more than one crystalline phase occurring within the liquid forming region then the desired phase can be chosen by adjusting the composition. Fig. 18 shows this situation where A is an oxide which will give good oxidation resistance, B is a low melting oxynitride of high O:N ratio and C is again an oxynitride but more refractory since its nitrogen content is higher than B,. It is generally the case that A nad C will perform better than B.

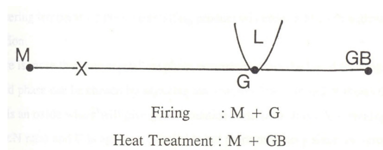

Figure 15. *The optimum phase relationships for achieving densification followed by devitrification [45]*

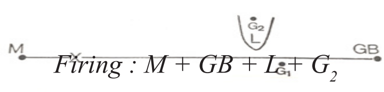

Firing : M + GB + L + G_2

HT : M + GB + G₁ + G₂

Figure 16. *Phase relationships for the case when the liquid phase does not cross the matrix-grain boundary phase join [45]*

Firing : M + G

HT: M + GB

Figure 17. *Phase relationships for the case where the liquid phase comfortably crosses the matrix-grain boundary phase [45]*

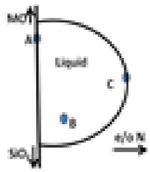

Figure 18. *Choice of different grain boundary phases [45]*

The effects of BET and AET post sintering heat treatment processes on phase development were investigated in 50Yb50Ce and Ce dopant systems (Fig. 19). BET is the most common method used to improve the high temperature properties of Si_3N_4 based ceramics [47]. BET is the devitrification of the glassy phase (glassy phase (solid) → crystalline phase (solid)) between 1100-1350°C after sintering. This process in many cases requires conversion from low density glass to high density crystal phase. As a result, small pores are formed at the interfaces due to the decrease in volume after devitrification. Another limitation of this method as well as the formation of porosity is that the crystalline phase composition to be formed must be well designed and long heat treatment time required for crystallization. In this study, heat treatment was performed for 12 hours at 1350°C for crystal phase formation. Another and new method for improving the high temperature properties of SiAlON ceramics is the crystallization of nearly the entire grain boundary phase by heat treatment (AET) above eutectic. By appropriate selection of the starting composition, the maximum solubility of the nitrogen in the system can be achieved, and the grain boundary liquid of the system is maintained, thereby allowing crystallization by heat treatment above the eutectic. Since the grain boundary phase is liquid in the AET process temperatures (1450-1650°Cs), it has advantages such as faster crystallization as well as less residual amorphous phase remaining. AET treatment was carried out at 1600°C for 2 hours. The phase characterization results of the designed compositions after the AET and BET processes are given in Figure 19. While 25A/50Yb50Ce composition did not observe crystal phase formation after sintering process, melilite phase formation after AET heat treatment and wollastonite (monoclinic structure) formed after BET heat treatment were determined. Wollastonite phase is in the chemical formula $CeSiO_2N$ and the N:O ratio is 0.42. Since cations with large ion size tend to form oxynitride phases, they form the melilite crystal phase of the Ce cation. ($Ce_2Si_{3-x}Al_xO_{3+x}N_{4-x}$). Since the melilite phase is a nitrogen-rich phase (N: O ratio 0.67), the grain boundaries remain oxygen-rich and the material's high resistance to oxidation at high temperature will increase, while creep resistance will decrease.

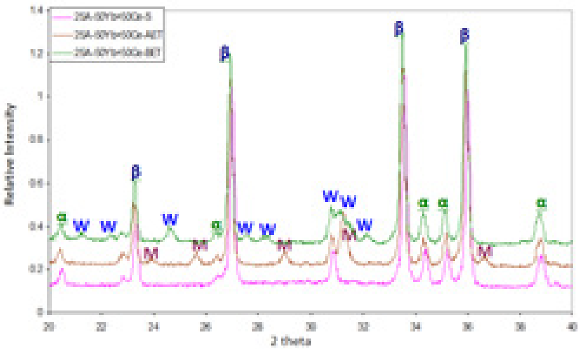

Figure 19. *XRD pattern of 25A/50Yb50Ce composition after sintering and after the AET and BET heat treatment (S: silicate phase, W: wollastonite phase (monoclinic structure) α: α- SiAlON phase, β: β-SiAlON phase)*

When looking at the XRD results of 25A/Ce composition no crystal phase formation was observed after sintering (Fig. 20). In addition, due to the large Ce^{3+} ion size (1.03 Å), it failed to stabilize the α'-SiAlON structure alone and the initially designed (25α:75β) phase ratios could not be obtained. Melilite phase after AET heat treatment and wollastonite (triclinic structure) phase were determined after BET heat treatment. When compared with 25A/50Yb50Ce composition, more wollastonite and melilite crystal phase formation was observed in 25A/Ce composition after AET and BET heat treatments. Slow or fast cooling rates affect the type of grain boundary phase (whether crystal or glassy). During slow cooling, crystal phase formation is observed as sufficient time is allowed for crystal phase formation. It was determined that crystal phase is obtained in one stage without post sintering heat treatment by applying controlled cooling regime during sintering since it provides time for atoms to be regularly arranged. As can be seen from Figure 21, similar Melilite phase crystallization was achieved after slow cooling and heat treated material.

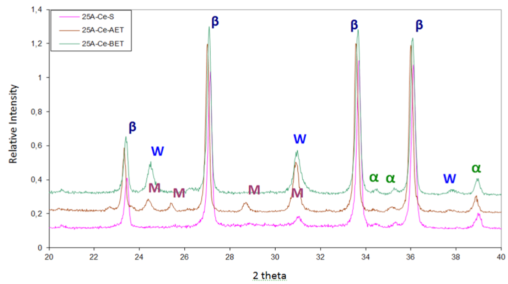

Figure 20. *XRD pattern of 25A/Ce composition after sintering and after the AET and BET heat treatment (W: wollastonite phase (triclinic structure), M: melilite phase, α: α- SiAlON phase, β: β-SiAlON phase)*

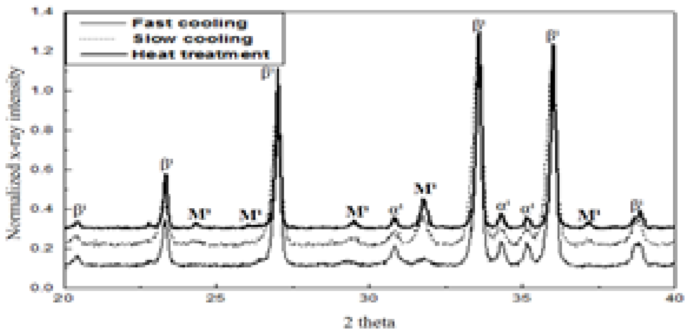

Figure 21. *Comparison of the crystallinity by fast cooling, slow cooling and heat treatment in Y–Sm–Ca containing system (heat treatment at 1600°C for 2 h (β': beta SiAlON phase, α': alpha SiAlON phase, M': melilite phase ($Ln_2Si_{3-x}Al_xO_{3+x}N_{4-x}$)).[46]*

In terms of microstructure development, there is no significant difference in the slow and fast cooled sample. However, grain growth was observed in the heat treated sample. (Fig. 22 a,b, c.) Slow cooling process was applied as follows: heating rate was 10°C / min from sintering temperature to 1700°C and heating rate 5°C / min to 1500°C [46]. Another example for crystallization with slow cooling is 90Yb:5Sm:5Ca cation system. The crystal phase formation was not observed in 25A/90Yb10Sm5Ca composition after rapid cooling, while silicate phase formation was observed after slow cooling. (see Fig. 23) [20].

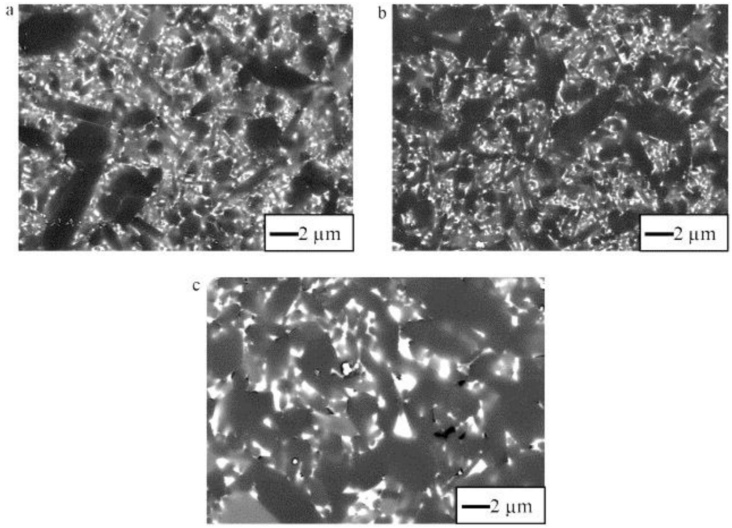

Figure 22. *Representative SEM images of Y–Sm–Ca doped SiAlONs after (a) fast cooling, (b) slow cooling and heta treatment [46]*

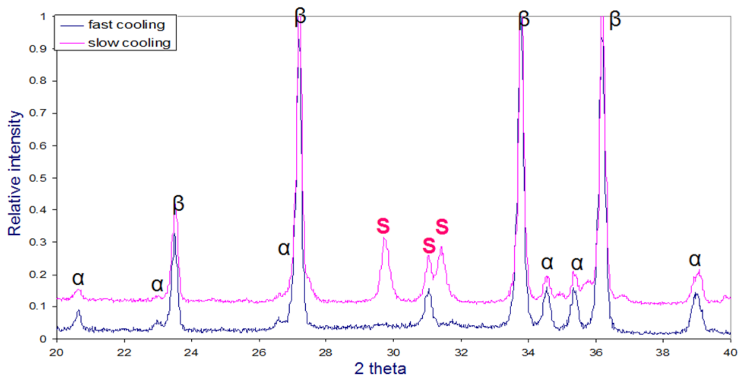

Figure 23. *Comparison of the crystallinity by fast cooling, slow cooling in Yb, Sm, Ca containing system (β: Beta SiAlON phase, α: Alpha SiAlON phase, S: Silicate phase ($Ln_2Si_2O_7$) [20].*

Vacuum Heat Treatment

It is well established that the intergranular glassy phase and its distribution within the grain boundaries of silicon nitride based ceramics is the most important single factor determining the chemical and mechanical performance of these materials at high temperatures [45]. In order to improve high temperature properties some methods were applied up to now. For example, the use of additives that provides high eutectic temperatures and which result in the formation of high-viscosity liquids rich in nitrogen with a high refractory character. For this reason, very high melting temperature sintering additives are favored. Although the pressure-less sintering of SiAlON ceramics with these additives quite easy, eutectic temperature quite low (1350°C) and the cost of oxide additives is high. Other common methods for removing (or minimizing) intergranular glassy phase involve the use of very expensive and pure and fine particle size of starting Si_3N_4 powders and also expensive sintering techniques (like GPS and HIP). Therefore new and cheaper techniques are needed for the production of dense, refractory silicon nitride based ceramics which contain very little residual grain boundary phase [45].

For that reason vacuum heat treatment is a cheaper technique to remove the sintering additive in gaseous form. In this technique, it is possible to completely remove the residual intergranular vitreous phase in Si3N4 ceramics by volatile metal oxides by post-preparative heat treatment in vacuum at 200-300 ° C below the original sintering temperature. In this case, the grain boundary M-Si-O-N phase is liquid at the vacuum heat treatment temperature, boils as a mixture of metal vapor and some shrinkage occurs in the system, densities above 99% are obtained. However, it is difficult to completely remove the grain boundary phase, since it is volatile removed from the system below the decomposition temperature of SiAlON when the grain boundary phase is rich in aluminum [45]. The only metals suitable for use as sintering additives, which could be removed by a subsequent vacuum heat treatment process are, Li, Na, K, Mg, Ca, Sr, Yb. From the list K has not been considered further because its very low boiling point creates problems in initial sintering; the volatile species SiO and Al_2O must also be included because they are relevant for the M-Si-O-N and M-Si-Al-O-N liquid phases formed during sintering [45].

Due to decomposition of SiAlON under vacuum, some experiments were carried out to study the effectiveness of hydrogen in the place of vacuum as an agent for the removal of grain boundary material. It was found that hydrogen (in a carbon environment) could satisfactorily remove volatile metals (e.g. Mg, Li), but the residual silica and nitrogen in the glass remained as the crystalline phase Si2N2O. This phase has comparable refractoriness to silicon nitride, and is therefore perfectly acceptable as an additional constituent of the microstructure, with the added advantage that it has a 10% lower density (2.82 compared with 3.20 g/cm3), as a result of which it fills up a considerable amount of the grain boundary volüme originally occupied by glass, and therefore less shrinkage is needed during the heat-treatment step to retain a good final density. Materials prepared in this way would be expected to show excellent creep and oxidation resistance up to temperatures in excess of 1450°C [45]. The vacuum heat-treated product is suitable for high temperature applications. Although its strength at room temperature is slightly lower than as-sintered products, this strength is maintained to at least 1500 ° C and improves the properties of pure silica layer formation on the surface in an oxidizing atmosphere. More importantly, by the absence of grain boundary phase, the mechanism of grain boundary diffusion of metallic materials into the bulk sample is avoided and therefore the corrosion resistance is considerably better compared to conventional materials [45].

Sintering with Hot Press (HP), Hot Isostatic Pressing (HIP), Gas Pressure Sintering (GPS) or Spark Plasma Sintering (SPS)

Due to high binding energies between the silicon and nitrogen atoms in silicon nitride structure, it is difficult to achieve completely dense structures from pure silicon nitride powders. On account of this sintering additives are necessary for full densification. The amount of sintering aids used varies according to the sintering technique used. For the sintering of SiAlON ceramics, gas pressure sintering (GPS), hot pressing (HP), hot isostatic pressing (HIP), pressure-less sintering, spark plasma sintering (SPS) and microwave sintering techniques are generally used.

The high amount of sintering aids is necessary for pressure-less sintering (PLS) technique to achieve completely dense structures. However, the high liquid phase amount increases the amount of intergranular phase and adversely affects the high temperature properties of the material. Therefore, sintered materials with PLS are suitable for long term use only at temperatures below 1000°C. Therefore pressure assisted sintering techniques were developed.

The grain boundary diffusion controlled material transport mechanism via the liquid phase from the interface to the pore region plays the dominant role during the liquid phase sintering of silicon nitride based ceramics [48].

$$\frac{dp}{dt} = \frac{((Db\delta)\varphi)}{d^3} f(\sum, \sigma)$$

Where φ is molecular volume of the diffusion species, d is the initial grain size, Db is the grain boundary coefficient, δ is the initial thickness (diffusion path) of the intergranular liquid phase, and f(Σ, σ) is stress function which involves the density dependent sintering potential, Σ and an effective stress σ due to the external pressure. From this equation it is clear that either an external pressure must be applied or the sintering temperature must be increased to compensate for liquid volume reduction and increase the driving force for grain boundary diffusion controlled material transport. The starting powders to form SiAlON at HP are heated to high temperatures under unidirectional pressure (20-50 MPa). The applied pressure enhances both re-arrangement and grain boundary diffusion. Tsuge et all showed that strong ceramics could be fabricated by hot pressing with very little additive but the major disadvantage of this technique is that only simple shapes can be produced and the process can not be easily automated [49].

Another method is to apply isostatic pressure (~ 300 MPa) and called as hot isostatic pressing. This technique is highly interesting as it allows the production of dense SiAlON ceramics with negligible residual glassy intergranular phase and hence this increases the high temperature properties. Ingelström and Ekström showed that glass-encapsulated hot isostatic pressing, silicon nitride could be densified with zero or only small (□1 w/o) additions of a sintering aid [50]. This allows production of very complex shapes products. The cost, like HP, is high, but reduces when large number of samples is involved.

Gas pressure sintering technique is a widely used sintering technique in the production of dense complex shape silicon nitride based ceramics. It has cost advantage over HIP and allows for the production of materials with better thermal and mechanical properties than pressure-less sintering. Nitrogen gas pressure on the GPS prevents thermal decomposition of the powder compact and allows sintering at elevated temperatures. High temperature properties are improved by enabling the use of less and more refractory sintering additives. Mitomo showed that the decomposition of Si_3N_4 is suppressed by heating under higher nitrogen pressures and this is the basis of gas pressure sintering (GPS) [6].

It is possible to sinter at high temperatures by GPS than by other methods and this accelerates material diffusion in grain boundaries. In a series of studies conducted by Gazza in 1983, used a two-step sintering cycle, using relatively less pressure (0.1 MPa) in the first step, called the pre-sintering step, and increased the nitrogen pressure to 2 MPa in the second step [51]. Open pores must be removed during the first step, or it will be impossible to complete the densification in the second step since highly pressurized gas trapped in the pores, inhibits complete densification or reduces density because of swelling of the pores as a result of thermal expansion of the gas. Hirosaki et al (1990) showed silicon nitride based ceramics could be sintered with very little additive to fully dense materials with significantly less glass phase content [52].

In the gas pressure sintering technique, the driving force is the sum of the capillary pressure and the applied external pressure and is given in the following equation:

$$P_t = \frac{\gamma_s}{r} + P_{appl.} f(\rho, geo)$$

Here, f (ρ, geo) is a function of relative density and grain geometry. Sintering rate increases with increasing sintering pressure. By applying extra pressure, the driving force and kinetics for densification are increased [53,54]. Spark plasma sintering (SPS) is a recently developed sintering technique which produces high quality materials in a very short time (10-15 min.) where fast heating and cooling rates can be applied (600°C / min) as a result of filling the gap between the powder particles with high sintering pressure (~ 50 MPa) and electrical energy. The high temperature properties of the material are also very good, since SPS allows the production of completely dense materials using a small amount of sintering aids [55].

High Temperature Applications of SiAlON Ceramics

Good resistance to high temperature and chemical attack, together with high thermal conductivity facilitate their use in burners, welding nozzles, heat exchangers and shielding tubes. Besides automotive applications include uses as tappets, shims and wear pads. SiAlON parts resist wetting by non-ferrous metal melts and withstand corrosive environments [56]. For gas turbines, furnaces, steam turbines and similar high-temperature engineering materials, creep is of high importance and is taken into account in calculations. SiAlONs are potential to be used for high temperature tribological applications since they are light, hard and have good chemical resistance [57,58]. Currently, cutting tools are the most important market.

Thermal shock resistance is also important where resistance to thermal cycling is a prerequisite, i.e. for cutting-tool inserts, molten-metal handling pipes, hot-dip ceramic hooks, thermocouple protection sheaths etc. [59]. In some applications, their performance is sometimes insufficient. Therefore composite approach is applied to increase the properties of SiAlON ceramics. SiC, TiN, TiC, TiCN, TiB_2, WC, $MoSi_2$, etc. phases are used as reinforcements for the SiAlON matrix [60-64].

CONCLUSION

This chapter has examined processing, microstructure and properties of SiAlON ceramics for the use of high temperature applications and methods to improve the high temperature properties. SiAlONs are of interest as engineering materials for high temperature (>1000°C) applications because they are designed to maintain good mechanical properties even up to 1350 °C. The most important parameter affecting high temperature properties is intergranular phase (nature amorphous or crystalline, chemistry/composition, coalescence behavior, refractoriness). Up to now there are lots of studies on the improving high temperature properties. They are basically reduction of sintering additive amount; selection of proper sintering aids to provide refractory intergranular phase; sintering with HIP, GPS and SPS with fully dense and less IGP; crystallization/removing of intergranular/grain boundary phases by slow cooling, heat treatment (AET and BET) and vacuum heat treatment methods. SiAlON ceramics have wide range of properties and hence high potential for many specific applications. With the improvement of the high temperature properties and the reduction of production costs, usage areas will increase.

REFERENCES

1. Collins, J. F., & Gerby, R. W. (1955). New refractory uses for silicon nitride reported. *JOM*, *7*(5), 612-615.

2. Wiederhorn, S. M., & Ferber, M. (2001). Silicon nitride for gas turbines. Current opinion in solid state & materials science, 5(4).

3. Mangels, J. A., & Tennenhouse, G. J. (1980). Densification of reaction-bonded silicon nitride. American Ceramic Society Bulletin, 59, 1216-1218.

4. Bowen, L. J., Weston, R. J., Carruthers, T. G., & Brook, R. J. (1978). Hot-pressing and the α-β phase transformation in silicon nitride. Journal of Materials Science, 13(2), 341-350.

5. Terwilliger, G. R. (1974). Properties of sintered Si3N4. *Journal of the American Ceramic Society*, *57*(1), 48-49.

6. Mitomo, M. (1976). Pressure sintering of Si 3 N 4. *Journal of Materials Science*, *11*(6), 1103-1107.

7. Oyama, Y., & Kamigaito, O. (1971). Solid solubility of some oxides in Si3N4. *Japanese Journal of Applied Physics*, *10*(11), 1637.

8. Jack, K. H., & Wilson, W. I. (1972). Ceramics based on the Si-Al-ON and related systems. *Nature physical science*, *238*(80), 28.

9. Jack, K. H. (1976). Sialons and related nitrogen ceramics. *Journal of materials science*, *11*(6), 1135-1158.

10. Ekström, T., & Nygren, M. (1992). SiAION ceramics. *Journal of the American Ceramic Society*, *75*(2), 259-276.

11. Mitomo, M., & Tajima, Y. (1991). Sintering, properties and applications of silicon nitride and sialon ceramics. *Journal of the Ceramic Society of Japan*, *99*(1154), 1014-1025.

12. Calis Acikbas , N., & Acikbas, G. (2018). Seramik Aşınma Parçaları (Ceramic Wear Parts), Geleceğin dünyasinda bilimsel ve mesleki çalişmalar - Mühendislik ve Teknoloji (1. basım) Ekin basin yayin dağitim ISBN: 978-605-327-789-7.

13. Fukushima, M. (2017). *Advanced Processing and Manufacturing Technologies for Nanostructured and Multifunctional Materials III* (No. 5). John Wiley & Sons.

14. Mandal, H., & Acikbas, N. C. (2013). Processing, characterization and mechanical properties of SiAlONs produced from low cost β-Si3N4 powder. *KONA Powder and Particle Journal*, *30*, 22-30.

15. Bowen, P., Highfield, J. G., Mocellin, A., & Ring, T. A. (1990). Degradation of aluminum nitride powder in an aqueous environmet. Journal of the American Ceramic Society, 73(3), 724-728.

16. Krnel, K., & Kosmač, T. (2001). Protection of AlN powder against hydrolysis using aluminum dihydrogen phosphate. Journal of the European Ceramic Society, 21(10-11), 2075-2079.

17. Kocjan, A., Krnel, K., & Kosmač, T. (2008). The influence of temperature and time on the AlN powder hydrolysis reaction products. Journal of the European Ceramic Society, 28(5), 1003-1008.

18. Olhero, S. M., Novak, S., Oliveira, M., Krnel, K., Kosmac, T., & Ferreira, J. M. F. (2004). A thermo-chemical surface treatment of AlN powder for the aqueous processing of AlN ceramics. Journal of materials research, 19(3), 746-751.

19. Krnel, K., Dražič, G., & Kosmač, T. (2004). Degradation of AlN powder in aqueous environments. Journal of materials research, 19(4), 1157-1163.

20. "Kesici Uç Uygulamaları için SiAlON Seramiklerinin Mikroyapı Tasarımı", TÜBİTAK-TEYDEB, (Yürütücü: Prof. Dr. Servet Turan) Proje No: No:3040287, (2004-2007).

21. Acikbas, N. C., Kara, F., & Mandal, H. (2009). Development of α-β SiAlON Ceramics From Different Si3N4 Starting Powders. In Key Engineering Materials (Vol. 403, pp. 107-108). Trans Tech Publications.

22. Özcan, S., Açıkbaş, G., Özbay, N., & Açıkbaş, N. Ç. (2017). The effect of silicon nitride powder characteristics on SiAlON microstructures, densification and phase assemblage. *Ceramics International*, *43*(13), 10057-10065.

23. Acikbas, N. C., Kumar, R., Kara, F., Mandal, H., & Basu, B. (2011). Influence of β-Si3N4 particle size and heat treatment on microstructural evolution of α: β-SiAlON ceramics. *Journal of the European Ceramic Society*, *31*(4), 629-635.

24. Acikbas N. Calis and Acikbas. G. (2016). Statistical Evaluation of Repeatability Analyses of SiAlON Production Process. 1072-1081.

25. Petzow, G., & Herrmann, M. (2002). Silicon nitride ceramics. In *High performance non-oxide ceramics II* (pp. 47-167). Springer, Berlin, Heidelberg.

26. Wachtman, J. B., Cannon, W. R., & Matthewson, M. J. (2009). *Mechanical properties of ceramics*. John Wiley & Sons.

27. Kurama, S., Herrmann, M., & Mandal, H. (2002). The effect of processing conditions, amount of additives and composition on the microstructures and mechanical properties of α-SiAlON ceramics. *Journal of the European Ceramic Society*, *22*(1), 109-119.

28. Hoffmann, M. J., & Petzow, G. (Eds.). (2012). *Tailoring of mechanical properties of Si3N4 Ceramics* (Vol. 276). Springer Science & Business Media.

29. Kumar, R., Acikbas, N. C., Kara, F., Mandal, H., & Basu, B. (2009). Microstructure–mechanical properties–wear resistance relationship of SiAlON ceramics. *Metallurgical and Materials Transactions A*, *40*(10), 2319-2332.

30. Acikbas, N. C., & Kara, F. (2017). The effect of z value on intergranular phase crystallization of α1/β1-SiAlON-TiN composites. Journal of the European Ceramic Society, 37(3), 923-930.

31. Ekström, T., & Persson, J. (1990). Hot hardness behavior of yttrium sialon ceramics. *Journal of the American Ceramic Society*, *73*(10), 2834-2838.

32. Fox, K. M., & Hellmann, J. R. (2008). Microstructure and creep behavior of silicon nitride and SiAlONs. *International Journal of Applied Ceramic Technology*, *5*(2), 138-154.

33. CHEN, C., & Tien, T. Y. (1987, January). High temperature mechanical properties of SiAlON ceramics: microstructural effects. In *Ceram. Eng. Sci. Proc.* (Vol. 8, No. 7, pp. 778-795).

34. Uludağ, A., & Turan, D. (2011). High temperature bending creep behavior of a multi-cation doped α/β-SiAlON composite. *Ceramics International*, *37*(3), 921-926.

35. Nickel, K. G. (1997). Corrosion of non-oxide ceramics. *Ceramics international*, *23*(2), 127-133.

36. Nordberg, L. O., Nygren, M., Käll, P. O., & Shen, Z. (1998). Stability and Oxidation Properties of RE-α-Sialon Ceramics (RE= Y, Nd, Sm, Yb). *Journal of the American Ceramic Society*, *81*(6), 1461-1470.

37. Persson, J., & Nygren, M. (1994). The oxidation kinetics of β-sialon ceramics. *Journal of the European Ceramic Society*, *13*(5), 467-484.

38. Deeley, G. G., Herbert, J. M., & Moore, N. C. (1961). Dense silicon nitride. *Powder metallurgy*, *4*(8), 145-151.

39. Kijima, K., & Shirasaki, S. I. (1976). Nitrogen self-diffusion in silicon nitride. *The Journal of Chemical Physics*, *65*(7), 2668-2671.

40. Butler, E., Lumby, R.J., Szweda, A., Lewis, M.H. (1984), Proceedings of the 1st International Symposium on Ceramic Components for Engine", Ed. By Somiya, S., Kanai, E. and Ando, K., 169.

41. Acikbas, N. C., & Demir, O. (2013). The effect of cation type, intergranular phase amount and cation mole ratios on z value and intergranular phase crystallization of SiAlON ceramics. *Ceramics International*, *39*(3), 3249-3259.

42. Acikbas, N. C., Kara, A., Turan, S., Kara, F., Mandal, H., & Bitterlich, B. (2007). Influence of type of cations on intergranular phase crystallisation of SiAlON ceramics. In *Materials science forum* (Vol. 554, pp. 119-122). Trans Tech Publications.

43. Kara, F., Mandal, H., Turan, S., Kara, A. and Calis Acikbas, N., (2008). "Development Strategies for SiAlON Ceramics", 2nd International Congress on Ceramics - ICC2 : A Global Road Map for Ceramic Materials and Technologies - Forecasting the Future, pp.119-128.

44. Becher, P. F., Painter, G. S., Sun, E. Y., Hsueh, C. H., & Lance, M. J. (2000). The importance of amorphous intergranular films in self-reinforced Si3N4 ceramics. *Acta materialia*, *48*(18-19), 4493-4499.

45. Mandal, H., (1992). Heat Treatment of SiAlON Ceramics, Ph.D. Thesis, University of Newcastle Upon Tyne , England.

46. Acikbas, N. C., Yurdakul, H., Mandal, H., Kara, F., Turan, S., Kara, A., & Bitterlich, B. (2012). Effect of sintering conditions and heat treatment on the properties, microstructure and machining performance of α-β-SiAlON ceramics. *Journal of the European Ceramic Society*, *32*(7), 1321-1327.

47. Mandal, H., & Thompson, D. P. (2000). New heat treatment methods for glass removal from silicon nitride and sialon ceramics. *Journal of materials science*, *35*(24), 6285-6292.

48. Hsueh, C., Evans, A. G., Cannon, R. M., & Brook, R. (1986). Viscoelastic stresses and sintering damage in heterogeneous powder compacts. *Acta Metallurgica*, *34*(5), 927-936.

49. Tsuge, A., Nishida, K., & Komatsu, M. (1975). Effect of Crystallizing the Grain-Boundary Glass Phase on the High-Temperature Strength of Hot-Pressed Si3N4 Containing Y2O3. *Journal of the American Ceramic Society*, *58*(7-8), 323-326.

50. Ingelstrom, N., & Ekstrom, T. (1987). Silicon Nitride Made by the Encapsulated HIP Technique. In *Hot Isostatic Pressing- Theories and Applications. Proceedings of the International Conference Lulea, Sweden, 15-16 June 1987,* (pp. 307-314).

51. Gazza, G. E. (1983). Influence of Composition and Process Selection on Densification of silicon Nitride. In *Progress in Nitrogen Ceramics* (pp. 273-282). Springer, Dordrecht.

52. Hirosaki, N., Okada, A., & Mitomo, M. (1990). Effect of oxide addition on the sintering and high-temperature strength of Si 3 N 4 containing Y 2 O 3. *Journal of materials science*, *25*(3), 1872-1876.

53. Kang, S. J. L. (2004). *Sintering: densification, grain growth and microstructure*. Elsevier.

54. Biswas, S. K., & Riley, F. L. (2001). Gas pressure sintering of silicon nitride—current status. *Materials chemistry and physics*, *67*(1-3), 175-179.

55. Shen, Z., & Nygren, M. (2001). Kinetic aspects of superfast consolidation of silicon nitride based ceramics by spark plasma sintering. *Journal of Materials Chemistry*, *11*(1), 204-207.

56. Riley, F. L. (2000). Silicon nitride and related materials. Journal of the American Ceramic Society, 83(2), 245-265.

57. Calis Acikbas , N., Ataman, A. & Acikbas, G. (2019). Production of SiAlON-Graphite Composites with Spark Plasma Sintering, III. International Scientific and Vocational Studies Congress - Engineering Proceeding Book, pp.450-454.

58. Acikbas, N. C. (2018). Tribological behavior of αı/βı-SiAlON-TiN composites. *Journal of the European Ceramic Society*, *38*(5), 2279-2288.

59. Acikbas, N. C., Tegmen, S., Ozcan, S., & Acikbas, G. (2014). Thermal shock behaviour of α: β-SiAlON–TiN composites. *Ceramics International*, *40*(2), 3611-3618.

60. Açıkbaş, G. A & Açıkbaş, N. Ç., (2018). Dependence of SiAlON-TiN composite properties on TiN reinforcement particle sizes. *Anadolu University Journal of Science and Technology A- Applied Sciences and Engineering*, *19*(2), 356-367.

61. Akin, S. R. K., Turan, S., Gencoglu, P., & Mandal, H. (2017). Effect of SiC addition on the thermal diffusivity of SiAlON ceramics. *Ceramics International*, *43*(16), 13469-13474.

62. Vleugels, J., Jiang, D. T., & Van der Biest, O. (2004). Development and characterisation of SiAlON composites with TiB 2, TiN, TiC and TiCN. *Journal of materials science*, *39*(10), 3375-3381.

63. Nordberg, L. O., & Ekström, T. (1995). Hot-Pressed MoSi2-Particulate-Reinforced α-SiAlON Composites. *Journal of the American Ceramic Society*, *78*(3), 797-800.

64. Mallik, A. K., Acikbas, N. C., Kara, F., Mandal, H., & Basu, D. (2012). A comparative study of SiAlON ceramics. *Ceramics International*, *38*(7), 5757-5767.

Chapter 6

ADVANCE OXIDATION PROCESS STUDY OF SUGAR INDUSTRY WASTEWATER WITH CLAY AS A CATALYST

***Şefika KAYA*[1]**
***Yeliz AŞÇI*[2]**

1 Ph.D., Department of Chemical Engineering, Eskisehir Osmangazi University, Eskisehir, Turkey.
2 Prof. Ph.D., Department of Chemical Engineering, Eskisehir Osmangazi University, Eskisehir, Turkey.

1. INTRODUCTION

Water is one of the most important substances for living things to survive. The water necessary for the needs of people is supplied from sources. The water used is given to surface waters or ground. Discharging wastewater to surface waters without any disposal process causes a constantly growing pollution. After the pollution of rivers, lakes and other water sources, this pollution removal causes enormous costs. In some cases, it is impossible to restore the deteriorated natural balance.

Wastewater treatment processes are divided into three groups as physical (screen, sand trap, flotation and sedimentation), chemical (sedimentation, adsorption, disinfection) and biological (activated sludge, trickle filter, biodiscs). Although physicochemical methods (coagulation-flocculation, filtration, adsorption, stripping with air) can be effective, they are not preferred because the pollutant is transferred from one environment to another [1]. Biological treatment cannot provide enough efficiency in removing toxic and persistent organics from waste water. Chemical processes based on advanced oxidation processes are used before biological treatment to remove toxicity and organic load from this type of waste water [2].

Recently, advanced treatment methods known as environmentally friendly are used in the treatment of wastewater by oxidizing waste water that is difficult to biodegrade to a more harmless form (eg carbon dioxide, water and inorganic salts). Advanced oxidation processes are one of these methods. Advanced oxidation processes are those that use hydroxyl radicals (OH•) as primary oxidation types. Hydroxyl radicals are highly reactive and non-selective due to their unpaired electrons. On the basis of advanced oxidation processes, it is based on the formation of small molecules and inorganic ions, as well as the removal of organic pollutants through oxidation reactions with hydroxyl radicals [3, 4].

The heterogeneous Fenton process, one of the advanced oxidation processes, can effectively remove refractory organic materials in water or soil. The heterogeneous Fenton process does not have the disadvantages of the homogeneous Fenton process, such as reduced reactivity due to catalyst consumption and the need for sludge treatment due to pH adjustments. It has become a promising environmentally friendly treatment technology for this reason. The heterogeneous Fenton process stands out among various advanced oxidation processes due to the structural stability and reusability of catalysts, wide pH range, high oxidation efficiency and low operating costs [5].

The sugar industry has an important place in the food industry in terms of the economic development of rural areas. A lot of water is consumed in each unit of the sugar production process and therefore waste water generation is too high [6]. Approximately 1000 L wastewater comes out of 1500-2000 L clean water [7].

Sugar factory wastewater contains various organic and inorganic substances. Organic substances are high in diffusion water and press water, and inorganic substances are more in beet flotation water. Although the wastewater of sugar factories contains inorganic substances, organic substances cause the main pollution. Inorganic substances are removed in settling pools and lagoons established in factories. As most of the organic substances are soluble in water, they go to the receiving environment. Therefore, wastewater from sedimentation ponds must be treated [8].

The wastewater generated contains very little organic and inorganic pollutants as well as a small amount of metals and nutrients [6]. Chemicals used in the production process also contribute to water pollution [9]. Additionally, the presence of nitrogen and phosphorus in the wastewater of the sugar industry causes excessive algae growth in lakes, ponds and streams [10]. In the wastewater of the sugar industry, biological methods are not suitable for systems where persistent organic and inorganic substances will be eliminated. Treatment processes are also slow due to their low treatment efficiency and are generally applied to low capacity plants [11, 12].

In recent years, more effective technologies and methods have come to the fore for the treatment of wastewater containing persistent organic pollutants [13]. In this study, heterogeneous Fenton process was carried out with wastewater taken from Eskişehir Sugar Factory. It is aimed to realize a heterogeneous Fenton process by using clay with high iron content instead of using iron solutions. In this way, it is aimed to prevent the catalytic sludge waste that is generated in large amounts in the classical (homogeneous) Fenton process. In the heterogeneous Fenton process, the reactions are the same as in the Fenton process. The only difference is to use clay with 8-9% iron content as catalyst instead of using iron solutions that will ensure homogeneity. The reason to choose the H_2O_2 used as oxidant in the Fenton process reaction is that its oxidation potential is more oxidizing, easy to find and low in cost compared to other oxidant substances.

2. MATERIALS AND METHOD

2.1. Materials

In this study the wastewater used were obtained from Eskisehir Sugar Factory operating in Turkey. The color of the wastewater used is black and its pH value is 7.3. The black color of the wastewater is generally due to the formation of various sulphides, especially iron sulfur [14]. Clay was used as a catalyst in the heterogeneous Fenton process experiments. The clay used in this study were obtained from a tile factory operating in Eskisehir in Turkey. Iron ratio of clay purchased from tile factory is around 8-9%. It is aimed to prevent the formation of solid waste sludge by using solid catalysts instead of iron solution in Fenton process.

2.2. Heterogeneous Fenton experiments

In the heterogeneous Fenton experiments, 100 ml of wastewater was taken into 250 ml glass flasks. The pH value of the wastewater sample was adjusted using 2M H_2SO_4 and 2M NaOH solutions. The desired amount of clay was added to the wastewater sample as a catalyst. Experiments were carried out in a water bath shaken at constant temperature for a predetermined period of time, with the last hydrogen peroxide solution added to the sample. After the experiments were completed, the reaction was stopped by adding 2M NaOH to the sample. Then, a clear solution was taken and color analysis was performed.

3. RESULTS AND DISCUSSIONS

3.1. Effect of the pH

For the optimal pH selection in the Heterogeneous Fenton process, studies at 5 different pH values were carried out. In order to determine the optimum pH value, the values of 2g clay and 200 ppm H_2O_2 solution were kept constant and they were studied in a shaking water bath at 30^{o}C for 120 minutes. The experimental results obtained were given in Figure 1.

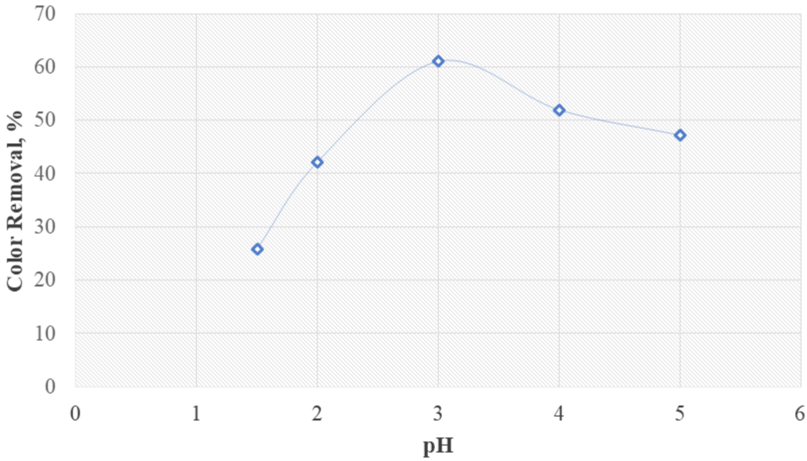

Figure 1. *The effect pH on heterogenous Fenton proces (H_2O_2=200 ppm, amount of clay 2g, temperature 30°C, time 2 hours).*

pH is an important parameter in oxidation processes. At very low pH values, the reaction of iron ion and H_2O_2 can be inhibited. The decrease in yield with increasing pH is explained by the loss of catalytic activity by the conversion of Fe(II) to Fe(III) colloids. When pH is higher than 3.5, Fe(II) ions are unstable, so the iron ion starts to precipitate as $Fe(OH)_3$ easily [15]. According to experimental results, optimum pH was determined as 3.

3.2. Effect of the amount of clay

In order to determine the optimum catalyst amount, 6 different catalyst amounts such as 0.5; 1; 2; 3; 4; 5 g were studied. In the study, by keeping the pH constant at 3, different amounts of catalysts were added and kept in a shaking water bath at 30°C for 120 minutes.

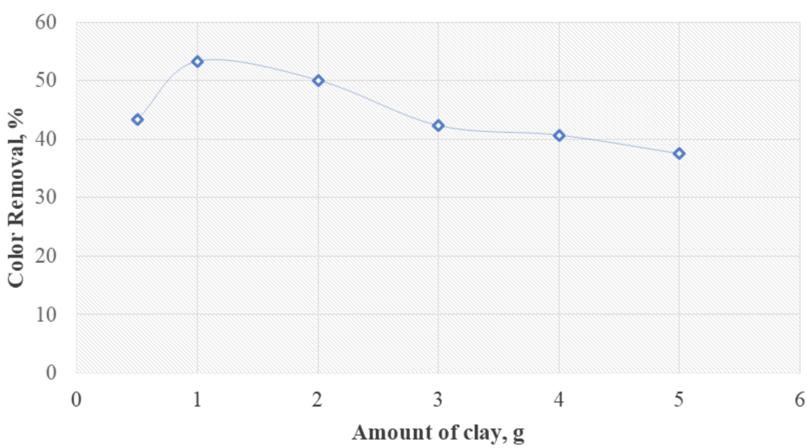

Figure 2. *The effect the amount of clay on heterogenous Fenton proces (pH=3, H_2O_2=200 ppm, temperature 30°C, time 2 hours).*

In our study, the optimum amount of clay for the heterogeneous Fenton process was determined to be 1 g, since it would be more advantageous in terms of both high color removal efficiency and economically. In the case of low concentrations of iron ions, fewer hydroxyl radicals form in the environment and no effective reaction occurs. High iron ion concentration has a negative effect on the pollution value of the wastewater [16]. In addition, it has been stated that if the iron ion concentration is above a certain ratio, the rate of disintegration will slow down, and the amount of suspended iron at the exit of the process will be high due to the use of excess iron ions [2].

3.3. Effect of the hydrogen peroxide concentration

By keeping pH (3), catalyst amount (1g), temperature (30°C) and reaction time (120 min) constant, working with 7 different ppm values in the range of 25-400 ppm, the effect of the hydrogen peroxide concentration was investigated.

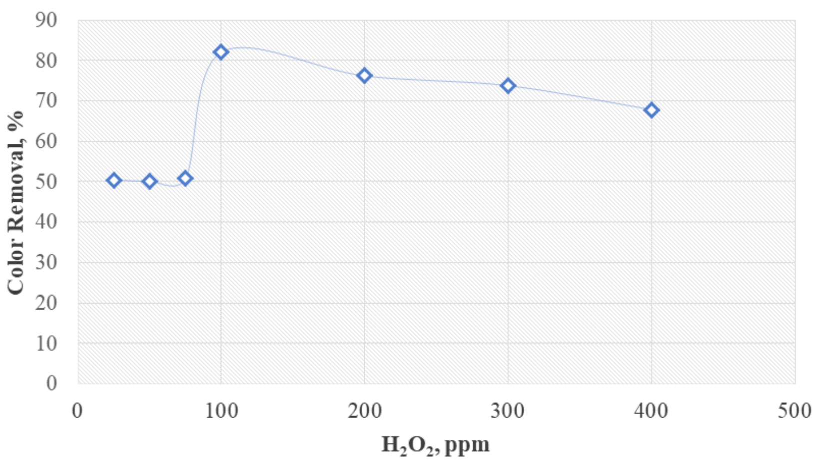

Figure 3. *The effect the hydrogen peroxide concentration on heterogenous Fenton proces (pH=3, amount of clay 1g, temperature 30°C, time 2 hours).*

According to the experimental results, 100 ppm H_2O_2 concentration at which the highest color removal efficiency was obtained was determined as the optimum value. The hydrogen peroxide concentration plays an important role in deciding the overall efficiency of the decomposition process. Generally, it has been observed that the treatment efficiency of wastewater increases with the increase in hydrogen peroxide concentration [17]. However, care must be taken when determining the hydrogen peroxide concentration to be studied. Hydrogen peroxide not used during the Fenton process contributes as a contaminant and is therefore not recommended in excess [18]. Therefore, the concentration of hydrogen peroxide should be adjusted so that the full amount is used.

3.5. Effect of the temperature and reaction time

In order to determine the optimum temperature value, pH (3), catalyst amount (1g) and hydrogen peroxide concentration (100 ppm) were kept constant and studied at 20 and 30°C. In order to determine the optimum reactin time value, 4 values between 5-120 minutes were studied at two temperature values (20 and 30°C).

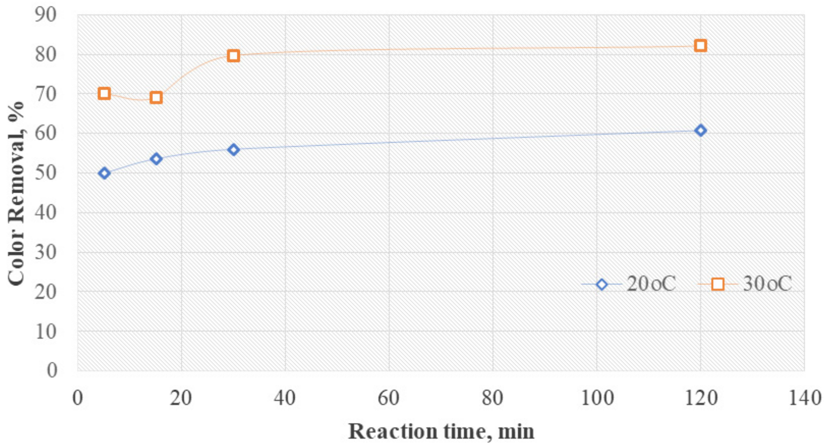

Figure 4. *The effect the temperature and reaction time on heterogenous Fenton proces (pH=3, amount of clay 1g, H_2O_2=100 ppm).*

The optimum temperature range of advanced oxidation processes is reported as 20-40°C. When the temperature is above 50°C, hydrogen peroxide spontaneously decomposes into H_2O and O_2. This situation causes a decrease in the oxidation efficiency. If the temperature is below 20°C, it slows down chemical reactions [19, 20]. As seen in Figure 4, the highest color removal efficiency was obtained at 30°C.

When the effect of reaction time on color removal was examined, the optimum point was chosen as 30 minutes, where the color removal was maximum. The maximum color removal this minute was 80%. When the Figure 4 was examined, it was observed that the color removal increased until the optimum reaction time and then almost remained constant.

4. CONCLUSION

In the study, removal of color of sugar industry wastewater was carried out by the heterogeneous Fenton process. The clay with 8-9% iron content was used as a catalyst in experimental studies. Optimum working points were determined by examining the color removal efficiencies with the heterogeneous Fenton process.

The effects of parameters such as pH, catalyst amount, hydrogen peroxide concentration, temperature and reaction time on the heterogeneous Fenton process were investigated. In this context, the parameters of pH (1.5-5), catalyst amount (0.5-5 g), H_2O_2 concentration (25-400 ppm), temperature (20 and 30°C) and time (5-120 minutes) were studied and the optimum value of each parameter was found. As a result of the experiments, optimum conditions were determined as pH 3, catalyst amount 1g, temperature 30°C, H_2O_2 concentration 100 ppm and reaction time 30 minutes.

In the literature studies, it is seen that the best removal for the Fenton process takes place under acidic conditions and the optimum temperature values are between 20-40°C. When the studies on Fenton process are examined, it is seen that the optimum pH value is mostly 3. The temperature is generally 30°C. Since the amount of clay can vary according to the iron content, it was decided that 1 gram of clay was appropriate considering the cost and literature researches. The duration varies according to the concentration and pollution of the initial wastewater, as in the studies examined.

The heterogeneous Fenton process, which is among the advanced oxidation processes, was chosen as the method to be applied because it is of great importance in terms of low cost, high color removal efficiency and hydroxyl radical generation.

REFERENCES

Çokay, E., Şengül, F., 2006, Treatment of Toxic Pollutants by Advanced Oxidation Processes, Dokuz Eylül University Faculty of Engineering Science and Engineering Journal, 8, 2, 1-9.

Gürtekin, E., Şekerdağ, N., 2008, An Advanced Oxidation Process: Fenton Process, Pamukkale University Engineering Faculty Journal of Engineering Sciences, 14, 230-234.

Legrini, O., Oliveros E., Braun A. M., 1993, Photochemical Processes For Water Treatment, Chem Rev., 93, 671-698.

Bolton, J.R., K.G., Bırcher, W. Tumas, C.A., Tolman, 2001, Figures Of Merit For The Technical Development And Application Of Advanced Oxidation Technologies For Both Electric And Solar Driven Systems, Pure Appl. Chem. 73, 4, 627-637.

Wang, D., Men, B., Yang, X., He, J., 2016, Interfacial Mechanisms Of Heterogeneous Fenton Reactionscatalyzed By İron-Based Materials: A Review, Journal Of Environment Science, 39, 97-109.

Ewa, E.E. Iwara, A.I., Adeyemi, J.A., Eja, E.I., Ajake, A.O. and Otu, C.A., 2011, Impact of industrial activities on water quality of Omoku Creek Sacha, Journal of Environmental Studies, 1. 8-16.

Asaithambi, P., Matheswaran, M., 2016, Electrochemical Treatment Of Simulated Sugar İndustrial Effluent: Optimisation And Modeling Using A Response Surface Methodology, Arabian Journal Chemistry, 988-999.

Bodakçi, H., 2015, Determination of Ideal Conditions for Treatment of Sugar Beet and Organic Wastewater and Purification of Brine Solution by Electrocoagulation Method, Ankara University, Master's Thesis.

Qureshi, A.L., Mahessar, A.A., Leghari, M.E., Lashari, B.K., Mari, F.M., 2015, Impact Of Releasing Wastewater Of Sugar İndustries İnto Drainage System Of Lbod Sindh, International Journal Of Environment Science Development, 6, 5, 381-386.

Sahu, O., 2019, Electro-Oxidation And Chemical Oxidation Treatment Of Sugar İndustrywastewater With Ferrous Material: An İnvestigation Of Physicochemical Characteristic Of Sludge, South African Journal Of Chemical Engineering, 28, 26-38.

Santhanakrishnan, T., Emelda, E.J., 2013, Effluent Treatment In Sugar Industry Waste Using Brine Shrimp, International Journal Of Advanced Life Sciences, 6, 5, 459-463.

Tchamango, S., Nanseu-Njiki, Ngameni, C.P., Hadjiev, E.D., Darchen A., 2010, Treatment Of Dairy Effluents By Electrocoagulation Using Aluminium Electrodes, Science Total Environment, 408, 947-952.

Moreira, F.C., Boaventura, R.A.R., Brillas, E. and Vilar, V.J.P., 2017, Electrochemical advanced oxidation processes: A review on their application to synthetic and real wastewaters, Applied Catalysis B: Environmental, 217–261.

Poddar, P.K., Sahu, O., 2017, Quality And Management Of Wastewater In Sugar Industry, Appl Water Sci 7, 461–468.

Neyens, E., Baeyens, J., 2003, A Review Of Classic Fenton's Peroxidation As An Advanced Oxidation Technique, Journal Of Hazardous Materials, B98, 33-50.

Chan, K., Chu, W., 2003, The dose and ratio effects of Fe(II) and H_2O_2 in Fenton's process on the removal of atrazine, Environmental Technology, 24, 703-710.

Kang, Y.W., Hwang, K.Y., 2000, Effects of Reaction Conditions on the Oxidation Efficiency in the Fenton Process, Water Res., 34, 2786–2790.

Lin, S.H., Lo, C.C., 1997, Fenton Process for Treatment of Desizing Wastewater, Water Res., 31, 2050–2056.

Duman, E., 2006, Investigation of the Purification of Pharmaceutical Industry Wastewater by Fenton Oxidation, Hacettepe University, Master's Thesis.

Aytaç, E., 2013, Oxidatıon of Aqueous Bisphenol A with the Fenton's Reagent: The Effects of Operatıng Parameters on Process Performance and Toxicity Evaluations, M.Sc. Thesis, Istanbul Technical University, 161.

Chapter 7

THE ENVIRONMENTAL PERFORMANCE EVALUATION OF OECD COUNTRIES THROUGH DATA ENVELOPMENT ANALYSIS

***Irmak TEMIZ*[1]**

***Yeliz BURUK SAHIN*[2]**

***Ezgi AKTAR DEMİRTAS*[3]**

1 Yüksek Mühendis, Eskisehir Osmangazi University, Department of Industrial Engineering, irmak.cicek1988@gmail.com

2 Dr. Öğr. Üyesi, Eskisehir Osmangazi University, Department of Industrial Engineering, yelizburuk@ogu.edu.tr

3 Prof Dr., Eskisehir Osmangazi University, Department of Industrial Engineering, eaktar@ogu.edu.tr

1. INTRODUCTION

The humanity has passed through several societal development stages as hunter-gatherer, agricultural, industrial and now is experiencing knowledge age and these stages have brought along the transformation from manufacturing/producing into consuming. Along with increasing population, the consumer society has come across with overconsumption and environmental hazards. Such problems as global warming, drought, climate change, decreasing supply of drinking water, and air pollution has come to a serious extent and have started to threaten all the mankind. This serious increase has made it necessary to take immediate action against environmental problems and initiate environmental protection measures. With the aim of creating a sustainable society, the governments are obliged to create and apply policies that will make a balance between economic development and environment protection. From the sustainability aspect, environmental assessments have an increasing significance and constitute the first and foremost step of policies related to green environment of countries.

For these reasons, the fact that countries specify their place in terms of environmental performance relative to others' is of much significance with regard to designating the reasons of being inefficient of under-performing countries, building environmental friendly strategies, and creating new policies. Along with rising significance of environmental protection, the use of Data Envelopment Analysis (DEA) has also increased within environment performance evaluations. DEA is based on linear programming and is a nonparametric method which aims to evaluate the relative efficiency of decision-making units. Different from parametric methods, it does not necessitate the functions correlating inputs and outputs (Hosseinzadeh-Bandbafha et al., 2018). DEA is particularly used in cases where multiple inputs and outputs could not be transformed into weighted input and output sets and is firstly used by Charnes et al. (1978) to measure the efficiency of state schools in the United States. DEA then has been used to evaluate the efficiency of universities, hospitals, banks, and firms in manufacturing sector and also to compare the efficiency of resource utilisation of countries and regions (Eva et al., 2016; Omrani et al., 2018; Dobos and Vörösmarty, 2019). No subjective comments are needed for the weights of utilised resources and emissions within the environment performance evaluations made through DEA since the weights are objectively determined by the model itself.

Another important point while evaluating the environment performance is that the inputs and outputs should be compatible with the targets of evaluated Decision Making Units (DMUs). While the variables are constituted by only inputs and outputs while making efficiency analysis through the DEA, there are inputs and two-group output variables during the environmental performance evaluation. "The outputs aimed to be achieved" as a result of used inputs during the production indicate the desired output while the environment-polluting outputs (wastes released into the air, water and soil, emissions, etc.) indicate undesirable outputs (Wang and Zhao, 2017).

Sueyoshi and Goto (2011) have presented a new DEA method combining operational and environmental efficiency analyses in which outputs are classified as desired and undesirable. This proposed technique has been applied on Japanese electricity distribution companies. With the aim of evaluating the energy and environmental efficiency of electricity distribution companies in 30 different regions in Japan between 1997 and 2010, Wang et al. (2013) have made use of multi-directional efficiency analysis and window analysis. Sueyoshi and Goto (2013) have combined DEA with Malmquist index in order to evaluate the environmental efficiency of 10 OECD (Organisation for Economic Co-operation and Development) countries. With the aim of measuring the environmental performance, Meng et al. (2013) have put forward a radial DEA approach composed of a static and dynamic environmental performance index value. This method was first used to build an environmental performance model between 1998 and 2009 for industrial organisations in different Chinese cities. Zhang et al. (2015) evaluated the ecological energy efficiency of China between 2001 and 2010. The results of all these studies have indicated that the Chinese government should immediately intensify its improvement efforts in central and western regions to maintain a sustainable development. Sözen and Karık (2017) have compared the renewable energy performances of 33 OECD and BRICS countries with those of Turkey between 2009 and 2013. Within this study in which they have formed two different models based on different inputs and outputs, they have carried out analyses to determine the efficiency scores in the course of time and technical enhancements through DEA and Malmquist Productivity Index (MPI). Mavi and Mavi (2019) have measured the energy and environmental efficiencies of OECD countries through DEA and analysed environmental performances via MPI. Besides, they have developed the model of common set of weights by using ideal point method.

The studies carried out to measure environmental performance has been presented in Table 1 by considering their input, desired output, undesirable output and the methods. When these studies are examined, it has been observed that the most common inputs and outputs while analysing the environmental performances are population, the consumption of fossil and non-fossil fuels, CO_2, SO_2, and NO_2 emissions, workforce, water and energy amounts, waste water and solid waste amounts, gross national domestic product, capital, and electricity consumption.

Table 1 *Literature Review*

Reference	Input	Output	Undesired Output	Methodology/ Approach
Guo et al. (2011)	Capital stock, Labour, Energy	Gross domestic product (GDP)	CO_2 emission	Environmental DEA model
Sueyoshi and Goto (2011)	Total assets, , # Employees	Total sales, # Customers	CO_2 emission	Range-Adjusted Measure, DEA
Wu et al. (2012)	Capital stock, Labour, Energy	Industrial value added	CO_2 emission	Dynamic energy performance index, DEA
Wang et al. (2013)	Energy, Labour, Capital stock	GDP	CO_2 emission	A multi-directional efficiency analysis and window analysis
Sueyoshi and Goto (2013)	Combustible, Nuclear, Hydro+renewable	Electricity	CO_2 emission	DEA, Malmquist index
Lin et al. (2013)	Labour, Capital, Energy	GDP	CO_2 emission	DEA, A directional distance function metafrontier approach
Meng et al. (2013)	Labour force, Energy	Industrial value added	CO_2 emission, Waste gas, Waste water, Solid waste	Non-radial DEA, static and a dynamic environmental performance index
Chen et al. (2014)	Energy, Social fixed assets investment	GDP	Raffle of waste water, solid, and gas	Linear monotonic decreasing trans-formation approach, DEA
Wu et al. (2014)	Investment in fixed assets, electricity	GDP	NO_2	Slacks-based measure
Zhang et al. (2015)	Capital, Labour, Energy	GDP	SO_2 emission, CO_2 emission chemical oxygen demand	A metafrontier slack-based efficiency measure approach
Wang et al. (2016)	Energy, Labour, Capital, R&D investment, IPC investment	Industrial value added	$CO_{2,}$ SO_2, solid emissions, waste water emissions	A non-radial DEA mode
Sözen and Karık (2017)	Electricity capacity, Energy supply Energy consumption, Energy production, Electricity consumption, Labour force/ population, Net capital account	Hydro capacity, Geothermal capacity, Solar photovoltaic capacity, Wind capacity, Electricity production from hydro, geothermal, solar photovoltaic, wind	-	DEA, Malmquist productivity index (MPI)
Yao et al. (2018)	Capital, Labour, Water, Energy	GDP	Solid, water, gas	SBM DEA
Mavi and Mavi (2019)	Labour, Energy	GDP, Renewable energy	Greenhouse gas emission, Municipal waste	Common weight analysis for MPI

Ouyang and Yang (2020)	Income, population, government spending, coal consumption, oil consumption, natural gas consumption, land	GDP, human development index, consumption	CO_2 emissions	A multiplicative network DEA

The purpose of this study is to analyse the environmental performance of OECD countries, specify the place of Turkey among these countries and propose some recommendations regarding to improve the current performance of Turkey. Since multiple input and output variables have been included, DEA method has been used after considering the advantages mentioned above. The distinctive feature of this study comes from the fact that the analyses and evaluations of environmental performances of countries have been carried out through input and output oriented CCR models with the assumption of constant returns to scale by dealing with such variables the first time as environmental tax and electricity production from renewable energy sources. Super efficiency model has been used to specify efficient countries in terms of environmental performance. Besides, window analysis has been used to make an evaluation in terms of time course. Lastly, the efficiency change between years has been measure through Malmquist TFP index.

2. MATERIALS AND METHODS

DEA has firstly been developed by Charnes et al. (1978) with the aim of measuring the relative efficiency of systems called DMUs manufacturing/producing similar products or services. This method allows measuring the relative total factor efficiency of DMUs in cases which there are many input and output variables having different units of measure and when they cannot be demeaned into a common criterion. DEA compares each of DMUs only with the best DMUs. Identified as the best, these DMUs comprises the efficient frontier and they constitute the benchmark with which any other DMUs will be measured against. The method assumes that the DMUs on the efficient frontier are relatively efficient. These are called reference sets of inefficient DMUs.

2.1. Input-Output Selection

Identifying the input and output variables used for determining DMUs and their efficiency in DEA is of significance in terms of the fact that the analysis will yield correct results. Using different input and output sets may cause changes within the efficiency value of DMUs. If an important variable is skipped within the model, the efficiency value of DMU actively using this variable will decrease. For this reason, the input and output variables to be used during the analysis should be cautiously and meticulously determined. The fact that redundant number of inputs and outputs are used within the model negatively affect the distinction power of the analysis. Therefore, the optimum number of inputs and outputs should be used in line with the purpose of the study. If there are many inputs and outputs, then the number of DMUs should be increased, as well.

If the number of selected input is (m) and output is (s) in a DEA model, it is compulsory for the reliability of the research to have at least 3*(m+s) + 1 decision making unit. According to Sherman (1984), the optimum number of decision making unit is n>m+s while n=number of observations, m=number of inputs, and s=number of outputs. The general view about this issue is that the number of DMUs should be at least twice as many as the number of inputs and outputs.

Since some of the outputs within the study are undesirable, the approaches related to this situation have been examined as well. Dyckhoff and Allen (2001) indicate three basic approaches for modelling undesirable outputs. In the first method, undesirable outputs of DEA are modelled as f (y) = 1 /y.

In his method, Rheinhard et al. (1999) have modelled undesirable outputs as inputs. As indicated by Scheel (2001), undesirable outputs could be considered as inputs. This transformation could be used with both the assumptions of constant returns to scale and variable returns to scale. The third approach could be used with only the assumption of variable returns to scale. The conversion of $f(y) = -y + \beta_i$ is used for undesirable outputs along with the use of transformation. In order to get rid of negative values, a positive β_i scalar having enough greatness should be added onto the undesirable output (Ali and Seiford, 1990). This study has adopted the first approach and has applied inverse function method for undesirable outputs.

2.2. **Model Selection**

It is possible to use both the assumptions of constant returns to scale (CRS) and variable returns to scale (VRS) in DEA. The CCR model measures the total efficiency with the assumption of CRS while BCC model measures the technical efficiency with the assumption of VRS. What kind of model should be set up depends on whether the inputs and outputs are controlled or not. The input oriented models examine the extent of decrease of inputs while the outputs are held at a certain level; however, the output oriented models examine the extent of increase of outputs while the inputs are constant at a certain level (Malana and Malano, 2006; Aldamak and Zolfaghari, 2017). In other words, the main aim of input oriented models is to use minimum number of inputs to produce the current output while the main aim of output oriented models is to reach the maximum number of outputs with the current input. An output oriented model should be set up if there is less or much control over the inputs and an input oriented model should be established if there is less or much control over the outputs. This study has made use of input and output oriented CCR models whose details are provided in the following parts.

Input Oriented CCR Model

In a process having n DMUs, n models are set up and the relative efficiency of each DMU is measured. n optimisation models are solved within this process. The objective function of models, for example for the DMU_k, coincides with the optimisation of ratio between the total weighted output and total weighted input (Cooper et al., 2011).

To maximize the efficiency of DMU k, the objective function and the constraints of the linearized input oriented CCR model is shown in Equation (1-4):

m: the number of input

s: the number of output

v_i: the weight of input i

X_{ik}: the amount of input i used by DMU_k

u_r: the weight of output r for DMU_k

Y_{rk}: the amount of output r produced by DMU_k

Y_{rj}: the amount of output r produced by DMU_j

X_{ij}: the amount of input i used by DMU_j

$\mathcal{E}$: very small positive integer.

$$E_k = \max\left(\sum_{r=1}^{s} u_r Y_{rk}\right) \tag{1}$$

$$\sum_{i=1}^{m} v_i X_{ik} = 1 \tag{2}$$

$$\left(\sum_{r=1}^{s} u_r Y_{rj}\right) - \left(\sum_{i=1}^{m} v_i X_{ij}\right) \leq 0 \quad \forall\, j = 1,..,n \tag{3}$$

$$u_r, v_i \geq \mathcal{E} \geq 0 \qquad i = 1, \dots, m \qquad r = 1, \dots, s \tag{4}$$

The data obtained through the solution of the model is the efficiency value of DMU_k (E_k). The fact that the value of efficiency is equal to 1 means that the DMU is efficient while the value less than 1 means the DMU is inefficient. Alternatively called envelopment model, the dual form could also be used within analyses.

Output Oriented CCR Model

To minimize the efficiency of DMU k, the objective function and the constraints of the linearized output oriented CCR model is shown in Equation (5-8).

$$E_k = \min\left(\sum_{r=1}^{m} v_i X_{ik}\right) \tag{5}$$

$$\sum_{r=1}^{p} u_r Y_{rk} = 1 \tag{6}$$

$$\left(\sum_{r=1}^{p} u_r Y_{rj}\right) - \left(\sum_{i=1}^{m} v_i X_{ij}\right) \geq 0 \qquad \forall\, j = 1, .., n \tag{7}$$

$$u_r, v_i \geq \varepsilon \geq 0 \qquad i = 1, \ldots, m \qquad r = 1, \ldots, s \tag{8}$$

While input/output oriented models give information about efficient and inefficient DMUs, they do not provide any information about the ranking of these units. Developed by Anderson and Petersen (1993), the super efficiency model particularly aims to solve this problem and enables ranking decision making units by making a comparison between them. Within this model, each of the efficient DMUs is excluded from efficient production frontier and their super efficiency scores are obtained by calculating the distance of each excluded DMU to the re-defined efficiency frontier. When each of the decision making units is ranked in an ascending sort in terms of their super efficiency score, the superiority relationship between them could be observed. Except the feature of being able to exclude the evaluated DMUs from the reference set, the super efficiency model is equal to dual CCR-DEA.

2.3. Window Analysis

Incorporating the time dimension into the DEA, the window analysis was developed by Charnes, Clark, Cooper and Golany in 1985. The window analysis is based on moving averages method and evaluates the performance of DMUs in a course of time by assuming them as a different unit in each period. This method increases the distinction power of the analysis by increasing the number of DMUs (Halkos and Tzeremes, 2009). However, it is worth noting that while DMUs from a specific period are evaluated relative to each other and themselves, it is assumed that no technological developments have been experienced during this period. Therefore, the analyses made during periods when there are little technological developments yield to more reliable results thanks to using short time periods.

When a series of N (n = 1, ... N) DMUs in a T (t = 1, ... T) time period is considered, on condition that r is the number of inputs and s is the number of outputs in each DMU, DMU nt indicates n observation within t time through input vector $(x_n^{1t}, x_n^{2t}, \ldots\ldots, x_n^{rt})$ and output vector $y_n^t = (y_n^{1t}, y_n^{2t}, \ldots\ldots, y_n^{st})$. Assuming that the window has started on the k time point (1≤k≤T) and the window width is w (1≤w≤T-k), then the input (X_{kw}) and output (Y_{kw}) matrix of each window (kw) is as shown in Equation (9-10) (Yang and Chang, 2009):

$$X_{kw} = (x_1^k, x_2^k, \ldots\ldots, x_N^k, x_1^{k+1}, x_2^{k+1}, \ldots\ldots, x_N^{k+1}, \ldots\ldots, x_1^{k+w}, x_2^{k+w}, \ldots\ldots, x_N^{k+w}) \quad (9)$$

$$Y_{kw} = (y_1^k, y_2^k, \ldots\ldots, y_N^k, y_1^{k+1}, y_2^{k+1}, \ldots\ldots, y_N^{k+1}, \ldots\ldots, y_1^{k+w}, y_2^{k+w}, \ldots\ldots, y_N^{k+w}) \quad (10)$$

The number of DMU, time period and window size are the concepts used in the analysis. The time period indicates the number of periods during which DMU will be examined. The window size could be identified by the researcher with regard to the number of data. For the advantages and disadvantages of narrow-wide window sizes, please refer Cooper et al. (2011).

2.4 Malmquist Total Factor Productivity (TFP) Index

Malmquist TFP index is used for measuring the extent and reasons of development of productivity in a course of time by using panel data. Developed by Malmquist (1953) with regard to distance functions, this index measures the change of TFP between two points by calculating the relative distance of each data point to common technology. The distance functions could be treated as input-output oriented (Deliktas, 2002). The Malmquist TFP index calculated with regard to distance functions with the assumption of constant returns to scale has been given in Formula 11. Within this index, (t) indicates the base year while (t+1) represents the following year.

$$M_0(x^{t+1}, y^{t+1}, x^t, y^t) = \overbrace{\frac{D_0^{t+1}(x^{t+1}, y^{t+1})}{D_0^t(x^t, y^t)}}^{Efficiency\ Change} \times \overbrace{\left[\left(\frac{D_0^t(x^{t+1}, y^{t+1})}{D_0^{t+1}(x^{t+1}, y^{t+1})}\right)\left(\frac{D_0^t(x^t, y^t)}{D_0^{t+1}(x^t, y^t)}\right)\right]^{1/2}}^{Technological\ Change} \quad (11)$$

The ratio out of the square brackets within the Formula (11) measures the change in technical efficiency between the years of (t) and (t+1) in terms of output-oriented approach. The change of efficiency (EC) is the ratio of technical efficiency during (t+1) period to that of (t) period. The geometric mean of the two ratios in the square brackets indicates the change of technology (TC) (x_{t+1} and x_t) occurred between the two periods. The change in the technical efficiency represents the catch-up effect related to production frontier while the technological change could be expressed as frontier shift (Mahadevan, 2002). The fact that M_0 index is greater than 1 means that the total factor productivity has increased within the period between (t) and (t+1) while a value of less than 1 means the total factor productivity has decreased within the same period (Coelli et al., 2005).

3. RESULTS AND DISCUSSION

The inputs used within this study in order to measure efficiency are **the amount of energy consumption (EC)** and **the number of labours (L)**. However, the increase in the energy consumption brings along the environmental problems. The emissions resulting from energy consumption causes water, air, and soil pollution and therefore, negatively affects the nature, human health, and bio-diversity. This relationship between energy and environment renders energy as an important factor of environmental performance evaluations. The amount of energy consumed in a year to produce electricity has been provided in a unit equivalent to a million-ton petroleum (mtoe) (an mtoe is equivalent of 4.1868x1016 Joules). The data has been obtained from the website of www.bp.com. The number of labours of OECD countries has been used as the input variable and these data have been obtained from www.oecd.org.

The outputs used to measure the efficiency and the details about the compilation of data have been provided in the following paragraphs.

- **CO_2 emissions:** The main sources of carbon dioxide emissions are electricity production through fossil fuels, industrial activities, settlements and transportation sector. However, 80-85 % of carbon dioxide released into the atmosphere comes from the burning of fossil fuels (petroleum and its derivatives, coal and natural gas). The climate change caused by greenhouse gas emissions is the biggest problem that humanity has ever come across. CO_2 emissions are the most released gas into the atmosphere and have the biggest responsibility in causing global warming and climate change. The burning of solid, liquid and gas fuels results in CO_2 emissions released into the atmosphere. The data measured as metric tonnes per capita has been obtained from http://data.worldbank.org. The emission data used as undesirable output has been applied inverse function method.

- **Combustible renewable waste (CRW):** The combustible and renewable wastes which measured as a percentage of the total energy consumption are composed of solid biomass, liquid biomass, biogas, industrial and municipal wastes and these wastes are used for energy production in several ways. Therefore, both the wastes are utilised and energy is produced. The data has been obtained from http://data.worldbank.org.

- **Electricity generation from renewable sources (EG-RNW):** Except from hydroelectric, this concept includes generation of electricity from such sources and methods as geothermal, sun, tides, winds, biomasses, and biofuels. The data has been expressed as the total percentage of energy and obtained from http://data.worldbank.org.

- **Gross Domestic Product:** The relationship between GDP and environmental pollution is explained by Environmental Kuznets Curve (EKC). According to the EKC hypothesis, while the environmental pollution increases during the first years of economic growth, the pollution decreases in the following years. Again, with regards to this hypothesis, since the production is mainly based on agricultural-activities in developing countries, the environmental pollution is not observed; however, during the first years of industrialisation, the primary aim is to increase the production and income. Therefore, rapid consumption of natural resources and utilisation of dirty technologies bring along the increase in both the production activities and environmental pollution, though. When the country reaches to a certain extent of income, the awareness of people and the activities of environmental organisations will increase the demand for a cleaner environment and therefore, the use of clean technologies will spread throughout the country. For these reasons, GDP which is an important indicator of economic growth is also one of the important indicators of environmental performance measurements. The data has been recorded in billion dollars and obtained from https://www.iea.org.

- **NOx (nitrogen oxide) and SOx (sulphur oxide) emissions:** Other air pollutants seriously harming the ecosystem and human health are NO_x and SO_x. The NOx emissions are the end product of every burning process and the majority of SOx emissions results from fossil power plants using large amounts of sulphurous solid and liquid fuels. Indicating the total emission amount per capita in metric tonnes, the data has been obtained from www.oecd.org.

- **Environmental Tax Revenue (ETR):** The purpose of environmental taxes is to decrease the economic activities directly or indirectly polluting the environment and encourage environmental friendly production and consumption methods. Environmental taxes are important tools for governments in terms of determining the relative prices of products and services. The environmental tax revenues indicated as % of GDP have been assumed as one of the important outputs. The data has been obtained from www.oecd.org.

Due to the reasons mentioned above and different from other studies in the literature, environmental taxes and electricity generation from renewable resources have been utilised as output variables within the study.

The data of 28 countries has been analysed in terms of output oriented

CCR model through the academic version of EMS 1.3 software and the efficiency scores (Column 3) and peers and peer weights for inefficient countries (Column 4) have been provided in Table 2. Statements out of brackets within benchmark column indicate the number of reference country (peer) while the statements in the brackets indicate peer weights, dual variables in other words, used to determine the target value of the related country.

Table 2 *Efficiency Scores and Benchmarks of OECD Countries*

No	Country	Score	Benchmarks (peers and peer weights)
1	Austria	111.41%	4 (0.82) 10 (0.24) 27 (0.55) 28 (0.03)
2	Belgium	114.78%	10 (0.83) 27 (1.25)
3	Canada	141.74%	10 (7.03)
4	Denmark	100.00%	
5	France	122.60%	10 (1.74) 27 (11.45)
6	Germany	123.25%	10 (1.56) 27 (17.48)
7	Greece	158.45%	4 (0.16) 27 (1.71)
8	Italy	114.58%	27 (10.72)
9	Nthrlds	120.51%	10 (0.84) 27 (3.07)
10	Norway	100.00%	
11	Portugal	115.33%	4 (0.45) 20 (0.71) 27 (0.19)
12	Spain	144.52%	27 (9.65)
13	Sweden	118.42%	4 (1.08) 10 (0.61) 27 (0.17)
14	Turkey	113.97%	27 (8.95)
15	United Kingdom	121.37%	27 (13.77)
16	United States	104.69%	10 (44.86) 27 (15.69)
17	Australia	121.86%	10 (1.88) 27 (3.32)
18	Czech Republic	174.04%	4 (0.29) 10 (0.24) 27 (1.77)
19	Finland	100.00%	
20	Hungary	100.00%	
21	Japan	148.38%	10 (1.12) 27 (29.23)
22	New Zealand	119.84%	4 (0.13) 24 (0.01) 27 (0.95)
23	Poland	160.74%	27 (6.74)
24	Slovak Republic	100.00%	
25	Chile	168.65%	4 (1.37) 24 (0.14) 27 (0.68)
26	Israel	102.10%	10 (0.02) 27 (1.73)
27	Ireland	100.00%	
28	Switzerland	100.00%	

As observed in Table 2, DMUs having 1 point are efficient while those having more than 1 point are inefficient. According to the data of last one year, of 28 countries, 7 are efficient and 21 are inefficient. Denmark, Norway, Finland, Hungary, Slovakia, Ireland, and Switzerland are efficient countries. The efficiency average of all countries has been measured as 122.19%.

21 countries have been found as inefficient with regard to environmental performance. Among efficient countries, Denmark has been the reference point of 7 countries while Norway, Hungary, Slovakia, Ireland and Switzerland have been the reference point of 12, 1, 2, 20 and 1 countries, respectively. Finland has not been referred by any country.

The method of target values related to outputs of inefficient countries has been sampled for Turkey and it has been concluded that Turkey, with a score of 113.97%, is an inefficient DMU. In order to take place among the efficient countries, Turkey whose target values have been given in Table 3 has to hold up Ireland as an example.

Table 3 *Output Target Values of Turkey*

Output Values of Turkey	Target Values of Turkey
CO_2= 0.220	0.140*8.949= 1.253
CRW= 2.930	3.99*8.949= 35.706
EG_RNW %= 4.760	21.8*8.949= 195.096
GDP = 1677.62	213.65*8.949= 1911.934
NO_X = 0.100	0.06*8.949= 0.537
SO_X = 0.040	0.240*8.949= 2.148
ETR %= 3.830	2.17*8.949= 19.419

In order to be efficient in terms of environmental performance, Turkey has to increase its $1/CO_2$ emission values which have been applied inverse function from 0.220 to 1.253. Therefore, as the $1/ CO_2$ value increases, the emission value of CO_2 will decrease. Similarly, the emission value of $1/NO_X$ has to be increased from 0.100 to 0.537 and that of SO_X has to be increased from 0.040 to 2.148. Besides, Turkey has to increase the amount of combustible and renewable waste by 32.776 units from 2.930 to 35.706 and its GDP by 234.314 from 1677.620 to 1911.934. The increase in each unit of GDP enables a six-thousandth rise in the efficiency. Moreover, if the revenue from environmental taxes is increased from 15.589% to 19.419%, Turkey will become an efficient country. However, such a high rate of increase in environmental taxes does not seem possible for developing countries whose GDP is relatively lower. 4.7% of electricity is generated from renewable resources in Turkey and since the target is 195%, it seems impossible to reach that goal.

Table 4 provides a summary of the target of output amounts calculated through output oriented CCR models and the target of input amounts calculated through input oriented CCR models for inefficient countries to become efficient. When the input target values are examined in Table 4, it could be observed that Turkey has to decrease its number of labours from 28.774 to 19.300.

Table 4 *Input and Output Target Values of Inefficient Countries*

	OUTPUTS						INPUTS		
DMU	CO_2	CRW	EG_ RNW	GDP	NO_X	**SO_x**	**ETR**	**EC**	**L**
Austria	0.249	21.999	58.088	407.463	0.085	0.646	5.114	33.800	4357.600
Belgium	0.267	9.177	28.716	519.695	0.100	0.559	4.482	55.800	4966.900
Canada	0.773	35.278	12.017	2.127.982	0.211	2.179	14.898	326.074	19124.500
Denmark	0.170	22.450	55.830	249.130	0.050	0.500	4.110	17.400	2905.600
France	1.794	54.417	252.561	2.973.034	0.739	3.287	28.534	237.600	29429.000
Germany	2.619	77.604	383.756	4.208.641	1.096	4.681	41.251	312.100	41961.300
Greece	0.267	10.526	**46.490**	406.482	0.111	0.493	4.389	26.300	4167.847
Italy	1.501	42.783	233.753	2.290.889	0.643	2.573	23.268	146.900	23126.564
Netherlands	0.522	16.445	68.300	909.051	0.209	0.996	8.432	80.900	8895.800
Norway	0.110	5.020	1.710	302.810	0.030	0.310	2.120	46.400	2721.400
Portugal	0.266	16.436	36.059	314.483	0.091	0.525	4.101	24.600	4864.975
Spain	1.351	38.502	210.362	2.061.645	0.579	2.316	20.940	132.200	20812.333
Sweden	0.276	28.042	65.208	492.093	0.083	0.772	6.121	49.625	5184.500
Turkey	1.253	35.706	195.086	1.911.934	0.537	2.148	19.419	122.600	19300.999
United Kingdom	1.927	54.928	300.108	2.941.196	0.826	3.304	29.873	188.600	29691.422
United States	7.131	287.800	418.708	16.936.238	2.287	17.672	129.149	2.296.500	155921.800
Australia	0.671	22.669	75.561	1.277.696	0.255	1.379	11.183	132.600	12268.400
Czech Republic	0.323	14.689	55.060	521.537	0.128	0.642	5.525	40.200	5297.900
Finland	0.120	26.930	18.910	207.560	0.040	0.130	2.880	26.700	2697.300
Hungary	0.230	7.910	9.650	228.330	0.080	0.360	2.600	20.000	4444.200
Japan	4.215	122.243	639.176	6.583.658	1.787	7.362	65.802	452.300	66087.500
New Zealand	0.156	6.711	27.850	235.382	0.064	0.292	2.595	15.326	2436.300

Poland	0.944	26.911	147.031	1.440.968	0.405	1.619	14.636	92.400	14546.593
Slovak Republic	0.180	7.180	7.440	146.720	0.060	0.120	1.730	15.500	2721.900
Chile	0.354	34.473	92.292	511.166	0.118	0.890	7.399	35.400	5961.965
Israel	0.244	6.989	37.746	374.845	0.104	0.421	3.791	24.500	3778.300
Ireland	0.140	3.990	21.800	213.650	0.060	0.240	2.170	13.700	2156.800
Switzerland	0.230	9.600	3.800	442.360	0.120	1.042	1.760	28.500	4695.600

In order for efficient countries to be sorted among themselves, the super efficiency model has been utilised and the results have been provided in Table 5. According to the data given in Table 5, the top three countries have been found as Denmark, Switzerland, and Finland. Even if it has the same amount of inputs with 59.26% (100-40.74), Denmark continues to be an efficient country. It is possible to make similar comments about other countries.

Table 5 *Super Efficiency Scores*

Efficient Countries	Super Efficiency Score	Rating
Denmark	40.74%	1.
Switzerland	73.39%	2.
Finland	77.39%	3.
Ireland	79.58%	4.
Norway	89.36%	5.
Slovak Republic	90.54%	6.
Hungary	92.72%	7.

The efficiency change of countries in three-year period has been evaluated through window analysis and the results have been given in Table 6. Due to the limited data, the window size has been determined as two. The Period 1 column indicates the efficiency values of first year with regard to the data of the same year. As for the efficiency scores of the second year, the first rows of Period 2 column give the first two years' data while the second rows contain the last two years' data (the data of the first year has been excluded from the calculation) related to the calculated efficiency scores of the second year. Period 3 column gives the efficiency scores of the third year calculated by the last two years' data.

According to the data in Table 6, Denmark and Ireland are efficient countries thanks to their stable performance each year. This result is supported by the zero value of range and standard deviation scores. Although the efficiency score of some countries as Norway has a little decrease within the years, they could be stated as generally efficient countries. Inefficient in the first year, Finland and Hungary has become efficient in the last two years. The best efficiency performance average belongs to Denmark and Ireland with 100 points and these countries are respectively followed by Switzerland, Finland, Norway, Slovakia, and Hungary. The worst average in efficiency performance belongs to Czech Republic with 173.30 points and it has to increase its outputs by 73.3% (1.733-1= 0.733) in order to be an efficient country. The highest values in range and standard deviation belong to Chile which has a fluctuating efficiency performance. It could be observed that Turkey is not an efficient country between these periods and due to the rises and falls in the efficiency value, it could be stated that Turkey has a fluctuating performance. The mean, range, and standard deviation of efficiency scores of Turkey have been found as 115.15, 10.94, and 4.54, respectively. Since the year and country based average efficiency value is 122.2, Turkey is in a better situation with an average of 115.15.

Table 6 *The Results of Window Analysis of Countries*

DMU	P1	P2	P3	Mean	Range	Std. Dev.
Austria	108.91	109.47	---	110.47	3.2	1.52
	---	112.11	111.39			
Belgium	112.09	113.52	---	114.44	5.26	2.23
	---	117.35	114.78			
Canada	145.24	143.45	---	143.78	3.5	1.55
	---	144.7	141.74			
Denmark	100	100	---	100	0	0
	---	100	100			
France	115.85	115.84	---	118.77	6.76	3.45
	---	120.77	122.60			
Germany	118.63	119.39	---	122.32	9.36	4.29
	---	127.99	123.25			
Greece	160.79	157.44	---	161.37	11.36	5.15
	---	168.8	158.45			
Italy	116.74	115.26	---	117.04	7	3.16
	---	121.58	114.58			
Netherlands	118.04	118.61	---	120.15	5.4	2.43
	---	123.44	120.51			
Norway	100	100	---	100.04	0.16	0.08
	---	100.16	100			
Portugal	100.95	110.28	---	110.57	14.72	6.87
	---	115.38	115.67			
Spain	146.87	140.72	---	145.21	8	3.45

	---	148.72	144.51			
Sweden	117.31	117.31	---	118.12	2.12	1.02
	---	119.43	118.42			
Turkey	120.85	109.91	---	115.15	10.94	4.54
	---	115.85	113.97			
United King.	129.61	126.42	---	127.66	11.88	5.04
	---	133.25	121.37			
United States	106.11	105.19	---	105.67	1.99	0.90
	---	106.68	104.69			
Australia	121.27	119.69	---	121.57	3.78	1.56
	---	123.47	121.85			
Czech Republic	168.63	170.52	---	173.30	11.36	4.99
	---	179.99	174.04			
Finland	101.44	100	---	100.36	1.44	0.72
	---	100	100			
Hungary	105.74	100	---	101.44	5.74	2.87
	---	100	100			
Japan	142.61	141.09	---	145.10	7.29	3.80
	---	148.30	148.38			
New Zealand	105.76	105.05	---	111.79	11.45	7.5
		116.5	119.84			
Poland	165.25	163.51	---	165.50	11.74	5.01
		172.48	160.74			
Slovak Repub.	100	101.30	---	100.82	1.99	0.99
	---	101.99	100			
Chile	138.94	122.55	---	139.35	46.11	20.72
	---	127.23	168.66			
Israel	138.02	135.99	---	129.82	41.06	18.72
	---	143.16	102.10			
Ireland	100	100	---	100	0	0
	---	100	100			
Switzerland	100	100	---	100.32	1.28	0.64
	---	101.28	100			
Mean	121	122.38	122.2	122.15		

In the last part of study, the efficiency change of 28 OECD countries has been measured through Malmquist TFP index and the results have been analysed by DEAP 2.1 package. The first three columns of Table 7 include the values of EC, TC, and TFP for the first and second years while the latter three columns contain the same values for the second and third years and the last three columns bear the data of average change of EC, TC, and TFP. Countries having a value of greater than 1 for their efficiency are those successfully reached to the production frontier. When the average changes are taken into consideration, it has been observed that of 28 countries, 12 have experienced a decrease while 8 countries have experienced an increase in their EC performance. 8 countries have experienced no change in their EC value. The countries increasing their EC value most are Israel, the United Kingdom, and Turkey by 15.6%, 3.3%, and 3%, respectively. On the other hand, the countries experiencing the biggest fall are Chile, Portugal, and New Zealand by 10.1%, 6.9%, and 6.3%, respectively. Countries having greater than 1 TC are those producing more outputs with the same amount of input by increasing their technological capacity. While it has been found out that all countries have increased their technological capacity, those having the biggest rise are Denmark by 4.8%, New Zealand by 4.5%, and Switzerland by 4.4%. In terms of TFP, 24 countries have increased their performance while 4 countries have experienced a fall in this index value. TFP value of 85.7% of the countries has increased while there has been a fall in the 14.3%. The biggest rise belongs to Israel with 19.8% while the sharpest fall has been experienced by Chile with 6.8%. The EC performance of Chile has been observed as the cause of this fall.

Table 7 Results of Malmquist TFP Index

	1st-2nd years			2nd-3rd years			Average		
DMU	EC	TC	TFP	EC	TC	TFP	EC	TC	TFP
Austria	0.987	1.008	0.995	0.983	1.025	1.007	0.985	1.016	1.001
Belgium	0.973	1.015	0.988	0.989	1.037	1.025	0.981	1.026	1.006
Canada	1.005	1.006	1.010	1.012	1.009	1.021	1.008	1.007	1.016
Denmark	1.000	1.001	1.001	1.000	1.098	1.098	1.000	1.048	1.048
France	0.994	1.007	1.000	0.945	1.044	0.986	0.969	1.025	0.993
Germany	0.988	1.005	0.994	0.969	1.048	1.015	0.978	1.026	1.004
Greece	1.025	1.004	1.029	0.990	1.076	1.065	1.007	1.039	1.047
Italy	1.022	0.994	1.017	0.993	1.069	1.061	1.008	1.031	1.039
Netherlands	0.985	1.010	0.995	0.984	1.042	1.025	0.985	1.026	1.010
Norway	1.000	0.996	0.996	1.000	1.024	1.024	1.000	1.010	1.010
Portugal	0.930	0.994	0.925	0.932	1.068	0.996	0.931	1.031	0.960
Spain	1.057	0.988	1.044	0.962	1.070	1.029	1.008	1.028	1.036
Sweden	0.991	1.013	1.004	0.983	1.030	1.013	0.987	1.022	1.009
Turkey	1.114	0.987	1.100	0.953	1.068	1.017	1.030	1.027	1.058

United Kingdom	1.039	0.987	1.025	1.028	1.038	1.098	1.033	1.027	1.061
United States	0.995	1.014	1.009	1.005	1.014	1.019	1.000	1.014	1.014
Australia	1.003	1.010	1.013	0.982	1.032	1.013	0.993	1.021	1.013
Czech Republic	0.979	1.010	0.989	0.980	1.054	1.033	0.979	1.032	1.010
Finland	1.000	1.045	1.045	1.000	1.002	1.002	1.000	1.023	1.023
Hungary	1.000	1.079	1.079	1.000	1.008	1.008	1.000	1.043	1.043
Japan	1.006	1.005	1.011	0.951	1.052	1.000	0.978	1.028	1.005
New Zealand	0.988	0.998	0.986	0.888	1.095	0.972	0.937	1.045	0.979
Poland	1.024	0.987	1.011	1.004	1.069	1.073	1.014	1.027	1.041
Slovak Republic	1.000	0.961	0.961	1.000	1.093	1.093	1.000	1.025	1.025
Chile	1.119	1.018	1.139	0.723	1.054	0.762	0.899	1.036	0.932
Israel	1.002	1.012	1.014	1.332	1.062	1.414	**1.156**	**1.037**	**1.198**
Ireland	1.000	1.033	1.033	1.000	1.053	1.053	1.000	1.043	1.043
Switzerland	1.000	1.000	1.000	1.000	1.090	1.090	**1.000**	**1.044**	**1.044**
Average	1.007	1.006	1.014	0.982	1.052	1.032	0.994	1.029	1.023
<1							12	-	4
=1							8	-	-
>1							8	28	24

4. CONCLUSION

While the environmental performance of OECD countries is analysed, the current situation in Turkey has been evaluated within this study. Such variables as environmental taxes and energy production from renewable resources have been assessed together through DEA method and several analyses have been carried out through input and output oriented CCR models under the assumption of constant returns to scale function.

When the recent OECD data has been examined, it could be observed that countries releasing the least CO_2 emissions are Switzerland, Hungary, and Portugal while those releasing the most CO_2 emissions are the USA and Australia. With its highly developed industry and large population, the USA is among the countries that release the most amount of CO_2 into the atmosphere. On the other hand, meeting 60% of its energy need from hydroelectric power plants, Switzerland is the country having the least amount of CO_2 emissions. As the most important action to prevent increasing environmental pollution is to reduce CO_2 emissions, people should increase energy efficiency, reduce energy consumption, make some technological changes to enable less use of energy, and using such low-carbon fuels as natural gas and non-fossil fuels rather than coal which contains high amounts of carbon.

When the amount of energy from combustible and renewable wastes is analysed, it could be observed that Denmark, Finland, and Sweden has the most amount of energy production from these resources. Meeting its energy need from renewable energy resources, Denmark aims to cease the complete use of fossil fuels and as for the wastes, Denmark either recycles the majority of them or meets its regional heating needs through the heat produced by the burning of wastes. 67% of its 11 million tonnes of waste is recycled while 27% is burnt in combustion plants. Denmark meets 20% of the country's heating need and 5% of its energy consumption through the energy obtained from wastes. Sweden treats domestic waste of the country with modern techniques and uses biogas obtained at the end of this process for both heating and generating electricity. Sweden uses 99% of domestic waste to generate electricity and uses the remaining 1% as agricultural fertilizer. Energy production from wastes is of much significance in terms of contributing many problems including global warming. Accordingly, the increased amounts of greenhouse gas emissions could be decreased. The fact that wastes are transformed into energy and industrial chemicals both decreases the dependence on external resources for energy and chemicals and provides economic benefits. As the income level of people or countries is increased, more environmental friendly products are produced and consumed.

It has been found out that the country having the largest amount of electricity generation from renewable resources is again Denmark. Being generated from a renewable resource, the wind energy is among the cleanest energy and Denmark meets one-third of the country's energy need from wind. On the other hand, Finland has efficient waste treatment facilities and power plants generating electricity from solid wastes.

Environmental taxes are of much significance in terms of protecting the environment, as well. The purpose of imposing such taxes is to direct manufacturers and consumers to environmental friendly activities by increasing the prices of products and services. Products having the potential of harming the environment are applied higher pricing and therefore, by steering the behaviour of individuals, production and consumption preferences are supposed to change. The fact that individuals contribute to the cost of protecting the environment is ensured only through environmental taxes. Reducing the production by creating a cost for products polluting the environment or for the firm manufacturing these products is a common policy applied throughout the world. Denmark has the highest amount of revenues coming from environmental taxes and is one of the first countries applying "Ecological Tax Reform" incorporating environmental taxes, efficient tools in improving the quality of natural environment and protecting it, and the use of revenues from these taxes. Therefore, it is possible to state that Denmark has pioneered the environmental tax applications.

The fact that inefficient countries determine the policies that will enable reaching the target values by taking countries such as Denmark and Sweden as a reference point and putting the applicable ones into practice will substantially reduce environmental threat.

Through the super efficiency model, efficient countries have been sorted and three years' performance evaluation has been carried out via window analysis. Denmark, Switzerland, and Finland has been found out as the most efficient countries at the end of the super efficiency analysis. According to the results of window analysis, Denmark and Ireland has been found as having the best efficiency performance and there has been observed periodical fluctuations in the performance of other countries.

Lastly, the change in the efficiency of countries between the years has been measured through Malmquist TFP index. According to the results, the countries increasing their EC value most are Israel, the United Kingdom, and Turkey by 15.6%, 3.3%, and 3%, respectively. Countries having the biggest rise in their TC have been found out as Denmark by 4.8%, New Zealand by 4.5%, and Switzerland by 4.4%. When the overall situation is analysed, TFP value of 85.7% of the countries has increased while there has been a fall in the 14.3%.

For the future studies, it could be recommended that the input and output selection could be carried out by expert views and such multiple-criteria decision making techniques as AHP and DEMATEL could be used. The methodology adopted within the study could be used as a guide for different efficiency analysis scenarios and DMUs.

REFERENCES

Aldamak, A. & Zolfaghari, S. (2017). Review of efficiency ranking methods in data envelopment analysis. *Measurement*, *106*, 161-172.

Ali A. I. & Seiford L. M. (1990). Translation invariance in data envelopment analysis. *Operations Research Letters*, *9*(6), 403–405.

Andersen, P. & Petersen, N.C. (1993). A procedure for ranking efficient units in data envelopment analysis. *Management Science*, *39*(10), 1261-1264.

Charnes A, Clark C. T, Cooper W. W & Golany B. (1985). A developmental study of data envelopment analysis in measuring the efficiency of maintenance units in the U.S. Air Forces. *Annals of Operations Research*, *2*(1), 95–112.

Charnes A. Cooper W. W. & Rhodes E. (1978). Measuring the efficiency of decision making units. *European Journal of Operational Research*, *2*(6), 429–444.

Chen, J., Song, M. & Xu, L. (2014). Evaluation of environmental efficiency in China using data envelopment analysis. *Ecological Indicators*, *52*, 577-583

Coelli, T. J., Rao, D. S. P., O'Donnell, C. J. and Battese, G. E. (2005). An introduction to efficiency and productivity analysis, Springer Science & Business Media.

Cooper, W. W., Seiford, L. M., & Zhu, J. (2011). Data envelopment analysis: History, models, and interpretations. In Handbook on data envelopment analysis, Springer, Boston, MA.

Deliktas, E. (2002). Efficiency and Analysis of Total Factor Productivity Growth in Private- Owned Manufacturing Industry in Turkey. *METU Studies in Development*, *29*(2), 247-284.

Dobos, I. & Vörösmarty, G. (2019). Inventory-related costs in green supplier selection problems with Data Envelopment Analysis (DEA). *International Journal of Production Economics*, *209*, 374-380.

Dyckhoff, H. & Allen, K. (2001). Measuring ecological efficiency with data envelopment analysis (DEA), *European Journal of Operational Research*, *132*(2), 312–325.

Eva, M., Sagarra, M. & Agasisti, T. (2016). Assessing organizations' efficiency adopting complementary perspectives: An empirical analysis through data envelopment analysis and multidimensional scaling, with an application to higher education. *In Handbook of operations analytics using data envelopment analysis*, Springer, Boston, MA.

Guo, X.D., Zhu, L., Fan, Y. & Xie, B.C. (2011). Evaluation of potential reductions in carbon emissions in Chinese provinces based on environmental DEA. *Energy Policy*, *39*(5), 2352-2360.

Halkos G.E. and Tzeremes N.G. (2009). Exploring the existence of Kuznets curve in countries' environmental efficiency using DEA window analysis. *Ecological Economics*, *68*(7), 2168–2176.

Hosseinzadeh-Bandbafha, H., Nabavi-Pelesaraei, A., Khanali, M., Ghahderijani, M. & Chau, K.W. (2018). Application of data envelopment analysis approach for optimization of energy use and reduction of greenhouse gas emission in peanut production of Iran. *Journal of cleaner production*, *172*, 1327-1335.

Lin, E.Y-Y., Chen, P-Y. & Chen, C-C. (2013). Measuring the environmental efficiency of countries: A directional distance function metafrontier approach. *Journal of Environmental Management*, *119*, 134-142.

Mahadevan, R. (2002). A DEA Approach to Understanding the Productivity Growth of Malaysia's Manufacturing Industries. *Asia Pasific Journal of Management*, *19*(4), 587-600.

Malana, N. M. & Malano, H. M. (2006). Benchmarking productive efficiency of selected wheat areas in Pakistan and India using data envelopment analysis. *Irrigation and Drainage: The journal of the International Commission on Irrigation and Drainage*, 55(4), 383-394.

Malmquist, S. (1953). Index numbers and indifference surfaces. *Trabajos de Estadistica, 4*(2), 209–242.

Mavi, N. K. & Mavi, R. K. (2019). Energy and environmental efficiency of OECD countries in the context of the circular economy: Common weight analysis for malmquist productivity index. *Journal of environmental management*, *247*, 651-661.

Meng, F. Y., Fan, L. W., Zhou, P. and Zhou, D. Q. (2013). Measuring environmental performance in China's ındustrial sectors with non-radial DEA, *Mathematical and Computer Modelling*, *58*(5-6), 1047-1056.

Omrani, H., Shafaat, K. & Emrouznejad, A. (2018). An integrated fuzzy clustering cooperative game data envelopment analysis model with application in hospital efficiency. *Expert Systems with Applications*, *114*, 615-628.

Ouyang, W. & Yang, J. B. (2020). The network energy and environment efficiency analysis of 27 OECD countries: A multiplicative network DEA model. *Energy*, *197*, 117161.

Rheinhard S., Lovell C. A. K., Thijssen G. (1999). Econometric estimation of technical and environmental efficiency: An application to Dutch dairy farms. *American Journal of Agricultural Economics*, *81*(1), 44–60.

Scheel H. (2001). Undesirable outputs in efficiency evaluations. *European Journal of Operational Research*, *132*(2), 400–410.

Sherman H. D. (1984). Data Envelopment Analysis as a New Managerial Audit Methodology-Test and Evaluation. *Auditing*, *4*(1), 35.

Sozen, A. & Karık, F. (2017). Comparison of Turkey's renewable energy performance with OECD and BRICS countries by multiple criteria. *Energy Sources, Part B: Economics, Planning, and Policy*, *12*(5), 487-494.

Sueyoshi, T. & Goto, M. (2011). Measurement of returns to scale and damages to scale for DEA-based operational and environmental assessment: how to manage desirable (good) and undesirable (bad) outputs? *European journal of operational research, 211*(1), 76-89.

Sueyoshi, T. & Goto, M. (2013). DEA environmental assessment in a time horizon: Malmquist ındex on fuel mix, electricity and CO_2 of ındustrial nations. *Energy Economics, 40*, 370–382.

Wang, J. & Zhao, T. (2017). Regional energy-environmental performance and investment strategy for China's non-ferrous metals industry: a non-radial DEA based analysis. *Journal of cleaner production*, *163*, 187-201.

Wang, J., Zhao, T. & Zhang, X. (2016). Environmental assessment and investment strategies of provincial industrial sector in China — Analysis based on DEA model. *Environmental Impact Assessment Review, 60*, 156-168.

Wang, K., Wei, Y. M. & Zhang, X. (2013). Energy and emissions efficiency patterns of Chinese regions: a multi-directional efficiency analysis. *Applied Energy*, *104*, 105-116.

Wu, F., Fan, L.W., Zhou, P. & Zhou, D.Q. (2012). Industrial energy efficiency with CO2 emissions in China: A nonparametric analysis. *Energy Policy*, *49*, 164–172.

Wu, J., An, Q., Yao, X. & Wang, B. (2014). Environmental efficiency evaluation of industry in China based on a new fixed sum undesirable output data envelopment analysis. *Journal of cleaner production*, *74*, 96-104.

Yang H. H. & Chang C. (2009). Using DEA window analysis to measure efficiencies of Taiwan's integrated telecommunication firms. *Telecommunications Policy*, *33*(1-2), 98–108.

Yao, X., Feng, W., Zhang, X., Wang, W., Zhang, C. & You, S. (2018). Measurement and decomposition of industrial green total factor water efficiency in China. *Journal of Cleaner Production*, *198*, 1144-1156.

Zhang, N., Kong, F. & Yu, Y. (2015). Measuring ecological total-factor energy efficiency ıncorporating regional heterogeneities in China. *Ecological Indicators*, *51*, 165-172.

Chapter 8

OVERVIEW OF BIOCOMPOSITES WITH PLANT-DERIVED COMPONENTS IN TERMS OF MATRIX AND REINFORCEMENT MATERIALS

***Ipek YALCIN ENIS*[1]**
***Hande SEZGIN*[2]**

1 Assist.Prof.Dr. Ipek Yalcin-Enis, Istanbul Technical University, Textile Technologies and Design Faculty, Textile Engineering Department, Turkey. ipekyalcin@itu.edu.tr
2 Dr. Hande Sezgin, Istanbul Technical University, Textile Technologies and Design Faculty, Textile Engineering Department, Turkey. sezginh@itu.edu.tr

Introduction

With the development of technical textiles, low-weight engineering materials based on textile-reinforced composites have become one of the most interesting areas for scientists (Badawi, 2007). From ship construction to building construction, household appliances to space technology, these composite materials, which are widely used in almost every field, are increasingly important in the engineering field (Sevkat et al., 2009; Ashrafi et al., 2012).

The fluctuation in oil prices and the resource decline increase people's awareness of renewable resources (Faruk et al., 2014). The increasing raw material prices of polymers and plastics, decreasing reserves and threats to the environment have revealed the importance of using natural materials for the development and production of polymer composites (Abdul Khalil et al., 2012). The development of biocomposites is driven at this point by the environmental concerns regarding the use of petroleum-based materials and rapid consumption of fossil resources (Haq et al., 2008; Sahoo et al., 2015).

The first studies in the emergence of biocomposite materials started with the use of natural fibers in composite materials (Sahoo et al., 2015). Natural fibers are preferred in composite structures due to their lightness, low cost, easy processability, biodegradability and nonabrasiveness (Sahoo et al., 2015; Manthey et al., 2013; Sahoo et al., 2018). Although the use of natural fibers in composite materials makes the composite structure "greener", it is not sufficient to call the material as a biocomposite. Matrix material should also have a biological content (Manthey et al., 2013; Fowler et al., 2006). Today, synthetic thermoplastics and thermosets dominate commercial biocomposite production (Fowler et al., 2006). Fiber reinforced polymers cause significant problems as they cannot be reused and / or recycled when their life is over. These materials are difficult to separate and recycle as the components are tightly linked and the structure is relatively stable (Fowler et al., 2006; Mohanty et al., 2000).

There are many types of bioresins based on their origins and structures (Sahoo et al., 2018). Tanin, lignin, furan, carbohydrates, itanoic acid, and proteins are some of the sources of bioresins (Sahoo et al., 2015; Raquez et al., 2010). Of all bioresins, plant-based ones are the most preferred bioresins for composite structures. Polymers made of plant oils are transformed into biomass and then reused (Sahoo et al., 2018). Thanks to these properties, plant-based oils reduce the carbon footprint of the composite material (Manthey et al., 2013). However, plant-based bioresins have lower mechanical, thermal and thermo-physical properties than synthetic resins (Haq et al., 2008). The most important features of biocomposites are their biodegradability in addition to low density, high toughness, acceptable specific strength properties, ease of separation, enhanced energy recovery, carbon dioxide retention (Fowler et al., 2006). Thus, biodegradable plastics and bio-based polymer products produced from renewable sources create sustainable and environmentally friendly products that can compete in the current market dominated by petroleum-based products (Abdul Khalil et al., 2012).

In this review, biocomposite components such as plant fibers as a reinforcement material, and plant oil-based bioresins as matrix material have been introduced. In addition, general information on biocomposite production techniques is addressed; studies on the production of biocomposite materials have been discussed comparatively and the current situation of the research topic in the literature has been analyzed.

Materials

Reinforcement Materials

The main task of reinforcement material is to improve the mechanical properties of the matrix material and thus the composite material, but all fiber types have different effects on the properties of the final composite material (Wambua et al., 2003). In general, the reinforcement material has properties such as providing the rigidity and strength of the material and carrying the applied loads (Faruk et al., 2014). While the use of synthetic fiber as a reinforcement material was dominant in the recent past, the use of natural fiber reinforcement material has gained momentum day by day (Abdul Khalil et al., 2012). Among synthetic fibers, carbon and glass fiber reinforcements come to mind in the presence of necessity of high mechanical properties but the interest in natural fiber reinforcements is increasing in non-carrier element designs (automotive panels, sports equipment, etc.) where medium mechanical properties are favored (Wambua et al., 2003).

The natural fibers used in biocomposites act as a reinforcement material by increasing the strength and hardness of the material. Natural fibers do not have the necessary thermal and mechanical properties required for engineering plastics. Moreover, while fibers such as glass and carbon can be produced in certain property ranges, the properties of natural fibers differ significantly. The source, origin, nature, physical and chemical composition of the natural fibers are important factors that affect the composite properties. However, the advantages of natural fibers over other reinforcing materials are low cost, low density, high toughness, acceptable specific strength, reduced tool wear, reduced skin and respiratory irritation, good thermal properties, ease of separation, improved energy recovery and biodegradability (Mohanty et al., 2000). Compared to glass and carbon, natural fibers have some undesirable properties like hydrophilic structure, low adhesion strength, low impact strength, low flame retardancy and varying physical-mechanical properties depending on the geography where they grew up (Manthey et al., 2013; Gowda et al., 1999; Ahmed and Vijayarangan, 2006). Using natural fibers, the weight can be reduced by 10%, production energy is saved by 80%, and the material cost is 5% less in comparison to glass fiber reinforced composites (Geethamma et al. 1998).

On the other hand, while the mechanical properties of the composites are influenced by the properties of the matrix and the reinforcing materials used, the ability of these materials to adhere to each other also plays a decisive role in the mechanical properties of final composite materials (Nayak et al., 2009). Cellulosic fibers have strongly hydrophilic nature due to the hydroxyl groups they contain. The hydrophilic nature of these fibers is the biggest cause of adhesion problems with hydrophobic polymer matrices. Processes such as; acetylation, silylation, and etc. are mostly preferred to reduce the hydrophilic properties of natural fibers and enhance the fiber-matrix interface (Fowler et al., 2006).

Natural fibers are divided into three main classes; animal fibers, plant fibers, and mineral fibers. Among them, plant fibers are the most preferred ones in composite materials (Ramamoorthy, 2015). Plant fibers used as reinforcement material in biocomposites, is classified as leaf, bast, fruit, seed, wood, grain, straw and grass fibers (Manthey et al., 2013). Cellulose, hemicellulose, and lignin are the main components of the plant fibers. The hydrogen bonds and other linkages are responsible for providing strength and stiffness to the plant fibers (Dilfi et al., 2018). The hydroxyls form hydrogen bonds inside the cellulose macromolecule itself and between other cellulose macromolecules and with hydroxyl groups of the air that result in a hydrophilic nature which may cause poor fiber-matrix interface (Joseph et al., 1999). Fiber-matrix adhesion, fiber volume fraction, fiber aspect ratio, fiber orientation, and stress-transfer efficiency of the interface are the main key factors that affect the final performance of the fiber-reinforced composites (Joseph et al., 1999).

Flax fibres which are grown in temperate climates, are strong and stiff. Especially in automotive industries, the use of flax reinforced composites come to fore instead of glass fiber reinforced composites (Kumar and Srivastava, 2017). Although flax has the best combination of cost, weight, strength and stiffness properties, jute is the most preferred bast fiber in composite production owing to its low cost, accessability, nonabrasiveness and moderate strength allowing high filling levels and resulting in cost-saving (Ahmad et al., 2015; Kumar and Srivastava, 2017; Dilfi et al. , 2018). Sisal is a lignocellulosic leaf fiber and extracted from Agave Sisalana plant. The moderately high specific strength and high stiffness of sisal fibers make these fibers promising alternatives as reinforcement materials especially in structural biocomposites (Joseph et al., 1999). Similar to sisal, hemp is also a widely used plant fiber as a reinforcement material owing to its high strength and stiffness. In recent years, there is an increase in the use of hemp fiber for various applications (Shahzad, 2011). Coconut is cultivated mostly for its fruits and the husks and shells of the plant are mostly disposed as waste. Coconut fiber (coir fibers) is extracted from the external shell of a coconut fruit thus these obtained waste components provide potential resource for natural fibers to be used as reinforcement materials (Adeniyi et al., 2019; Prasad et al., 2017). Since the coir fibers have curvy structure, it is not easy to orient these fibers during composite production. Therefore, these fibers are mostly reinforced as randomly distributed fibers. In automotive, aeronautical and construction industries, coir fibers are mostly preferred due to their non-toxic, light-weight, eco-friendly and low cost features (Prasad et al., 2017). With its high amount of lignin content, coir fibers are known as one of the hardest natural plant fibers (Fouladi et al., 2011). Moreover, this high lignin thus low cellulose content leads to high weather resistance because it absorbs less water. It has better thermal stability than other natural fibers (Johnson et al., 2017, Haque et al., 2009). The oil palm fibers are lignocellulosic fibers achieved from empty fruit and bunch fibrous mesocarp of oil palm tree as waste material after oil extraction (Joseph et al., 2006). They show similarity to coir fibers in cellular structure (Joseph et al., 1999). These coir and oil palm fibers are mostly used as a reinforcement in clay, cement, and different polymers since they are hard and tough (Joseph et al., 2006). Out of 300 species, around 20 species of banana plants are used for consumption. Banana fibers as lignocellulosic bast fibers, are obtained from the pseudo-stem of these banana plants with good mechanical properties. Since the banana cultivation is in abundance in tropical countries, these fibers can be utilized in various applications (Mahesh et al., 2020).

One of the drawbacks of the natural fibers is the variety in their composition depending upon factors such as source, age, retting and separating techniques, geographic origin, rainfall during growth, and constituents' content which results in different properties (Shahzad, 2011). Comparative specific features of the selected plant fibers mostly used as reinforcement materials are listed in Table 1.

Table 1. *Comparative specific properties of plant fibers*

	Cellulose [%]	Hemi-cellulose[%]	Lignin [%]	Moisture Content [%]	Density [g/cm³]	Tensile Strength[MPa]	Young Modulus[GPa]	Elongation at Break [%]
Jute Fiber	61-71 (Rahman and Khan, 2007) 59-71.5 (Dittenber and GangaRao, 2012)	13.6-20.4 (Rahman and Khan, 2007; Dittenber and GangaRao, 2012)	12-13 (Rahman and Khan, 2007; Dittenber and GangaRao, 2012)	12.6 (Rahman and Khan, 2007) 12.5-13.7 (Dittenber and GangaRao, 2012)	1.3-1.4 (Ramamoorthy, 2015) 1.3-1.49 (Dittenber and GangaRao, 2012)	393-773 (Rahman and Khan, 2007) 600-1100 (Manthey et al., 2013) 320-800 (Dittenber and GangaRao, 2012)	13-26.5 (Rahman and Khan, 2007) 10-30 (Manthey et al., 2013)	1.16-1.5 (Rahman and Khan, 2007) 1-1.8 (Dittenber and GangaRao, 2012)
Flax Fiber	71 (Rahman and Khan, 2007) 62-72 (Dittenber and GangaRao, 2012)	18.6-20.6 (Rahman and Khan, 2007; Dittenber and GangaRao, 2012)	2.2 (Rahman and Khan, 2007) 2-5 (Dittenber and GangaRao, 2012)	10 (Rahman and Khan, 2007) 8-12 (Dittenber and GangaRao, 2012)	1.5 (Ramamoorthy, 2015) 1.4-1.5 (Dittenber and GangaRao, 2012) [v]	345-1100 (Rahman and Khan, 2007) 800-1500 (Prabhakaran, 2014) 343-2000 (Dittenber and GangaRao, 2012)	60-80 (Manthey et al., 2013) 27.6-103 (Rahman and Khan, 2007; Dittenber and GangaRao, 2012)	2.7-3.2 (Rahman and Khan, 2007) 1.2-3.3 (Dittenber and GangaRao, 2012)
Sisal Fiber	65 (Mukherjee and Satyanarayana, 1984) 60-78 (Dittenber and GangaRao, 2012)	12 (Mukherjee and Satyanarayana, 1984) 10-14.2 (Rahman and Khan, 2007)	9.9 (Mukherjee and Satyanarayana, 1984) 8-14 (Dittenber and GangaRao, 2012)	10 (Mukherjee and Satyanarayana, 1984) 10-22 (Dittenber and GangaRao, 2012)	1.45 (Mukherjee and Satyanarayana, 1984) 1.3-1.5 (Rahman and Khan, 2007)	468-640 (Rahman and Khan, 2007) 600-700 (Manthey et al., 2013) 363-700 (Dittenber and GangaRao, 2012)	5.5-12.6 (Rahman and Khan, 2007) 9.4-22 (Ramamoorthy, 2015) 9-38 (Dittenber and GangaRao, 2012)	4.3 (Joseph et al., 1999) 2-7 (Dittenber and GangaRao, 2012)
Hemp Fiber	90 (Shahzad, 2011) 68-74.4 (Dittenber and GangaRao, 2012)	15-22.4 (Dittenber and GangaRao, 2012)	3.7-10 (Rahman and Khan, 2007)	6.2-12 (Dittenber and GangaRao, 2012)	1.4-1.5 (Dittenber and GangaRao, 2012) [V]	310-750 (Shahzad, 2011) 550-900 (Manthey et al., 2013) 270-900 (Dittenber and GangaRao, 2012)	30-60 (Shahzad, 2011; Ramamoorthy, 2015) 23.5-90 (Dittenber and GangaRao, 2012)	2-4 (Shahzad, 2011) 1-3.5 (Dittenber and GangaRao, 2012)
Coir Fiber	36-43 (Rahman and Khan, 2007; Dungani et al., 2016) 32-43.8 (Dittenber and GangaRao, 2012)	0.15-0.25 (Dungani et al., 2016)	40-45 (Dittenber and GangaRao, 2012) 41.2-45.3 (Dungani et al., 2016)	8 (Rahman and Khan, 2007)	1.15-1.46 (Dittenber and GangaRao, 2012)	131-175 (Rahman and Khan, 2007) 580 (Joseph et al. 1999) 95-230 (Dittenber and GangaRao, 2012)	4-6 (Rahman and Khan, 2007) 2.8-6 (Dittenber and GangaRao, 2012)	15-40 (Rahman and Khan, 2007) 15-51.4 (Dittenber and GangaRao, 2012)
Oil Palm Fiber	60-65 (Dittenber and GangaRao, 2012) 44.2-49.6 (Dungani et al., 2016)	18.3-33.5 (Dungani et al., 2016)	11-29 (Dittenber and GangaRao, 2012) 17.3-26.5 (Dungani et al., 2016)	8.56 (Sudiyani et al., 2008)	0.7–1.55 (Dittenber and GangaRao, 2012)	150-500 (Dittenber and GangaRao, 2012)	80-248 (Dittenber and GangaRao, 2012)	17-25 (Dittenber and GangaRao, 2012)
Banana Fiber	63-64 (Mukherjee and Satyanarayana, 1984) 63-67.6 (Dittenber and GangaRao, 2012)	19 (Mukherjee and Satyanarayana, 1984) 10-19 (Dittenber and GangaRao, 2012)	5 (Mukherjee and Satyanarayana, 1984; Dittenber and GangaRao, 2012)	10-11 (Mukherjee and Satyanarayana, 1984) 8.7-12 (Dittenber and GangaRao, 2012)	1.35 (Mukherjee and Satyanarayana, 1984; Dittenber and GangaRao, 2012)	540 (Joseph et al., 1999) 500 (Dittenber and GangaRao, 2012)	12 (Dittenber and GangaRao, 2012)	3 (Joseph et al., 1999) 1.5-9 (Dittenber and GangaRao, 2012)

Matrix Materials

The matrix material provides the shape, surface appearance and resistance to environmental factors of the composite materials. Most of the matrix materials (80%) are composed of non-renewable petroleum resources. Damages to the environment, climate change, and declining fossil resources have led companies and scientists to search for alternative matrix materials, and thus bio-based plastics have emerged (Faruk et al., 2014). Although some of bioresins are not biodegradable, they are preferred due to their affordable prices and structural properties similar to petroleum-based resins (Francucci et al., 2013).

Since ancient times, pine resin has been used in decorative and protective lacquer materials. As time went on, a wide variety of natural resins were developed in addition to pine resin, and they are used in many different areas. Starch, one of these, was rediscovered as a plastic material, although it was actually a polymer found in nature (Faruk et al., 2014). Studies on bioresins have gained momentum, taking into account the decline of oil reserves and environmental concerns (Wambua et at., 2003).

Plant oils are triglycerides composed of triple fatty acids linked to glycerol with ester bonds. Fatty acids differ according to the oil source and growth conditions (Jiang, 2015). The iodine value and double bonds of fatty acids determine the degree of unsaturation. Higher values indicate a higher degree of unsaturation. Unsaturated fatty acids are modified to form reactive sites and chemical reactions continue during the thermoset curing process (Ramamoorthy, 2015; Ramamoorthy et al., 2012). The most important properties of functional vegetable oils are their degree of unsaturation, stereochemistry and length of fatty acids (Pin et al., 2015). Thus, the degree of unsaturation of fatty acids plays an important role in the production of thermoset resins because vegetable oils must be functionalized in order to be used as a thermoset resin. Bioresins can be used as a blend of all synthetic resins (Jiang, 2015). Unlike biomass in polydisperse polymeric form, plant oils exist as a monodisperse low molecular weight material structure, which is almost pure triacylglycerol. Due to this feature, these oils are used in the production of monomers for the polymer industry at a low cost (Kong et al., 2012). The thermoset bioresins obtained from plant oils (soybean oil, linseed oil, etc.) are quite remarkable in natural resins and offer an alternative to commercial equivalents such as epoxy, vinylester, and polyester. (Francucci et al., 2013; Ramamoorthy, 2015). Contrary to synthetic resins, they are derived from plants and contain carboxylic acid, oil and isoprene-based hydrocarbons (Jiang, 2015). Oil-based bioresins have many advantages over petroleum-based resins. Besides their biodegradability and dimensional stability, many of them are also front-run with low cost (Habib and Bajpai, 2011; Francucci et al., 2013; Jiang, 2015). They are also odorless and non-toxic during production which can be resulted from its hardener content, which is the main part of the bioresin system, generally contains blocked isocyanate and keeps the function of the harmful components from going out (Jiang, 2015).

Plant oils consisted of high fatty acid esters with unsaturated fraction such as linoleic acid have better properties than the ones having lower degree of unsaturation such as linolenic acid, oleic acid, and with saturated fraction such as stearic acid and palmitic acid. This is the reason why linseed oil and soybean oil are mostly used as starting monomers for bioresins. They have enhanced properties among other oils owing to more than 50% unsaturated triglyceride content (Mustapha et al., 2019).

Several chemical modifications are required for these monomers to be used in applications. Epoxidation and acrylation are the two main processes in which they are modified or functionalized to produce bioresins from plant oils. The most commonly used process among many applications is the epoxidation of double bonds. The acrylation process is a reaction in which epoxidized plant oils are exchanged for other functions. After this reaction, a polymer is obtained in the form of acrylated epoxidized plant oil. The acrylation process provides the material a lower curing temperature, shorter curing time and improved material properties (Sadiq et al., 2018). In recent years, scientists focus on the development of new polymers with low toxicity and migration based on epoxidized plant oils that can be used instead of phthalates (Pin et al., 2012).

Among these resins, soybean oil-based resin is the leading one due to its unique composition (53% linoleic acid, 23% oleic acid, 11% palmitic acid, 8% linolenic acid and 4% stearic acid) (Meier et al., 2007; Gerbase et al., 2002). Acrylated epoxidized soybean oil (AESO) is a relatively commercially available resin type produced by the chemical modification of soybean oil. AESO production occurs in two steps. Soybean oil is first epoxidized and epoxidized soybean oil is obtained. It is then functionalized with acrylate groups and AESO is produced (Ramamoorthy, 2015; Ramamoorthy et al., 2012). Due to their long aliphatic chain structure and low crosslinking density, functionalized soybean oil-based bioresins cannot provide sufficient mechanical and thermal properties. They are often mixed with petroleum-based polymers to improve their properties (Sahoo et al., 2015; Sahoo et al., 2018). In addition, it is stated in the literature that epoxidized soybean oil (ESO) is blended with epoxy to toughen the composite structure (Sahoo et al., 2018). The most common application areas of bio-based composites are automotive and structural applications (Sahoo et al., 2018). In addition to soybean oil, the epoxidized lindseed oil (ELO) attracts attention due to its low volatility, high resistance to solvents, low migration tendency and flexible structure that increases mechanical properties. It is also known that ELO-based composites have better thermo-mechanical properties than bifunctional epoxy-based ones with same hardener (Pin et al., 2015). The most epoxidized oil among plant oils is linseed oil due to the excess of double bonds found in linolenic acid chains (Lutton et al., 2017). On the other hand, industrial hemp oil has an important potential of use as a raw material of bioresin, thanks to its fatty acid profile (Francucci et al., 2013). As a byproduct of hemp fiber production, hemp oil shows an important potential as a bioresin raw material, as it contains high levels of linoleic and linolenic acid (Manthey et al., 2013). Palm oil is the world's highest yield oil crop with 5 to 10 times higher production per hectare compared to other plant oils (Mustapha et al., 2014). Soybean oil, rapeseed oil and sunflower oil follow palm oil as production capacity, respectively (Kong et al., 2012; Kadem et al., 2018). Palm oil, which is abundant in tropical regions, is of great interest in the composite industry (Lutton et al., 2017). Although cottonseed oil, a by-product of cotton, which is the highest production plant fiber in the textile industry, is generally used in the food industry, studies are underway for the use of this high volume oil in different sectors (Lutton et al., 2017). Flax seeds, radish seeds, olive seeds, castor oil, grapeseed oil, sunflower and camelina oil, rapeseed, canola and corn oil, pine oil, tung oil, corn, peanut oil have also been placed as potential materials in polymer science besides mostly used soybean, lindseed, and hemp oils (Ramamoorthy, 2015; Ramamoorthy et al., 2012; Lutton et al., 2017). Fatty acids, double bonds and iodine values of common plant oils are given in Table 2.

Table 2. *Fatty acids, double bonds and iodine values of common plant oils (Lu and Larock, 2009).*

Plant Oils	Palmitic [%]	Stearic [%]	Oleic [%]	Linoleic [%]	Linolenic [%]	Avg. double bonds / triglyceride [%]	Iodine Value [mg/100g]
Soybean	11	4	23.4	53.3	7.8	4.6	117-143
Linseed	5.5	3.5	19.1	15.3	56.6	6.6	168-204
Palm	42.8	4.2	40.5	10.1	-	1.7	44-58
Canola	4.1	1.8	60.9	21	8.8	3.9	110-126
Sunflower	5.2	2.7	37.2	53.8	1	4.7	110-143
Cottonseed	21.6	2.6	18.6	54.4	0.7	3.9	90-119
Coconut	9.8	3	6.9	2.2	-	-	6-11
Olive	13.7	2.5	71.1	10	0.6	2.8	75-94
Corn	10.9	2	25.4	59.6	1.2	4.5	102-130
Sesame	9	6	41	43	1	3.9	103-116
Castor	1.5	0.5	5	4	0.5	2.7	82-88

Manufacturing Methods

The techniques used in the production of biocomposites are the same as those used in the production of conventional composite materials (Fowler et al., 2006). The main methods used for the production of thermoset polymer matrix composites are; hand lay-up technique, vacuum infusion method, and compression molding (Jiang, 2015).

Hand lay-up is the simplest method of production, in which the felt or woven fibers are laid in the mold and the matrix forming resin is applied. In this process, it is important that the resin should penetrate well into the fiber or fabric. In compression molding, the composite components are transformed into hot press molds. While the compression molding method has advantages such as the ability to produce complex shapes and the advantages of different wall thicknesses, the technique is more expensive than other methods because of the metal molds (Fuqua et al., 2012; Arıcasoy, 2016). In the case of vacuum infusion, large sandwiches are usually laid on the glass surface, then a vacuum bag is placed at the top layer to absorb the air inside and, if necessary, the material is allowed to cure in the oven or in the atmosphere conditions (Advani and Hsiao, 2012; Campbell, 2010).

The curing characteristics of bioresins are of paramount importance, as their physical properties and processability largely depend on the reaction rate and the degree of curing (Francucci et al., 2013). One of the greatest challenges of biocomposite production is this high curing temperature of biopolymers because many natural fibers are degraded at high temperatures (Jiang, 2015). Natural fibers need to be used at relatively low processing temperatures due to the possibility of fiber degradation at high temperatures (Mohanty et al., 2000). Thermal degradation of natural fibers occurs in two stages. The first one is the degradation of hemicellulose that occurs around 200°C, the second is the degradation of lignin at 280-300°C (Manthey et al., 2010). Thermoset biopolymers with high curing temperature which often exceeds 150°C, limits their use with natural fibers that are not resistant to high temperatures (Fowler et al., 2006).

Current studies

Studies on biocomposites consisting of plant oil-based bioresins and plant fibers in the literature mostly focus on the use of plant oil-based resins in a mixture of sythetic resins such as; AESO-styrene (Lee et al., 2013; O'Donnell et al., 2004), AESO-polyester (Wu & Li, 2017; Miyagawa et al., 2007), AESO-vinylester (Grishchuk and Karger- Kocsis, 2011), AESO-epoxy (O'Donnell et al., 2004; Miyagawa et al., 2007; Sahoo et al., 2018, Kocaman and Rahmetli, 2016; Ozkur et al., 2020), ESO-epoxy (Bakar et al., 2018; Sahoo et al. 2017), ELO-epoxy (Sahoo et al., 2018); epoxidized palm oil (EPO)-polyester (Mustapha et al., 2018; Mustapha et al., 2020), epoxidized methyl linseedate (EML)/ methyl ester of soybean oil (MESO)-unsaturated polyester (Mehta et al., 2004), and neem oil (NO)-phenolic resin (Manna et al., 2012) mixtures. The general outcomes show that the content of bioresins mostly reduce the tensile strength of the composites but improves the plasticity of the synthetic resin it is used with.

As above mentioned handicaps of the plant oil-based resins, there are limited but promising studies in which these plant oil-based bioresins are used as the only matrix material together with the natural fiber reinforcements.

In a study of the utilization of AESO in composite structures, Lee et al. (2013) examined the effects of different surface treatments (acetylation, silane and peroxide treatment) on chemical, morphological and interface properties of ramie fiber-reinforced AESO biocomposites. Results showed that all treatments reduced the hydrophilicity of the ramie fiber and removed the impurities from the fiber surface. Chemically treated ramie fibers caused a reduction in their water affinity thus enhanced the adhesion between ramie fiber and AESO resin. Moreover, in the silane treated samples, the interface shear strength was found higher than the other specimens, and it was stated that the interface which is one of the most important characteristics for biocomposites could be improved by applying silane treatment to the fibers.

In a study of Liu et al. (2018), biocomposite materials were produced using hemp fiber, AESO resin and two different bifunctional isocyanates (isocyanatoethyl methacrylate (IEM) and 3-isopropenyldimethylbenzyl isocyanate (TMI)), and the effect of different proportions of isocyanates (10 and 15% by weight) on the properties of the composite material was investigated. The properties of the produced composites were compared with the properties of pure AESO and AESO-styrene mixed composite materials. The results showed that both IEM and TMI increased the curing efficiency of AESO, decreased its viscosity and strengthened the bond it formed with hemp fiber. It was observed that the IEM-15 sample showed closer tensile and flexural strength with the styrene-containing composite material, while the TMI-15 sample had higher tensile modulus, flexural strength, and flexural modulus than the styrene-containing sample. As a result, it was seen that IEM and TMI could be an alternative material to styrene which was mixed with AESO in biocomposite production.

Akesson et al. (2009) examined the mechanical properties of natural fiber (air-laid hemp and linen mats) reinforced AESO biocomposites. Composite production was carried out by spray-up technique followed by compression molding. Tensile strength and dynamic mechanical thermal analysis tests have shown that the mechanical properties of composite materials increased with increasing fiber amount. The tensile modulus of samples with 70% reinforcement ratio varied between 5.8 - 9.7 GPa, and the flexural modulus varied between 3.7 -7.2 GPa according to the reinforcement type. It has also been understood that AESO resin could be reinforced with 70% by weight of fiber without any problems in production. It is concluded that this high fiber ratio has some advantages for composites such as higher mechanical strength, lower cost, and more renewable materials.

Kadem et al. (2018) produced biocomposite materials using sunflower oil and Alfa fiber in this study. Sunflower oil, used as resin, was first epoxidized and then acrylated (AESFO). Boron trifluoride (0.5 and 1 wt%) and cobalt octoate (0, 0.01, 0.02 to 0.03 wt%) were added to the AESFO resin as cationic initiator and catalyst, respectively, and copolymerized with styrene (30, 40 to 50 wt%). As a result of the preliminary analyses (stress at break, Young's modulus and elongation at break), the best AESFO/styrene/boron trifluoride/cobalt octoate ratio was determined as 50/50/0.5/0.02 and biocomposite production started. Alfa fibers were treated with a 5% NaOH solution and both treated and untreated fibers were added to the matrix material in proportions of 5, 7.5 and 10% by weight. The results obtained showed that the best tensile and thermal properties were obtained with the 7.5% treated Alfa fiber added sample.

In another study, Liu et al. (2016) produced a biocomposite using hemp fiber as a reinforcement material and AESO copolymerized with N-vinyl-2-pyrrolidone as a matrix material and added isophorone diisocyanate (IPDI) to the produced composite material to improve its properties. Fourier-transform infrared spectroscopy and nuclear magnetic resonance spectroscopy analyses results showed that the addition of IPDI strengthened the bond formed between AESO and hemp fibers and consequently improved the static and dynamic mechanical properties (tensile and flexural properties, storage modulus) of the composite material, but reduced its thermal durability. It has also been observed that the addition of IPDI to AESO resin reduced the viscosity and the curing temperature.

Adekunle et al. (2011) used thermoset polymer from soybean oil, jute woven fabrics and carded lyocell fiber to produce composites from renewable materials. Composites were designed in three categories; three different woven jute fabric reinforced panels, lyocell fiber reinforced panels and the hybrid panels consisting of sandwich structures of jute fabrics (outer part) and lyocell fibers (core part). Resin impregnation was realized by hand spraying and compression molding technique is used for manufacturing. According to the results, among the samples produced, the best mechanical properties (tensile strength: 144 MPa, tensile modulus: 18 GPa, bending strength: 217 MPa, bending modulus: 13 GPa, impact strength: 35 kJ /m^2) were obtained with lyocell reinforced composites. On the other hand, with the use of lyocell in hybrid composite, the mechanical properties were improved but lower storage modulus was obtained. As a result, the use of lyocell fiber in hybrid composites can overcome the limitations of woven fabrics.

Khot et al. (2011) aimed to produce strong composite structures by reinforcing AESO with various ratios of hemp and linen fibers. A resin transfer molding technique was used for manufacturing of composites. Results are compared with glass fiber reinforced composites. According to the results, the highest mechanical properties were obtained with glass reinforced samples. When 20% hemp reinforced composites (tensile strength 35 MPa, flexural strength 35.7-51.3 MPa) and linen reinforced composites (tensile strength 20-30 MPa, bending strength 45-65 MPa) were compared, it was found that the hemp reinforced structures had higher tensile strength, while the linen reinforced samples had higher bending strength. As a result, a hybrid model is suggested to combine the advantages of natural- and synthetic fiber-reinforced composites.

In a study of Fombuena et al. (2019), biocomposites consisting of epoxidized linseed oil (ELO) and flax fabric were produced by resin transfer molding technique. As a crosslinking agent, a 1:1 mixture of nadic methyl anhydride (MNA) and maleinized linseed oil (MLO) were used. Before production, flax fibers were treated using amino-silane, glycidyl-silane and maleic anhydride to enhance the interface of reinforcement and matrix materials. Test results showed that composites have higher mechanical properties when MNA was used alone as a hardener. When MNA and MLO were used together, impact resistance was increased 43% thus more ductile panels were manufactured due to the the presence of long fatty acid chains of MLO. Moreover, the maleic anhydride treatment improved the ductility of the composites due to the esterification of cellulose surface (Fombuena et al., 2019).

Liu et al. (2016) produced a biocomposite consisting of carded hemp fiber mats (5 plies) as a reinforcement material and AESO, as a matrix, using hot press machine. An N-vinyl-2-pyrrolidone (NVP) was used as the crosslinking agent and the results of this composite sample (NVP-AESO) were compared with styrene-based composite samples (St-AESO). The results showed that NVP-AESO samples containing 20% NVP by weight had higher glass transition temperature compared to St-AESO samples containing 20% St. In addition, its mechanical properties were found closer to each other. Increased NVP ratio (40% by weight) resulted in higher tensile strength, tensile modulus, flexural strength, flexural modulus, storage modulus compared to St-AESO samples. Consequently, the NVP–AESO resin could be used instead of traditional St-AESO resin since this novel resin system has comparable rheological behavior and lower curing temperature compared to the St–AESO resin. Moreover, NVP–AESO composites revealed enhanced matrix-fiber interface due to high reactivity of NVP monomers resulting in excellent mechanical properties (Liu et al., 2016).

In another study on the use of AESO in composite materials, Ramamoothy et al. (2012) produced AESO composite plates reinforced with woven and non-woven jute fabrics, non-woven lyocell, viscose matt and woven glass fabric to evaluate the mechanical properties (tensile, impact and bending strength) and moisture absorptions. Compression molding technique was used for composite production. Results indicated that the highest mechanical properties were obtained with glass and lyocell reinforced samples, while moisture absorption was found to be lowest in the samples reinforced with glass, lyocell and jute fibers. Moreover, the hybrid composites showed better mechanical properties compared to the woven and nonwoven jute fiber composites however, to improve the mechanical properties of the jute fiber reinforced composites, the ratio of of lyocell or glass fiber in the hybrid composite should be increased.

Application Areas

Some bioplastics have a lower performance factor than petroleum-based plastics and their shelf life is very short. Moreover, since the bio-products are more recent to be produced on the market, production price tags are not as cost-effective as fossil waste plastics production (Faruk et al., 2014). Therefore, these features limit their usages in several application areas. However, sustainable and environmentally friendly biocomposites owing to their comparable advantages such as biodegradability, low density, high toughness, acceptable specific strength properties, enhanced energy recovery, carbon dioxide retention, compete in the current market dominated by petroleum-based products (Abdul Khalil et al., 2012; Fowler et al., 2006). Automotive, construction, furniture and packaging industries are among the application areas where biocomposite materials are mostly preferred (Fowler et al., 2006).

Conclusion

With the increasing importance of environmental factors, the use of natural materials in the production of composite materials is increasing. Bioresins synthesized from renewable sources such as plant oils attract the attention of researchers in terms of sustainability, while natural fibers that offer many advantages are preferred as reinforcement materials. In recent years, studies on how bioresins obtained from the synthesis of vegetable fatty acids (soybean oil, flaxseed oil, etc.) take the place of synthetic resins have been the focus of researchers. Thus, plant oil-based resins become promising matrix materials for biocomposites owing to their tailored performance suited for engineering applications. Considering sustainability and environmental factors, it can be said that biocomposites obtained from natural fiber reinforced bioresins are one of the most important materials of the 21st century.

REFERENCES

Abdul Khalil H.P.S., Bhata U.H., Jawaid M., Zaidon A., Hermawan D. and Hadid Y.S. (2012). Bamboo fibre reinforced biocomposites: A review, *Materials & Design*, 42, 353-368.

Adekunle K., Patzelt C., Kalantar A. and Skrifvars M. (2011). Mechanical and viscoelastic properties of soybean oil thermoset reinforced with jute fabrics and carded lyocell fiber, *Journal of Applied Polymer Science,* 122(5), 2855–2863.

Adeniyi A.G., Onifade D.V., Ighalo J.O. and Adeoye, A.S. (2019). A review of coir fiber reinforced polymer composites. *Composites Part B: Engineering*, 176, 107305.

Advani S.G. and Hsiao K.T. (2012). Manufacturing techniques for polymer matrix composites (PMCs). Elsevier.

Ahmad F., Choi H. S. and Park M. K. (2015). A review: Natural fiber composites selection in view of mechanical, light weight, and economic properties, *Macromolecular Materials and Engineering*, 300(1), 10–24.

Ahmed K.S. and Vijayarangan S. (2006). Elastic property evaluation of jute-glass fiber hybrid composite using experimental and CLT approach, *Indian Journal of Engineering and Materials Science*, 13, 435-442.

Åkesson D., Skrifvars M. and Walkenström P. (2009). Preparation of thermoset composites from natural fibres and acrylate modified soybean oil resins, *Journal of Applied Polymer Science*, 114(4), 2502–2508.

Arıcasoy, O. (2016). Istanbul Chamber of Commerce Composite Sector Report.

Ashrafi B., Díez-Pascual A. M., Johnson L., Genest M., Hind S., Martinez-Rubi Y., González-Domínguez J. M., Martínez M. T., Simard B., Gómez-Fatou M. A. and Johnston A. (2012). Processing and properties of PEEK/glass fiber laminates: Effect of addition of single-walled carbon nanotubes, *Composites Part A: Applied Science and Manufacturing*, 43, 1267–1279.

Badawi S. S. (2007). Development of the weaving machine and 3D woven spacer fabric structures for lightweight composites materials, (*PhD Thesis*), Technical University of Dresden, Dresden.

Bakar M.B.A., Masri M.N., Amini, M.H.M., Thirmizir M.Z.M. and Salim, M.S. (2018). Mechanical, thermal and morphological properties of epoxy resin toughened with epoxidized soybean oil, *AIP Conference Proceedings*, 2030(1), 1-8.

Campbell F.C. (2010). Structural Composite Materials. ASM International.

Dilfi K.F.A, Balan A., Bin H., Xian G. and Thomas S. (2018). Effect of surface modification of jute fiber on the mechanical properties and durability of jute fiber-reinforced epoxy composites, *Special Issue: Epoxy Composites,* 39, E2519-E2528.

Dittenber D.B. and GangaRao H.V.S. (2012). Critical review of recent publications on use of natural composites in infrastructure, *Composites Part A: Applied Science and Manufacturing*, 43(8), 1419–1429.

Dungani R., Karina M., Subyakto, Sulaeman A., Hermawan D. and Hadiyane A. (2016). Agricultural waste fibers towards sustainability and advanced utilization: A review, *Asian Journal of Plant Sciences*, 15, 42-55.

Faruk O., Bledzki A. K., Fink H. P. and Sain M. (2014). Progress report on natural fiber reinforced composites, *Macromolecular Materials and Engineering*, 299(1), 9-26.

Francucci G, Cardona F. and Manthey N.W. (2013). Cure kinetics of an acrylated epoxidized hemp oil-based bioresin system, *Journal of Applied Polymer Science*, 128(3), 2030-2037.

Geethamma V.G., Mathew K.T., Lakshminarayanan R. and Sabu T. (1998). Composite of short coir fibers and natural rubber: Effect of chemical modification, loading and orientation of fiber, *Polymer,* 6, 1483-1490.

Habib F. and Bajpai M. (2011). Synthesis and characterization of acrylated epoxidized soybean oil for uv cured coatings, *Chemistry and Chemical Technology*, 5(3), 317-326.

Fouladi M.H., Ayub M. and Nor J.M. (2011). Analysis of coir fiber acoustical characteristics*, Applied Acoustics*, 72(1), 35-42.

Fombuena V., Petrucci R., Dominici F., Jordá-Vilaplana A., Montanes N. and Torre L. (2019). Maleinized linseed oil as epoxy resin hardener for composites with high bio content obtained from linen byproducts. *Polymers*, 11(2), 301.

Fowler P.A., Hughes J.M. and Elias R.M. (2006). Biocomposites: technology, environmental credentials and market forces, *Journal of the Science of Food and Agriculture*, 86(12), 1781-1789.

Fuqua M.A., Huo S. and Ulven C.A. (2012). Natural fiber reinforced composites, *Polymer Reviews*, 52, 259-320.

Gerbase A.E., Petzhold C.L. and Costa A.P.O. (2002). Dynamic mechanical and thermal behavior of epoxy resins based on soybean oil, *Journal of the American Oil Chemists' Society*, 79, 797-802.

Gowda T.M., Naidu A.C.B. and Chhaya R. (1999). Some mechanical properties of untreated jute fabric-reinforced polyester composites, *Composites Part A: Applied Science and Manufacturing*, 30, 277–284.

Grishchuk S., Karger-Kocsis J. (2011). Hybrid thermosets from vinyl ester resin and acrylated epoxidized soybean oil (AESO), *eXPRESS Polymer Letters*, 5(1), 2-11.

Haq M., Burgueño R., Mohanty A.K. and Misra M. (2008). Hybrid bio-based composites from blends of unsaturated polyester and soybean oil reinforced with nanoclay and natural fibers, *Composites Science and Technology*, 68, 3344-3351.

Haque M., Hasan M., Islam S. and Ali E. (2009). Physico-mechanical properties of chemically treated palm and coir fiber reinforced polypropylene composites, *Bioresource Technology*, 100(20), 4903-4906.

Jiang L. (2015). New manufacturing process for biocomposite sandwich parts using a myceliated core, natural reinforcement and infused bioresin, (*PhD Thesis*), Rensselaer Polytechnic Institute, Troy, New York.

Johnson R.D.J., Prabu V.A., Amuthakkannan P. and Prasath K.A. (2017). A review on biocomposites and bioresin based composites for potential industrial applications, *Reviews on Advanced Materials Science*, 48, 112-121.

Joseph P.V., Joseph K. and Thomas S. (1999). Effect of processing variables on the mechanical properties of sisal-fiber-reinforced polypropylene composites, *Composites Science and Technology*, 59(11), 1625-1640.

Joseph K., Filho R.D.T., James B., Thomas S. and Carvalho L.H. (1999). A review on sisal fiber reinforced polymer composites, *Revista Brasileira de Engenharia Agrícola e Ambiental*, 3(3), 367-379.

Joseph S., Joseph K. and Thomas S. (2006). Green composites from natural rubber and oil palm fiber: Physical and mechanical properties, *International Journal of Polymeric Materials and Polymeric Biomaterials*, 55(11), 925-945.

Kadem S., Irinislimane R. and Belhaneche-Bensemra N. (2018). Novel Biocomposites Based on Sunflower Oil and Alfa Fibers as Renewable Resources, *Journal of Polymers and the Environment*, 26, 3086–3096.

Khot S.N., Lascala J.J., Can E., Morye S.S., Williams G.I., Palmese G.R., Kusefoglu S.H. and Wool R.P. (2011). Development and application of triglyceride-based polymers and composites, *Journal of Applied Polymer Science*, 82(3), 703–723.

Kocaman S. and Ahmetli G. (2016). Eco-friendly natural filler based epoxy composites, *International Journal of Chemical, Molecular, Nuclear, Materials and Metallurgical Engineering,* 10, 471-474.

Kumar A and Srivastava A. (2017). Preparation and mechanical properties of jute fiber reinforced epoxy composites. *Industrial Engineering and Management*, 6(4), 234.

Kong X., Omonov T.S. and Curtis J.M. (2012). The development of canola oil based bio-resins, *Lipid Technology,* 24(1), 7-10.

Lee T.S., Choi H.Y., Choi H.N., Lee K.Y., Kim S.H., Lee S. G. and Yong D. K. (2013). Effect of surface treatment of ramie fiber on the interfacial adhesion of ramie/acetylated epoxidized soybean oil (AESO) green composite, *Journal of Adhesion Science and Technology*, 27(12), 1335-1347.

Liu W., Xie T. and Qiu R. (2016). Improvement of properties for biobased composites from modified soybean oil and hemp fibers: Dual role of diisocyanate, *Composites: Part A*, 90, 278–285.

Liu W., Chen T., Xie T. and Qiu R. (2016). Soybean oil-based thermosets with N -vinyl-2-pyrrolidone as crosslinking agent for hemp fiber composites. *Composites Part A: Applied Science and Manufacturing*, 82, 1–7.

Liu W., Fei M., Ban Y., Jia A., Qiu R. and Qiu J. (2018). Concurrent improvements in crosslinking degree and interfacial adhesion of hemp fibers reinforced acrylated epoxidized soybean oil composites, *Composites Science and Technology*, 160, 60-68.

Lu Y. and Larock, R. C. (2009). Novel polymeric materials from vegetable oils and vinyl monomers: Preparation, properties, and applications, *ChemSusChem,* 2, 136-147.

Lutton R.E.M., Taylor S., Sonebi M. and Murphy A. (2017). Commercial potential of bioresins and their success in thermosetting composites: An overview, *2nd International Conference on Bio-based Building Materials & 1st Conference on Ecological Valorisation of Granular and Fibrous Materials*, June 21th - 23th 2017, Clermont-Ferrand, France.

Mahesh D., Kowshigha K.R., Raju, N.V. and Aggarwal P.K. (2020). Characterization of banana fiber-reinforced polypropylene composites, *Journal of the Indian Academy Wood Science*, 17, 1–8.

N.W., F., G. and T. (2013). Thermo-mechanical properties of epoxidized hemp oil-based bioresins and biocomposites, *Journal of Reinforced Plastics and Composites*, 32(19), 1444-1456.

Manthey N.W., Cardona F., Aravinthan T., Wang H. and Cooney T. (2010). Natural fibre composites with epoxidized vegetable oil (EVO) resins: A review, *Southern Region Engineering Conference*, 11-12 November 2010, Toowoomba, Australia.

Mehta G., Mohanty A.K., Misra M. and Drzal L.T. (2004). Biobased resin as a toughening agent for biocomposites, *Green Chemistry*, 6(5), 254.

Meier M.A., Metzger J.O., Schubert U.S. (2007). Plant oil renewable resources as green alternatives in polymer science, *Chemical Society Reviews*, 36, 1788–1802.

Miyagawa H., Mohanty A.K., Burgueno R., Drzal L.T. and Misra M. (2007). Novel biobased resins from blends of functionalized soybean oil and unsaturated polyester resin, *Journal of Polymer Science Part B: Polymer Physics*, 45, 698-704.

Mohanty A. K., Misra M. and Hinrichsen G. (2000). Biofibres, biodegradable polymers and biocomposites: An overview, *Macromolecular Materials and Engineering*, 276/277, 1–24.

Mukherjee P.S. and Satyanarayana K.G. (1984). Structure and properties of some vegetable fibers, *Journal of Materials Science*, 19, 3925-3934.

Mustapha S.N.H., Aminuldin A., Zakaria S, Ramli R.A., Salim N. and Roslan R. (2018). Mechanical and thermal properties of calcium carbonate filled kenaf reinforced unsaturated polyester/epoxidized palm oil composite, *AIP Conference Proceedings 2030*.

Mustapha S.N.H., Farahaika C.W.N., Norizan C.W., Roslan R. and Mustapha R. (2020). Effect of kenaf/empty fruit bunch (EFB) hybridization and weight fractions in palm oil blend polyester composite, *Journal of Natural Fibers,* https://doi.org/10.1080/15440478.2020.1788686.

Mustapha R., Rahmat A.R., Abdul Majid R. and Mustapha S.N.H. (2019). Vegetable oil-based epoxy resins and their composites with bio-based hardener: a short review. *Polymer-Plastics Technology and Materials*, 1–16.

Mustapha S.N.H., Rahmat A.R., Arsad A. and Yeong S.K. (2014). Novel bio-based resins from blends of functionalised palm oil and unsaturated polyester resin, *Materials Research Innovations*, 18, 326-330.

Nayak S.K., Mohanty S. and Samal S.K. (2009). Influence of short bamboo/glass fiber on the thermal, dynamic mechanical and rheological properties of polypropylene hybrid composites, Materials Science and Engineering: A, 523, 32–38.

O'Donnell A., Dweib M.A. and Wool R.P. (2004). Natural fiber composites with plant oil-based resin, *Composites Science and Technology*, 64, 1135-1145.

Ozkur S., Sezgin H., Akay E., Yalcin-Enis I. (2020). Hybrid bio-based composites from blends of epoxy and soybean oil resins reinforced with jute woven fabrics, *Materials Research Express*, 7, 1-15.

Pin J.M., Sbirrazzuoli N. and Mija A. (2015). From epoxidized linseed oil to bioresin: An overall approach of epoxy/anhydride crosslinking, *ChemSusChem*, 8(7), 1232-1243.

Prabhakaran S., Krishnaraj V., Senthilkumar M. and Zitoun R. (2014). Sound and vibration damping properties of flax fiber reinforced composites, *Procedia Engineering*, 97, 573 – 581.

Prasad G.L.E., Gowda B.S.K. and Velmurugan R. (2017). A study on impact strength characteristics of coir polyester composites, *Procedia Engineering*, 173, 771 – 777.

Rahman M.M. and Khan M.A. (2007). Surface treatment of coir (Cocos nucifera) fibers and its influence on the fibers' physico-mechanical properties, *Composites Science and Technology,* 67, 2369–2376.

Ramamoorthy S.K, Di Q., Adekunle K. and Skrifvars M. (2012). Effect of water absorption on mechanical properties of soybean oil thermosets reinforced with natural fibers, *Journal of Reinforced Plastics and Composites*, 31(18), 1191-1200.

Ramamoorthy S.K. (2015). Properties and performance of regenerated cellulose thermoset biocomposites, *(PhD Thesis),* University of Borås, Sweden.

Raquez J.M., Deléglise M., Lacrampe M.F. and Krawczak P. (2010). Thermosetting bio-materials derived from renewable resources. A critical review, *Progress in Polymer Science*, 35, 487–509.

Sadiq A.S., Bello A.A., Tokan A. and Abdulsam S. (2018). Production and analysis of bioresin from mango (mangifera indica) kernel oil, *International Journal of Modern Research in Engineering and Technology*, 3(12), 5-16.

Saha P., Manna S., Sen R., Roy D. and Adhikari B. (2012). Durability of lignocellulosic fibers treated with vegetable oil–phenolic resin. *Carbohydrate Polymers,* 87(2), 1628–1636.

Sahoo S.K., Khandelwal V. and Manik G. (2018). Influence of epoxidized linseed oil and sisal fibers on structure–property relationship of epoxy biocomposite, *Polymer Composites,* 39, 2595-2605.

Sahoo S.K., Mohanty S. and Nayak S.K. (2017). Mechanical, thermal, and interfacial characterization of randomly oriented short sisal fibers reinforced epoxy composite modified with epoxidized soybean oil, *Journal of Natural Fibers*, 14, 357-367.

Sahoo S.K., Mohanty S. and Nayak S.K. (2015). Synthesis and characterization of bio-based epoxy blends from renewable resource based epoxidized soybean oil as reactive diluent, *Chinese Journal of Polymer Science,* 33, 137−152.

Sahoo S.K., Mohanty S. and Nayak S.K. (2015). Toughened bio-based epoxy blend network modified with transesterified epoxidized soybean oil: Synthesis and characterization, *RSC Advances*, 5, 13674-13691.

Sahoo S.K., Mohanty S. and Nayak S.K. (2015). Study on the effect of woven sisal fiber mat on mechanical and viscoelastic properties of petroleum based epoxy and bioresin modified toughened epoxy network, *Journal of Applied Polymer Science,* 132, 1-12.

Sahoo S.K., Mohanty S. and Nayak S.K. (2018). Mechanical, dynamic mechanical, and interfacial properties of sisal fiber-reinforced composite with epoxidized soybean oil-based epoxy matrix, *Polymer Composites*, 39, 2065-2072.

Sahoo S.K., Khandelwal V. and Manik G. (2018). Sisal fibers reinforced epoxidized nonedible oils based epoxy green composites and its potential applications, *Green Composites*, Singapore: Springer.

Sevkat E., Liaw B., Delale F. and Raju B.B. (2009). Drop-weight impact of plain-woven hybrid glass–graphite/toughened epoxy composites, *Composites Part A: Applied Science and Manufacturing*, 40, 1090–1110.

Shahzad A. (2011). Hemp fiber and its composites – a review, *Journal of Composite Materials*, 46(8), 973-986.

Sudiyani Y., Alawiyah S. and Sembiring K.C. (2008). Alkali pretreatment and enzymatic saccharification of oil palm empty fruit bunch fiber for production of ethanol, *Proceeding of The International Seminar on Chemistry 2008*, 30-31 October 2008, Jatinangor.

Wambua P., Ivens J. and Verpoest I. (2003). Natural fibres: can they replace glass in fibre reinforced plastics?, *Composite Science and Technology*, 63, 1259–1264.

Wu Y. and Li K. (2017). Replacement of styrene with acrylated epoxidized soybean oil in an unsaturated polyester resin from propylene glycol and maleic anhydride, *Journal of Applied Polymer Science,* 134(28), 45056.

Chapter 9

THE ROLE OF BIOPOLYMER SELECTION IN THE DESIGN OF ELECTROSPUN SMALL CALIBER VASCULAR GRAFTS TO REPLACE THE NATIVE ARTERIAL STRUCTURE

Janset OZTEMUR[1]
Ipek YALCIN ENIS[2]

1 Janset Oztemur, Istanbul Technical University, Textile Technologies and Design Faculty, Textile Engineering Department, Turkey. oztemurj@itu.edu.tr Orcid ID: https://orcid.org/0000-0002-7727-9172

2 Assist. Prof.Dr. Ipek Yalcin-Enis, Istanbul Technical University, Textile Technologies and Design Faculty, Textile Engineering Department, Turkey. ipekyalcin@itu.edu.tr Orcid ID: https://orcid.org/0000-0002-7215-3546

1. Introduction

Not included in the infectious diseases category, cardiovascular diseases (including coronary heart disease and stroke) are the most common disease worldwide and accounted for an estimated 17.8 million deaths in 2017. More than three-quarters of these deaths occurred in low-income and middle-income countries (Kaptoge et al., 2019). Deaths from cardiovascular diseases triggered by the increased stress level brought about by rural to urban resettlement and unhealthy eating habits increased by 21.1% between 2007 and 2017 (Fuster, 2014; Roth et al., 2018). According to the data of the World Health Organization, it is estimated that the annual incidence of deaths due to cardiovascular diseases worldwide will reach 23.6 million by 2030 (World Health Organization, 2020)

While mild cardiovascular diseases are treated with modification of dietary, lifestyle changes, and medications, treatment options for more damaged blood vessels usually consist of replacing the diseased part with a portion of the autologous (native) vessel via bypass method (Pashneh-Tala, MacNeil, & Claeyssens, 2016). Although autologous vessels are considered to be a quite good candidate for cardiovascular diseases, reasons such as alteration of the vascular structure (atherosclerosis), dimensional incompatibility of the autologous vessel, donor morbidity and the patient's previous vascular change or other diseases pose a risk (Liu et al., 2020; Zamani et al., 2017). On the other hand, saphenous vein, which is the most preferred autologous vein in bypass procedures, carries the risk of structural deterioration when exposed to blood pressure as well as vascular occlusion (Bos, Poot, Beugeling, Van Aken, & Feijen, 1998; Eschenhagen, Reichenspurner, & Zimmermann, 2013). Therefore, the necessity of finding alternative solutions to overcome the problems experienced in autologous vessels has been among the prominent issues in recent years. However, allografts taken from donors or cadavers, and xenografts obtained from animals are alternatives, they cannot fully meet this need due to the lack/incompatibility of donors and their short life (Hasan et al., 2014). For all these reasons, artificial grafts, which offer more risk-free and easier application, promise for patients who need vascular replacement.

Today, artificial vessels/prostheses based on polyethylene terephthalate (PET), polytetrafluoroethylene (PTFE), and polyurethane (PU) are successful and commercially available for large diameter (> 6mm) vessels. However, these polymers do not provide success in small diameter (<6mm) vascular graft applications due to the discrepancy at the anastomosis point of the artificial graft and native blood vessel which causes unordinary blood flow, thrombosis, and intimal hyperplasia (Seifalian et al., 2003). Moreover, the use of the aforementioned polymers in small vessels, in addition to having properties such as inadequate structural porosity, insufficient cell adhesion, and proliferation, low elasticity level, also causes restenosis (narrowing of the vessel and thus the restriction of the blood) and various infections (Liu et al., 2020; Spadaccio et al., 2016). Considering autologous vascular insufficiency and the inconvenience of existing commercial polymers, extensive studies are needed on a wide variety of subheadings ranging from material selection, production technology, construction features to modification techniques to develop biocompatible small caliber vascular grafts.

Tissue engineering is an alternative issue that offers the formation of scaffolds (including vascular grafts) that allow the tissue to produce its extracellular matrix (ECM) using biodegradable polymers (J. Wu et al., 2018). Even though there are many fabrication techniques to produce tissue-engineered fibrous scaffolds electrospinning is one of the most cost-effective and simple methods of producing polymer fibers ranging from under-micron sizes to above-micron sizes (Rogina, 2014; Subbiah, Bhat, Tock, Parameswaran, & Ramkumar, 2005). Moreover, this technique allows obtaining the desired properties in the final structure due to its high surface to volume ratio, adjustable porosity, and controllable pore architecture such as the size and shape, as well as a wide range of biomaterial utilization (Bhardwaj & Kundu, 2010; Kai, Liow, & Loh, 2015a). On the other hand, as in other tissue engineering applications, the main goal in vascular grafts is to mimic the native vascular structure, so the material to be chosen should meet the needs of the vascular structure such as re-endothelialization and cell attachment (Hiob, She, Muiznieks, & Weiss, 2017).

In this review, the requirements to mimic the native artery, promising natural and synthetic biopolymers, and recent studies based on their use in electrospun scaffolds for small caliber vascular grafts are discussed in detail to highlight the importance of search for novel material for researchers.

2. How to Imitate a Native Artery Structure?

The native artery has a highly complex, multi-layered structure, and in a replacement vascular graft design each layer is expected to be imitated by considering the physical, mechanical, histological and topographic features of each layer of the native vessel (Adhikari, Tucker, & Thomas, 2019) . The vascular structure consists of three main layers: tunica intima, tunica media and tunica adventitia. The tunica intima, the innermost part of the three concentric layers closest to the blood flow, consists mainly of a simple but regular single endothelial cell layer (EC) containing connective tissues, and is directly connected to the basement membrane. Also, biological signaling events, orientation of endothelial cells, intracellular protein expression, cytoskeleton construction, anti-platelet aggregation, and cell-cell interactions can be regulated in this layer. (Jia, Li, Weng, Gu, & Chen, 2020). Tunica media is the habitat of spindle-shaped smooth muscle cells (SMC). Having low tensile strength in the middle layer, elastin functions as a relaxant stress behavior and distributes stress evenly across the wall of the vessel to the stronger collagen fibers (Goins, Webb, & Allen, 2019). Tunica adventitia, the outermost layer of fibroblast cells, consists of an extracellular collagen matrix which contains perivascular nerve cells, and is responsible for preventing vasodilation and deformation under physiological stress (Goins et al., 2019; Yalcin Enis & Gok Sadikoglu, 2018).

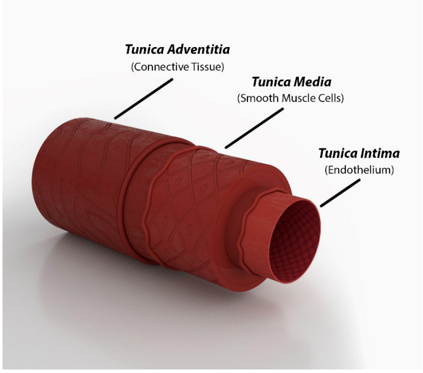

Figure 1. *The structure of a native artery*

Dynamic-mechanical compliance between the native artery and the vascular graft is highly crucial; otherwise, problems such as flow separation and low wall shear stress may arise as well as the failure of blood flow and intimal hyperplasia may be faced (Montini-Ballarin et al., 2017). One of the main elements of this compliance is the elastin/collagen structure that forms the basis of the natural vascular structure. The vascular structure shows low modulus response at low strain first due to low modulus elastin, while at higher tensions it shows stiffening behavior by straightening elastin and high modulus collagen fibers; furthermore, this mechanical behavior is called the J-shaped structure (Zhalmuratova et al., 2019). Imitation of this structure in accordance with mechanical needs affects the elastic behaviors such as the formation of the J-shape structure, which is an extremely critical feature (Montini-Ballarin et al., 2016). The researchers aim to design vascular grafts that behave as a J-shaped structure under pressure in their studies by utilizing both natural (Akentjew et al., 2019) and synthetic polymers (Rapoport et al., 2012; Yang et al., 2016). Arteries whose constituent components are collagen and elastin are constantly exposed to pressure and shear stress due to the flow of blood with a velocity of 1.2 cm/s and a pressure of 87 mmHg, continuously. This biomechanical stretch and un-stretch cycle causes momentary dimensional changes in artery diameter. (Hoskins et al., 2017). Therefore, a tissue-engineered vascular graft (TEVG) should be resistant to blood pressure and stretching cycle. Moreover, TEVGs should have a mechanical strength similar to native vessels, with a burst pressure of approximately 2000 mmHg to prevent aneurysmal expansion (Seifu, Purnama, Mequanint, & Mantovani, 2013). This aneurysm problem for vascular graft designs is also discussed by Yalcin Enis et al., not in terms of the compliance difference between the scaffold and the native vessel but the difference through the length of the fibrous scaffold because of nonhomogeneous fiber distribution obtained (Figure 2) (Yalcin Enis, Horakova, Gok Sadikoglu, Novak, & Lukas, 2017). The vascular scaffolds should also have dynamic compliance and sufficient suture retention when surgically sutured with the native artery (Zamani et al., 2017).

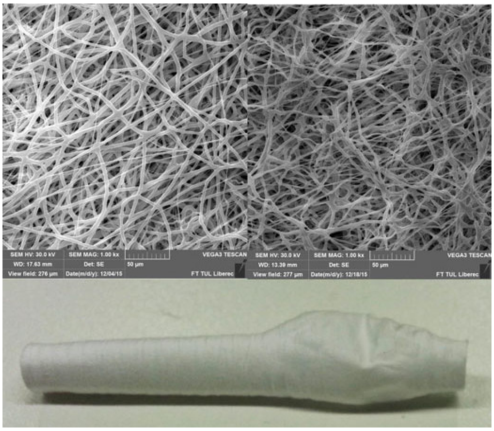

Figure 2. *Scanning electron microscope (SEM) images of a tubular vascular graft structure; (a) before burst pressure testing, (b) after testing (aneurysm part). Aneurysm part of the scaffold (c) Reprinted from (Yalcin Enis et al., 2017).*

Table 1. *Mechanical properties of native human blood vessels*

Type of Blood Vessel	Elastic Modulus (MPa) Circ./Long.*	Ultimate Stress (MPa) Circ./Long.	Strain at Failure (%) Circ./Long.	Burst Pressure (mmHg)	Suture Retention (N)	Compliance (%/100mmHg)	Reference
Saphenous vein	42.62 ±27.76 /130.2 ±56.36	3.01 ±1.91 /13.22 ±5.73	NA	NA	NA	NA	(Donovan et al., 1990)
	NA	NA	11±5/17±10	1599±877	1.76-2.45	0.7-2.6	(Konig et al., 2009; Zamani et al., 2017)
Internal mammary artery	8 /16.8	4.1/4.3	134/59	NA	NA	NA	(Hasan et al., 2014)
	NA	NA	NA	3196±1264	1.35±4.5	11.5±3.9	(Konig et al., 2009)

***Circ.,** circumferential; **Long.,** longitudinal

On the other hand, each layer of the multilayered arteries has different mechanical properties and each layer serves different functions. Therefore, the morphological, topographic, mechanical, and biological properties of each layer should be unique. For instance, the innermost layer is expected to have low porosity that allows the proliferation of endothelial cells but also prevents blood leakage, while the middle and outer layers are expected to have a larger porosity suitable for SMCs diffusion (Wu et al., 2018). Moreover, a suitable vascular graft should provide adequate anti-thrombogenicity to the structure to prevent coagulation or stenosis after implantation and promoting proper endothelialization (Joshi et al., 2020).

These properties are largely related to the material selection and optimization of the construction parameters (Figure 3). Although natural polymers are preferred in terms of biocompatibility in many studies, these polymers are insufficient in terms of their mechanical properties. At this point, synthetic biopolymers come to the fore.

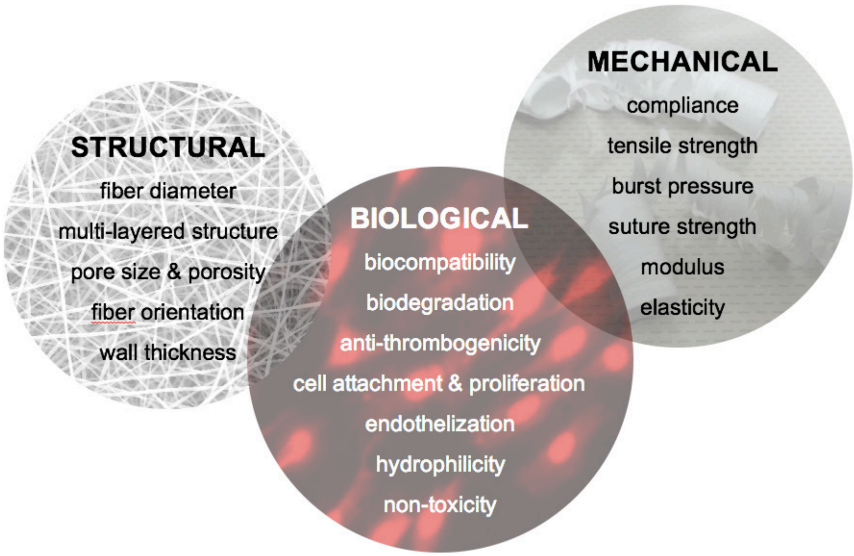

Figure 3. *Design parameters of a native artery*

3. Biopolymers

The scaffold material plays a key role to obtain an effective regenerated vascular construction likewise in all tissue engineering strategies because it provides the basic structure for cell growth (Thomas, Lekshmi, & Nair, 2013). Although it is highly preferred in large diameter grafts, the use of polymers such as PET, ePTFE, and PU in small diameter grafts is limited due to incomplete endothelialization and intimal hyperplasia caused by the long stay of these polymers in the body (Hiob et al., 2017). Polymers that can be degraded in the biological environment and do not show toxic effects in this process are also very advantageous materials because there is no need for a second operation to remove the graft from the body (Kai, Liow, & Loh, 2015b; Xue & Greisler, 2003). Hence, biodegradable polymers have become promising materials for vascular grafting applications.

The biodegradable polymers can be divided into two groups as natural and synthetic. The natural biodegradable polymers are very successful in biocompatibility and cell activities, while synthetic ones have properties such as high strength and controllable degradation (Thomas et al., 2013).

3.1.Natural biopolymers

Biopolymers that are derived from natural sources are widely used in biomedical applications as they are highly biocompatible and offers opportunity to enhanced cell activities such as cell adhesion, growing, proliferation, and cell to cell signalling (Shojaee & Bashur, 2017)

Collagen: Collagen is the main protein in the extracellular matrix structure (Zhou, Cao, Ma, & Lin, 2010). There are two major types of collagens: fibrillar and non-fibrillar. For most animal tissues, fibrillar collagen forms (collagen type I, II, III, VI and XI) elongated fibril structures which are recognised for their structural function in mechanical support. Collagen type I is one of the most commonly used collagen types in tissue engineering applications. Moreover, non-fibrillary collagens can be classified into sub-categories including the network-forming collagens (collagen types IV and VII), fibril-associated collagens (FACITs, collagen types IX and XII), and membrane-associated triple helix collagens (MACITs) (Copes, Pien, Van Vlierberghe, Boccafoschi, & Mantovani, 2019). Even though collagen has excellent biocompatibility and weak antigenicity, it suffers from the mechanical properties (Lee, Singla, & Lee, 2001).

Elastin: Elastin is also one of the core components of the extracellular vascular matrix that provides elasticity and strength (Koens et al., 2010) . In addition to its desirable mechanical properties, elastin serves as a major promoter for vascular cells, prohibiting for smooth muscle cell migration and proliferation, and improving endothelial cell attachment and proliferation (Wise et al., 2011).

Gelatin: Gelatin is a type of protein that includes 19 aminoacids in its structure (Vroman & Tighzert, 2009). It is derived from the collagen by hyrolisation method. Although gelatin is preferred owing to its fluid loss prevention feature, it is generally used in a mixture of other biopolymers due to the insufficient mechanical and degredation features (Gu et al., 2016).

Silk Fibroin: Silk fibroin is a protein based polymer which is derived from animal sources (Catto et al., 2015). It is composed of highly repeated primary sequence which results in great homogeneity in the secondary ß-sheet structure, a high crystalline characteristics and impressive mechanical features. As silk is an attractive biodegradable material in terms of not only its mechanical properties but also suitability for cell activities and biocompatibility, it has a great place in small vascular graft studies (Marelli et al., 2012). Moreover, it can be conveniently processed into a number of structures including hydrogels, films, porous scaffolds, and micro/nano particles (Chan et al., 2019).

Chitosan: Chitosan is a biocompatible, biodegradable, nontoxic, and non-antigenic biopolymer sourced from crustaceans such as crabs and shrimps (Zhu et al., 2009). Further, it has a rigid and crystalline structure due to the strong intermolecular hydrogen bonds in the structure (Vroman & Tighzert, 2009). For this reason, it is mostly used in a blend of softer polymers in order to be used in tissue engineering applications.

Keratin: Keratin is a biocompatible polymer that is suitable for cell adhesion and exhibits hydrophilic behavior thanks to the Ar-Gly-Asp (RGD) sequence and various carboxyl and amino-pendant groups in its structure (Yen, Chen, Huang, Kuo, & Lin, 2015).

3.2. Synthetic biopolymers

Synthetic polymers are widely used to acquire scaffolds with sufficient mechanical properties which keep their strength for relatively long periods of time and allow the regeneration of new tissues. The mechanical properties of synthetic polymers can be managed effectively compared to natural polymers, so they allow the development of tissue engineering structures with improved mechanical properties (Song, Feijen, Grijpma, & Poot, 2011).

Poly (ε-caprolactone) (PCL): PCL is a synthetic polyester which, under physiological conditions, can be degraded by hydrolysis of its ester bonds (Mohandesnezhad et al., 2020). Also, it is an aliphatic polyester that has been widely utilized in long-term tissue engineering applications such as vascular grafts due to its low biodegradation rate, superior biocompatibility, and suitability for cell acitivities (Ren et al., 2015).

Poly (lactic acid) (PLA): PLA is a commercially available bio-based polymer used in a variety of applications due to its high strength, modulus and biodegradability. It is formed by bacterial fermentation of biomass such as sugar or starch, or polymerization of lactic acid, which can be formed by chemical synthesis (Murariu & Dubois, 2016). At the same time, its bioabsorbable and biocompatible properties make PLA an extremely promising material for medical applications (Saini, Arora, & Kumar, 2016).

Poly (glycolic acid) (PGA): As a synthetic aliphatic polyester, PGA is one of the most commonly used biomaterials in tissue engineering applications (Matsuzaki, John, Shoji, & Shinoka, 2019). Despite its high mechanical strength and biocompatibility, its hard structure limits the use of PGA (Dehnavi, Parivar, Goodarzi, Salimi, & Nourani, 2019). For this reason, it is used as a copolymer or blended with other biopolymers that shows high elongation at breakage values.

4. Current Studies

4.1. Based on natural biopolymers

Natural polymers are preferred for vascular grafts due to aforementioned numerous advantages but their insufficient mechanical properties limit their use alone thus they are mostly used in a blend of other natural polymers or biomaterials.

In a study of Jia et al. (2019), a biomimetic extracellular matrix electrospun vascular graft was produced by using collagen and hyaluronic acid (HA) due to the rapid endothelization capacity of collagen-HA composition. The ratio of collagen-HA was defined as 8:2 and 1,1,1,3,3,3-hexafluoroisopropanol (HFIP) was used as a solvent. Likewise other studies in the literature, the fiber diameter increased (402 ± 298 to 1132 ± 729 nm) with increasing the collagen-HA concentration (6 to 10%). Also, the scaffolds were seeded with porcine iliac artery endothelial cells (PIECs). 4 hours after cell seeding, it was observed that PIECs adhered to the surface, and after 72 hours the number of cells began to increase. Such findings suggested the promise of this collagen-HA electrospun nanofibers as a nominee for interior layer vascular tissue-engineered scaffolding with the enhancement of the mechanical properties. Zhou et al. (2010) designed a tubular vascular graft structure based on collagen/silk fibroin (Col/SF) blends (blend ratios differ as 0/100, 5/100, 10/100, and 20/100) by using electrospinning technique. All the electrospinning parameters were kept constant (20 kV voltage, 0.015 ml/min feed rate, and 20 cm tip to collector distance). SF was dissolved in $CaCl_2/H_2O/C_2H_5OH$ and collagen was dissolved in acetic acid. According to the morphological analysis results, the crystallinity and the fiber diameter increased with increasing collagen content in the blend (1.11±0.20 µm, 1.29±0.28 µm, 1.40±0.28 µm, and 2.45±0.80 µm). On the other hand, all the samples had water uptake capacity higher than 70% which is dedicated to the high porosity of the electrospun materials and hydrophilic response of the structure. Although the tensile strengths of the samples varied between 1.5-2.5 MPa, the elongation at break values decreased when the collagen concentration reached 10%. This rapid decline in elongation at break values was clarified by the increasing crystallinity of SF. Similar to Zhou et. al, Marelli et al. (2012) produced an electrospun small caliber tubular vascular graft with

SF and collagen type I. In this study, electrospun SF was constructed, then hybridization process was carried out by dynamic dipping of the SF tubular structure in the collagen solution. The hybrid structure had SF fibers with average diameter of 750 nm and 70 nm diameter of collagen fibrils. Also, this hybrid structure showed enhanced mechanical and biological response compared to the neat SF fibrous structure since the hybridization process strengthened the material's mechanical qualities by forming bonds of physical or chemical nature between the two proteins. While SF had 2.62±0.21 N ultimate tensile strength (UTS), SF-C hybrid structure had UTS of 3.17±0.32 N. Moreover, the burst pressure and compliance (at 80-120 mmHg) were recorded as 894 ±2 4.91 mmHg and 3.24 ± 058 %/mmHg for SF-C, and 575.67 ± 17.47 mmHg and 3.51 ± 0.42 %/mmHg for SF, respectively. Although cell metabolic activity was observed in both samples 1,3,5 and 7 days after cell seeding, it has been said that the activity in SF-C was higher than the SF, and the hybrid structure gave rise to the construct cytocompatibility. Sato et al. (2010) aimed to construct electrospun small diameter vascular graft (ES) using Bombyx mori silk fibroin. To enhance the mechanical strength and water permeability of the vascular graft, the scaffolds were covered by a silk-based sponge, and the combined structure was named as ESSC. According to the results it was seen that with the increase in the concentration of silk from 3% to 8%, fiber diameters increased from 936±479 nm to 2137±1244 nm. The water permeability value of 10-40 ml/min/cm^2, which was attributed as a threshold value for vascular grafts, decreased from 227±25 ml/min/cm^2 to 30±5.3 ml/min/cm^2 with the addition of sponge to the vascular graft structure, but this value was also satisfactory. Moreover, the electrospun silk graft had a convincing compliance (2.4%/100 mmHg) which was higher than the compliance of native saphenous vessels. Tensile strength of ES was measured as 74±0.40 and 2.76±0.13 MPa and elastic modulus of ES was measured as 1.70±0.16 and 4.94±0.16 MPa for circumferential and longitudinal directions, respectively; whereas these values were improved in ESSC scaffolds (tensile strength 28±0.81/3.83±0.48 MPa; elastic modulus 2.91±0.67/6.63±0.77 MPa, for circumferential and longitudinal directions, respectively) with additional silk-based sponge structure. Yen et al. (2015) investigated the performance of keratin/silk fibroin electrospun membranes for vascular graft applications. In this study, it was considered to combine the cell adhesion properties of keratin with the mechanical strength of silk fibroin. The weight ratios of fibroin/silk were defined as 9:1 (FK91), 8:2 (FK82), 7:3 (FK73), and fibroin (F). Moreover, degummed silk fibroin dissolved in $CaCl_2/H_2O/C_2H_5OH$, then keratin/silk fibroin blend was dissolved in formic acid. Due to the morphology analysis results, the fiber diameter increased (2.27 ± 0.65 to 5.74 ± 1.04) with the increment of fibroin content in the structure and a porous structure was obtained with appropriate pore sizes. Since fibroin had high tensile strength, the ultimate tensile strength increased with the increment of the ratio of fibroin in the structure. The ultimate tensile strength values of FK73, FK82, FK91, and F were measured as 1.74±0.12MPa, 1.81±0.10MPa, 2.02 ± 0.06MPa, and 2.09±0.06MPa, respectively. The increased keratin ratio gave the structure a hydrophilic behavior by reducing the contact angle thus, the cell adhesion response was also enhanced with keratin addition. In consequence, FK82 was found to be suitable for vascular graft structure in terms of ultimate tensile strength, cell adhesion, and microstructural properties.

4.2. Based on synthetic biopolymers

Synthetic biopolymers can also be used alone, in a mixture with other synthetic polymers or in the form of copolymers to meet the desired properties of vascular grafts.

Yalcin et al. (2014) presented a study in which the design parameters were determined to mimic the real vascular structure in morphological, mechanical, and biological aspects and to create a biodegradable small caliber vascular graft structure. At a concentration of 18 w/v % solution was prepared by utilizing PCL (45,000 Mn) and chloroform/ethanol (9/1 v/v) solvent system. The tubular scaffolds were constructed with a diameter of 6 mm and a wall thickness of 250 µm. The scaffold surface consisted of homogeneous and bead-free fibers, and the diameter of the fibers was measured between 0.25-0.75 µm in the first peak and 1.75-2.25 µm in the second peak. While the porosity and the pore size were measured as 29-36.39% and 8.60-29 µm^2, respectively by a static software program; 49.7-93.83 µm^2 pore sizes were achieved by bubble method which tests under dynamic conditions. Except for 250 r/min, a tensile strength of 1 MPa was obtained at all rotational speeds (1000, 5000 and 10,000 r/min) in radial direction, while the tensile strength was recorded between 0.1-0.4 MPa at all rotational speeds in the 90° direction. This was due to the numerically increased radially oriented fibers contributing to the maximum tensile strength. Likewise, in the axial directions of scaffolds produced at 5000 and 10,000 r/min speeds, higher elongation at break values were achieved as 324% and 386%, respectively. The relatively low elongation at break value of 224% in the 90° at 15,000 r/min can be explained by the substantial decrease in the amount of interconnecting fibers that can withstand loading. Furthermore, the biocompatibility of PCL was found sufficient for all the samples produced at different rotational speeds by MTT test using 3T3 fibroblasts, and after 7 days of the culture, cell proliferation was observed. In a later study of Yalcin et al. (2017), a 6 mm diameter bilayer vascular graft was fabricated using electrospinning method. PCL (45,000 and 80,000 Mn) and poly (lactid-co-caprolactone) (PLC) (70/30 molar ratio) were used as the main polymers. PCL (45,000 Mn) was dissolved in chloroform/ethanol, and PCL (80,000) and PLC were dissolved in chloroform/ethanol/acetic acid. Bilayer structures were produced from combinations of each polymer types including randomly distributed inner layer (produced at 5000 min^{-1}) and radially oriented (produced at 15, 000 min^{-1}) outer layer. Diameters of randomly distributed fibers were higher than that of oriented fibers for PCL (45,000 Mn) (4.02±1.22 µm for random fibers, and 3.47±0.88 µm for oriented fibers) and PCL (80,000Mn) samples (2.96±0.88 µm for random fibers and 2.50±0.85 µm for oriented fibers) which was thought to be caused by mechanical stress. In contrast, due to the highly elastic behavior of PLC, the randomly distributed fiber diameter was lower compared to the oriented fibers for PLC surfaces (4.01±1.01 µm for random fibers and 4.59±1.42 µm for oriented fibers). The bilayer tubular structure with the highest ultimate tensile strength of 2.7 MPa belonged to PLC+PCL_80 and its elongation at break was measured as 650%. Owing to the high elastic response, PLC samples showed the highest burst resistance (1500 mmHg). Jia et al. (2020), designed a biomimetic trilayer tubular vascular scaffolds from biodegradable polymers. They used PCL as an intima layer due to its super biocompatibility and low degradation rate, poly(lactic-co-glycolide) (PLGA) as a media layer, and polyurethane (PU) for adventitia which is the outer layer because of its both biocompatibility and mechanical properties. The inner and outer layers were produced by electrospinning method while the media layer is produced via freeze-drying method due to macropore and high connectivity possibilities. The researchers obtained oriented PCL and PU nanofibers, and PLGA fibrous structure which has significantly high porosity (83.73 ± 1.23 %) and large pore sizes (47.93 ± 18.73 µm). PCL and PU layers were thermally treated for effective crosslinking thus a trilayer scaffold was achieved with enhanced mechanical properties. It was demonstrated that electrospun PCL and PU structures had higher degradation rate (24.86±7.29 % and 12.62±1.59 % at week 6, respectively) than PLGA scaffold (3.01±0.54 % at week 6) since ultrafine electrospun fibers have more interaction with lysozyme because of its high surface area. Consequently, a trilayer tubular biocompatible and biodegradable vascular graft was produced which has good endothelialization with restrained thrombosis and hyperplasia in the PCL intima layer, cell penetration due to large pore size in PLGA media layer, and high-level tensile strength in PU adventitia layer. In this detailed study, Abudula et al. (2019) aimed to develop an electrospun cellulose nanofibril (CNF) reinforced vascular grafts structure using PLA and poly (butylene succinate) (PBS) biopolymers. CNF was chosen because of its nanoscale property that helps to achieve better orientation and strong adsorption ability of moisture useful for medical applications. PLA/PBS blend was used at different ratios (100/0, 75/25, 60/40, 50/50, 40/60, 35/65, 25/75 and 0/100), and the polymer blend was dissolved in chloroform/acetone (3/1) solvent system at a constant 6% concentration. For the CNF reinforced system, the ratios were kept as 50/50 for PLA/(PBS+CNF), and the CNF concentration was varied between 1-5%. With the addition of the PLA into the solution, the viscosity increased and the bead-free structures were obtained. On the other hand, the fiber diameter decreased with the CNF reinforcement (1019±75 nm for PLA, 409±51 nm for hybrid structure with 50/50 of PLA/PBS, 379±46 nm for composite fiber with 1% CNF, and 267±27 nm for composite fiber with 5% CNF). The optimal mechanical performance was obtained using PLA/PBS blend with a 50/50 ratio which has 112.5±1.5% elongation at break and 98.6±4.6 MPa elastic modulus in addition to highest tensile strength (2.77±0.23 MPa). Moreover, 5% CNF reinforcement enhanced the tensile strength of the PLA/PBS blend to 3.46±0.28 MPa. As a result of the water contact angle analysis, it was observed that the contact angle varied between 69 and 114.1° and this angle decreased and hydrophilicity increased with CNF induction. In addition to the morphological and mechanical investigations, cell activity analysis displayed that PLA/PBS blends had better cell adhesion compared to the neat PLA and PBS. 7 and 14 days after the cell seeding, PLA/PBS (50/50) and CNT reinforced PLA/PBS scaffolds had higher cell proliferation than neat PLA and neat PBS. Montini-Ballarin et al. (2016) actualized a study that points to the mechanical behaviors of an electrospun bilayer vascular grafts. In this study, a segmented poly(ester urethane) (SPEU) named PHD and poly(L-lactic acid) (PLLA) were used to imitate the mechanical features of elastin and collagen, respectively. While PHD was dissolved in 2,2,2-trifluoroethanol (TFE); dimethylformamide (DMF)/dichloromethane (DCM) (40/60) mixture was used as a solvent for PLLA. Then, two types of solutions were blended at 90/10 (for the outer layer) and 50/50 wt/wt (for inner layer) ratios to prepare PLLA/PHD solutions. 5 mm diameter of vascular grafts were produced with different wall thicknesses. According to the uniaxial tensile test, the stress-strain curve of the PHD showed an elastic behavior like elastin, and the slope of the PLLA resembled collagen which has a more stiff structure. Moreover, the bilayer structure had Young's modulus values of 6.24±1.69 MPa in the circumferential direction and 29.54±5.85 MPa in the axial direction. Moreover, with high strain values of bilayer scaffolds (%142-233), they exhibited more flexible structure than the rigid Dacron and Goretex commercial grafts. The suture strengths of scaffolds were between 0.98-2.45 N and the strength increased as the wall thickness of the graft increased. On the other hand, the compliance values of vascular grafts were between 1.59-1.72% (80-120mmHg), and although it was lower than the coronary artery, it showed J-shaped behavior like in the native blood vessel. Furthermore, the burst pressures were 1232-1775 mmHg (for axial elongation L/L0=1) which is closer to human saphenous veins. Zhai et al. (2013) designed a potential vascular graft for substitution of the femoral artery by using P(LLA-CL) block copolymer which has hydrophobicity, enhanced mechanical property, good degradation rate, and elastic property, and heparin biomaterial that was used for its feature to increase proliferation of endothelial cells (ECs) and inhibit the proliferation of vascular SMCs. The scaffold was produced by a coaxial electrospinning method as it is an effective method to gain favor from both the strong properties of P(LLA-CL) and heparin. Heparin was utilized as a core component to be encapsulated while the P(LLA-CL) copolymer as the shell component. Besides the P(LLA-CL)/heparin blend, P(LLA-CL) scaffold was produced to determine the effect of heparin on the morphology and the cell activity. The results obtained in dry conditions showed that the tensile strength and strain values for P(LLA-CL) were 18.34 ± 0.18 MPa and 504 ± 21.62%, respectively, while for P (LLA-CL) / heparin it was 17.56 ± 0.43 MPa and 460 ± 33.14, respectively. It can be said that all results are suitable for vascular grafts. At the end of the study, both P(LLA-CL) and P(LLA-CL)/heparin vascular grafts were implanted to Beagle dogs, and all of the scaffolds resulted in success. However, the P(LLA-CL)/heparin composite has been said to be a much better candidate for blood vessel repair, as it has a 100% patency rate in the early stage, 50% in the medium term, and 25% in the long term.

4.3. Based on blended biopolymers

Since both natural and synthetic biopolymers have numerous advantages but also noticeable barriers, the blend of natural and synthetic biopolymers for vascular applications is among the research topics of interest to researchers.

McClure et al. (2012) designed electrospun trilayered vascular grafts using PCL, elastin (ELAS), collagen (COL), and silk (SF), also accomplished of their mechanical investigations. All the materials were dissolved in HFIP; moreover, ternary polymer systems were used at different rates. ELAS-based solutions were blended in 45-45-10, 55-35-10, 65-25-10 ratios of PCL-ELAS-COL and PCL-ELAS-SF, while SF and COL based solutions were blended in 45-10-45, 55-10-35, and 65-10-25 ratios of PCL-ELAS-COL and PCL-ELAS-SF. Scaffolds were crosslinked with either 1-ethyl-3-(3-dimethyl aminopropyl)-carbodiimide (EDC) or genipin (GEN). While the tensile strength of EDP crosslinked ELAS based scaffolds was between 0.4-2.3 MPa, those with GEN crosslinked ones were between 0.3-2 MPa and the peak stress increased with the decrease in elastin amount in the structure and the increase in the amount of PCL. On the other hand, EDC cross-linked 65-10-25 ratio PCL-ELAS-COL based (modulus of 13.5 + 3.08 MPa), and EDC cross-linked 65-25-10 based PCL-ELAS-COL based (modulus of 13.2 + 1.0 MPa) has been identified as the hardest structures. Besides, the average burst strength of the PCL-ELAS-COL scaffold varying between 1500-3500 had 45-45-10 and 65-25-10 medial layers, while the higher the amount of PCL in the adventitia layer, the burst resistance also increased. According to the compliance analysis performed in a 4 week degradation process, it was determined that the compliance of the adventitial layer with GEN crosslink at the ratio of 55-10-35 and the medial layer of the 55-35-10 ratio of PCL-ELAS-COL based scaffold at the 0, 1, 2 and 4 weeks increased over time. However, in PCL-ELAS-SF scaffolds, no increase in compliance was observed during the degradation process. Wu et al. (2018) designed a trilayer tubular vascular graft that has axially aligned (PLCL)/collagen (COL) fiber-based inner layer, circumferentially oriented PLGA/silk yarn-based middle layer, and a random PLCL/COL fiber-based outer layer. PLCL/COL blend was dissolved in 1,1,1,3,3,3-hexafluoro-2-propanol (HFIP) at 10% concentration, and PLGA/silk composite was dissolved in HFIP at 15% concentration. Axially aligned PLCL/COL fibers were produced by electrospinning which has a collector in a magnetic field, then the double nozzle electrospinning system was used for PLGA/silk yarns. Finally, random PLCL/COL fibers were created by a simple single-nozzle electrospinning system for the outer layer. Axially aligned PLCL/COL fibers and random PLCL/COL fibers had diameters of 336.90±107.27 nm and 361.15±136.91 nm, respectively. On the other hand, the PLGA/silk oriented yarns had the 206.17±46.23 µm diameter, and the pore size was measured as 39.02±6.25 µm. The trilayer tubular structure had about 50 N tensile force and 100% strain in the axial direction. Since all layers had satisfactory mechanical behaviors, PLCL/COL fiber surfaces were seeded with human umbilical vein endothelial cells (HUVECs) and PLGA/SF fiber surface was seeded with SMCs. As a result, it was observed that the cells continued to survive and proliferated after 1, 3 and 6 days of the cell transplantation thus each layer was found both mechanically and biologically suitable for vascular grafts. Hajiali et al. (2011) aimed to produced PGA/gelatin-based nanofibrous scaffolds for vascular graft applications by using the electrospinning technique. PGA/gelatin blends with different weight ratios (100/0, 90/10, 70/30, and 50/50) were dissolved in hexafluoroisopropanol, and the solution concentration was kept in constant as 10 wt%. The morphological analysis showed that the neat PGA surface has a beady structure while the continuous and bead-free fibers occured with the induction of gelatin; moreover, the higher the gelatin ratio in the structure, the greater the fiber diameter (87.72±23.34 nm for neat gelatin fibers, and 863.96±265.09 nm for PGA/gelatin (50/50) fibers). Similar to fiber diameter, the pore size increased from 0.317 to 20.465 µm with the increasing gelatin content. Compared to the pure PGA sheet, PGA/gelatin 10% sheet (650 kPa tensile strength and 30-40 MPa modulus), PGA/gelatin 30% sheet (1 MPa tensile strength and 32 MPa modulus), and PGA/gelatin 50% sheet (1.907 MPa tensile strength and 72 MPa modulus) were improved in terms of tensile strength and Young's modulus values. The scaffolds were seeded with two types of cells; HUVECs and human umbilical artery smooth muscle cells (HUASMCs), and the cell viabilities were controlled at day 1, 3, and 5. At the end of the 5th day, the viability of HUVECs was mostly seen in PGA/10 wt% gelatin, while the viability of HUASMCs was mostly seen in PGA/30 wt% gelatin. Based on the results, it was concluded that using PGA/10 wt% gelatin as the inner layer and PGA/30 wt% gelatin in the outer layer of a bilayer tubular vascular graft structure would be promising. Stitzel et al (2006). conducted a study involving the production of an electrospun small diameter vascular graft, and morphological, mechanical, and biological analysis of the grafts produced. Collagen and elastin were used to support the scaffold biologically and a high molecular weight PLGA (Mw 110,000) was used for mechanical performance. This polymer mixture was dissolved at a concentration of 15% in HFIP, and the isotropic electrospun fibrous scaffolds were constructed with a diameter of 4.75 mm and a thickness of 1 mm. Also, the diameter of randomly oriented fibers was 0.720±0.35 μm. Mechanical analysis results showed that the strains are almost identical in the axial and circumferential directions before failure occurred at a strain of 40%, and the burst pressure was 1425 mmHg. These findings indicated that these scaffolds possessed sufficient strength and elasticity to be used as replacements for native vessels. On the other hand, 70-80% of both ECs and SMCs survived according to the MTT and neutral red biocompatibility assay after the day 1,3,5, and 7. Moreover, after 4 days, a confluent layer of endothelial cells on the inner surface and after 3 days, smooth muscle cells on the outer surface of the scaffold were determined. Consequently, it was stated that when the scaffold was implanted subcutaneously in mice, no physical or biological damage was encountered. Joshi et al. (2020) aimed to produced heparin loaded polycaprolactone (PCL)/gelatin (PG) nanofibers via co-axial electrospinning and co-cultured it with mesenchymal stem cells (MSCs) and HUVECs to the potential use of vascular grafts. PCL was used as a core part due to its biocompatibility and high strength and PG was preferred as a shell part as it is a natural material and it provided significant biocompatibility. PCL (in 7-10% concentration) and PG (in 8-10% concentration) were dissolved in 2,2,2 Trifluoroethanol (TFE). After the fibrous mats were produced they were cross-linked in the glutaraldehyde vapor; also, the scaffolds were heparinized. According to the morphological analysis, smooth and bicomponent fibers structures were obtained, and the mean fiber diameters of 1.3 μm for 10%PCL-10%gelatin, 1.13 μm for 8%PCL-10%gelatin, and 400 nm or 7%PCL-8%gelatin were measured. PCL-gelatin nanofiber structure had enhanced tensile properties in contrast to gelatin-based structure due to the PCL backbone which provided better mechanical properties. In consequences of the platelet adhesion test, appropriate antithrombogenic characteristics through heparin functionalization was also obtained. In a similar study of Joshi et al., Coimbra et al. (2017) using coaxial electrospinning technology, produced bicomponent fiber structured scaffolds for vascular grafts consisting of PCL as core and functionalized gelatin (GelMA) as a sheet. Core-shell fibrous meshes were prepared using three separate GelMA to PCL weight ratios (25/75, 50/50 and 75/25). Also, PCL was dissolved in TFE, and GelMA was solubilized in a 2,2,2-trifluoroethanol (TFE) / glacial acetic acid (AAc) mixture (4/1 v/v). According to the results obtained from the morphological analysis, continuous and bead-free fibers could not be obtained from the 25GelMA/75PCL sample, while continuous fibers with a diameter of 600 nm were obtained on the 50GelMA/75PCL and 75GelMA/25PCL surfaces. Moreover, while the water contact angle was 110° on the pure PCL-based surface, it was stated that as the amount of gelatin in the structure increased, the water contact angle decreased from 100° to 40° and the structure gained hydrophilic character, thus increasing the cell adhesion availability. On the other hand, in the analysis performed 1 day after cell seeding, cell attachment and proliferation were found to be quite successful on the GelMA/PCL surface. In a study by Wang et al. (2013), heparin grafted PLA and chitosan (CS) based conduits with core-sheath nanofiber structure were produced for vascular applications. PLA solution was prepared by dissolving in DMF, and chitosan powder was mixed with PEO then dissolved into the formic acid. PLA was used as a core, and chitosan was used as a shell (at 1/3 and 1/1 of PLA/CS proportion). While the fibers at 3/1 ratio were uniform and the mean diameter was 600 nm, uniform fiber structures with a 1/1 ratio could not be obtained and it exhibited a higher mean diameter (2 μm). On the other hand, the crosslinking was applied to the fibrous surfaces to improve the mechanical features of the scaffolds. The neat PLA-based surface had approximately 60 MPa elastic modulus and 1-2 MPa tensile breaking strength whereas the PLA/CS bicomponent structure had an enhanced modulus of approximately 110 MPa and tensile breaking strength of 2-3 MPa. The PCL/ CS surface acted better in terms of cell activity in comparison to the cell culture sample. The relative rate of growth of PCL/CS nanofibers was 90% and that of pure PLA 70%. On the other hand, if the findings of the MTT were compared, the growth in the number of cells in PCL/CS nanofibers (from 68 to 92.4%) was counted greater than in PLA nanofibers (from 63.7 to 70.3%).

5. Conclusion

Although synthetic materials such as ePTFE, PET and PU have been used in artificial vascular prosthesis applications for many years, they are insufficient in small diameter vascular applications and cause problems such as intimal hyperplasia since they are not biodegradable materials. Reasons such as an insufficient number of donors and tissue incompatibilities limit the use of autografts. In this context, the need for the discovery of new materials is obvious. The use of biomaterials has gained considerable importance in recent years since they contain features such as biocompatibility, biodegradability, cell activity, and suitable mechanical strength. Moreover, electrospinning facilitates the creation of the desired small diameter artificial vascular structure including nano/microscale fibers with adjustable pore architecture and appropriate fiber morphology. When the diversity in biopolymers meets unlimited design parameters that can be adjusted through electrospinning, it offers researchers endless combinations to design the best graft that can mimic the target tissue in the best possible way. All these studies focusing on small caliber vascular grafting studies hold great promise for patients suffering from cardiovascular diseases.

REFERENCES

Abudula, T., Saeed, U., Memic, A., Gauthaman, K., Hussain, M. A., & Al-Turaif, H. (2019). Electrospun cellulose Nano fibril reinforced PLA/PBS composite scaffold for vascular tissue engineering. *Journal of Polymer Research*, *26*(5). https://doi.org/10.1007/s10965-019-1772-y

Adhikari, K. R., Tucker, B. S., & Thomas, V. (2019). Tissue engineering of small-diameter vascular grafts. *Biointegration of Medical Implant Materials*, *1957*, 79–100. https://doi.org/10.1016/B978-0-08-102680-9.00004-4

Akentjew, T. L., Terraza, C., Suazo, C., Maksimuck, J., Wilkens, C. A., Vargas, F., … Acevedo, J. P. (2019). Rapid fabrication of reinforced and cell-laden vascular grafts structurally inspired by human coronary arteries. *Nature Communications*, *10*(1), 1–15. https://doi.org/10.1038/s41467-019-11090-3

Bhardwaj, N., & Kundu, S. C. (2010). Electrospinning: A fascinating fiber fabrication technique. *Biotechnology Advances*, *28*(3), 325–347. https://doi.org/10.1016/j.biotechadv.2010.01.004

Bos, G. W., Poot, A. A., Beugeling, T., Van Aken, W. G., & Feijen, J. (1998). Small-diameter vascular graft prostheses: Current status. *Archives of Physiology and Biochemistry*, *106*(2), 100–115. https://doi.org/10.1076/apab.106.2.100.4384

Catto, V., Farè, S., Cattaneo, I., Figliuzzi, M., Alessandrino, A., Freddi, G., … Tanzi, M. C. (2015). Small diameter electrospun silk fibroin vascular grafts: Mechanical properties, in vitro biodegradability, and in vivo biocompatibility. *Materials Science and Engineering C*, *54*, 101–111. https://doi.org/10.1016/j.msec.2015.05.003

Chan, A. H. P., Filipe, E. C., Tan, R. P., Santos, M., Yang, N., Hung, J., … Wise, S. G. (2019). Altered processing enhances the efficacy of small-diameter silk fibroin vascular grafts. *Scientific Reports*, *9*(1), 1–14. https://doi.org/10.1038/s41598-019-53972-y

Coimbra, P., Santos, P., Alves, P., Miguel, S. P., Carvalho, M. P., de Sá, K. D., … Ferreira, P. (2017). Coaxial electrospun PCL/Gelatin-MA fibers as scaffolds for vascular tissue engineering. *Colloids and Surfaces B: Biointerfaces*, *159*, 7–15. https://doi.org/10.1016/j.colsurfb.2017.07.065

Copes, F., Pien, N., Van Vlierberghe, S., Boccafoschi, F., & Mantovani, D. (2019). Collagen-based tissue engineering strategies for vascular medicine. *Frontiers in Bioengineering and Biotechnology*, *7*(JUL), 1–15. https://doi.org/10.3389/fbioe.2019.00166

Dehnavi, N., Parivar, K., Goodarzi, V., Salimi, A., & Nourani, M. R. (2019). Systematically engineered electrospun conduit based on PGA/collagen/bioglass nanocomposites: The evaluation of morphological, mechanical, and bio-properties. *Polymers for Advanced Technologies*, *30*(9), 2192–2206. https://doi.org/10.1002/pat.4648

Donovan, D. L., Schmidt, S. P., Townshend, S. P., Njus, G. O., & Sharp, W. V. (1990). Material and structural characterization of human saphenous vein. *Journal of Vascular Surgery*, *12*(5), 531–537. https://doi.org/10.1016/0741-5214(90)90005-U

Eschenhagen, T., Reichenspurner, H., & Zimmermann, W. H. (2013). Tissue-Engineered Cardiovascular Products. In *Principles of Tissue Engineering: Fourth Edition* (Fourth Edi). Elsevier. https://doi.org/10.1016/B978-0-12-398358-9.00084-7

Goins, A., Webb, A. R., & Allen, J. B. (2019). Multi-layer approaches to scaffold-based small diameter vessel engineering: A review. *Materials Science and Engineering C*, *97*(November 2018), 896–912. https://doi.org/10.1016/j.msec.2018.12.067

Gu, B. K., Park, S. J., Kim, M. S., Lee, Y. J., Kim, J. Il, & Kim, C. H. (2016). Gelatin blending and sonication of chitosan nanofiber mats produce synergistic effects on hemostatic functions. *International Journal of Biological Macromolecules*, *82*, 89–96. https://doi.org/10.1016/j.ijbiomac.2015.10.009

Hajiali, H., Shahgasempour, S., Naimi-Jamal, M. R., & Peirovi, H. (2011). Electrospun PGA/gelatin nanofibrous scaffolds and their potential application in vascular tissue engineering. *International Journal of Nanomedicine*, *6*, 2133–2141. https://doi.org/10.2147/ijn.s24312

Hasan, A., Memic, A., Annabi, N., Hossain, M., Paul, A., Dokmeci, M. R., … Khademhosseini, A. (2014). Electrospun scaffolds for tissue engineering of vascular grafts. *Acta Biomaterialia*, *10*(1), 11–25. https://doi.org/10.1016/j.actbio.2013.08.022

Hiob, M. A., She, S., Muiznieks, L. D., & Weiss, A. S. (2017). Biomaterials and Modifications in the Development of Small-Diameter Vascular Grafts. *ACS Biomaterials Science and Engineering*, *3*(5), 712–723. https://doi.org/10.1021/acsbiomaterials.6b00220

Hoskins, P. R., Lawford, P. V., Hardman, D., Hose, R., Narracott, A. J., Keevil, S. F., … Wilkinson, I. B. (2017). Cardiovascular Biomechanics. In P. R. Hoskins, P. V. Lawford, & B. J. Doyle (Eds.), *Cardiovascular Biomechanics*. Cham: Springer International Publishing. https://doi.org/10.1007/978-3-319-46407-7

Jia, W., Li, M., Kang, L., Gu, G., Guo, Z., & Chen, Z. (2019). Fabrication and Comprehensive Characterization of Biomimetic Extracellular Matrix Electrospun Scaffold for Vascular Tissue Engineering Applications. *Journal of Materials Science*, *54*(15), 10871–10883. https://doi.org/10.1007/s10853-019-03667-6

Jia, W., Li, M., Weng, H., Gu, G., & Chen, Z. (2020). Design and comprehensive assessment of a biomimetic tri-layer tubular scaffold via biodegradable polymers for vascular tissue engineering applications. *Materials Science* *and Engineering C*, *110*(February), 110717. https://doi.org/10.1016/j.msec.2020.110717

Joshi, A., Xu, Z., Ikegami, Y., Yamane, S., Tsurashima, M., & Ijima, H. (2020). Co-culture of mesenchymal stem cells and human umbilical vein endothelial cells on heparinized polycaprolactone/gelatin co-spun nanofibers for improved endothelium remodeling. *International Journal of Biological Macromolecules*, *151*, 186–192. https://doi.org/10.1016/j.ijbiomac.2020.02.163

Kai, D., Liow, S. S., & Loh, X. J. (2015a). Biodegradable polymers for electrospinning: Towards biomedical applications. *Materials Science and Engineering C*, *45*, 659–670. https://doi.org/10.1016/j.msec.2014.04.051

Kai, D., Liow, S. S., & Loh, X. J. (2015b). Biodegradable polymers for electrospinning: Towards biomedical applications. *Materials Science and Engineering C*, *45*, 659–670. https://doi.org/10.1016/j.msec.2014.04.051

Koens, M. J. W., Faraj, K. A., Wismans, R. G., Van Der Vliet, J. A., Krasznai, A. G., Cuijpers, V. M. J. I., … Van Kuppevelt, T. H. (2010). Controlled fabrication of triple layered and molecularly defined collagen/elastin vascular grafts resembling the native blood vessel. *Acta Biomaterialia*, *6*(12), 4666–4674. https://doi.org/10.1016/j.actbio.2010.06.038

Konig, G., McAllister, T. N., Dusserre, N., Garrido, S. A., Iyican, C., Marini, A., … L'Heureux, N. (2009). Mechanical properties of completely autologous human tissue engineered blood vessels compared to human saphenous vein and mammary artery. *Biomaterials*, *30*(8), 1542–1550. https://doi.org/10.1016/j.biomaterials.2008.11.011

Lee, C. H., Singla, A., & Lee, Y. (2001). Biomedical applications of collagen. *International Journal of Pharmaceutics*, *221*, 1–22. https://doi.org/https://doi.org/10.1016/S0378-5173(01)00691-3

Liu, F., Liao, X., Liu, C., Li, M., Chen, Y., Shao, W., … He, J. (2020). Poly(l-lactide-co-caprolactone)/tussah silk fibroin nanofiber vascular scaffolds with small diameter fabricated by core-spun electrospinning technology. *Journal of Materials Science*, *55*(16), 7106–7119. https://doi.org/10.1007/s10853-020-04510-z

Marelli, B., Achilli, M., Alessandrino, A., Freddi, G., Tanzi, M. C., Farè, S., & Mantovani, D. (2012). Collagen-Reinforced Electrospun Silk Fibroin Tubular Construct as Small Calibre Vascular Graft. *Macromolecular Bioscience*, *12*(11), 1566–1574. https://doi.org/10.1002/mabi.201200195

Matsuzaki, Y., John, K., Shoji, T., & Shinoka, T. (2019). The evolution of tissue engineered vascular graft technologies: From preclinical trials to advancing patient care. *Applied Sciences (Switzerland)*, *9*(7). https://doi.org/10.3390/app9071274

McClure, M. J., Simpson, D. G., & Bowlin, G. L. (2012). Tri-layered vascular grafts composed of polycaprolactone, elastin, collagen, and silk: Optimization of graft properties. *Journal of the Mechanical Behavior of Biomedical Materials*, *10*, 48–61. https://doi.org/10.1016/j.jmbbm.2012.02.026

Mohandesnezhad, S., Pilehvar-Soltanahmadi, Y., Alizadeh, E., Goodarzi, A., Davaran, S., Khatamian, M., … Akbarzadeh, A. (2020). In vitro evaluation of Zeolite-nHA blended PCL/PLA nanofibers for dental tissue engineering. *Materials Chemistry and Physics*, *252*(January), 123152. https://doi.org/10.1016/j.matchemphys.2020.123152

Montini-Ballarin, F., Calvo, D., Caracciolo, P. C., Rojo, F., Frontini, P. M., Abraham, G. A., & V. Guinea, G. (2016). Mechanical behavior of bilayered small-diameter nanofibrous structures as biomimetic vascular grafts. *Journal of the Mechanical Behavior of Biomedical Materials*, *60*, 220–233. https://doi.org/10.1016/j.jmbbm.2016.01.025

Montini-Ballarin, F., Suárez-Bagnasco, D., Cymberknop, L. J., Balay, G., Caracciolo, P. C., Negreira, C., … Abraham, G. A. (2017). Elasticity response of electrospun bioresorbable small-diameter vascular grafts: Towards a biomimetic mechanical response. *Materials Letters*, *209*, 175–177. https://doi.org/10.1016/j.matlet.2017.07.110

Murariu, M., & Dubois, P. (2016). PLA composites : From production to properties ▯. *Advanced Drug Delivery Reviews*, *107*, 17–46. https://doi.org/10.1016/j.addr.2016.04.003

Pashneh-Tala, S., MacNeil, S., & Claeyssens, F. (2016). The tissue-engineered vascular graft - Past, present, and future. *Tissue Engineering - Part B: Reviews*, *22*(1), 68–100. https://doi.org/10.1089/ten.teb.2015.0100

Rapoport, H. S., Fish, J., Basu, J., Campbell, J., Genheimer, C., Payne, R., & Jain, D. (2012). Construction of a tubular scaffold that mimics j-shaped stress/strain mechanics using an innovative electrospinning technique. *Tissue Engineering - Part C: Methods*, *18*(8), 567–574. https://doi.org/10.1089/ten.tec.2011.0286

Ren, X., Feng, Y., Guo, J., Wang, H., Li, Q., Yang, J., … Li, W. (2015). Surface modification and endothelialization of biomaterials as potential scaffolds for vascular tissue engineering applications. *Chemical Society Reviews*, *44*(15), 5680–5742. https://doi.org/10.1039/c4cs00483c

Rogina, A. (2014). Electrospinning process: Versatile preparation method for biodegradable and natural polymers and biocomposite systems applied in tissue engineering and drug delivery. *Applied Surface Science*, *296*, 221–230. https://doi.org/10.1016/j.apsusc.2014.01.098

Saini, P., Arora, M., & Kumar, M. N. V. R. (2016). Poly(lactic acid) blends in biomedical applications. *Advanced Drug Delivery Reviews*, *107*, 47–59. https://doi.org/10.1016/j.addr.2016.06.014

Sato, M., Nakazawa, Y., Takahashi, R., Tanaka, K., Sata, M., Aytemiz, D., & Asakura, T. (2010). Small-diameter vascular grafts of Bombyx mori silk fibroin prepared by a combination of electrospinning and sponge coating. *Materials Letters*, *64*(16), 1786–1788. https://doi.org/10.1016/j.matlet.2010.05.024

Seifalian, A. M., Salacinski, H. J., Tiwari, A., Edwards, A., Bowald, S., & Hamilton, G. (2003). In vivo biostability of a poly(carbonate-urea) urethane graft. *Biomaterials*, *24*(14), 2549–2557. https://doi.org/10.1016/S0142-9612(02)00608-7

Seifu, D. G., Purnama, A., Mequanint, K., & Mantovani, D. (2013). Small-diameter vascular tissue engineering. *Nature Reviews Cardiology*, *10*(7), 410–421. https://doi.org/10.1038/nrcardio.2013.77

Shojaee, M., & Bashur, C. A. (2017). Compositions Including Synthetic and Natural Blends for Integration and Structural Integrity: Engineered for Different Vascular Graft Applications. *Advanced Healthcare Materials*, *6*(12), 1–14. https://doi.org/10.1002/adhm.201700001

Song, Y., Feijen, J., Grijpma, D. W., & Poot, A. A. (2011). Tissue engineering of small-diameter vascular grafts: A literature review. *Clinical Hemorheology and Microcirculation*, *49*(1–4), 357–374. https://doi.org/10.3233/CH-2011-1486

Stitzel, J., Liu, J., Lee, S. J., Komura, M., Berry, J., Soker, S., … Atala, A. (2006). Controlled fabrication of a biological vascular substitute. *Biomaterials*, *27*(7), 1088–1094. https://doi.org/10.1016/j.biomaterials.2005.07.048

Subbiah, T., Bhat, G. S., Tock, R. W., Parameswaran, S., & Ramkumar, S. S. (2005). Electrospinning of nanofibers. *Journal of Applied Polymer Science*, *96*(2), 557–569. https://doi.org/10.1002/app.21481

Thomas, L. V., Lekshmi, V., & Nair, P. D. (2013). Tissue engineered vascular grafts - Preclinical aspects. *International Journal of Cardiology*, *167*(4), 1091–1100. https://doi.org/10.1016/j.ijcard.2012.09.069

Vroman, I., & Tighzert, L. (2009). Biodegradable polymers. *Materials*, *2*(2), 307–344. https://doi.org/10.3390/ma2020307

Wang, T., Ji, X., Jin, L., Feng, Z., Wu, J., Zheng, J., … He, N. (2013). Fabrication and Characterization of Heparin-Grafted Poly-L-lactic acid−Chitosan Core−Shell Nanofibers Scaffold for Vascular Gasket. *ACS Applied Materials and Interfaces*, *5*, 3757–3763. https://doi.org/dx.doi.org/10.1021/am400369c

Wise, S. G., Byrom, M. J., Waterhouse, A., Bannon, P. G., Ng, M. K. C., & Weiss, A. S. (2011). A multilayered synthetic human elastin/polycaprolactone hybrid vascular graft with tailored mechanical properties. *Acta Biomaterialia*, *7*(1), 295–303. https://doi.org/10.1016/j.actbio.2010.07.022

World Health Organization. (2020). Cardiovascular Diseases. Retrieved from https://www.who.int/health-topics/cardiovascular-diseases/#tab=tab_1

Wu, J., Hu, C., Tang, Z., Yu, Q., Liu, X., & Chen, H. (2018). Tissue-engineered Vascular Grafts: Balance of the Four Major Requirements. *Colloids and*

Interface Science Communications, *23*(February), 34–44. https://doi.org/10.1016/j.colcom.2018.01.005

Wu, T., Zhang, J., Wang, Y., Li, D., Sun, B., El-Hamshary, H., … Mo, X. (2018). Fabrication and preliminary study of a biomimetic tri-layer tubular graft based on fibers and fiber yarns for vascular tissue engineering. *Materials Science and Engineering C*, *82*, 121–129. https://doi.org/10.1016/j.msec.2017.08.072

Xue, L., & Greisler, H. P. (2003). *Biomaterials in the development and future of vascular grafts*. 472–480. https://doi.org/10.1067/mva.2003.88

Yalcin Enis, I., & Gok Sadikoglu, T. (2018). Design parameters for electrospun biodegradable vascular grafts. *Journal of Industrial Textiles*, *47*(8), 2205–2227. https://doi.org/10.1177/1528083716654470

Yalcin Enis, I., Horakova, J., Gok Sadikoglu, T., Novak, O., & Lukas, D. (2017). Mechanical investigation of bilayer vascular grafts electrospun from aliphatic polyesters. *Polymers for Advanced Technologies*, *28*(2), 201–213. https://doi.org/10.1002/pat.3875

Yalcin, I., Horakova, J., Mikes, P., Sadikoglu, T. G., Domin, R., & Lukas, D. (2016). Design of Polycaprolactone Vascular Grafts. *Journal of Industrial Textiles*, *45*(5), 813–833. https://doi.org/10.1177/1528083714540701

Yang, S. kyeong, Shafiq, M., Kim, D., Park, C., Jung, Y., & Hyun, S. (2016). Characterization and preparation of bioinspired resorbable conduits for vascular reconstruction. *Macromolecular Research*, *24*(4), 371–379. https://doi.org/10.1007/s13233-016-4042-4

Yen, K. C., Chen, C. Y., Huang, J. Y., Kuo, W. T., & Lin, F. H. (2015). Fabrication of keratin/fibroin membranes by electrospinning for vascular tissue engineering. *Journal of Materials Chemistry B*, *4*(2), 237–244. https://doi.org/10.1039/c5tb01921d

Zamani, M., Khafaji, M., Naji, M., Vossoughi, M., Alemzadeh, I., & Haghighipour, N. (2017). A Biomimetic Heparinized Composite Silk-Based Vascular Scaffold with sustained Antithrombogenicity. *Scientific Reports*, *7*(1), 1–14. https://doi.org/10.1038/s41598-017-04510-1

Zhai, W., Qiu, L. jun, Mo, X. mei, Wang, S., Xu, Y. fei, Peng, B., … Zheng, J. hua. (2013). Coaxial electrospinning of P(LLA-CL)/heparin biodegradable polymer nanofibers: potential vascular graft for substitution of femoral artery. *Journal of Biomedical Materials Research - Part B Applied Biomaterials*, *107*(3), 471–478. https://doi.org/10.1002/jbm.b.32972

Zhalmuratova, D., La, T. G., Yu, K. T. T., Szojka, A. R. A., Andrews, S. H. J., Adesida, A. B., … Chung, H. J. (2019). Mimicking "j-Shaped" and Anisotropic Stress-Strain Behavior of Human and Porcine Aorta by Fabric-Reinforced Elastomer Composites. *ACS Applied Materials and Interfaces*, *11*(36), 33323–33335. https://doi.org/10.1021/acsami.9b10524

Zhou, J., Cao, C., Ma, X., & Lin, J. (2010). Electrospinning of silk fibroin and collagen for vascular tissue engineering. *International Journal of Biological Macromolecules*, *47*(4), 514–519. https://doi.org/10.1016/j.ijbiomac.2010.07.010

Zhu, C., Fan, D., Duan, Z., Xue, W., Shang, L., Chen, F., & Luo, Y. (2009). Initial investigation of novel human-like collagen/chitosan scaffold for vascular tissue engineering. *Journal of Biomedical Materials Research - Part A*, *89*(3), 829–840. https://doi.org/10.1002/jbm.a.32256

Chapter 10

A JAVASCRIPT FRAMEWORK FOR VOICE BROWSING

İzer ÖZLÜ[1]
Özgün YILMAZ[2]

1 B.Sc., Ege University, Department of Computer Engineering, izerozlu@gmail.com
2 Assoc. Prof. Dr., Ege University, Department of Computer Engineering, ozgun.yilmaz@ege.edu.tr

1. Introduction

World Wide Web (WWW) is a rich source of information. It is used for communication, banking, business, education, socialization, e-Health, e-Government, and etc. (Efthimiou et al., 2019). WWW is accessed through web browsers, which employ graphical user interfaces (GUIs) to interact with the users. Most of the websites present their content visually and make the user interact with the website through peripheral devices such as mouse and keyboard (Griol, Manuel Molina, & Corrales, 2011; Pérez, 2019). Interaction with computers through these traditional devices require fine motor skills. Therefore, it is impossible or at least difficult for the motor-handicapped or visually impaired users to interact with the web browser (Rozado, Niu, & Lochner, 2017; Sengupta, Ke, Menges, Kumar, & Staab, 2018).

A solution to this problem might be voice browsing. Voice browsing facilitates speech recognition to extract commands. Then the extracted commands are executed. It is used for navigation and interacting with the web site.

In this paper, a Javascript framework, namely Speech-to-Command, for supporting web developers to integrate voice commands into their software is proposed. It integrates Google Cloud Speech-to-Text (GCST) service and other Javascript libraries (RecordRTC and JEST) to accomplish voice browsing and provides the developers an easy way of doing this. Converting voice commands to text is achieved by using a third-party service, Google Cloud Speech-to-Text. Once the text representation of a voice command is obtained from GCST, it is analyzed and tokenized and the developer can define actions to be taken based on the commands.

The subsequent sections of this paper are as follows: In Section 2, related research is surveyed. In Section 3, developed framework is described. In Section 4, an initial experiment conducted to evaluate the system and its results are presented. Finally, in Section 5, conclusion and future work are discussed.

2. Related Work

Web Speech API defines a JavaScript API to enable web developers to incorporate speech recognition and synthesis into their web pages (Natal, Shires, & Jägenstedt, 2020). It is free and has a good documentation. Most of the browsers support Web Speech API. The limitations of Web Speech API are that it accepts short recordings and there might be some inconsistencies from browser to browser.

Amazon Transcribe is part of Amazon Web Services (AWS) and provides developers to add speech to text capability to their applications.

Amazon Transcribe uses deep learning to transform audio speech to text quickly and accurately. Amazon Transcribe targets converting customer service calls, closed captioning, and subtitling, and media assets to create a fully searchable archive. Amazon Transcribe Medical can be used to transform medical speech to text for clinical documentation applications (Amazon Web Services, Inc., 2020). These topics are irrelevant to voice browsing and voice commands. Also, Amazon Transcribe has a steep learning curve.

The IBM Watson Speech to Text service converts audio speech to text using deep learning. One advantage of this service is that grammar knowledge and language structure are also considered to accurately transcribe speech to text (IBM, 2020).

Google Cloud Speech to Text service facilitates deep learning to transcribe human speech to text. GCST lets the users choose from a selection of trained models for voice control optimized for domain-specific quality requirements (Google Cloud, 2020). This is the reason we choose GCST in this work for speech recognition. Also, GCST performed slightly better than the other speech to text technologies.

Sengupta et al. (2018) investigates integrating voice and gaze-based modalities to provide a better hands-free web browsing experience for end-users. A multimodal browsing method formed by combining eye gaze and voice inputs is demonstrated. The initial evaluation of the system shows that multimodality improved performance.

Pérez (2019) presents, Handsfree for Web, a browser extension that enables to execute voice commands for the current website or the browser itself. It supports two kinds of commands, atomic, and segmented. Handsfree for Web uses Web Speech API to convert speech into text.

Rozado et al. (2017) describes the FaceSwitch, which supports motor-impaired users to interact with a computer hands-free. The FaceSwitch combines gaze-based modality with video-based face gestures modality. In the resulting multimodal system, gaze pointing is used for target selection and facial gestures are used for target-specific action commands.

In this paper, a Javascript framework to support voice browsing is proposed. Google Cloud Speech-to-Text is used to convert voice commands to text commands. Once the text representation of a voice command is obtained from GCST, it is analyzed and tokenized and the developer can define actions to be taken based on the commands. It integrates GCST and other Javascript libraries (RecordRTC and JEST) to accomplish voice browsing and presents the developers an easy way of doing this.

3. Speech-to-Command Framework

The developers, who are planning to use Speech-to-Command, only need to provide an API key by registering with Google Speech-to-Text service. In order to extract commands, Speech-to-Command divides the text into segments. The default segments consist of *verb*, *target object*, *connective* and *source object*. *Verb* indicates the action to be taken. *Target object* is the entity affected by the taken action. *Connective* is the word(s) in between the *target* and the *source* objects. *Source object* is the entity used by the action to affect *target object*. In every command, there should be at least one verb. Target, source and connective segments are optional. In Figure 1, an example command and its segments are shown. With this command, the user wants to enter his institution information to the related form field. Another example is when the user wants to submit the form, "submit" voice command is sufficient which consists of only a verb.

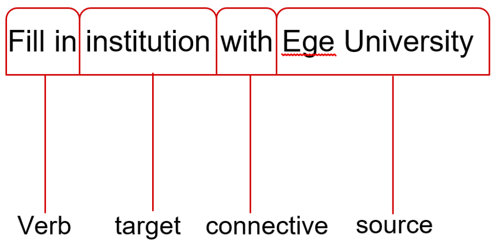

Figure 1. *A segmented command*

The workflow of speech to text transformation is divided into two figures. Figure 2 shows the process from acquiring a voice command to preparing it for sending. Figure 3 shows the process from sending the audio data to construction and finally execution of the command. When a voice command is recorded, it is sent to the Google Cloud Speech-to-Text service. HTTP requests are used to communicate with Google Cloud Speech-to-Text service to provide flexibility. Then, text representation of the speech is received from the server. Verb segment is determined by comparing with the list of defined commands. Every command should have a verb and every verb has a command structure and if the command has a connective, the connective separates target and source objects. Target and source objects are obtained by parsing the remainder text divided by the connective. Target object can also be a keyword such as *next*, *previous*, *first*, *second*, etc. These keywords are useful in easily navigating through controls in a form. In the end, a command object is constructed consisting of verb, connective, source, and target objects. Then, this command is executed by invoking the callback function, provided by the developer. Verbs, connectives, and keywords for target objects can be defined by the developer.

In the implementation, five verbs are defined. These are the following verbs:

- focus
- fill / fill in
- click
- clear
- submit

Focus command is for focusing on a target visual control such as a text box, check box, command button, link, etc. Focus verb also accepts keywords such as *next* and *previous*. "Focus next" voice command focuses on the next element. "Focus surname" command focuses on the element named *surname*.

Fill / fill in verb is used to enter text into text input controls without using the keyboard. *Fill* command is used when the user wants to edit currently focused control and there is no target object. On the contrary, *fill in* is used to edit a specified target control. "fill in name with John Doe" enters *John Doe* in the *name* field. "fill with John Doe" enters *John Doe* into the focused control.

Similarly, *clear* verb clears the text input of the controls. It can optionally have a target control as an argument. *Submit* command is used for submitting forms and does not have any arguments. It is used instead of clicking the submit button. Finally, *click* verb is used for clicking clickable controls. "Click left" and "click right" voice commands are used for clicking left and right mouse buttons, respectively. "click" command is regarded as left click. Click command takes optionally one argument that is the name of the target control. "click cancel" command imitates left-clicking on the cancel button.

One of the functionalities that our framework offers is voice recording. Although, MediaRecorder API (Mozilla, 2020b) is the default API that is provided by the browsers to record sound, it does not support linear16 format required by Google Speech-to-Text service. RecordRTC (Khan, 2020), an open-source third-party library, is used to record voice in linear16 format.

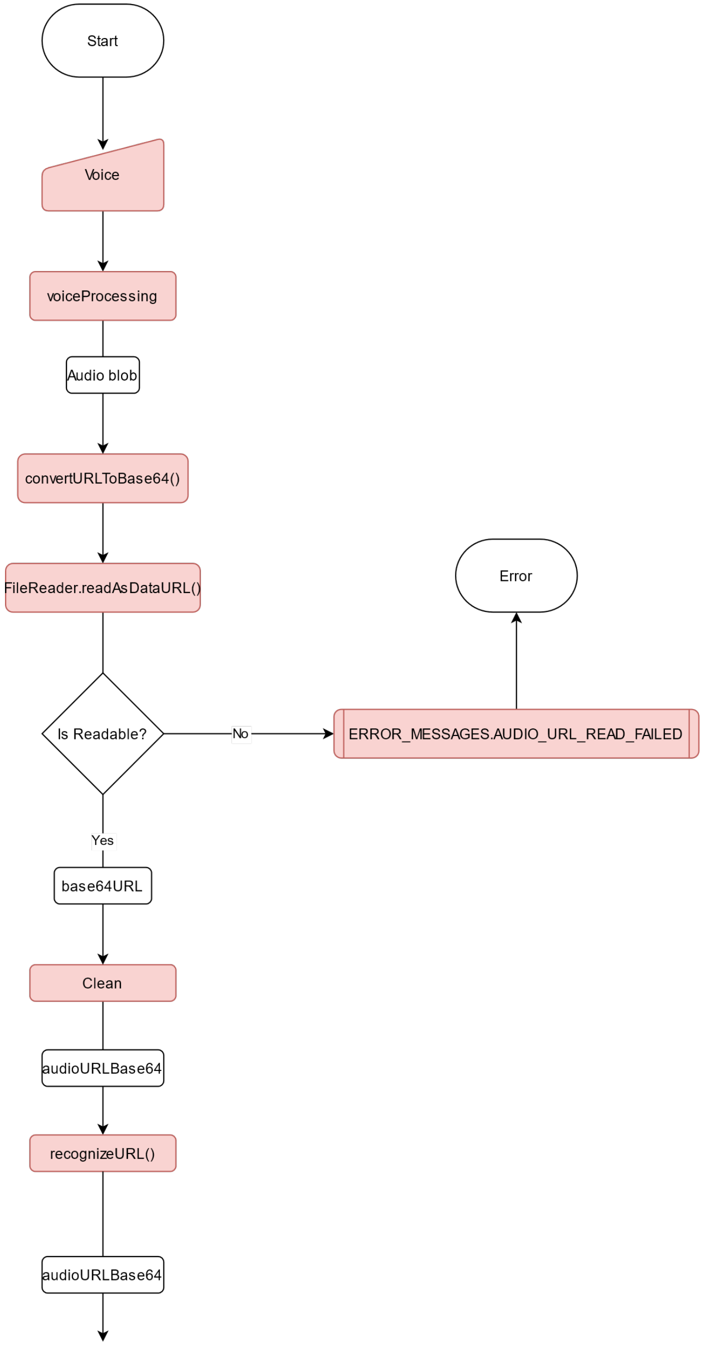

Figure 2. *The process of preparing a voice command for sending*

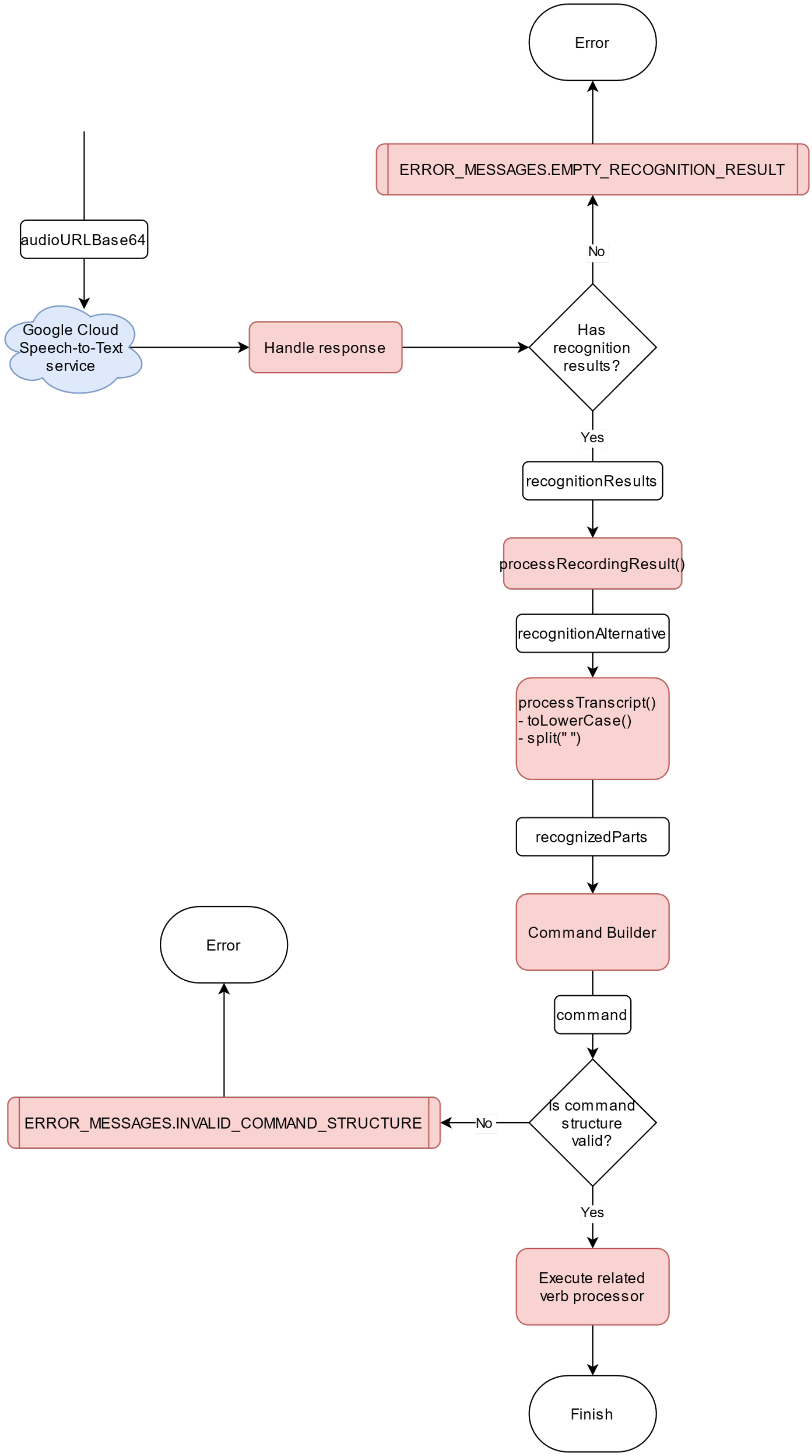

Figure 3. *The process of constructing a command from its text representation*

After the voice is recorded, it needs to be converted to a Base64 string. To achieve this, it is first stored as a blob (Mozilla, 2020a), the blob is converted to Base64 string and then geared for sending to the Speech-to-Text service. Google Speech-to-Text service provides a RESTful API to convert Base64 string to text. After the constructed string is sent, a response in JSON format is received. The response contains alternative text representations each having a confidence probability.

In Speech-to-Command, the first response is processed. It is tokenized and partitioned by searching the verb list. If there is no errors or inconsistencies, a rule object is constructed consisting of verb, connective, target, and source objects.

For every verb, an average of six unit tests are created. A Javascript unit testing framework, Jest, is used because the framework is encoded in Typescript and it targets browsers. Recognized words and the command structure are both tested.

To demonstrate the capabilities of Speech-to-Command, a sample web application is developed. This application also acts as a guide to potential users. In this application, it is intended to fill in a form and submit it.

To demonstrate the sample application, a set of voice commands listed in Table 1 are given and executed by the application. Figure 4 shows the application before the voice commands are given and Figure 5 shows the resulting form, just before "submit" command is spoken. Figure 6 shows the target web page after submit command is executed.

Table 1. *Voice commands in given order*

clear surname
focus surname
fill in surname with black
submit

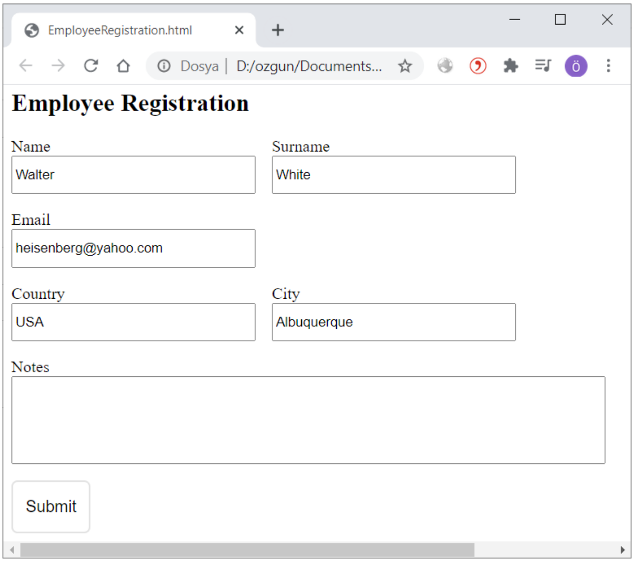

Figure 4. *The application before the voice commands are given*

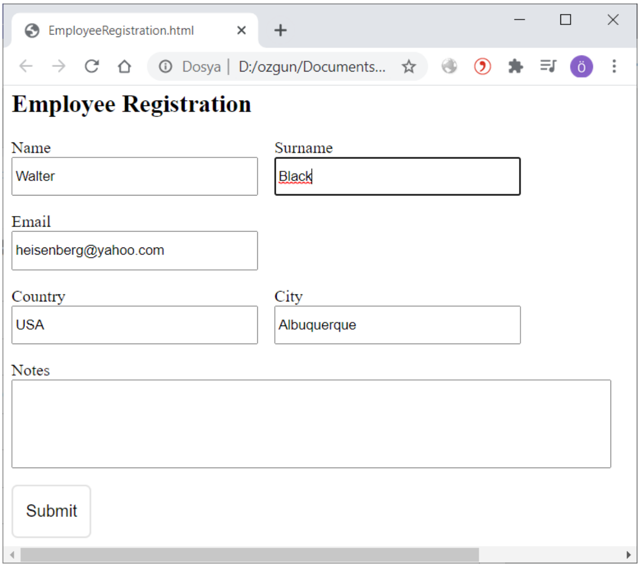

Figure 5. *The application just before the submit command*

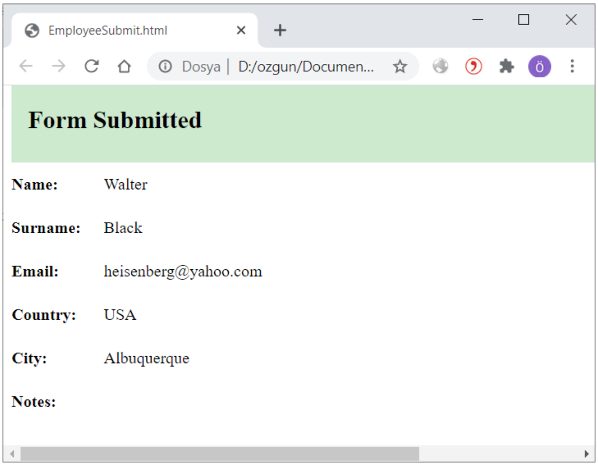

Figure 6. *The application after the submit command is executed*

4. Evaluation

In this section, an experiment considering voice commands each having a different verb and if applicable different command structure was conducted to measure the success rates. Each different command was spoken out loud 10 times and speech to text conversion success was recorded. As mentioned earlier speech to text conversion is performed by Google Cloud Speech-to-Text service. The success rates corresponding to each command is listed in Table 2. The resulting success rates are acceptable. GCST sometimes mixes words that are phonetically similar. During testing, it is deduced that *fill in* command can be interpreted as *phil*, *phil in*, *phil's*, *phil's in* and *chilling*.

As a workaround to this problem, all of the listed wrong interpretations of the *fill in* command are regarded as *fill in* command. As a result, success rate of fill in command is increased. This does not cause a problem because there are no verbs phonetically similar to *fill in*. The success rates of each command are acceptable, and the lowest success rate belongs to *fill in surname with black* command, which is 70%. The success rates also depend on the target and source words. For example, *clear address* command will have success rate different than *clear surname*.

Table 2. *Success rates of related voice commands*

Command	**Success rate**
clear	80%
clear surname	80%
focus surname	80%
focus next	100%
focus previous	80%
fill in surname with black	70%
fill in with white	80%
submit	90%

5. Conclusion

Voice recognition has become an increasingly important concept in recent years. Browsing the web with voice commands is also possible through voice recognition. In this paper, a framework to aid developers in developing voice browsing web applications in an integrated manner is proposed. The most important aspect of voice browsing is converting user's voice into text. For this purpose, Google Cloud Speech-to-Text service is used. The developed framework is extensible, as the developers can introduce their own verbs and command structures and define corresponding actions that should be taken. In this initial version of our framework, five verbs are introduced as a starting point. Every verb is unit-tested and verified. Although, an initial experiment is conducted using five voice commands and the results were satisfactory, more rigorous testing should be conducted to test commands with different target and source combinations. In the future, we are planning to add more built-in verbs to the library.

REFERENCES

Amazon Web Services, Inc. (2020, August 18). Amazon Transcribe – Speech to Text - AWS. Retrieved from https://aws.amazon.com/transcribe/

Efthimiou, E., Fotinea, S.-E., Goulas, T., Vacalopoulou, A., Vasilaki, K., & Dimou, A.-L. (2019). Sign Language Technologies and the Critical Role of SL Resources in View of Future Internet Accessibility Services. *Technologies*, *7*(1), 18. https://doi.org/10.3390/technologies7010018

Google Cloud (2020, August 25). Speech-to-Text: Automatic Speech Recognition. Retrieved from https://cloud.google.com/speech-to-text

Griol, D., Manuel Molina, J., & Corrales, V. (2011). The VoiceApp System: Speech Technologies to Access the Semantic Web. *Advances in Artificial Intelligence*, *7023*, 393–402.

IBM (2020). Speech to Text - IBM Cloud. Retrieved from https://cloud.ibm.com/catalog/services/speech-to-text#about

Khan, M. (2020, April 29). RecordRTC. Retrieved from https://recordrtc.org/

Mozilla (2020a, August 31). Blob. Retrieved from https://developer.mozilla.org/en-US/docs/Web/API/Blob

Mozilla (2020b, August 31). MediaRecorder. Retrieved from https://developer.mozilla.org/en-US/docs/Web/API/MediaRecorder

Natal, A., Shires, G., & Jägenstedt, P. (2020). Web Speech API. Retrieved from https://wicg.github.io/speech-api/

Pérez, J. (2019). Handsfree for Web: A Google Chrome Extension to Browse the Web via Voice Commands. In *W4A '19, Proceedings of the 16th Web For All 2019 Personalization - Personalizing the Web*. New York, NY, USA: Association for Computing Machinery. https://doi.org/10.1145/3315002.3332443

Rozado, D., Niu, J., & Lochner, M. (2017). Fast Human-Computer Interaction by Combining Gaze Pointing and Face Gestures. *ACM Transactions on Accessible Computing*, *10*(3), 1–18. https://doi.org/10.1145/3075301

Sengupta, K., Ke, M., Menges, R., Kumar, C., & Staab, S. (2018). Hands-Free Web Browsing: Enriching the User Experience with Gaze and Voice Modality. *2018 ACM Symposium on Eye Tracking Research & Applications (Etra 2018).* Advance online publication. https://doi.org/10.1145/3204493.3208338

Chapter 11

TOPOLOGY OPTIMIZATION FOR ADDITIVE MANUFACTURING IN THE AVIATION AND AUTOMOTIVE INDUSTRY

Neslihan TOP[3]
İsmail ŞAHİN[4]
Harun GÖKÇE[5]

3 Arş. Gör. Neslihan Top, Gazi Üniversitesi
4 Doç. Dr. İsmail Şahin, Gazi Üniversitesi
5 Dr. Harun Gökçe, TÜBİTAK-Sage

1. INTRODUCTION

Optimization is an engineering process performed to achieve the best result under specified limits. In mechanical design processes, engineers and designers have to make managerial and technological decisions at many stages of the system. It is aimed to minimize the effort spent with optimization studies and to maximize efficiency (Tejani, 2012; Gökçe et al., 2019). Optimization is the process of reaching the ideal solution and increasing performance in current conditions with the restrictions imposed. It can also be defined as a technology where improvements are made such as increasing capacity and efficiency and reducing cost and material use by using resources such as labour, equipment, materials and time in the most efficient way (Gass, 2000). By using this technology, a solution close to ideal is sought to give better performance to the system. The optimization process improves the quality and accelerates the decision-making process by ensuring that problems are solved accurately and effectively in real-time (Winston, 2003; Şahin, 2018).

With the advances in computer technology, high performance and minimum weight have been the focus of structural design applications. Optimization processes in structural design applications; can be performed as shape, size and Topology Optimization (TO). Among these methods, TO gives engineers and designers the most creative results. Studies are carried out to optimize the material distribution on the part with TO. With the developments provided by TO, structural design applications have gradually increased, especially in the automobile, aviation and biomedical industries (Gökçe et al., 2019; Liu et al., 2018; Zhu et al., 2009). The most important reason for this situation is that the design can determine its optimum geometry within the defined constraints. Stronger, lighter and original designs can be obtained with this method. The TO process is shown in Figure 1.

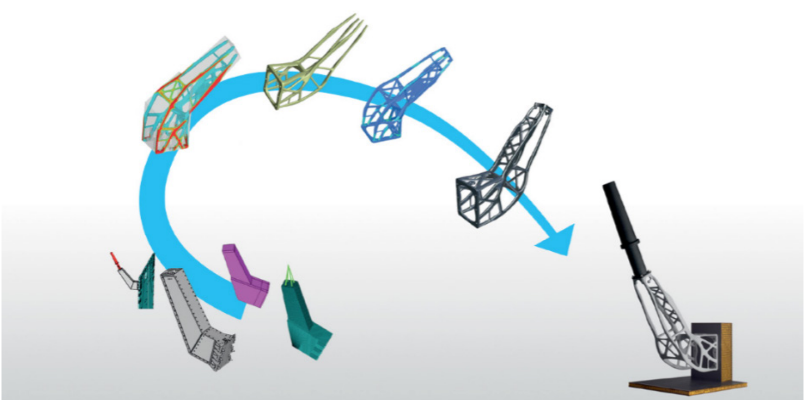

Figure 1.Topology optimization process (Le, 2017)

Structural optimization techniques (Figure 2) grouped as size, shape and TO change the part shape or material distribution to achieve the optimum structure under various constraints (Poyraz, 2004). First of all, the first optimum topology is created with existing methods and transformed into suitable designs. Then shape optimization is used to accurately shape the contours of the model and, if necessary, the final dimensions of the model are determined by size optimization.

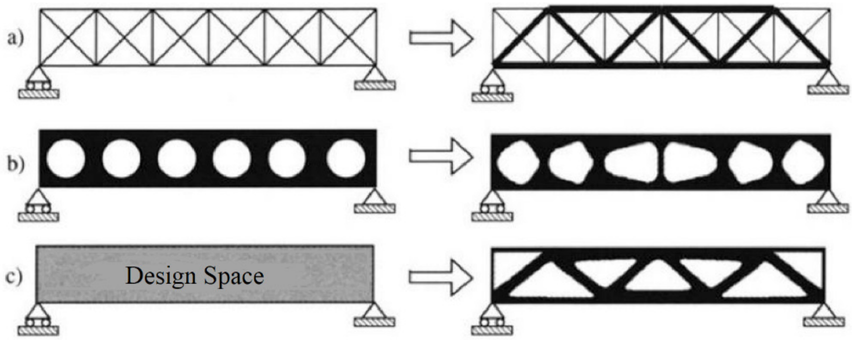

Figure 2. Structural optimization a) size optimization, b) shape optimization, c) topology optimization (URL 1)

Dimensional optimization aims to find the optimal cross-sectional area of each element in the structure and change its dimensions to reach the ideal form. Shape optimization is the optimization of the external shape of the structure without changing its connections. TO explains how the elements that make up the structure can best create connections (Thummar, 2014). Therefore, TO is the most general definition of structural optimization. It is to optimize the material distribution to reach the ideal structure (Nadir et al., 2004; Top et al., 2019).

The improvements provided by optimization techniques have increased the use of these techniques and have also been reflected in the design processes. Structural optimization methods are widely used in Computer Aided Design (CAD) processes to reduce cost and shorten the production process. With structural optimization methods, designers and engineers can have an idea about the general shape of the product in the early stages of design, and the closest design solution to the ideal can be obtained with the restrictions placed in the specified area (Göv, 2007).

In this chapter, the TO process, one of the optimization techniques used to achieve the ideal design, and the production of parts obtained by this method with Additive Manufacturing (AM) technologies are discussed. The complex structure of the parts obtained as a result of TO makes it difficult to produce these parts by traditional methods. For this reason, AM technologies are preferred, which enable production from a CAD file in a single process step during the production phase. It is widely used in the aerospace and automotive industry due to light and durable parts with TO. At the end of the study, TO applications of sample parts used in the sectors mentioned above were introduced.

2. TOPOLOGY OPTIMIZATION

TO is an application that provides the best improvement on the geometry and material distribution of the structure. It is important that the optimized part can be edited according to the desired changes (URL 2, URL 3). With optimization, it is aimed to achieve the best form by reducing the weight of the piece without changing its function. It is widely used in the aerospace and automotive industries, especially to produce lightweight yet durable parts.

TO is used with the aim of the optimal distribution of the material in a designated area. The regions that have the least effect on the general strength and natural frequency of the building are determined and the regions that need to be removed from the building are defined. It has been found that it is efficient to use existing designs to strengthen, reduce their weight, and achieve the ideal form. In the process of arranging the material distribution with the TO method, the creation of holes, protrusions, grooves in the structure, creation or deletion of new elements are performed (Saleem et al., 2008). With this application, the weight of the part is reduced and the ideal structure is achieved without changing the function. For this reason, it has become an effective tool in space, aerospace, automotive and medical industries for the design of the lightest and highest performance parts (Zhu et al., 2016).

TO is applied as a powerful conceptual design tool in different engineering disciplines. Application difficulties have been experienced due to the transformation of the ideally shaped part obtained as a result of the optimization process into computer-aided design data and the complexity of the production process (Chuang et al., 2017). The easiest way to transform the model obtained as a result of the process into a ready-made printing model has been determined as AM technologies that enable the production of structures with complex geometries in a single process step. The model obtained after the optimization process can be saved in Stereolithography (STL) format and sent directly to production and printed. Since the material distribution on the model is optimized, the amount of material used in printing will also decrease, thus reducing production costs.

In the TO process, firstly, a three-dimensional (3D) model of an original design is prepared in CAD programs. Structural analysis process is initiated in accordance with the specified limitations. After the analysis is completed, the stress distributions on the model are determined and the regions that do not have a significant contribution to load carrying are removed from the part. The final model obtained is remodeled in CAD software and the status of meeting the determined loads is tested with the Finite Element Analysis (FEA) method. This process is repeated until the desired result is achieved. When the target model is reached, the production process starts with AM.

TO is a method used to provide properties such as strong design, minimum weight and ideal form in the process of reaching the ideal structure of any design without losing its function. The main purpose in TO method is to regulate the material distribution. For this purpose, the creation of holes, protrusions, and grooves in the structure, creation or deletion of new elements are performed (Saleem et all, 2008). The optimal material distribution is achieved by dividing the design space into N finite elements with the restriction and load introduced. The application, which starts by deciding which part to apply the TO, is carried out by imposing the necessary limitations and selecting the power application and optimization rate. The optimal material distribution is achieved by dividing the design space into N finite elements with the restriction and load introduced (Yang and Chuang, 1994). The structure and original design obtained after the process are not functionally different. TO can be applied to parts designed with add-ons brought to CAD programs before production. In recent years, it is seen that TO applications have been used extensively, especially in studies for AM (Top et al., 2018; Şahin et al., 2019).

In recent years, TO has become a rapidly growing research area with its application in many fields such as mechanical, civil and automotive engineering, and continues to develop in order to bring the shape of a design field to the best possible topology. Suggested approaches for topology optimization of continuous structures; It is divided into two categories: Heuristic Methods and Mathematical Based Methods.

Examples of heuristic methods are Evolutionary Structural Optimization / Bi-directional Evolutionary Structural Optimization (ESO / BESO) methods, which are more intuitive and involve less mathematical processing (Querin el al, 1998). Homogenization Method (HM) (Bendsøe and Kikuchi, 1988) Level set Method (Allaire et al., 2004) and Solid Isotropic Material with Penalization method Penalization (SIMP) (Rozvany et al., 1992) can be cited as examples of math-based methods.

The most popular mathematical method for TO is the SIMP method. SIMP, a density-based method, was first proposed by Bendsoe and Kikuchi (1988), Rozvany et al. (1992) was developed by. Density-based methods work on a fixed finite element domain that aims to minimize an objective function by determining whether each finite element should consist of solid or void (Deaton & Grandhi, 2014). One of the commonly used methods is the SIMP method.

The purpose of optimization in the SIMP method is to estimate the optimal distribution of materials within a given design area for specific load conditions, boundary conditions, production constraints and performance requirements. This estimation is accomplished by finding the densities of the segment elements divided into finite elements. The density calculation is made using the displacement amounts of finite elements (Yaman, 2019). The definition of a density-based topology optimization problem, as in all optimization problems, consists of an objective function (Equation 1), constraints (Equation 3), and discrete representation of the physical system. The purpose of SIMP is to arrange the densities of finite elements by considering the general fit (C) of the part. In SIMP, general compliance is seen as a minimization problem and is defined as in Equation 1 (Bendsøe and Kikuchi, 1988).

$$\min C = u^T K(\rho), u \tag{1}$$

In Equation 1, C defines the general congruence, ρ the design variable representing the density vector, u the universal displacement vector, and K the universal stiffness matrix. Density is the key factor in minimizing overall compatibility. The densities of the finite elements that make up the part are found by using the displacement amount (Equation 2) (Yaman, 2019).

$$\rho = (\rho_1, \rho_2, \ldots\ldots, \rho_n)^T, u \tag{2}$$

The constraints used in SIMP consist of universal stiffness matrix (K), volume ratio (f) and universal charge (F) and density vectors (ρ) (Equation 3).

$$\begin{aligned} &K(\rho)U = F \\ &V_\rho / V_0 - f \leq 0 \\ &0 \leq \rho \leq 1 \end{aligned} \tag{3}$$

In Equation 3 V_ρ represents the material volume and V_0 represents the design area volume. The universal hardness matrix is calculated with the help of Equation 4.

$$K = \sum_{i=1}^{n} \rho_i^p K_0 \tag{4}$$

Where ρ_i *i.* the density of the element, K_0 indicates the hardness matrix of the element corresponding to ρ_i =1, and p indicates the penalty coefficient. The distributed function of design variables in density-based topology optimization is interpreted as the ρ_e material density of each finite element. The values of the density ratio;

$$0 \leq \rho_{\min} \leq \rho_e \leq 1 \tag{5}$$

and/or

$$0 \leq \rho_e \leq 1 \tag{6}$$

defined in ranges. Here 0 is an empty element, 1 is a solid element, $\rho_{\min}$ is the minimum density value and ρ_e is the density of each finite element. The zero density causes problems such as singularity in finite element matrices and in some cases the inability of the material to reappear in a zero density area (Deaton & Grandhi, 2014). In TO, the density is desired to be 0 or 1, the formation of fractional densities in the design is undesirable. In SIMP, the penalty coefficient (*p)* is used to prevent this situation (Gunwant & Misra, 2012). When the penalty coefficient is selected greater than 1, there are only finite elements with 0 and 1 density values after optimization. The optimum design process is completed by deleting elements with 0 density and obtaining geometry (Yaman, 2019).

3. TOPOLOGY OPTIMIZATION FOR ADDITIVE MANUFACTURING

AM, or 3D printing as it is popularly known, is the creation of a 3D object from a CAD model or a digital 3D model (Top at al, 2018). Designed parts are produced from 3D model created in CAD programs. This technology has been developed to produce prototypes of physical models as quickly as possible by heat or chemical treatments of polymer, composite or resin, and it accelerates the launch of products by greatly reducing errors in new product development (Santos, 2006). Producing layer by layer, not by extracting material, reduces material consumption. This feature makes AM a more efficient production method compared to traditional methods.

3D model of the design should be created before printing with AM technologies. The 3D model is obtained either by means of a CAD program or by scanning (reverse engineering) the real product with optical or laser 3D scanners. The prepared model is transferred to the appropriate software, slicing on the z-axis before printing and the sliced model data is transferred to the 3D printer (Figure 3). In order to transfer data between these softwares and 3D printers, the model is saved in STL format. A model saved in STL format does not contain attributes such as texture, color. It only defines the model as triangular regions and soft surfaces are more often expressed with triangles (Santos et al., 2006).

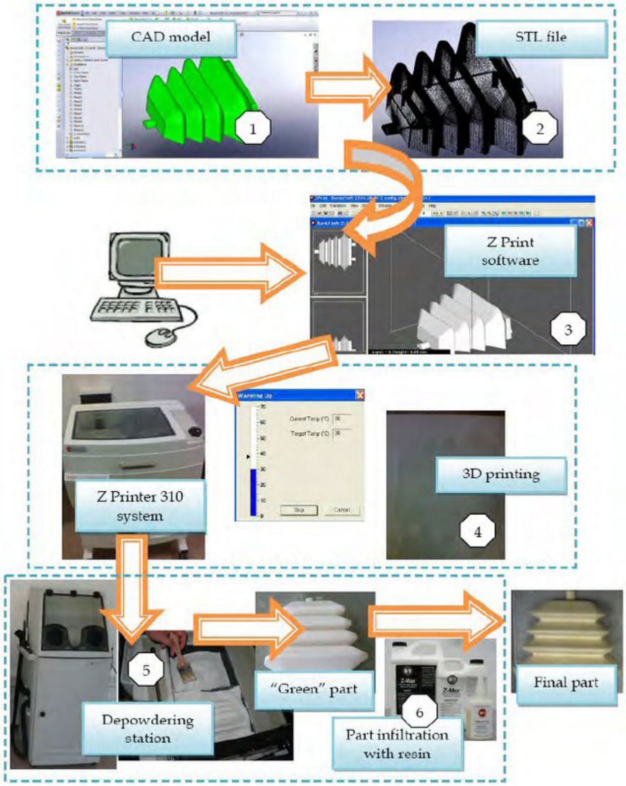

Figure 3.The production process with generalized additive manufacturing technologies (Udroiu & Nedelcu, 2011)

The fact that the prepared design file is easily transferable, easy to use and setup, the necessary arrangements and changes can be made quickly, the time and cost of product creation can be calculated in advance increases the preference of AM technologies (Kemal & Turan, 2018). In addition, the easy manufacturability of individual designs and structures with complex geometries and the variety of materials have increased the use and importance of this technology by designers and engineers. Production of functional parts, customized and geometrically complex products have been developed in the 3D printing process.

The current spread of AM technology has allowed designers and engineers to use TO techniques when designing new products. Combined with 3D printing, TO can result in lightening, improved structural performance, and a shortened design-to-production cycle. Because even though designs are efficient, they may not be realized with more traditional production techniques (Top at al., 2018).

One of the reasons why these technologies are preferred is that damage estimation can be made in computer environment with AM technologies before printing. One of the various optimization techniques used for damage estimation is TO. The rapid proliferation of AM technologies has increased the use of TO in engineers' product design. The advantages that AM offers in producing parts that are difficult to produce with traditional manufacturing encourage the use of TO techniques. With TO, it is aimed to reach the ideal form without changing the function of the part to be printed. It also contributes to cost reduction by using less material in the production of the part (Top at al., 2018).

Advances in AM technologies have led to a paradigm shift in the design process. The fact that even parts with complex geometries can be produced in a single process step with this technology has eliminated the worry of manufacturability and has led to an increase in creativity. Caged designs that can be easily produced thanks to AM technologies are the best example of this situation. The reason for using lattice structures in design is to change traditional solid form materials, reduce weight and increase multifunctional features. One of the methods used to produce lattice structures, TO is an effective tool to obtain optimal forms (Cheng et al., 2018). By using TO in the AM process, it is easier to evaluate the structural performance of the part obtained as a result of optimization by making trial productions, thus the design cycle can be shortened effectively (Wang et al., 2017). Topology optimization is a simulation-oriented method applied to create conceptual structures. The structures obtained as a result of the process are generally organic and it is not possible to produce without simplifying the model with traditional manufacturing methods. For this reason, the emergence of AM technologies has enabled TO results to be applied (Brackett et al., 2011; Top et al., 2019).

4. SAMPLE TO TOPOLOGICAL OPTIMIZATION APPLICATIONS

4.1. In Aviation

Aircraft design is complex and there are many parameters, variables, and constraints to consider during the design process. The structural lightweight of the aircraft is important in structural design. TO is preferred in the design of aviation personnel with its ability in load distribution and re-determination of material order. With TO, it is possible to obtain lightweight structures while meeting design constraints (Wang, 2018).

Recent studies show that the combination of TO and AM applications is effective in the design of aviation components. In a study conducted by the European Aeronautic Defense and Space company (EADS), the mass of the hinge bracket of Airbus 320 was reduced by 64% (Figure 4) (Tomlin and Meyer, 2011).

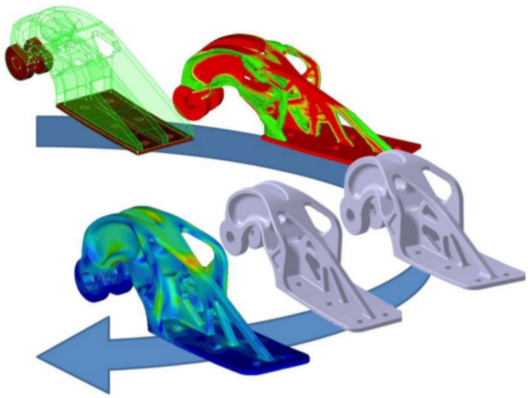

Figure 4. TO of Hing bracket (Tomlin and Meyer, 2011)

Nowadays, many parts of aviation vehicles are targeted to be produced with AM technologies and are subject to TO studies. This is because most of the aviation and space applications are suitable for AM (Schiller, 2015). Aerospace bracket (Guanghui et al., 2020), Turbojet engine holding bracket (Figure 5) (Gökçe et al., 2019), carrier brackets (Figure 6) (Şahin et al., 2019), aircraft rib (Stanford and Dunning, 2015) can be given as an example of TO studies conducted on aviation personnel. Similar studies have shown that the parts designed with topology optimization, which confirms the operation of EADS, are quite light and have optimum strength. For example, in a study on the design of the turbojet engine holding bracket with TO, the holding bracket was reduced by 60% compared to the original part. Gebisa and Lemu (2017) managed to reduce the turbojet engine holding bracket by 65%, which is a popular example in TO studies.

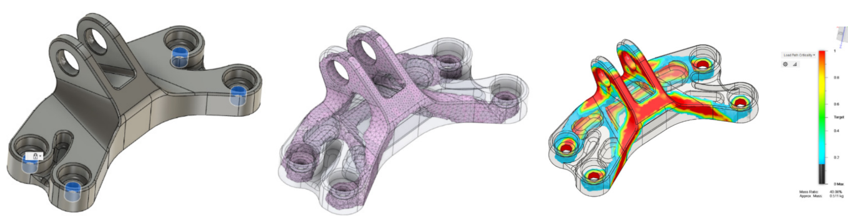

(a) (b) (c)

Figure 5. Turbojet engine holding bracket TO process (a) CAD model (b) Optimized model (c) FEA model (Gökçe et al., 2019)

Retaining brackets have important functions in both aviation and mechanical systems. As a carrier and guiding element, it is one of the critical elements in mechanical systems. For this reason, the aviation applications of TO have been extensively studied. Saebra et al. (2016) work on the optimum design of the aviation bracket to be produced with Selective Laser Melting (SLM) is one of them. In the study, the part was reduced by 54% with TO. In another study, the holding brackets used to hold the opening covers of the landing gear on the aircraft were discussed. The bracket to be produced with Selective laser sintering (SLS), one of the AM technologies, is lightened by 30% with TO. We see a similar result in the design of aircraft frame structures with TO (Wang, 2018). In the study, the aircraft frame structure, which was 51.338 kg before optimization, was reduced to 31.726 kg after optimization, and a reduction of 38.2% was achieved.

Figure 6. a) Aircraft landing gear holder bracket, b. Bracket 3D model, c. De-meshing the part surface d) The image of the part as a result of topology optimization (Şahin et al., 2019)

4.2. In Automotive

The rapid depletion of natural resources causes studies to improve resource consumption to be the focal point of engineering. The fuel required for moving vehicles is one of the best examples. In automotive design, reducing the amount of fuel consumption is an important issue to be considered in terms of CO2 emission reduction as well as reducing vehicle driving costs. The fuel consumption of vehicles is undoubtedly important in terms of careful use of limited resources and developing environmentally friendly technologies, but this situation affects the future of brands dramatically. Vehicle weight is a parameter that directly affects fuel consumption. Reducing vehicle weight not only improves fuel consumption but also increases the speed of the engine, which reduces the energy required to move the vehicle (Sudin et al., 2014). Studies have shown that every 100 kg reduction in vehicle weight leads to fuel savings of 0.4 L / 100 km for automobiles and approximately 0.5 L / 100 km for light trucks (MIT, 2008). With the opportunities it offers in automotive design, TO is widely used to reduce vehicle weight, which directly or indirectly affects vehicle performance, and to determine the best layout of vehicle structural components (Yang and Chahande, 1995).As in aviation, bracket optimization is common in automotive applications. In addition, many components that affect vehicle weight and performance are the subject of TO studies (Sun et.al, 2018; Cavazutti et.al, 2011; Shi et.al, 2009; Sargini et.al., 2020; Sudin et.al., 2014. ; Top et.al., 2019; Patel et.al., 2017; Top et.al., 2018).

TO applications give successful results in lightening vehicle body components. For example, Sun et al. (2018) As a result of the design of the

TWB indoor panel with Multi-objective TO, they reduced the door weight by 27.6%. The effect of reducing vehicle weight on design costs increases in parallel. In a study where the city bus body was designed with TO, it was observed that the design cost of the vehicle, whose weight was reduced by 30%, decreased by 40% (Shi et.al, 2009). In addition, while board space increased by 19%, energy consumption and emission decreased by 40%. In another study conducted to lighten the bus roof frame, the roof frame was reduced by 3.43% (Zhong et. Al., 2016). The opportunities offered by TO attract the attention of automobile manufacturers and are used effectively in designs. TO and mechanical design of the Ferrari chassis is one of the successful examples (Cavazutti et. Al., 2010). The chassis weight of the model created with TO has been significantly reduced.

As vehicle components become smaller, another issue to be considered in TO studies is AM technologies. AM technologies that enable metal-based production such as SLS and SLM are among the production methods used in TO studies. The design of the automotive breake pedal with TO and its production with AM is an interesting subject in this area. Sudin et al.'s pedal design with TO is 22% lighter than traditional pedals without compromising performance criteria (Sudin et. Al., 2014). Sargini et al., Redesigned with TO, reduced the weight of the arm brake pedal by 54% (Sargini et al., 2020). In the study, the production of arm brake pedal with AM was also confirmed. Figure 7. Arm brake shows the TO process of the pedal.

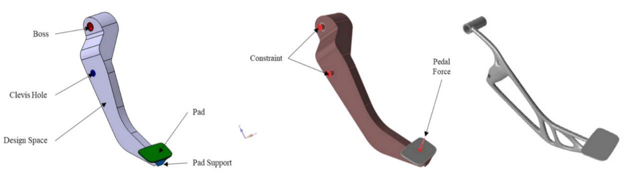

(a) *(b)*

Figure 7. Arm brake pedal TO process: (a) 3D model and boundaries conditions (b) The topology optimized design (Sargini et. al., 2020)

The performance of different materials is also tested in the design of vehicle components with RO. For example, Patel et al., In their study where they optimized Hand brake level with two different materials (S235 and A356), achieved a weight reduction of up to 10% with S235 and up to 65% with A356 (Patel et. Al., 2017). In the design of the bracket used for the handbrake mechanism of Ball et al, with TO for AM, the bracket was reduced by 42.96% (Figure 8) (Top et. Al., 2019). The researchers suggested that the bracket be manufactured with SLS.

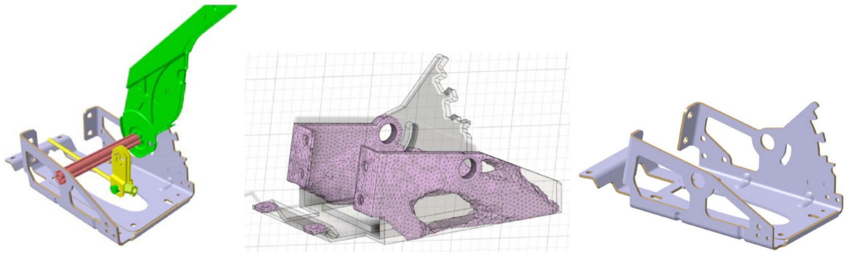

(a) (b) (c)

Figure 8. Handbrake mechanism bracket (Top et. Al., 2019) (a) Mechanism (b) Topology optimization result (c) Topology optimized bracket

5. CONCLUSION

With TO, it is aimed to transform existing solid models produced by traditional methods or a newly designed product into the most ideal form. TO consists of modeling the part with different methods (with CAD or Reverse Engineering methods) and determining the required boundary conditions for FEA analysis. This process involves obtaining the ideal part model suitable for the structural requirements of the part. The process is considered successful if the TO applied geometry is able to carry loads while lightening the weight. It is very difficult to produce parts designed with TO, using traditional production techniques. For this reason, the production of parts designed with TO using AM technologies is increasingly common. In this case, the effect of AM technologies becoming more accessible and increasing production speed is great.

TO applications are used with different prevalence in almost all areas of engineering. However, the most common areas of application are aviation and automotive sectors. When combined with AM technologies, the advantages offered by TO in design provide great convenience to designers and engineers working on automotive and aircraft design. Studies show that TO applications do not compromise strength while designing vehicle components lighter than traditional methods. Both aviation and automotive components can be produced lighter, with optimum strength, cheaper and faster with TO applications. Production with topologically optimized parts not only produces cost-effective vehicle components in the automotive and aerospace sector, but also serves the purpose of environmentally friendly design by reducing fuel consumption. Nowadays, the use of TO in product design is progressing to become an integral process of automotive and aircraft desi

In addition to the many advantages of using TO in design, as the design area expands, there are difficulties in the CAD and FEA stages. For this reason, as the design becomes more complex, the processor capacity of the computers must be increased. Parallel to this, problems may occur in the transfer of data. Mesh number, size, and existing algorithms remain a major challenge in CAD, Computer Aided Engineering (CAE) and TO applications. Due to the amorphous structure of some parts, there are difficulties in the formation of the FEA model, and even it cannot be modeled. Another problem is that parts that have been redesigned with TO can be produced and their aesthetics are not acceptable. In these cases, the organic shape is simplified and converted to standard geometries. In this transformation process, organic models are interpreted using typical CAD methods, but greatly optimism may be lost in this step (Liu et. Al., 2018).

Despite all the difficulties arising from the limitations of software, hardware and current AM technology, TO studies are increasing day by day. The solution of all factors (support material, low production volume, long manufacturing time, etc.) that increase the manufacturing time in AM comes to TO. For this reason, it is not possible to think the future of TO independently from AM. TO studies should focus on the issues such as support material minimization, low volume production, manufacturing time minimization in order to address the problems encountered in AM applications. We can also add topologically optimized design studies for multi-material AM solutions (Liu et. Al., 2018). The development of algorithms to solve the smoothing problem of parts designed with TO will prevent the loss of the optimality of the smoothed parts for production. The strength of the material obtained by additive manufacturing and the materials obtained from the subtractive method may have structural strength differences. It is expected that activities aimed at increasing the quality of materials obtained by powder metallurgy will develop simultaneously with TO. The developments experienced and the expectations of the sector from TO and AM will cause the intensification of practical industrial studies in the coming years.

REFERENCES

Allaire, G., Jouve, F., & Toader, A. M. (2004). Structural optimization using sensitivity analysis and a level-set method, *Journal of computational physics*, 194(1), 363- 393.

Stanford, B. K., & Dunning, P. D. (2015). Optimal topology of aircraft rib and spar structures under aeroelastic loads, *Journal of Aircraft*, 52(4), 1298-1311.

Bendsøe, M. P., & Kikuchi, N. (1988). Generating optimal topologies in structural design using a homogenization method, *Computer methods in applied mechanics and engineering*, 71(2), 197-224.

Brackett, D., Ashcroft, I., & Hague, R. (2011, August). Topology optimization for additive manufacturing. In *Proceedings of the solid freeform fabrication symposium, Austin, TX* (Vol. 1, pp. 348-362).

Cavazzuti, M., Baldini, A., Bertocchi, E., Costi, D., Torricelli, E., & Moruzzi, P. (2011). High performance automotive chassis design: a topology optimization based approach, *Structural and Multidisciplinary Optimization*, *44*(1), 45-56.

Cheng, L., Liu, J., Liang, X., & To, A. C. (2018). Coupling lattice structure topology optimization with design-dependent feature evolution for additive manufactured heat conduction design. *Computer Methods in Applied Mechanics and Engineering*, *332*, 408-439.

Chuang, C. H., Chen, S., Yang, R. J., & Vogiatzis, P. (2018). Topology optimization with additive manufacturing consideration for vehicle load path development. *International Journal for Numerical Methods in Engineering*, *113*(8), 1434-1445.

Deaton, J. D., & Grandhi, R. V. (2014). A survey of structural and multidisciplinary continuum topology optimization: post 2000. *Structural and Multidisciplinary Optimization*, *49*(1), 1-38.

Gass, S.I., "Making Decisions with Precision", Business Week October 30, (http://www.businessweek.com/archives/2000/b3705139.arc.htm?campaign_id=search#B3705139), (2000).

Gebisa, A. W., & Lemu, H. G. (2017). A case study on topology optimized design for additive manufacturing. In *IOP Conference Series: Materials Science and Engineering*, 276(1), 012026.

Gökçe H., Şahin İ., Top N. (2019). Turbojet motor tutma braketinin topoloji optimizasyon destekli yapısal tasarımı, *Uluslararası bilim, teknoloji ve sosyal bilimlerde güncel gelişmeler sempozyumu*, 2, 407-412. (Tam Metin Bildiri/Sözlü Sunum).

Göv, İ., Kütük, M. A., Topoloji Optimizasyonunda Eleman Silme Metodunun Uygulanması, XV. *Ulusal Mekanik Kongresi*, ISPARTA, (2007).

Guanghui, S. H. I., Chengqi, G. U. A. N., Dongliang, Q. U. A. N., Dongtao, W. U., Lei, T. A. N. G., & Tong, G. A. O. (2020). An aerospace bracket designed by thermo-elastic topology optimization and manufactured by additive manufacturing. *Chinese Journal of Aeronautics*, 33(4), 1252-1259.

Gunwant, D., Misra, A., (2012). Topology optimization of continuum structures using optimality criterion approach in ANSYS, *International Journal of Advances in Engineering & Technology,* 5(1), 470-485.

Kemal, Ş., Turan, O. (2018). 3B Yazıcı Teknolojilerinin Karşılaştırmalı Analizi, *Stratejik Ve Sosyal Araştırmalar Dergisi*, 2(2), 97-116.

Le, K. L. (2017). Generative Design with solidThinking Inspire, Arcada University of Applied Sciences, Plastics Technology Degree Thesis.

Liu, J., Gaynor, A. T., Chen, S., Kang, Z., Suresh, K., Takezawa, A., ... & Cheng, L. (2018). Current and future trends in topology optimization for additive manufacturing, *Structural and Multidisciplinary Optimization*, 57(6), 2457-2483.

Liu, S., Li, Q., Liu, J., Chen, W., & Zhang, Y. (2018). A realization method for transforming a topology optimization design into additive manufacturing structures, *Engineering*, 4(2), 277-285.

MIT 2008. On the Road in 2035: Reducing Transportation's Petroleum Consumption and GHG Emissions. Massachusetts Institute of Technology (2008). http://web.mit.edu/sloan-auto-lab/research/beforeh2/otr2035/On%20the%20Road%20in%202035_MIT_July%202008.pdf

Nadir, W., Kim, I. Y., & de Weck, O. (2004). Structural shape optimization considering both performance and manufacturing cost. In *10th AIAA/ISSMO Multidisciplinary Analysis and Optimization Conference* (p. 4593).

Patel, M. V., Sarawade, S. S., & Gawande, S. H. (2017). Topology optimization and stress validation of the hand brake lever. *International Review of Mechanical Engineering*, 11(7), 442-447.

Poyraz, M., "Bir Kamyon Şasinin Yapısal Optimizasyonu", İstanbul Teknik Üniversitesi Fen bilimleri Enstitüsü Makine Mühendisliği Bölümü Yüksek Lisans Tezi, (2004).

Querin, O. M., Steven, G. P., & Xie, Y. M. (1998). Evolutionary structural optimisation (ESO) using a bidirectional algorithm. Engineering computations.

Rozvany, G. I., Zhou, M., & Birker, T. (1992). Generalized shape optimization without homogenization, *Structural optimization*, 4(3-4), 250-252.

Saleem, W., Yuqing, F., & Yunqiao, W. (2008). Application of Topology Optimization and Manufacturing Simulations-A new trend in design of Aircraft components. In *Proceedings of the International MultiConference of Engineers and Computer Scientists* (Vol. 2).

Santos E.C., Shiomi, M., Osakada, K., Laoui, T. (2006). Rapid manufacturing of metal components by laser forming, *International Journal of Machine Tools and Manufacture*, 46(12-13), 1459-1468.

Sargini, M. I. M., Masood, S. H., Palanisamy, S., Jayamani, E., & Kapoor, A. (2020). Finite element analysis of automotive arm brake pedal for rapid manufacturing. In *IOP Conference Series: Materials Science and Engineering* (Vol. 715, No. 1, p. 012020). IOP Publishing

Schiller, G. J. (2015). Additive manufacturing for Aerospace. In *2015 IEEE Aerospace Conference* (pp. 1-8). IEEE.

Seabra, M., Azevedo, J., Araújo, A., Reis, L., Pinto, E., Alves, N., ... & Mortágua, J. P. (2016). Selective laser melting (SLM) and topology optimization for lighter aerospace componentes. *Procedia Structural Integrity*, 1, 289-296.

Shi, J. F., & Sun, J. H. (2009). Overview on innovation of topology optimization in vehicle CAE. In *2009 International conference on electronic computer technology* (pp. 457-460). IEEE.

Sudin, M. N., Tahir, M. M., Ramli, F. R., & Shamsuddin, S. A. (2014). Topology optimization in automotive brake pedal redesign, *International Journal of Engineering and Technology (IJET)*, 6(1), 398-402.

Sun, G., Tan, D., Lv, X., Yan, X., Li, Q., & Huang, X. (2018). Multi-objective topology optimization of a vehicle door using multiple material tailor-welded blank (TWB) technology, *Advances in Engineering Software*, 124, 1-9.

Şahin İ. (2018). Mühimmat Sistemlerinde Kullanılan Askı Kancalarında Geometri Tabanlı Topoloji Optimizasyonu, *3'rd International Symposium on Industrial Design Engineering* (Tam Metin Bildiri/Sözlü Sunum).

Şahin, İ, Top, N, Gökçe, H., Eldem, C. (2019). Uçak braketinin SIMP topoloji optimizasyon metodu ile yeniden tasarımı, *2. Uluslararası Türk Dünyası Mühendislik ve FenBilimleri Kongresi*, 464-472. (Tam Metin Bildiri/ Sözlü Sunum).

Tejani, G. G. (2012). Design optimization of the rubber compression moulding machine structure. Master Thesis, Gujarat Technological University in Partial Fulfillment of the Requirements for the Degree of Master of Engineering in Machine Design.

Thummar, D R. (2014). Truss Topology Optimization Using Modified Genetic Algorithm, Master of Technology in Machine Design, Department of Mechanical Engineering School of Engineering, RK University, Rajkot, Gujarat-360020.

Tomlin, M., & Meyer, J. (2011). Topology optimization of an additive layer manufactured (ALM) aerospace part. In *Proceeding of the 7th Altair CAE technology conference* (pp. 1-9).

Top N., Gökçe H., Şahin İ. (2019). Eklemeli İmalat İçin Topoloji Optimizasyonu: El Freni Mekanizması Uygulaması, *Selçuk Teknik Dergisi*, 18(1), 1-13.

Top, N., Şahin, İ., Gökçe H., Başak, H. (2018). 3B Yazıcı Teknolojisi için Topoloji Optimizasyonu: Otomotivde Salıncak Kolu Üzerine bir Çalışma, *3'rd International Symposium on Industrial Design Engineering* (Tam Metin Bildiri/Sözlü Sunum).

Udroiu, R., & Nedelcu, A. (2011). Optimization of additive manufacturing processes focused on 3D Printing. In Rapid Prototyping Technology-Principles and Functional Requirements. IntechOpen.

URL 1: [Online] 2015, http://volkan.com.tr/volmagazine/topoloji-optimizasyonu/

URL 2: [Online] 2015, http://info.simuleon.com/blog/how-topology-optimization-adds-innovation-for-3dprinted-products.

URL 3: [Online] Midas Informatıon Technology Co.,Ltd. Topology Optimization. http://www.midasnfx.com/products/analysis_sub.asp?strSearchKey=Optimization&n Cat3=582.

Wang K, Ho C. C., Zhang C., Wang B. (2017). A review on the 3D printing of functional structures for medical phantoms and regenerated tissue and organ applications, *Engineering*, 3(5), 653–62.

Wang, Z. L. (2018). Topological Optimization of Aircraft Frame Structures with the Variable Density Method. In *MATEC Web of Conferences* (Vol. 198, p. 05008). EDP Sciences.

Winston, W.L. (2003). "Operations Research: Applicatios and Algorithms", 4. baskı, International Thomson Publishing, Belmont, CA.

Yaman, U. (2019). Topoloji Optimizasyonu Yapılmış Parçaların 3B Yazıcılar ile Doğrudan Üretilmesi, *Gazi Üniversitesi Fen Bilimleri Dergisi Part C: Tasarım ve Teknoloji*, 7(1), 236-244.

Yang, R. J., & Chahande, A. I. (1995). Automotive applications of topology optimization. *Structural optimization*, *9*(3-4), 245-249.

Yang, R. J., Chuang, C. H. (1994). Optimal topology design using linear programming, *Computers & structures*, 52(2), 265-275.

Zhong, W., Su, R., Gui, L., & Fan, Z. (2016). Multi-objective topology and sizing optimization of bus body frame. *Structural and Multidisciplinary Optimization*, 54(3), 701-714.

Zhu, J. H., Zhang, W. H., & Xia, L. (2016). Topology optimization in aircraft and aerospace structures design, *Archives of Computational Methods in Engineering*, 23(4), 595-622.

Zhu, J., Zhang, W., & Beckers, P. (2009). Integrated layout design of multi-component system, *International journal for numerical methods in engineering*, 78(6), 631-651.

Chapter 12

ON PERFORMANCE OF FLOWER POLLINATION ALGORITHM IN TRAINING NEURAL NETWORK

Ebubekir KAYA[1]

1 Ebubekir KAYA: ebubekir@nevsehir.edu.tr, ebubekirkaya@yandex.com Department of Computer Engineering, Engineering -Architecture Faculty, Nevsehir Haci Bektas Veli University, 50300, Nevsehir, Turkey

1. INTRODUCTION

Artificial intelligence is the modeling of intelligent behavior in nature. Inspired by these intelligent behaviors, many artificial intelligence techniques have been proposed. Heuristic algorithms, neural networks and neuro-fuzzy are among these techniques. The artificial neural network (ANN) has had a wide usage area due to its advantages. System modeling, forecasting, manufacturing, signal processing, social sciences, pattern recognition are some of the areas where it is used **(Abiodun et al. 2018; Lachhwani, 2020)**. One of the important issues for ANN is the learning process. In particular, it is seen in the literature that derivative-based and heuristic methods are used.

Heuristic optimization algorithms are used successfully in solving many real problems in different fields **(Karaboga et al. 2014)**. The high performance of these algorithms has recently increased the number of heuristic optimization algorithms in the literature. Genetic algorithm (GA), particle swarm optimization (PSO), artificial bee colony (ABC), harmony search (HS), firefly algorithm (FA), cuckoo search (CS), tabu search (TS), simulated annealing (SA), differential evolution (DE), gravitational search algorithm (GSA), teaching–learning-based optimization (TLBO) and imperialist competitive algorithm (ICA) are popular heuristic algorithms **(Sarmah, 2020; Hussain et al. 2019)**. The flower pollination algorithm (FPA) examined within the scope of the study was developed in 2012 **(Yang, 2012)** and applied in a wide area. Detailed information about FPA is given in the following sections.

One of the important areas where heuristic optimization algorithms are used is ANN training. Different heuristic algorithms have been used successfully in the training of ANN and effective results have been obtained. This situation has increased the relationship between ANN and heuristic algorithm. The use cases of some heuristic algorithms in ANN training are examined by considering Web of Science and the result is presented in Table 1. GS, PSO, DE and ABC algorithms are used extensively in training neural network. HS, FA, CS, TS, SA, GSA, TLBO and ICA are in an upward trend.

The FPA algorithm is a new approach for ANN training. For this reason, the number of studies is limited. Since FPA was proposed, it has been used to solve many real-world problems. Computer science, bioinformatics, operation search, imaging science, food industry, meteorology, medicine, education and engineering are some of the areas where it is used **(Abdel-Basset & Shawky, 2019)**. The use of FPA in different areas shows that it is effective in problem solving. Although FPA is new in ANN training, it is possible to find some studies in the literature. Chiroma et al. **(Chiroma et al. 2016)** trained ANN by utilizing FPA for forecasting the Organization of the Petroleum Exporting Countries (OPEC) petroleum consumption. They compared their proposed method with ANN training approaches based on GA, PSO, ABC and BP. Their study showed that FPA-based ANN training is effective in solving the related problem. Chatterjee et al. **(Chatterjee et al. 2018)** proposed a hybrid approach based on ANN and FPA for rainfall prediction. In their study, the hybrid approch is compared with multilayer perceptron feed-forward network. They stated that their method was successful compared to the traditional method. Dutta & Kumar **(Dutta & Kumar, 2018)** suggested a model of liquid flow processes by using neural network and FPA. Liang et al. **(Liang et al. 2020)** proposed a model based on backward propagation network and FPA for intelligent diagnosis of natural gas pipeline defects. In their study, backward propagation network was optimized via improved FPA.

Table 1. Statistical information about the number of publications based on neural network.

Algorithm	Number of publication
GA	1598
PSO	564
DE	115
ABC	50
CS	32
FA	31
ICA	25
GSA	19
HS	17
SA	16
TLBO	11
TS	7
FPA	4

ANN studies based on FPA are limited. In fact, this situation shows that it is a new field of study for the solution of different real world problems. When the literature is reviewed, there is no comparison and analysis study using test functions on ANN training based on FPA. This situation makes the performance of this method uncertain. In this study, ANN training with FPA is carried out on XOR problem, 3 bit parity problem, nonlinear dynamic systems. It is aimed to convey information to the researchers about the performance of FPA with the application results.

2. METHODS

2.1. Flower Pollination Algorithm

FPA that models the pollination process in flowering plants was proposed by Xin-She Yang in 2012 **(Yang, 2012; Yang et al. 2014).**

General information about pollination process and FPA is as follows:

There are many flowering plants with various characteristics in nature. The pollination is critical for these plants. So, it is required for reproduction in flowering plants. Furthermore, it allows optimal reproduction of the flower. The pollination takes place in two different ways: biotic and abiotic.

Most of the pollination in flowers is biotic. The pollinator is needed for biotic pollination. Insect, bird, bat, etc. animals play an active role as pollinators in biotic pollination process. The ability of animals to fly allows for pollinate at greater distances. Abiotic pollination is also generally provided by wind and diffusion. According to biotic pollination, it occurs in a smaller area.

Th pollination is provided in two ways: cross-pollination and self-pollination. Th cross-pollination occurs with the flower of a different plant. If pollination occurs with the same plant species, it calls as self-pollination. Another important feature is flower constancy. Some pollinators use flower constancy and only visit certain types of flowers **(Yang, 2012; Yang et al. 2014)**.

There are 4 assumptions that make up the basic structure of this algorithm:

1) Biotic and cross-pollination are factors in the global pollination process. Levy distribution is effective in the flight of pollinators.

2) Abiotic and self-pollination process may be considered as local pollination.

3) Flower constancy is a reproduction probability associated with the similarity of the two flowers.

4) A switch probability (p) is used for switching between global and local pollination.

Flower Pollination Algorithm (or simply Flower Algorithm)

Objective min *or* max $f(\mathbf{x})$, $\mathbf{x} = (x_1, x_2, ..., x_d)$
Initialize a population of n flowers/pollen gametes with random solutions
Find the best solution $\mathbf{g}_*$ *in the initial population*
Define a switch probability $p \in [0, 1]$
while *(t <MaxGeneration)*
    for $i = 1 : n$ *(all n flowers in the population)*
      if *rand* $< p$,
        Draw a (d-dimensional) step vector L which obeys a Lévy distribution
        Global pollination via $\mathbf{x}_i^{t+1} = \mathbf{x}_i^t + L(\mathbf{g}_* - \mathbf{x}_i^t)$
      else
        Draw ϵ *from a uniform distribution in [0,1]*
        Randomly choose j and k among all the solutions
        Do local pollination via $\mathbf{x}_i^{t+1} = \mathbf{x}_i^t + \epsilon(\mathbf{x}_j^t - \mathbf{x}_k^t)$
      end if
      Evaluate new solutions
      If new solutions are better, update them in the population
    end for
      Find the current best solution $\mathbf{g}_*$
end while

Figure 1. Pseudo code of Flower Pollination Algorithm (FPA)

The working principles of FPA are based on local and global pollination. Biotic and cross-pollination and flower constancy are related to the global pollination process. In FPA, it is obtained by the new solution generation mechanism via (1).

$$x_i^{t+1} = x_i^t + \gamma L(x_i^t - g_b) \quad (1)$$

Here x_i^t is the pollen i, $g_b$is also the current best solution. γ is a scalling factor to control the step size. Flight of pollinators is realized by the Levy distribution. L is the value obtained from the Levy distribution.

In FPA, abiotic and self-pollination process may be considered as local pollination. So, local pollination takes place in a narrower region. In this process, flowering plants pollinate with different flowers of the same plant species in their neighborhood. Local pollination is modeled using (2).

$$x_i^{t+1} = x_i^t + \in (x_j^t - x_k^t) \quad (2)$$

Where x_j^t and x_k^t are pollens belong to different flowers of the same plant species in their neighborhood. $\in$ is a local random walk and a random value that conforms to a uniform distribution in [0,1].

The execution of global and local pollination process directly affects the success of FPA. So it is important to determine the global and local pollination time. FPA also has an important control parameter to balance these processes. It is a switch probability (p). p value is in the range of [0, 1]. As p value approaches 1, the effect of global pollination increases. Likewise, as p value approaches 0, the effect of local pollination increases. Pseudo code belong to working mechanism of FPA is given in Figure 1.

2.2. Artificial Neural Network (ANN)

ANN, one of the artificial intelligence techniques, models the working system of neurons in our brain. An ANN is formed by the interconnection of artificial neurons. As can be seen in Figure 2, an output value is obtained with some processes in neurons. The neurons are connected to each other by synaptic weights. All weighted inputs are processed in the transfer function. Each neuron can have a bias value. If a neuron has a bias value, it is included in the process. The output obtained from the transfer function is processed in the activation function and the output of a neuron is obtained. Sigmoid is used as activation function in applications. The equation of the Sigmoid function is given in (3).

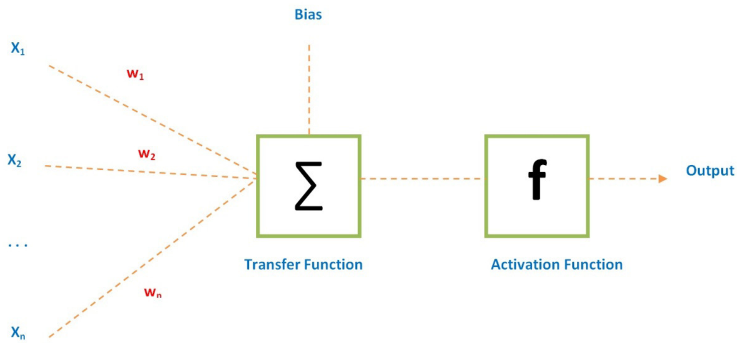

Figure 2. General scheme of artificial neuron

$$f(x) = \frac{1}{1+e^{-x}} \tag{3}$$

ANNs are divided into two classes as feed forward neural networks and feed backward neural networks. Feed forward neural network is divided into groups such as single layer perceptron, multilayer perceptron and radial basis function network. Bayesian regularized neural network (BRANN), Kohonen's self organizing map (SOM), Hopfield networks, competitive networks and art models are types of feed backward neural network **(Abiodun et al. 2018).** In this study, feed forward neural network is used. An example of feed forward neural network is given in Figure 3.

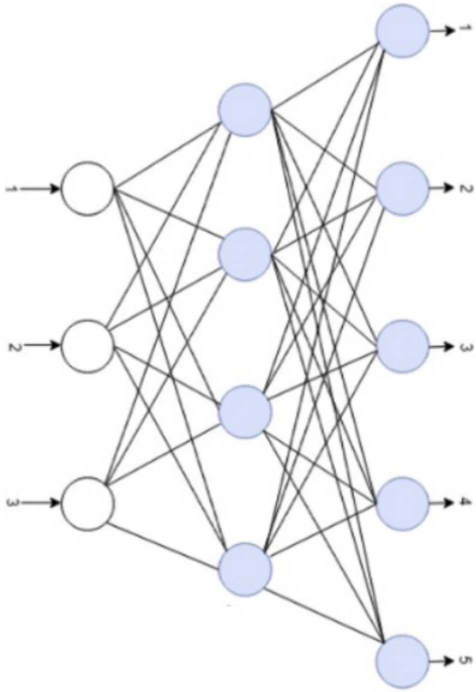

Figure 3. An example for feed forward neural network

An appropriate neural network model should be created in order to obtain effective results in solving the problem. The basic steps to be followed to determine a suitable neural network are given below **(Lachhwani, 2020)**:

- The input and output values of the model should be determined.
- The scaling range of the values to be used in the model should be determined. Data should be normalized in the range [0, 1] or [-1,1].
- The number of neurons in the layers and an activation function for each neuron should be determined.
- Weight values, bias and other parameters should be produced.
- An appropriate optimization algorithm should be determined for the training process. For each iteration, the parameters mentioned above should be updated.
- The training process should continue until the termination criteria.
- After the training process, the optimized neural network should be tested.

3. RESULTS

In this study, the performance of FPA on ANN training is evaluated. In this context, the applications are carried out on 4 different examples. The first example is on the solution of the XOR problem. The input / output values of the XOR problem are presented in Table 2. In Example 2, the studies are carried out on the 3 bit parity problem. The input / output values for Example 2 are shown in Table 3. Example 3 represents a nonlinear dynamic problem consisting of 2 inputs and 1 output. The equation of Example 3 is obtained by using (4) and (5). In Example 4, a nonlinear dynamic system with 3 inputs and 1 output is analyzed. This system is achieved using (6) and (7).

Table 2. XOR Test Problem (Example 1)

Input 1	Input 2	Output
0	0	0
0	1	1
1	0	1
1	1	0

Table 3. 3 bit Parity Test Problem (Example 2)

Input 1	Input 2	Input 3	Output
0	0	0	0
0	0	1	1
0	1	0	1
0	1	1	0
1	0	0	1
1	0	1	0
1	1	0	0
1	1	1	1

$$y_{t+1} = -0.2y_t^3 + u_t \tag{4}$$

$$u_t = \sin\left(\frac{2\pi t}{10}\right) + \sin\left(\frac{2\pi t}{25}\right) \tag{5}$$

$$y_{t+1} = \frac{y_t(y_{t-1} + 2)(y_t + 2.5)}{8.5 + y_t^2 + y_{t-1}^2} + u_t \tag{6}$$

$$u_t = \begin{cases} 2\cos(2\pi t/100), & t \le 200 \\ 1.2\sin(2\pi t/20), & 200 < t \le 500 \end{cases} \tag{7}$$

Sigmoid function is used as activation function in applications and the results have been obtained for different network structures. FPA has 2 important control parameters. These are population size and switch probability. The results obtained according to the changes of these parameters have been examined in detail. In all applications, the number of evaluations is taken as 100000. RMSE (root mean square error) is used as the error value. (8) is used in the calculation of RMSE. Here y_j is the real output. $\bar{y_j}$ is the estimated output. n denotes the number of samples. Each application is run 30 times and the average error value and standard deviation are calculated.

$$RMSE = \sqrt{\frac{1}{n}\sum_{j=1}^{n}(y_j - \bar{y_j})^2} \tag{8}$$

Table 4. Results of ANN training based on FPA (p=0.8)

Example	Network Structure	Number of parameters	Population Size (n)					
			10		20		50	
			RMSE	Std.	RMSE	Std.	RMSE	Std.
1	2-3-1	13	**0.00027**	0.00081	0.00130	0.00190	0.00745	0.00607
	2-4-1	17	0.00050	0.00071	0.00232	0.00241	0.00756	0.00496
	2-5-1	21	0.00070	0.00136	0.00277	0.00263	0.00613	0.00391
2	3-3-1	16	0.21117	0.14908	0.22475	0.12421	0.32668	0.04091
	3-4-1	21	0.13341	0.13848	0.22462	0.10634	0.28027	0.05668
	3-5-1	26	0.04602	0.08020	0.18788	0.10664	0.23585	0.07788
	3-10-1	51	**0.01682**	0.04741	0.04457	0.02850	0.09100	0.01768
3	2-5-1	21	0.01326	0.00207	0.01399	0.00190	0.01760	0.00119
	2-10-1	41	**0.01096**	0.00283	0.01557	0.00176	0.01703	0.00125
	2-15-1	61	0.01220	0.00296	0.01637	0.00120	0.01727	0.00115
4	3-5-1	26	**0.01370**	0.00468	0.01951	0.00398	0.02884	0.00378
	3-10-1	51	0.01483	0.00411	0.02377	0.00339	0.03713	0.00412
	3-15-1	76	0.01647	0.00497	0.02813	0.00405	0.04592	0.00691

In Table 4, the results belonging to ANN training by using FPA for the solution of 4 examples are given. The results are obtained for population sizes 10, 20 and 50. Also, different ANN structures are used. In Example 1, it is observed that as the population size increases, the solution quality decreases. The error value for n = 10 in 2-3-1 network structure is obtained as 0.00027. This value is found as 0.00130 and 0.00745 for n=20 and n=50 respectively. Similar increases in error have been observed in other network structures. As the number of neurons in the hidden layer increased, the number of parameters to be optimized increased. Parallel to this, the system becomes more complex. As a result, as the number of parameters increases, more unsuccessful solutions are obtained. For Example 1, the best result is obtained with 2-3-1 network structure and n = 10. Example

2 consists of 3 inputs and 1 output. The network structures such as 3-3-1, 3-4-1, 3-5-1 and 3-10-1 have been used in applications. Since Example 2 is a more difficult problem than Example 1, the number of neurons in the hidden layer directly affects the success. As the number of neurons in the hidden layer increased, the quality of the solution improves. While the error value is found 0.21117 with 3-3-1 network structure and n = 10, it is 0.01682 in 3-10-1 network. As in Example 1, increasing of population size decreases solution quality and the best result is found with n = 10. In Example 3, a nonlinear dynamic system is identified. In this example, the results are obtained on 2-5-1, 2-10-1 and 2-15-1 networks. The close results have been obtained in all networks. The best result is found with 2-10-1. The low population size is more effective in this example. In this network, 0.01096 is found for n = 10. For Example 4, the best result is found with n = 10 and 3-5-1 network structure. The rate of performance decreases with the increase in the number of parameters. As seen in Table 4, effective standard deviation values have been reached for the best solutions. This situation shows that similar results are obtained. As a reminder, starting populations are determined randomly in each application. Low standard deviation also increases the robustness of the solution. Quality solutions are obtained on 4 examples for p = 0.8 and n = 10. Generally, networks with fewer parameters have been more successful. The effect of this situation in terms of convergence is examined in Figure 4. In Example 1, the network structure with 2-3-1 shows its effectiveness after 4000 iterations. At first, due to the number of parameters is low, the speed of convergence remains low. In Example 2, the best convergence speed is obtained in 3-10-1. Solution quality and speed of convergence are parallel. In Example 3, the convergence speed appears to be better at 2-10-1. There is no obvious difference between 2-5-1 and 2-15-1 network structures In Example 4, the 3-5-1 network structure is more effective in both solution quality and convergence speed. In Figure 5, the effect of population size on convergence is examined. As the population size increases in all examples, convergence performance decreases. The best convergence is obtained for n = 10.

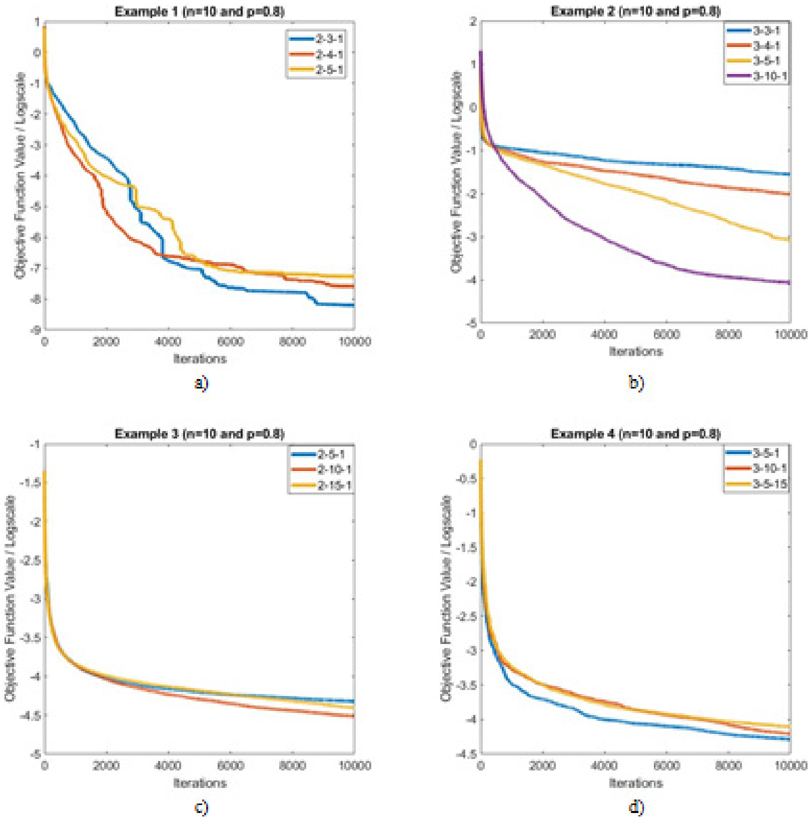

Figure 4. Comparison of convergence for different network structures on Example 1, 2, 3 and 4

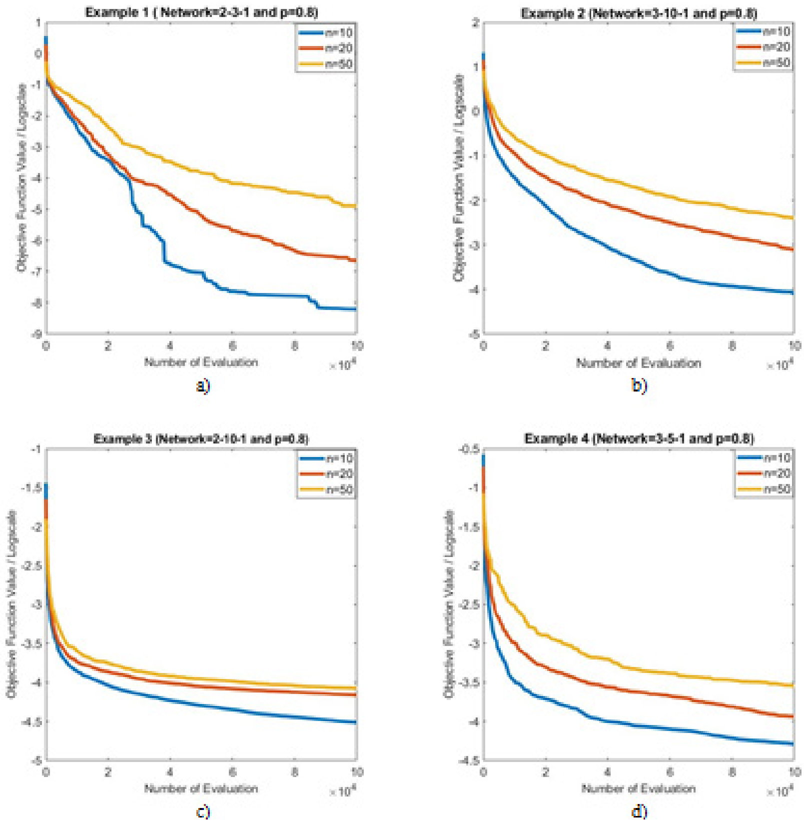

Figure 5. Comparison of convergence for different population size on Example 1, 2, 3 and 4

Table 5. Examination of effect of switch probability in neural network training based on FPA (Population Size=10)

Example	Network Structure	Switch Probability (p)				
		0.5 RMSE	0.6 RMSE	0.7 RMSE	0.8 RMSE	0.9 RMSE
1	2-3-1	**0.00015**	0.00022	0.00049	0.00027	0.00068
2	3-10-1	**0.00457**	0.00644	0.00733	0.01682	0.03040
3	2-10-1	0.01122	**0.01057**	0.01148	0.01096	0.01329
4	3-5-1	0.01429	**0.01267**	0.01286	0.01370	0.01593

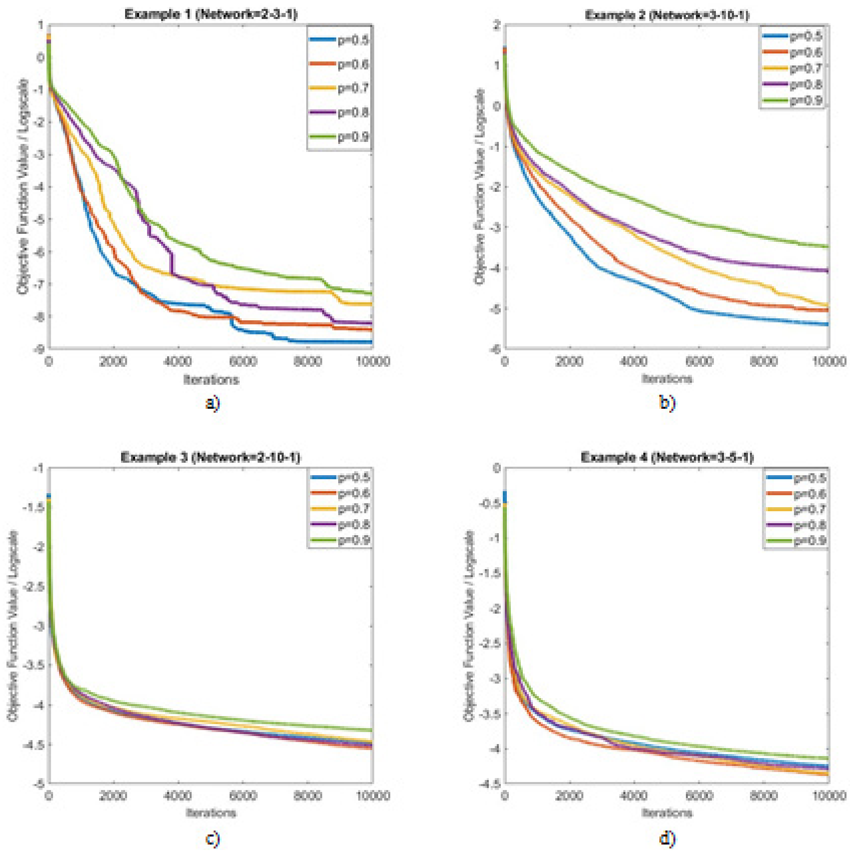

Figure 6. Comparison of convergence for different switch probability valueson Example 1, 2, 3 and 4

One of the important control parameters of FPA is switch probability (p). This control parameter takes a value between [0, 1]. Global pollination and local pollination process is determined by this parameter. If this parameter approaches 1, it is understood that global pollination is more effective. Global pollination is very effective in FPA's solution quality and speed of convergence. For this reason, solution qualities for different values of p are examined and the results are presented in Table 5. In Example 1, as p value approaches 1, the solution quality decreases. The best result is found when p = 0.5. In Example 2, high p values decrease the quality of the solutions. The best error value is obtained as 0.00457 in p=0.5. In Example 3, the similar results are obtained when p<0.9. The best solution is found with p = 0.6. In Example 4, the effective results are obtained by p= 0.6 and p=0.7. When Table 5 is evaluated in general, more successful results are obtained with p = 0.5 and p = 0.6 in ANN training. The effect of p values on convergence is examined in Figure 6. In the first 2 examples, the effect of different p values on convergence is clearly seen. A more successful convergence graph is obtained with a value of p = 0.5 where the solution quality is better. In the last two examples, their convergence is similar due to the close proximity of the solutions. The effective convergences are obtained except p = 0.9.

Table 6. Comparison of PSO, HS and FPA in ANN training (number of evaluation=100000)

Example	Network Structure	Algorithm		
		PSO $_{RMSE}$	HS $_{RMSE}$	FPA $_{RMSE}$
1	2-3-1	**0.00002**	0.02917	0.00022
2	3-10-1	0.07993	0.07252	**0.00644**
3	2-10-1	0.01733	0.02318	**0.01057**
4	3-5-1	0.03633	0.02762	0.01267

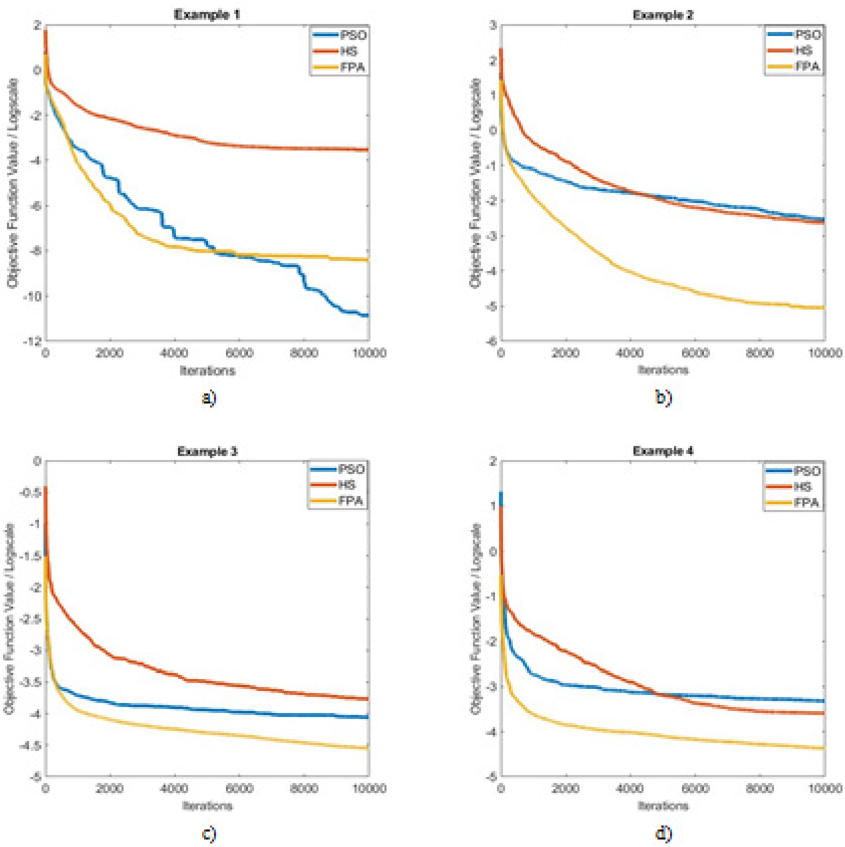

Figure 7. Comparison of convergence of PSO, HS and FPA in ANN training.

Table 7. The control parameters values used

Algorithms	Control Parameters	Values
PSO	Population Size	10
	Intertia Weights	[0.9,0.6]
	Maximum Number of Iterations	10000
HS	Memory Size	10
	Consideration Rate	0.95
	PAR	0.3
	Maximum Number of Iterations	10000
FPA	Population Size	10
	Switch Probability	0.6
	Number of Cycles	10000

The performance of FPA in ANN training is compared with PSO and HS and the results are given in Table 6. The control parameter values used in FPA, PSO and HS are shown in Table 7. In Example 1, the best result is found with PSO. However FPA is better than HS in Example 1. In Example 1, 2 and 3, FPA is more effective than PSO and HS. In Figure 7, the convergence charts of PSO, HS and FPA are compared. It is observed that FPA has a better convergence in all examples except Example-1. In Example 1, FPA is also more effective than PSO in the first 5000 iterations. This shows that FPA is effective in low and high iterations depending on the example.

4. CONCLUSION

When the literature is examined, it is seen that FPA is used successfully in the solution of many real world problems. On the other hand, FPA-based neural network studies are limited. This study aims to provide information about the usability of FPA in ANN training. For this reason, ANN is trained by using FPA for the solution of XOR problem, 3 bit parity problem and 2 nonlinear dynamic systems. The feed forward neural network is used in applications.

The network models with different neuron numbers have been used in applications. As is known, the increase in the number of artificial neurons increases the number of parameters to be optimized. It has been observed that increasing the number of neurons does not always lead to effective results. In some problems, more effective results are obtained with network structures with few neurons. Whereas, the more effective results are found by using more complex network structures in some problems. In fact, this is directly related to the complexity of the problem.

There are two important control parameters in FPA. These are population size and switch probability. The effects of both parameters on

ANN training are examined. The increase in population size (n) decreases the solution quality. The effective results are obtained for n=10. Although it varies according to the examples, as p value approached 1, the solution quality and convergence are negatively affected. It is observed that $p < 0.7$ is effective in ANN training.

Finally, the performance of FPA is compared with the performances of PSO and HS in ANN training. It has been observed that FPA is more effective than PSO and HS in terms of convergence and solution quality in ANN training.

REFERENCES

Abdel-Basset, M., & Shawky, L. A. (2019). Flower pollination algorithm: a comprehensive review. Artificial Intelligence Review, 52(4), 2533-2557.

Abiodun, O. I., Jantan, A., Omolara, A. E., Dada, K. V., Mohamed, N. A., & Arshad, H. (2018). State-of-the-art in artificial neural network applications: A survey. Heliyon, 4(11), e00938.

Chatterjee, S., Datta, B., & Dey, N. (2018). Hybrid neural network based rainfall prediction supported by flower pollination algorithm. Neural Network World, 28(6), 497-510.

Chiroma, H., Khan, A., Abubakar, A. I., Saadi, Y., Hamza, M. F., Shuib, L., ... & Herawan, T. (2016). A new approach for forecasting OPEC petroleum consumption based on neural network train by using flower pollination algorithm. Applied Soft Computing, 48, 50-58.

Dutta, P., & Kumar, A. (2018). Modeling and Optimization of a Liquid Flow Process using an Artificial Neural Network-Based Flower Pollination Algorithm. Journal of Intelligent Systems, 29(1), 787-798.

Hussain, K., Salleh, M. N. M., Cheng, S., & Shi, Y. (2019). Metaheuristic research: a comprehensive survey. Artificial Intelligence Review, 52(4), 2191-2233.

Karaboga, D., Gorkemli, B., Ozturk, C., & Karaboga, N. (2014). A comprehensive survey: artificial bee colony (ABC) algorithm and applications. Artificial Intelligence Review, 42(1), 21-57.

Lachhwani, K. (2020). Application of neural network models for mathematical programming problems: a state of art review. Archives of Computational Methods in Engineering, 27(1), 171-182.

Liang, X., Liang, W., & Xiong, J. (2020). Intelligent diagnosis of natural gas pipeline defects using improved flower pollination algorithm and artificial neural network. Journal of Cleaner Production, 121655.

Sarmah, D. K., Kulkarni, A. J., & Abraham, A. (2020). Heuristics and Metaheuristic Optimization Algorithms. In Optimization Models in Steganography Using Metaheuristics (pp. 49-61). Springer, Cham.

Yang, X. S. (2012, September). Flower pollination algorithm for global optimization. In International conference on unconventional computing and natural computation (pp. 240-249). Springer, Berlin, Heidelberg.

Yang, X. S., Karamanoglu, M., & He, X. (2014). Flower pollination algorithm: a novel approach for multiobjective optimization. Engineering optimization, 46(9), 1222-1237.

Chapter 13

FLOW PROFILES IN FLUID BED DRYERS

Sultan KEPÇEOĞLU[1]

Aytaç MORALAR[2]

Soner ÇELEN[3]

1 Sultan KEPÇEOĞLU, ASOS Proses Makina San. ve Tic. A.Ş

2 Aytaç MORALAR, Tekirdağ Namık Kemal University

3 Soner ÇELEN, Tekirdağ Namık Kemal University

1. INTRODUCTION

Drying is the process of removing liquid substances such as water in solid substance in order to slowing down or stopping chemical reactions and microbial spoilage [1]. During the drying process, a constant mass and heat transfer occurs. Mass transfer is an important feature of processes that preserve food by reducing the presence of water for microbial activity and spoilage reactions [2]. Drying is used in many sectors such as food, sludge, construction, medicine, chemical, mining and recycling [3-7]. Its advantages are listed as reducing the amount of fermentation in the product, increasing the storage capacity, recycling of waste as energy, reducing packaging and shipping costs, obtaining products with commercial value [2, 8].

Fluid bed process or fluidization process is the process of suspending the product by passing air strong enough to overcome the gravitational force affecting each particle. Moisture contained in the fluidized product is evaporated by the help of hot air and removed from the environment. Solid particle's contact with air is much more than other methods. It is a process which the end product reaches equal temperature and humidity in, since it is an ideal mixture [9].

The product fed in fluid bed dryer is a system that is made on a perforated sheet and formed a bed. Perforated sheet directs the air flow and provides equal fluidization of the product. This process is used in different types of machines such as batch type fluidized bed dryer, vibrating fluid bed dryer, spray fluid bed dryer, static fluid bed dryer and hybrid static fluid bed dryer, etc.

In the modeling of fluid bed dryers, calculations are made according to the input moisture value of the product, the desired output moisture value, capacity and final product temperature. The manufacturer should determine the parameters that are ideal for the product in fluid bed modeling. This parameters can be listed as particle diameter, bed height, drying air velocity, air temperature, dryer length, sieve structure, need for a mixer.

CFD (Computational Fluid Dynamics) analysis is used in fluid bed dryer modeling. CFD analysis method examines the air flow's behavior in the dryer, pressure drop and temperature parameters. The accuracy of the calculations is tested with the analyzes made and the preciseness of the results before manufacturing is determined. On fluid bed dryers, many studies have been carried out in different fields [10-18].

The aim of this study is to find ideal boiling speed by the calculating the minimum fluidization rate while designing a fluid bed dryer, and to calculate the required fan power at this boiling speed. To determine the most ideal flow profile according to the changing bed height, particle diameter and velocity, and to design with a policy of minimum cost and maximum efficiency is aimed. To that end, velocity profiles formed according to air velocity, particle diameter and bed height parameters in static fluid bed dryer were examined. The calculations' accuracy has been checked with the analysis made in the MFIX analysis program. Thus, it is aimed that the parameters can be adjusted optimally in the dryer process to be made.

2. MATERIAL AND METHOD

2.1. Fluid Bed Dryer

The main reasons for choosing a fluid bed dryer: It provides homogeneous solid mixture, rapid heat mass transfer and obtains products with the same moisture value as a result of the process. Fluid bed dryers can be used in different processes such as mixing, cooling, granulation, coating and burning. An example fluid bed dryer system is shown in Figure 2.1. In the system, a suction fan, cyclone to the catch escaped products, and a filter can be added to keep the product escaping from the cyclone. After the waste air is filtered, some fresh air is added to the system again in systems that energy recovery is desired. Different equipment permutations are available in different processes and the main equipment can be considered as dryer, discharge and suction fan, heater group.

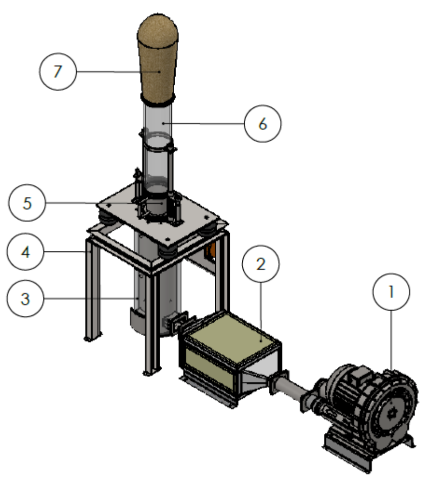

Figure 2.1. *Fluid bed dryer1: Fan (TMM - Type: EJ9KB - Power: 4kW - Flow: 470 m³ /h - Maximum Pressure: 225 mbar), 2: Resistance Heater (Max.180-250 ° C), 3: Hot Air Supply Line, 4: Chassis, 5: Sample Cup, 6: Sight Glass Column, 7: Cloth Filter*

2.2. Fluidization

Fluidization process is the process of suspending particles by passing pressurized air or fluid at a speed to overcome gravity and affect the particles to be fluidized [19].

This is called a fixed bed if the particles remain constant while the fluid passes through the product to be fluidized. The first speed at which the particles start to move with the fluid is the minimum fluidization speed and the product bed in this case is called the fluidized bed [20].

Conditions occurring in the bed according to the air velocity in fluid bed dryers are shown in Figure 2.2. Bubbles increase, causing large gaps and severe boiling in the dryer when air is introduced into the system faster than the fluidization speed [21].

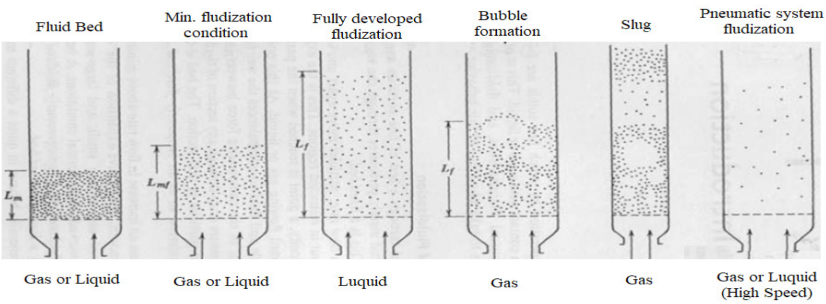

Figure 2.2. *Bubbles that may occur in the fluidized bed [22]*

2.3. Velocity Profiles

In theory, it can be examined under two parts, these are ideal fluid and real fluid. The velocities of the fluid elements are constant and parallel to each other and the ideal fluid friction value is considered to be zero. Real fluids are fluids whose viscosity values are examined.

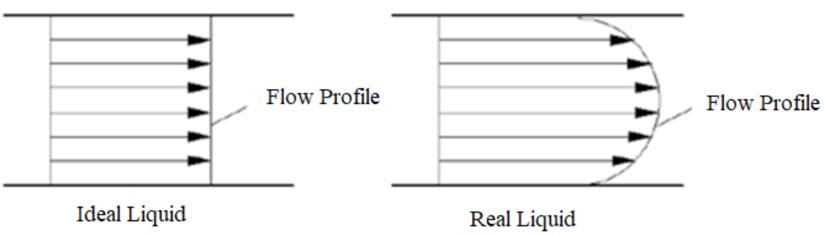

Figure 2.3. *The speed profiles of ideal fluid and real fluid*

2.4. Mathematical Modeling

The necessary calculations are made according to the physical properties of the product to be dried and desired product properties as the final product. The first calculation to be made in the fluid bed dryer design is the minimum fluidization rate and the pressure drop in conformity. Then, fan selection is made by adding other pressure losses in the system. The energy required for the product which is wanted to be dried to reach the desired moisture value is calculated and the required power for the heater is decided. In this study, energy calculations are not mentioned, studies have been made on pressure drop.

2.4.1. Minimum fluidization speed

The air velocity at which the boiling motion begins by overcoming the gravity with the fluid air in the fluidized bed dryer is called minimum fluidization. Air increases the gap distance between the particles and guarantee that the particles have a boiling movement in the bed making contact with air at the maximum level. The minimum fluidization rate varies depending on the density of the air, the viscosity, the number of Reynolds, the particle diameter of the product and the product density. Wen and Yu [23] minimum fluidization rate equation is accepted in the literature and is as in equation 2.1 [24].

$$u_{mf} = \frac{\mu}{\rho_g . d_p}[(33{,}7^2 + 0{,}0651Ar)^{0{,}8} - 33{,}7] \tag{2.1}$$

2.4.2. Archimedes number

Archimedes number examines the motion of fluids due to density differences. The Archimedes number is calculated since the motion of two or more fluids with different densities is subject in fluidized beds. The Archimedes number depends on density, viscosity, product density, particle diameter and gravity of the air, calculated by equation 2.2.

$$Ar = \frac{p_g . d_p^3 . (p_p - p_g) . g}{\mu^2} \tag{2.2}$$

Correlation between Reynolds number and Archimedes number is calculated by correlation in equation 2.3

$$Ar = 1650. Re_{mf} + 24{,}5. Re_{mf}^2 \tag{2.3}$$

2.4.3. Porosity Value During Boiling

Porosity is used to describe the intergranular air gap. There is a porosity value which express the air gap between the particles when the bed type is fixed in the fluid bed dryer. The porosity value changes due to the interaction of air and particles with each other during fluidization. In this study, the porosity value in the minimum fluidization rate in the equation 2.4 was accepted as the same as the porosity value in the fixed bed since the minimum fluidization speed and the air velocities applied in the fixed bed position are very close.

$$\varepsilon = \varepsilon_{mf}.\left(\frac{Re_p + 0{,}02.Re_p^2}{Re_{mf} + 0{,}02.Re_{mf}^2}\right)^{0{,}21} \tag{2.4}$$

2.4.4. Pressure Drop Calculation

In contact with air, the product bed in the fluid bed dryer creates resistance. This resistance causes the air pressure to drop as it passes through the bed. This pressure drop is calculated by converging with Todes' equation in equation 2.5 [25].

$$\Delta P = h.\rho_g.U^2\left[\frac{150.(1-\varepsilon)}{Re_p.\varphi} + \frac{7}{4}\right]\frac{1-\varepsilon}{\varphi.d_p.\varepsilon^3} \tag{2.5}$$

2.5. Analysis Method

The MFIX program is used in the analysis of this study. The drag model Symlal- O'Brien is used between particles and air. The Syamlal-O'Brien drag model is used to determine the hydrodynamics of the bed in turbulent fluidization. Temperature was determined as 25 ° C in analyzes. The dryer model applied in the MFIX program is shown in Figure 2.5. Air intake is defined as under the geometry, air outlet is from the top, and the side walls are defined as a non-slip surface. Geometry is 200 mm in the x direction and 1500 mm in the y direction. The analysis was carried out in two dimensions. The bed height, air velocity and particle diameter were taken as variables in the analysis.

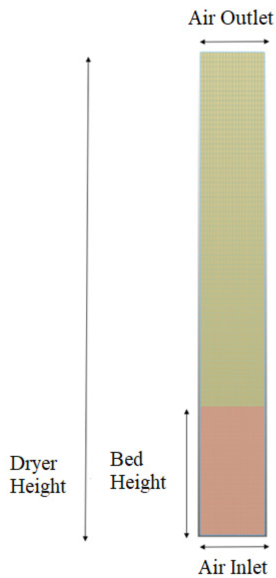

Figure 2.5. *MFIX dryer model*

2.6. Parameters

In this study, fluid velocity, particle diameter and bed height are the parameters that are effective in determining the flow profile. The effects of the parameters were compared to each other and among themselves.

2.6.1. Constant parameters

In the analysis studies, the product was determined as sand. Its density has been accepted as 1631 kg / m^3. The initial porosity value was taken as 0,55 in all analyzes. The energy calculation is not included in the analyzes, and the temperature has been taken constant throughout the entire solution area. For this reason, the viscosity value of the air has been taken as 1,836.10^{-5} kg / m.s. Geometry measurements were kept the same in the analyzes made.

2.6.2. Velocity parameter

The velocity parameter values are shown in Table 2.1 and the effect of the velocity has been examined by taking the particle diameter and bed height constant.

Table 2.1 *Velocity Parameter Value Range Table*

Number	Velocity (m/s)	Particle Diameter (m)	Bed Height (m)
1	0,6	0,0024	0,3
2	0,7	0,0024	0,3
3	0,8	0,0024	0,3
4	0,9	0,0024	0,3
5	1	0,0024	0,3
6	1,1	0,0024	0,3
7	1,2	0,0024	0,3
8	1,3	0,0024	0,3
9	1,4	0,0024	0,3

2.6.3. Particle Diameter Parameter

Particle diameter parameter values are shown in Table 2.2 and the effect of particle diameter has been examined by taking the air velocity and bed height mixed.

Table 2.2 *Particle diameter parameter value range table*

Number	Velocity (m/s)	Particle Diameter (m)	Bed Height (m)
1	1,2	0,0022	0,3
2	1,2	0,0023	0,3
3	1,2	0,0024	0,3
4	1,2	0,0025	0,3
5	1,2	0,0026	0,3

2.6.4. Bed Height Parameter

Bed height parameter values are shown in Table 2.3 and effect of bed height has been examined by taking the air velocity and particle diameter constant.

Table 2.3. *Particle diameter parameter value range table*

Number	Velocity (m/s)	Particle Diameter (m)	Bed Height (m)
1	1,2	0,0024	0,20
2	1,2	0,0024	0,25

3	1,2	0,0024	0,30
4	1,2	0,0024	0,35
5	1,2	0,0024	0,40

3. RESULTS AND DISCUSSION

3.1. Velocity Parameter Mathematical Modeling Results

The pressure drop change was observed at close values since the product fluidized t speeds after the minimum fluidization speed of 0.95 m/s (Table 3.1). In Figure 3.1, it is understood more clearly in terms of the slope where the rate of change becomes stable.

Table 3.1. Mathematical result table of velocity parameter

No	V	d_p	h	μ	p_g	p_p	ε	Re_p	Ar	Re_{mf}	u_{mf}	ΔP
1	0,6	0,0024	0,3	2E-05	1,186	1631	0,55	92,99	8E+05	147,6	0,95	357,3
2	0,7	0,0024	0,3	2E-05	1,186	1631	0,55	108,49	8E+05	147,6	0,95	465,9
3	0,8	0,0024	0,3	2E-05	1,186	1631	0,55	123,98	8E+05	147,6	0,95	588,6
4	0,9	0,0024	0,3	2E-05	1,186	1631	0,55	139,48	8E+05	147,6	0,95	725,3
5	1	0,0024	0,3	2E-05	1,186	1631	0,56	154,98	8E+05	147,6	0,95	808,3
6	1,1	0,0024	0,3	2E-05	1,186	1631	0,58	170,48	8E+05	147,6	0,95	817,7
7	1,2	0,0024	0,3	2E-05	1,186	1631	0,599	185,98	8E+05	147,6	0,95	823,9
8	1,3	0,0024	0,3	2E-05	1,186	1631	0,618	201,47	8E+05	147,6	0,95	827,1
9	1,4	0,0024	0,3	2E-05	1,186	1631	0,635	216,97	8E+05	147,6	0,95	827,6

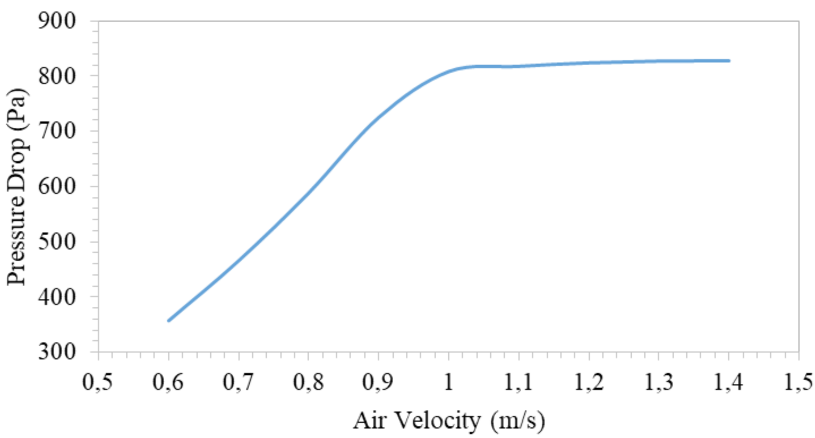

Figure 3.1. *Effect graph of the speed parameter on the pressure drop - Theoretical*

3.1.1. Mathematical Modeling Results For Particle Diameter Parameter

The effect of particle diameter on the change in pressure drop was investigated at 1.2 m/s velocity value, which is higher than the minimum fluidization velocity and 0.3 bed height. Figure 3.2 shows the result that increasing particle diameter increases the pressure drop in direct proportion.

Table 3.2. *Mathematical result table for particle diameter parameter*

No	V	d_p	h	µ	p_p	p_p	ε	Re_p	Ar	Re_{mf}	u_{mf}	ΔP
1	1,2	0,0022	0,3	2E-05	1,1856	1631	0,614	170	6E+05	126,25	0,89	811,13
2	1,2	0,0023	0,3	2E-05	1,1856	1631	0,606	178	7E+05	136,8	0,92	878,08
3	1,2	0,0024	0,3	2E-05	1,1856	1631	0,599	186	8E+05	147,61	0,95	823,88
4	1,2	0,0025	0,3	2E-05	1,1856	1631	0,593	194	9E+05	158,67	0,98	828,7
5	1,2	0,0026	0,3	2E-05	1,1856	1631	0,586	201	1E+06	169,98	1,01	832,66

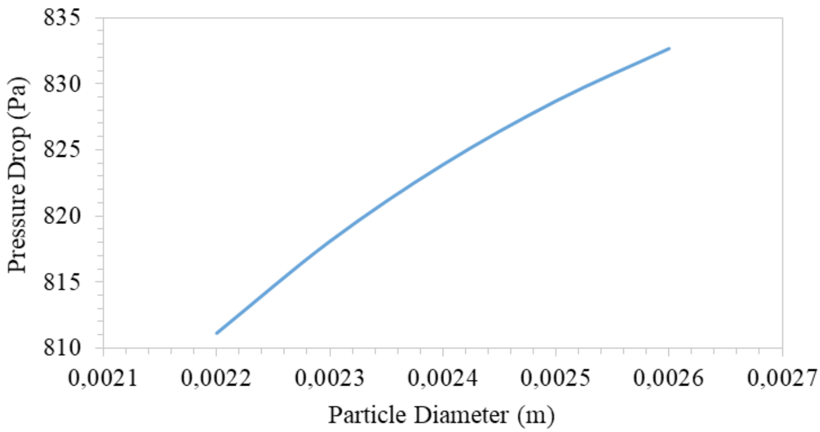

Figure 3.2. *Effect graph of the particle diameter parameter on the pressure drop - Theoretical*

3.1.2 Mathematical Modeling Results for Mattress High Parameter

The parameter that most affects the pressure drop in the fluid bed dryer is the bed height. Figure 3.3 shows the speed of impact of the bed height on the pressure drop.

Table 3.3. *Mathematical result table for the bed height parameter*

No	V	d_p	h	μ	p_p	p_p	ε	Re_p	Ar	Re_{mf}	u_{mf}	ΔP
1	1,2	0,0024	0,2	2E-05	1,1856	1631	0,599	186	6E+05	147,61	0,95	549,25
2	1,2	0,0024	0,25	2E-05	1,1856	1631	0,599	186	7E+05	147,61	0,95	686,57
3	1,2	0,0024	0,3	2E-05	1,1856	1631	0,599	186	8E+05	147,61	0,95	823,88
4	1,2	0,0024	0,35	2E-05	1,1856	1631	0,599	186	9E+05	147,61	0,95	961,19
5	1,2	0,0024	0,4	2E-05	1,1856	1631	0,599	186	1E+06	147,61	0,95	1098,51

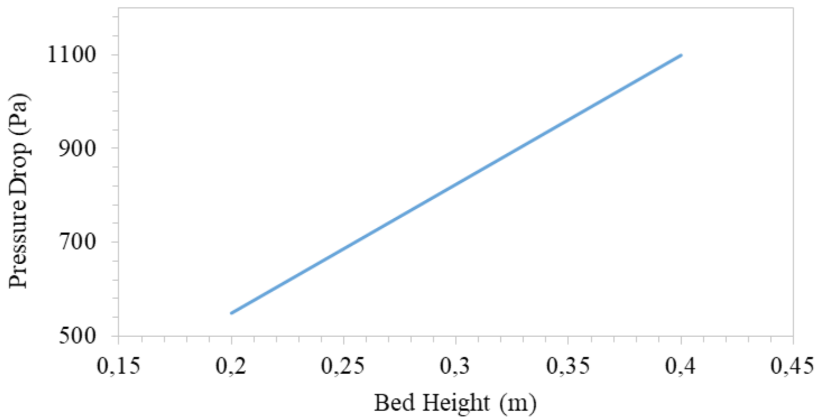

Figure 3.3. *Effect graph of the bed height parameter on the pressure drop-Theoretical*

3.2. Analysis Results

3.2.1. Velocity Parameter Analysis Results

Pressure drop was examined according to the variable speed parameter in MFIX program. In the analysis that are made in Figure 3.4, the change caused by the increasing air velocity in the pressure drop, Figure 3.7 shows the boiling motion in the 5th second of the anal.

Table 3.4 *Analysis result table of velocity parameter*

No	V	d_p	h	ΔP
1	0,6	0,0024	0,3	288
2	0,7	0,0024	0,3	377
3	0,8	0,0024	0,3	475
4	0,9	0,0024	0,3	581
5	1	0,0024	0,3	672
6	1,1	0,0024	0,3	749

7	1,2	0,0024	0,3	800
8	1,3	0,0024	0,3	838
9	1,4	0,0024	0,3	837

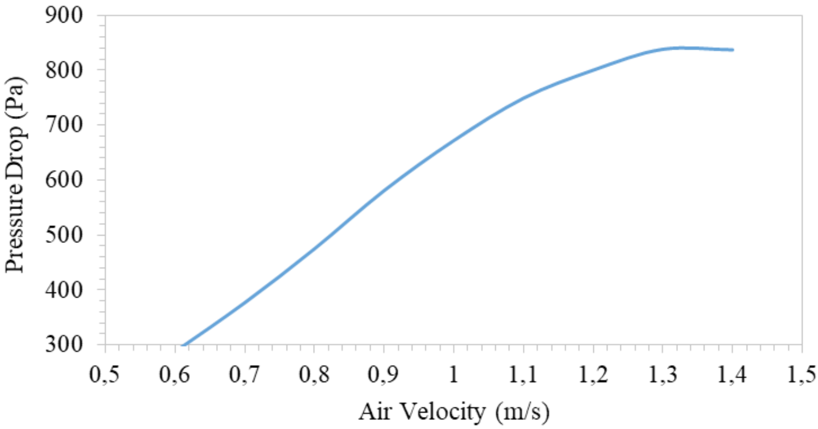

Figure 3.4. *Effect graph of the velocity parameter on the pressure drop-Analysis*

The pressure value required to pass from the fixed bed to the fluidized bed, a this is because the porosity in the fixed bed cases smaller than the porosity in fluidized bed. As can be seen in Figure 3.5, since the pace between particles is greater after the boiling starts, the resistance created by bearing is less.

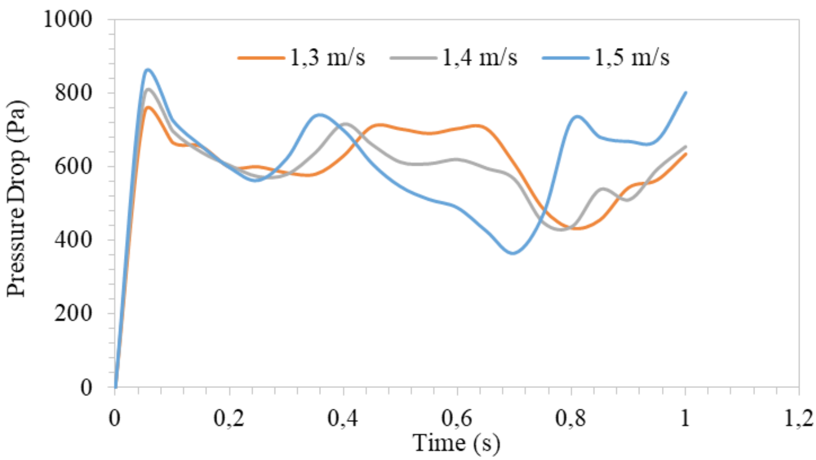

Figure 3.5. *Pressure drop time graph of the fluid bed velocity parameter*

The pressure time change shown in figure 3.6 belongs to the fixed bearing system. Since there is no fluidization movement in the fixed bed condition, the air pressure will remain constant after overcoming the bearing resistance.

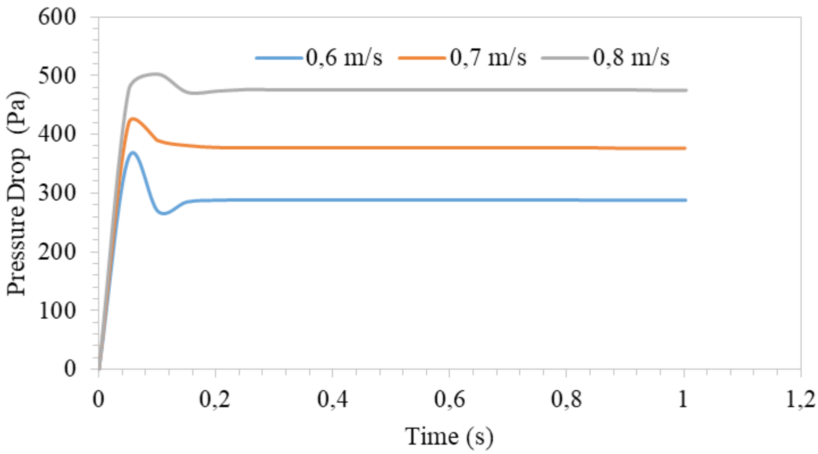

Figure 3.6. *Pressure drop time graph of fixed velocity parameter*

The velocity parameter of the analysis and the images of the 5th second boiling are shown in Figure 3.7.

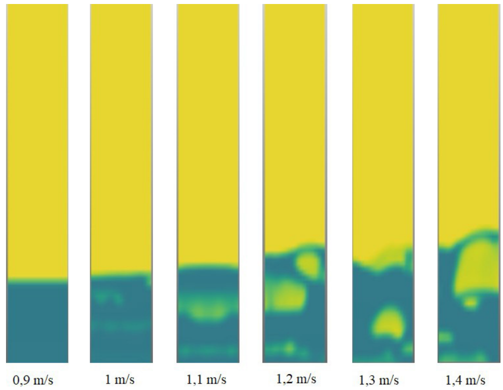

Figure 3.7. *MFIX analysis velocity parameter 5 second boiling images*

3.2.2. Particle Diameter Parameter Analysis Results

In the MFIX program, the effect f varying particle diameters on pressure drop was investigated. As the particle diameter increases, the air gaps increase and thus the porosity value decreases. Due to the close particle diameters selected in this study, The rate of change of porosity value is low. For this reason, pressure losses in different particle diameters have been found to be close and are shown in Figure 3..8. The boiling movements in the fifth second of the analysis are shown in Figure 3.9.

Table 3.5. *Analysis result table of particle diameter parameter*

No	V	d_p	h	ΔP
1	1,2	0,0022	0,3	793,85
2	1,2	0,0023	0,3	824,6
3	1,2	0,0024	0,3	800
4	1,2	0,0025	0,3	759,67
5	1,2	0,0026	0,3	779,62

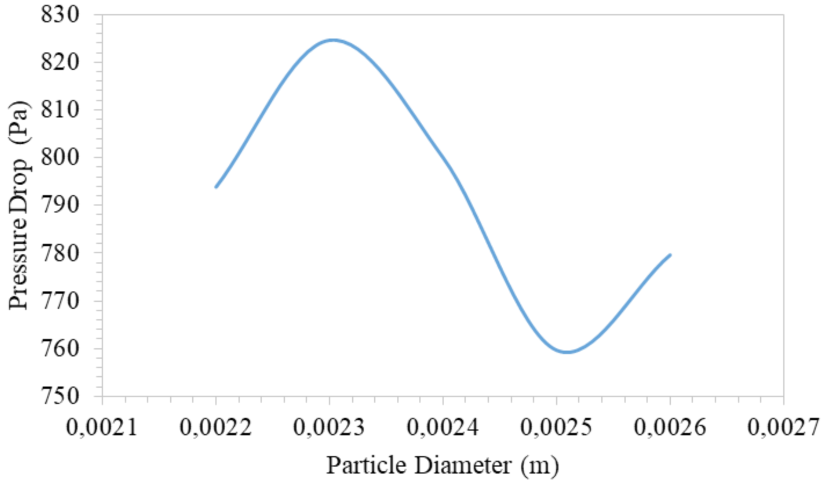

Figure 3.8. *Effect graph of the particle diameter parameter on the pressure drop – Analysis*

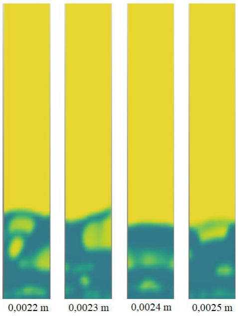

Figure 3.9. *MFIX analysis particle diameter parameter 5 second boiling images*

3.2.3. Bed Height Analysis Results

The variation of pressure drop according to 5 different bed heights varying between 0.2 and 0.4 meters was investigated. It was observed that the pressure drop increased with increasing bed height. In Figure 3.10, pressure drop value increasing due to increased bearing resistance, Figure 3.11 shows CFD analysis 5th second boiling movements.

Table 3.6. Analysis table of bed height parameter

No	V	d_p	h	ΔP
1	1,2	0,0024	0,2	412
2	1,2	0,0024	0,25	601,6
3	1,2	0,0024	0,3	800
4	1,2	0,0024	0,35	974
5	1,2	0,0024	0,4	1244

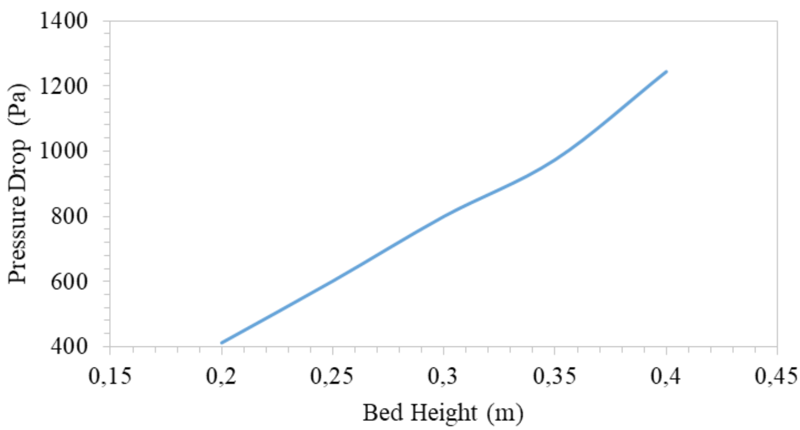

Figure 3.10. *Effect graph of the bed height parameter on the pressure drop - Analysis*

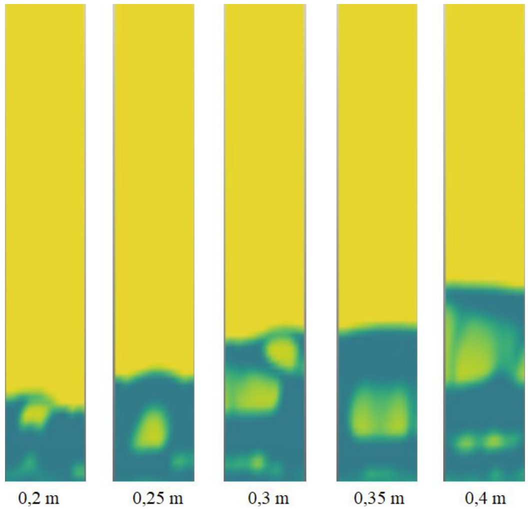

Figure 3.11. *MFIX analysis bed height parameter 5th second boiling images*

3.3. Comparison of Mathematical Calculations with Analysis Results

In the comparison of the calculations and analysis results, it was concluded that the values were consistent. In Figure 3.11-3.13, respectively, the effect of particle diameter, velocity parameter and bed height parameter on pressure drop are theoretical and analysis comparison charts. Theoretical and analysis comparison and deviation values of the analysis results are given in Table 3.7.

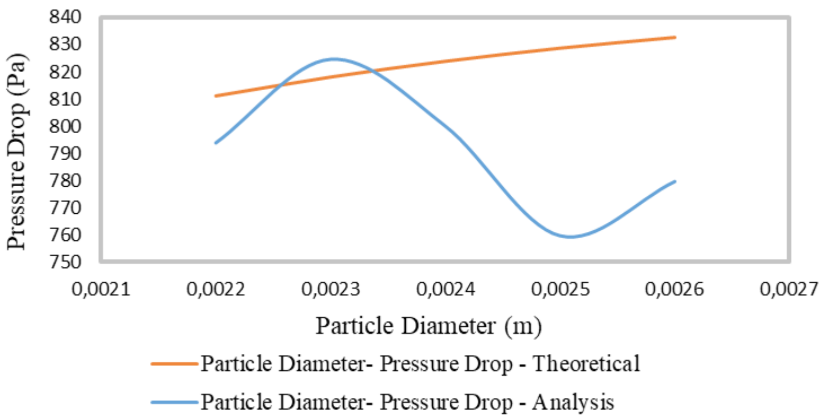

Figure 3.11. *Theoretical and analysis comparison of the effect of bed height parameter on pressure drop*

Table 3.7. *Comparison of analysis results with calculations and deviation table*

	Parametre No				
	1	2	3	4	5
Velocity - Theoretical	808,27	817,66	823,88	827,14	827,62
Velocity - Analysis	672,00	749,00	800,00	838,00	837,00
Velocity - Deviation	16,86	8,40	2,90	1,31	1,13
Particle Diameter - Theoretical	811,13	818,08	823,88	828,70	832,66
Particle Diameter - Analysis	793,85	824,60	800,00	759,67	779,62
Particle Diameter - Deviation	2,13	0,80	2,90	8,33	6,37
Bed Height - Theoretical	549,25	686,57	823,88	961,19	1098,51
Bed Height - Analysis	412,00	601,60	800,00	974,00	1244,00
Bed Height - Deviation	24,99	12,38	2,90	1,33	13,24

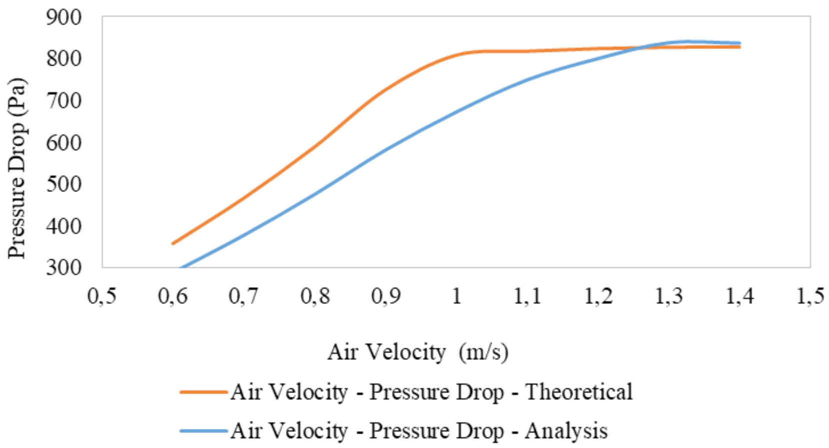

Figure 3.12. *Comparison chart of the theoretical and analysis results of the velocity parameter.*

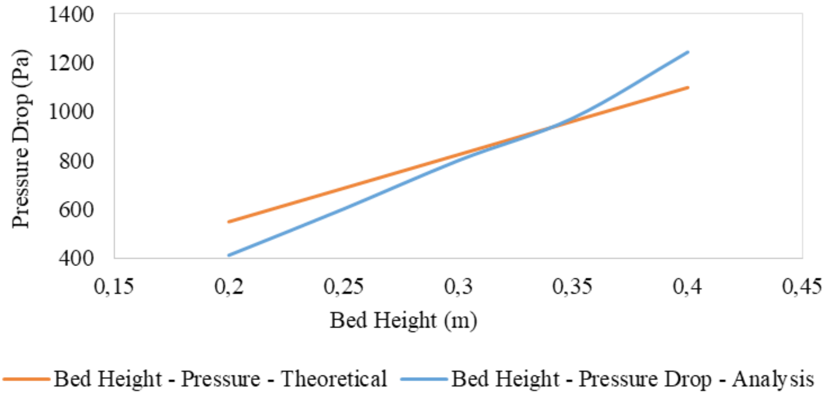

Figure 3.13. *Comparison chart of the theoretical and analysis results of the bed height parameter.*

When the effect rates of the parameters on the pressure drop are compared in Figure 4.14, it is observed that the most affecting parameter is the bed height. This argument is valid for values beyond the minimum fluidization rate. At values below the minimum fluidization velocity, no comparison can be made since there is a fixed bed.

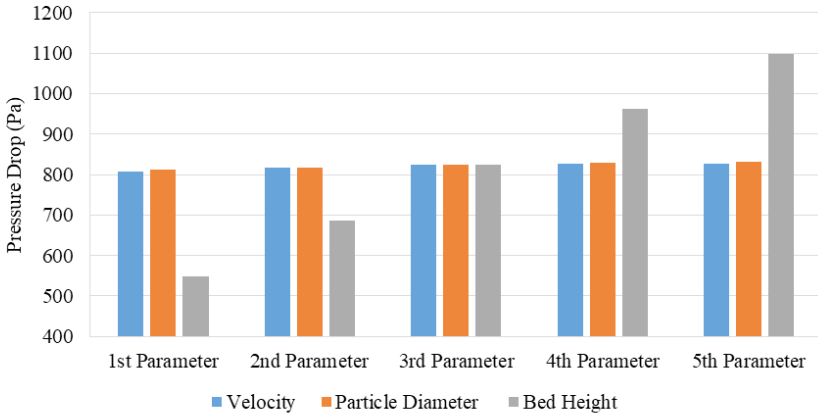

Figure 4.14 *Pressure drop impact chart according to the parameters*

4. CONCLUSIONS

In this study, the effect of fluid bed dryer parameters on pressure drop and flow profile was investigated. The effect of air velocity was observed as the first parameter. In the theoretical calculations and analysis of the velocity parameter, the bed height is 0.3 m and the particle diameter is 0.0024 m. First, the minimum fluidization speed was calculated and found to be 0.95 m / s. Below this value, no boiling action takes place and the fixed bed condition is valid. 0.6, respectively; 0.7; 0.8; 0.9; one; 1.1; 1,2; 1.3; Calculations and analyzes were made for 1,4 m / s velocities. At speeds after 0.95 m / s, which is the minimum fluidization speed, the pressure drop change occurs less because the counter pressure value required to overcome the resistance in the bed changes slightly.

Particle diameter 0.0022; 0.0023; 0.0024; 0.0025; The effect of the change in the range of 0.0026 m on the pressure drop was investigated. In the theoretical calculations and analysis of the particle diameter parameter, the bed height is 0.3 m and the air velocity is 1.2 m / s.

When calculations and analysis results were compared, it was observed that 0.1mm particle diameter increase had little effect on pressure drop. The reason for the low change can be assumed as the porosity value has slightly increased.

Bed height parameter, respectively 0.2; 0.25; 0.3; 0.35; Its effect on pressure drop was examined by taking 0.4 m. In the theoretical calculations and analysis of the bed height, the air velocity is 1.2 m / s and the particle diameter is 0.0024 m constant. It has been observed that the increase in bed height also increases the pressure drop. The higher the bed height, the more the resistance the air must overcome.

Acknowledgements

We thank ASOS Proses Makine San. ve Tic. A.Ş. for allowing the use of its laboratories as authors..

REFERENCES

Çelen, S., Arda, S. O. And Karataşer, M. A. (2018). Modeling of Drying Behavior Using Microwave Conveyor Dryer Assisted Solar Energy, El-Cezerî Journal of Science and Engineering, 5(1), 267-271.

Kovacı, T., Dikmen, E. and Şencan Şahin, A. (2018). Drying Systems, Energy Consumption and Product Quality and Sample System Design, Journal of Technical Sciences, 8(2), 25-39.

Çelen, S. and Aktaş, T. Effects of Hot Air and Vacuum Drying Methods on Drying Kinetics and Some Quality Characteristics of Traditionally Produced Couscous in Turkey, Philippine Agricultural Scientist, 2019, 102 (4), 322-329.

Çelen, S. Effect of Microwave Drying on the Drying Characteristics, Color, Microstructure, and Thermal of Trabzon Persimmon, 2019, Volume 8, Issue 2, 84.

Köse Tınmaz E., Çelen, S., Çelik S. Ö. Conventional and microwave drying of hydrocarbon cutting sludge, Environmental Progress & Sustainable Energy, 38(4), 1-7, 2019

Akyıldız, A. and Çelen, S. Effect of microwave curing on strength of mortar and drying behaviour, International Journal of Current Research, 9(02), 46636-46639, 2017.

Altıner, M. and Yildirim, M., 2011. Drying of Afsin-Elbistan Lignite and Effect of Moisture Content on Impact Strength, Ç.Ü Fen ve Mühendislik Bilimleri Dergisi, 26-3.

Çelen, S., Karataşer, M. A. and Moralar, A. Comparison Of Drying Time Of Microwave And Hybrid Dryer, International Scientific Conference 17-18 November 2017, Gabrovo, Bulgaria.

Çalhan, R., Kaya, D., Tulger, G.,, Eyidoğan, M., 2012. Organik Gübre Kurutma Teknolojileri: Akışkan Yataklı Kurutucular, Mühendis ve Makina Sayı: 634 Cilt: 53.

Çalban T. (2006). The effects of bed height and initial moisture concentration on drying lignite in a batch fluidized bed. Energy Sources Part A, 28(5), 479-485. doi:10.1080/009083190928029

Assari M.R., Basirat Tabrizi H., & Saffar-Avval M. (2006). Numerical simulation of fluid bed drying based on two-fluid model and experimental validation. Applied Thermal Engineering, 27(2007), 422-429.

Boonloi A., & Promvonge P. (2006, November 21-23). Drying kinetic of pepper corns in a fluidized-bed with helical distributor plate. The 2nd Joint International Conference on “Sustainable Energy and Environment (SEE 2006)”, Bangkok, Thailand.

Bait R.G., Pawar S.B., Banerjee A.N., Mujumdar A.S., & Thorat B.N. (2011). Mechanically agitated fluidized bed drying of cohesive particles at low air velocity. Drying Technology, 29(7), 808-118. doi:10.1080/07373937.2010.541574

Merzsch M., Lechner S., & Krautz H.J. (2012). Heat-transfer from single horizontal tubes in fluidized beds: influence of tube diameter, moisture and diameter-definition by geldart C fines content. Powder Technology, 235(2013), 1038-1046.

Tayyeb N., Arezou J., Kainmehr M.H., & Mortaza A. (2013). CFD simulation and optimization of factors affecting the performance of a fluidized bed dryer. Iranian journal of chemistry and chemical engineering (IJCCE), 32(4), 81-92.

Zhonghua W., & Mujumdar A.S. (2007). CFD modeling of the gas-particle flow behavior in spouted beds. Powder Technology, 183(2008), 260-272.

Hamzehei M. (2011). CFD modeling and simulation of hydrodynamics in a fluidized bed dryer with experimental validation. ISRN Mechanical Engineering. 2011(131087), 1-9.

Mahmoodi B., Hosseini S.H., & Ahmadi G. (2017). CFD-DEM simulation of a pseudo-two-dimensional spouted bed comprising coarse particles. Particuology, 43(2019), 171-180.

Kurtuluş O. (2007). Akışkan Yatakta Kurutma Prosesinin İncelenmesi (Yüksek Lisans Tezi). Yıldız Teknik Üniversitesi, İstanbul

Deniz Z. (2010). Akışkan Yataklı Kurutucu Modellemesi ve Analizi (Yüksek Lisans Tezi), İstanbul Teknik Üniversitesi, İstanbul

Erbaş, O. (2007). Dolaşımlı Akışkan Yatakta Isı Transferi Mekanizması ve Bu Mekanizmanın Kuramsal ve Deneysel Analizi (Doktora Tezi), Gazi Üniversitesi, Ankara.

Kunii D., Levenspiel O. (1977), Fluidizzation Engineering, John Wiley & Sons Inc., ISBN 0-88275-542-0

Wen, C.Y. and Yu, Y.H., 1966. Mechanics of Fluidization, Chemical Engineering Progress Symposium Series, 62, 100-110.

Güngör, A., 2006. Modelling Of Cırculating Fluıdized Bed Combustors, Doktora Tezi, İstanbul Teknik Üniversitesi, İstanbul.

Naterer, G. F., Heat Transfer in Single and Multiphase Systems, CRC Press, 640 Pages, 2019.

Chapter 14

CURRENT STUDIES ON WIRELESS SENSOR NETWORKS

Murat DENER[1]

1 Assoc. Prof. Dr. Gazi University, Graduate School of Natural and Applied Sciences Information Security Engineering, muratdener@gazi.edu.tr

1. INTRODUCTION

Today, the concept of smart cities consisting of smart systems has highlighted many issues in technology. The main ones are Wireless Sensor Networks, which contain sensor nodes, which are the raw material of smart cities, and examine their behavior and organization. Wireless Sensor Networks, which emerged for network installation in places where people could not reach (valleys, borders) previously, where a network could not be established, can be seen in all areas with the development of technology. Wireless Sensor Networks are the basis of many smart systems such as smart home systems used in homes, smart systems used in agriculture, air pollution measurement warning systems, smart intersection systems, and smart irrigation systems. The reason why Sensor Networks are used in smart systems is that they have many advantages.

There are three parts for the installation of smart systems. The first part, we can send any kind of value, measured from sensor. The second part, we can use any kind of protocol to communicate this information. And finally, we have external systems in order to show this data. With smart city systems, people's quality of life increases and the standard of living rises. At the same time, the city administration becomes easier. The hazards that may occur with the smart environment can be perceived in advance and the green areas are taken into consideration. The quality of our drinking water increases with smart water systems. Leakage and loss can be detected by smart measurement. Hazards can be detected in safety and emergency systems. The quality of the products increases. The number of deaths due to disease decreases.

Figure 1. Smart sytems with Wireless Sensor Networks

As you can see, all smart systems are possible with WSNs. The system you need can be realized at low cost through sensor networks.

Wireless Sensor Networks have increased their usage areas and their importance in the sector with the developments in recent years. It is a modular, user-friendly system that can be used in many areas in accordance with the purpose, offers practical solutions to the user and does not require infrastructure. Wireless Sensor Networks is a synchronized organization consisting of sensors that provide the perception of the environment with wireless service. It can be changed according to the conditions of the environment and integrated into the environment. With this feature, it is used with many technologies and systems. In particular, sensor technology used in every field today attracts the attention of users at all levels with projects such as smart homes and IoT technology. It has applications in many different fields such as military field, wildlife, industry, health and daily life. It causes questioning the reliability of a system that is used in such a wide and different area. Although their reliability is ensured, sensor networks contain some security problems depending on the environment and protocols in which they are used. Security is more important, especially if the purpose of use is military and critical areas. When the working environments of the sensors are sometimes outdoors, they are more vulnerable to attack. It is possible to prevent physical attacks with some precautions. On the other hand, attacks can sometimes come from internal and sometimes external networks. It is possible to group these attacks according to the specified criteria. These attacks cause some damage to the system and users. Although the working principle is similar to computer networks, such attacks are more affected than computer networks. Information security, confidentiality, integrity and accessibility are the most basic requirements of information security. These requirements apply to Wireless Sensor Networks. Therefore, these requirements are expected to be fulfilled in a secure sensor network.

2. WIRELESS SENSOR NETWORKS

Sensor Networks consist of many sensor nodes. Sensor node components are given in Figure 1.

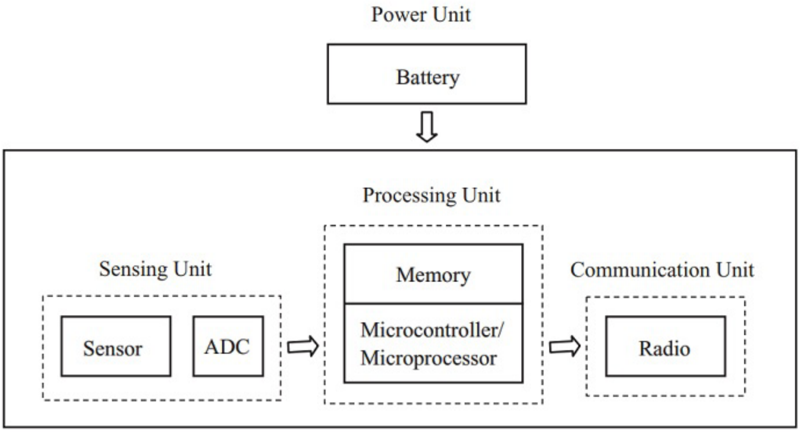

Figure 1. Sensor node components

The sensing unit has the desired sensor. For example, a sensor used for the detection of forest fires is temperature, fire sensor is installed in a node, while a sensor used for the detection of floods is installed in a water level sensor. Processor and Memory are located in the Processing Unit. Calculation and storage operations are carried out here. After the measurement of the data detected from the sensor, its calibration, etc. different calculations are included here. With the Transceiver circuit, data is transmitted to other sensor nodes or base station with the help of cooperation. Existing wireless modules (ZigBee, WiFi, Bluetooth, LoraWAN etc.) can be used here. In the power unit, the energy of the sensor node is provided. Thus, three main functions of the sensor node arise: detection, calculation, communication. There are 5 layers in Wireless Sensor Networks. These are given in Figure 2.

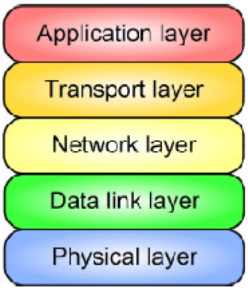

Figure 2. Layers in Wireless Sensor Networks

Physical layer is the layer responsible for frequency selection, formation of carrier frequency, signal detection, modulation. The data link layer is the layer responsible for media access control (MAC), error checking, data frame detection, data encryption. The network layer deals with the routing of the data transmitted by the transport layer. The transport layer controls data flow. Different types of applications can be developed thanks to the detection processes. These applications are used thanks to the application layer.

Protocols and transactions can be performed more easily if layered structure is dominant in Sensor Networks. Because the task and responsibility of each layer is different. Studies on Sensor Networks in the literature can be listed as follows: Increasing Energy Efficiency, Reducing Delay, Increasing Efficiency, Increasing Security, Developing Protocols, Algorithms for Different Layers, etc. In order to prove the validity of each study, simulation programs such as ns-2, QUALNET, MATLAB are used, and sometimes applications can be made over real sensor nodes.

3. SMART SYSTEMS WITH WIRELESS SENSOR NETWORKS

In the current period, cities cannot fully meet people's needs due to irregular and unplanned migration. With the increasing population growth in cities, especially in metropolises, the need for employment, housing, nutrition and infrastructure arises. Due to global climate change, agriculture, water, energy, natural disasters need to be monitored and controlled. Due to the long life expectancy of people, health, care and education needs arise. With the decrease in resources, environmental pollution increases, economic problems begin and the need for nutrition increases. The need for energy, high technology, security and communication is increasing. It is possible to meet the increasing need by making cities smart.

Smart city; It aims to increase the quality of life of citizens by creating sustainable mechanisms. In this respect, the smart city issue should be considered as a concept that includes different economic, human or legal elements, rather than just a technological issue. The main purpose of the smart city initiative is to guarantee the sustainability of cities, to facilitate living conditions by increasing social activities and to ensure maximum energy efficiency. Smart city areas include: Smart Environment. Smart Security, Smart People, Smart Structures, Smart Economy, Smart Space Management, Smart Health, Smart Governance, Information Technologies, Smart Transportation, Smart Energy, Communication Technologies, Information Security, Smart Infrastructure, Disaster and Emergency Management, Geographic Information Systems.

All of these systems can be made with wireless sensor network infrastructure. Therefore, it is clear that wireless sensor networks will always be in our lives for many years. Rising global trends and new technologies in smart cities with Wireless Sensor Networks are: Big Data, Social Networks, Climate Change, Open Data, Block Chain, Internet of Things, Urbanization and Population Growth, Artificial Intelligence, Sharing Economy, Urban Transformation, Autonomous / Connected Tools, Solution as a Service, Cloud Computing.

4. CURRENT STUDIES

In this section, by scanning the Web of Science database, the obtained studies have been examined and in the literature, what has been studied and what has been done in Wireless Sensor Networks is given in detail. Subjects are categorized and presented.

In recent years, studies on security in Wireless Sensor Networks are as follows.

In the study [1], security is emphasized. It has been stated that there may be malicious users who secretly listen to the channel during the application. To tackle this problem, a stochastic beamforming algorithm is proposed in the paper.

In the study [2], the limitations of Wireless Sensor Networks were mentioned, at the same time, it was stated that they were used in security applications such as military and health. In the study, Denial-of-Service attacks and defense methods in Wireless Sensor Networks are explained layer by layer. The study was examined in detail and the attacks-defense methods were listed by us in Table 1.

Table 1. Dos Attacks and Defense Methods in Wireless Sensor Networks

Layer	Attacks	Defenses
Physical Layer	Jamming Attack	Spread spectrum Jamming report Path re-routing
	Node Tampering	Go blind technique Camouflaging
Link Layer	Collision attacks	Error correcting codes
	Interrogation Attacks	Anti-replay MAC layer authentication
	Denial of Sleep	Packet authentication Collaborative hierarchical model
Network Layer	Spoofing Attack	Repeated game theory etc.
	Black Hole Attack	Acknowledgement mechanism Multi-path routing
	Hello Flooding Attack	Clustering approaches

Transport Layer	Synchronization Flood Attacks	Reducing connections Client puzzle TCP SYN cookies
	De-synchronization Attacks	Full packet authentication
	Content Attacks	Message observation mechanism
Application Layer	Overwhelming the Sensors	Sensor Modification
	Path-Based-DoS Attack	One Way Hash Chain

It is stated that defense methods are mostly acknowledgments, encryption, authentication, etc. in the stud. Because of the limited possibilities of nodes in Sensor Networks, the written defense methods should not be complex. Effective defense methods should be written in a simple way, and energy efficiency, which has an important role in Sensor Networks, should not be forgotten.

It is very important to provide security and privacy in Wireless Sensor Networks applications. They have stated [3] that current authentication and key generation techniques are insecure. Therefore, in order to dominate these vulnerabilities, they have proposed a new secure authenticated key establishment scheme.

Intrusion Detection systems are widely used as a defense method in wireless sensor networks. Thanks to these systems, malicious users who want to access the network without permission can be caught. As is known, there is extra energy consumption in such defense methods. Therefore, the life of the network can be shortened. Hence, their goal is the design of a reliable and energy-efficient monitoring system that resists internal security attacks. They present DAMS (Distributed and Adaptable Monitoring System) [4] that extends LEACH protocol with a trust-based and energy-efficient clustering protocols for both cluster heads and monitors election. It is stated that the new system improves energy efficiency and package delivery rates compared to other Leach alternatives.

In recent years, studies on clustering in Wireless Sensor Networks are as follows.

In the study [5], it is emphasized that random selection methods are used in the selection of the head of the cluster and that candidates suitable for being the head of the cluster can be skipped in these methods. To solve this problem, energy efficient fuzzy logic based clustering protocol (NEEF) is proposed in the study. The proposed protocol consists of four stages. These; The pre-deployment phase, the per-cluster selection phase, the cluster creation phase, and the data dissemination phase. The factors used in the fuzzy logic process are: primary factors, remaining energy and communication cost, secondary factors, node density and distance to base station. The proposed protocol was compared with SCHFTL and DFCR in MATLAB environment and successful results were obtained.

In wireless sensor networks, K-mean clustering algorithms are among the potential solutions that extend the life of the network. But in these algorithms, wrong selection of K value creates unbalanced clustering energy consumption. In order to eliminate these disadvantages, a new clustering technique using X-means algorithm is proposed in the study [6]. The proposed technique has been simulated in MATLAB environment and it has been observed that it gives better results than K-means clustering.

Clustering; It refers to the collaboration of sensor nodes to increase scalability, energy savings and durability. A group of sensor nodes can transmit their sensed values to remote stations through clusters controlled by cluster heads. Clusters are associated with the link between the cluster head and its node members, as well as the link between clusters and the base station. Performance parameters in Wireless Sensor Networks can be increased with clustering. One of the most important factors in clustering algorithms is choosing the right cluster head. In the paper [7], a Cuckoo search optimization algorithm using a fuzzy type-2 logic-based clustering strategy is suggested.

In recent years, studies on routing in Wireless Sensor Networks are as follows.

Wireless sensor networks are used in many areas as well as in environmental applications. Sensor nodes used in monitoring systems for natural disasters such as volcanic conditions and natural disasters such as storms and earthquakes may face many dangers. In such applications, nodes can be damaged faster, malicious people can damage nodes more easily. Accordingly, a safe, load balanced routing (SLBR) protocol has been proposed in the study [8] to be used in such applications.

As it is known, Drones are Unmanned Aerial Vehicles that can be easily steered with a remote control or software management. It reduces the cost considerably in aerial imaging, facilitates control mechanisms and is used in many business areas. Drones are also frequently used in gathering information from the environment. In the study [9], a drone-supported wireless sensor network was examined, it was aimed to coordinate the routing of information, to investigate several drone trajectories or route shapes and to examine their effects on information. This study was carried out within the scope of the project - Pilot Sensor Networks System for Monitoring Agricultural Areas - financed by the European fund. A new drone-powered distributed algorithm has been proposed for data acquisition in a wireless sensor network.

Green communications was first mentioned in the study [10]. Green communication refers to a new lifestyle and environmentally friendly methods. It also helps reduce the costs of communication infrastructures and service providers. In the paper, a bi-adjusting duty cycle schedule (BADCS) scheme that meets the green communication concept is proposed.

A new routing protocol has been proposed for less energy consumption in wireless sensor networks. In the work [11], they present a competent adhoc sensor routing (CASeR) protocol for delay reduction, reliable data communication, and efcient energy usage in mobile WSNs (MWSNs).

The path followed by sensor nodes in wireless sensor networks is very important. Excessive communication over a weak node, congestion due to heavy use of any path, all occur due to the wrong path selection. In the work [12] proposes an energy and congestion aware routing (ECAR) algorithm inheriting the concepts of the potential field.

In the work [13], they determine a multicast optimal route (OR) at a specific deadline for mobile sinks (MSs) using network coding (NC) in wireless sensor networks (WSNs).

A new routing mechanism has been proposed in the study [14]. The routing approach is not only the solution to improve the quality but also improves the WSN performance.

In recent years, studies on localization in Wireless Sensor Networks are as follows.

Positioning is a very important role in Wireless Sensor Network applications. For example, in forest fire detection systems, which is an environmental monitoring application, if the sensor nodes are not positioned correctly, the application will not work correctly. They added a self-adaptive function [15] that matches the positioning requirements for the explosion search mechanism of the fireworks algorithm.

In this study [16], monitoring and positioning processes were carried out using the received signal strength indicator (RSSI).

The study [17] proposes a simple yet new method of geographic routing to perform routing when location and channel errors occur. In the algorithm, it is proposed that next hop node is selected based on the combined probability of distance, estimated location error and estimated channel access probability associated with neighbor nodes.

Locating sensor nodes is one of the biggest challenges in wireless sensor networks. Most of the time, positioning operations are a one-time process. However, landslides or any other event may occur in real time applications. Nodes in the network may need to be relocated. In the paper [18], a new positioning algorithm for displaced sensor nodes is proposed. Particle swarm optimization (PSO) was used in the algorithm.

In most wireless sensor network applications, service cannot be provided without geolocation data, especially during disaster management. Recently, nodes are detected or their positions are learned through GPS-based mobile nodes. In the study [19], energy efficiency of mobile nodes is emphasized.

In recent years, studies on coverage in Wireless Sensor Networks are as follows.

Extending the coverage of sensor nodes is an important and critical issue for Wireless Sensor Networks. An energy-efficient distributed algorithm for target coverage preservation (DATCP) has been proposed in the study [20]. The implemented algorithm was compared with LEACH (multihop), CPCP, EADC, ECDC, and PCACP in terms of energy efficiency and successful results were obtained.

The work [21] investigates extending the lifetime of the WSN in the context of target coverage problems. To tackle this problem, they propose a scheduling technique for WSN based on a novel concept within the theory of learning automata (LA) called pursuit LA.

In recent years, other studies that have been done in Wireless Sensor Networks, especially focusing on energy efficiency, are as follows.

A smart carrier sense multiple access (SCSMA) was proposed in the study [22]. Control messages come into play when secure transmission of messages is required. It is extremely important that the control messages do not overlap and work effectively. Under normal circumstances, nodes use the CSMA method to avoid conflicts. It is known to avoid conflicts with the random withdrawal technique found in the CSMA method. CSMA's deficiencies were corrected with the NCR algorithm and Blind Learning Algorithm used as methods in the study. Comparison was made in terms of Energy Consumption and Throughput criteria and it was found to be better than 802.15.4 with RTS/CTS, a-RtsCts-CSMS/CA, and Slotted CSMA/CA.

As is known, Wireless Sensor Networks can be used actively in many areas including military and environmental. Due to the limited possibilities of Sensor Nodes, the location of the sensor nodes is very important in any application. Proper positioning of sensor nodes is critical to the performance and lifetime of the network. A new dynamic deployment approach based on metaheuristic Whale Optimization Algorithm has been proposed in the study [23].

Videos are compressed with the Distributed Video Coding technique. It is also used in Wireless Sensor Networks due to its low memory requirement. In the study [24], error control mechanism is proposed for reliable multimedia communication.

Since the sensor nodes in wireless sensor networks are located in a wide area, sending messages is not performed with a single hop. Sensor nodes must find a route and can send data using the multi-hop technique. In the paper [25], multihop V-MIMO technique is used for long range communication in the WSN.

In the article [26], the concept of class of service was adopted to prioritize heterogeneous, resulting in an optimized prioritized backoff MAC scheme called Class of Service Traffic Priority-based Medium Access Control.

Data fusion is essentially an information integration problem. This method combines data from multiple sensors to make a better analysis and make better decisions than using a single sensor for the relevant situation. They propose a data fusion method [27] based on an extreme learning machine optimized by particle swarm optimization for wireless sensor networks.

Congestion may occur due to several reasons like data packet collision, transmission channel contention and bufer overfow. Studies on congestion processes have been done in the article [28].

In the paper [29], the authors have been proposed an Adaptive Neuro Fuzzy Inference System based Relay Selection scheme. The proposed scheme enhance the network lifetime.

5. CONCLUSIONS

Wireless Sensor Networks can now be seen in all areas. Sensors are found everywhere in our homes, roads, buildings, parking lots and lands and measurements are made. The necessary work flows are created according to the measurement results. When the latest up-to-date studies are examined, it is seen that there are more studies in the fields of security, clustering, routing, positioning, coverage, and energy efficiency. Since each application is unique in Wireless Sensor Networks, there is no standard. Therefore, each study has its own acceptances and outputs. In summary, it is understood that energy efficiency and security issues will always be ahead in Wireless Sensor Networks.

REFERENCES

1. Hu, Z.T., Jin, Y., Liu, H.J. (2020). A Stochastic Beamforming Algorithm for Wireless Sensor Network with Multiple Relays and Multiple Eavesdroppers, *Wireless Personal Communications*, DOI: 10.1007/s11277-020-07778-1.

2. Ul Islam, M.N., Fahmin, A., Hossain, M.S., Atiquzzaman, M. (2020). Denial-of-Service Attacks on Wireless Sensor Network and Defense Techniques, *Wireless Personal Communications*, DOI: 10.1007/s11277-020-07776-3.

3. Jabbari, A., Mohasefi, J.B. (2020). User-sensor mutual authenticated key establishment scheme for critical applications in wireless sensor networks, *Wireless Networks*, DOI: 10.1007/s11276-020-02451-8.

4. Abdellatif, T., Mosbah, M. (2020). Efficient monitoring for intrusion detection in wireless sensor networks, *Concurrency and Computation-Practice & Experience*, DOI: 10.1002/cpe.4907.

5. Dwivedi, A.K., Sharma, A.K. (2020). Neef: A Novel Energy Efficient Fuzzy Logic Based Clustering Protocol for Wireless Sensor Network, *Scalable Computing-Practice and Experience*, *21*(3), 555-568.

6. Radwan, A., Kamarudin, N., Solihin, M.I., Leong, H., Rizon, M., Desa, H., Bin Azizan, M.A. (2020). X-means Clustering for Wireless Sensor Networks, *Journal of Robotics Networking and Artificial Life*, *7*(2), 111-115.

7. Mittal, N., Singh, S., Singh, U., Salgotra, R. (2020). Trust-aware energy-efficient stable clustering approach using fuzzy type-2 Cuckoo search optimization algorithm for wireless sensor networks, *Wireless Networks*, DOI: 10.1007/s11276-020-02438-5.

8. Palani, U., Amuthavalli, G., Alamelumangai, V. (2020). Secure and load-balanced routing protocol in wireless sensor network or disaster management, *IET Information Security*, *14*(5), 513-520.

9. Skiadopoulos, K., Giannakis, K., Tsipis, A., Oikonomou, K., Stavrakakis, I. (2020). Impact of drone route geometry on information collection in wireless sensor networks, *Ad Hoc Networks*, DOI: 10.1016/j.adhoc.2020.102220.

10. Li, G.P., Li, F.F., Wang, T., Gui, J.S., Zhang, S.B. (2020). Bi-adjusting duty cycle for green communications in wireless sensor networks, *Eurasip Journal on Wireless Communications and Networking*, DOI: 10.1186/s13638-020-01767-5.

11. Kumaran, K.M., Chinnadurai, M. (2020). A Competent Ad-hoc Sensor Routing Protocol for Energy Efficiency in Mobile Wireless Sensor Networks, *Wireless Personal Communications*, DOI: 10.1007/s11277-020-07741-0.

12. Jain, A., Pattanaik, K.K., Kumar, A., Bellavista, P. (2020). Energy and congestion aware routing based on hybrid gradient fields for wireless sensor networks, *Wireless Networks*, DOI: 10.1007/s11276-020-02439-4.

13. Kharati, E., Khalily-Dermany, M. (2020). Determination of the Multicast Optimal Route for Mobile Sinks in a Specified Deadline Using Network Coding and Tabu Search Algorithm in Wireless Sensor Networks, *Iranian Journal of Science and Technology-Transactions of Electrical Engineering*, DOI: 10.1007/s40998-020-00369-7.

14. Verma, U.S., Gupta, N. (2020). Wireless Sensor Network Path Optimization Using Sensor Node Coverage Area Calculation Approach, *Wireless Personal Communications*, DOI: 10.1007/s11277-020-07706-3.

15. Huang, M.G., Yu, B. (2020). Range-Based Positioning with Self-Adapting Fireworks Algorithm for Wireless Sensor Networks, *Mathematical Problems in Engineering*, DOI: 10.1155/2020/9286438.

16. Ramli, N.A.M., Rahiman, M.H.F., Malik, M.F.A., Kamarudin, L.M., Mohamed, L., Zakaria, A., Abdullah, M.S.M. (2020). A Design and Development of a Wireless Sensor Network for Potential Monitoring and Localization, *Journal of Electrical Engineering & Technology*, DOI: 10.1007/s42835-020-00515-5.

17. Katti, A., Lobiyal, D.K. (2020). Energy Efficient Location Error Resilient Connectivity in Wireless Sensor Networks, *Wireless Personal Communicaions*, DOI: 10.1007/s11277-020-07735-y.

18. Kanwar, V., Kumar, A. (2020). DV-Hop localization methods for displaced sensor nodes in wireless sensor network using PSO, *Wireless Networks*, DOI: 10.1007/s11276-020-02446-5.

19. Han, G.J., Yang, X., Liu, L., Zhang, W.B., Guizani, M. (2020). A Disaster Management-Oriented Path Planning for Mobile Anchor Node-Based Localization in Wireless Sensor Networks, *IEEE Transactions on Emerging Topics in Computing*, *8*(1), 115-125.

20. Nguyen, T.G., Phan, T.V., Nguyen, H.H., Aimtongkham, P., So-In, C. (2020). An efficient distributed algorithm for target-coverage preservation in wireless sensor networks, *Peer-To-Peer Networking and Applications*, DOI: 10.1007/s12083-020-00987-2.

21. Upreti, R., Rauniyar, A., Kunwar, J., Haugerud, H., Engelstad, P., Yazidi, A. (2020). Adaptive pursuit learning for energy-efficient target coverage in wireless sensor networks, *Concurrency and Computation-Practice & Experience*, DOI: 10.1002/cpe.5975.

22. Nguyen, T.T., Oh, H. (2020). SCSMA: A Smart CSMA/CA Using Blind Learning for Wireless Sensor Networks, *IEEE Transactions on Industrial Electronics*, *67*(12), 10981-10988.

23. Ozdag, R., Canayaz, M. (2020). A new metaheuristic approach based on orbit in the multi-objective optimization of wireless sensor networks, *Wireless Networks*, DOI: 10.1007/s11276-020-02454-5.

24. Nikzad, M., Bohlooli, A., Jamshidi, K. (2020). An adaptive, cross layer error control scheme for Distributed Video Coding over Wireless Multimedia

Sensor Networks, *Multimedia Tools and Applications*, DOI: 10.1007/s11042-020-09594-y.

25. Singh, M.K., Amin, S.I. (2020). Energy efficient wireless sensor network using optimum hops and virtual MIMO technique, *SN Applied Sciences*, DOI: 10.1007/s42452-020-03360-3.

26. Gupta, U., Bhattacharjee, V., Bishnu, P.S. (2020). Outlier Detection in Wireless Sensor Networks Based on Neighbourhood, *Wireless Personal Communications*, DOI: 10.1007/s11277-020-07722-3.

27. Cao, L., Cai, Y., Yue, Y.G. (2020). Data Fusion Algorithm for Heterogeneous Wireless Sensor Networks Based on Extreme Learning Machine Optimized by Particle Swarm Optimization, *Journal of Sensors*, DOI: 10.1155/2020/2549324.

28. Yadav, S.L., Ujjwal, R.L. (2020). Mitigating congestion in wireless sensor networks through clustering and queue assistance: a survey, *Journal of Intelligent Manufacturing*, DOI: 10.1007/s10845-020-01640-8.

29. Jain, N.K., Yadav, D.S., Verma, A. (2020). An Adaptive Neuro Fuzzy Inference System (ANFIS) Based Relay Selection Scheme for Cooperative Wireless Sensor Network, *Wireless Personal Communications*, DOI: 10.1007/s11277-020-07698-0.

Chapter 15

A MODEL PROPOSAL FOR DIGITAL TRANSFORMATION OF CITIES

Murat DENER[1]

1 Assoc. Prof. Dr. Gazi University, Graduate School of Natural and Applied Sciences Information Security Engineering, muratdener@gazi.edu.tr

1. INTRODUCTION

In order to be a country that produces technology, there is a need for a society that can use technology to improve the quality of life, administrations that can use its resources effectively and efficiently, and an internationally competitive production sector [1]. In order to get the place we deserve in the developing world, our cities must be made smart from end to end. In this direction, digital transformation is needed. Digital transformation is to generate value from data using the ultimate goal Technologies [2]. Sensors only generate data. These produced data are transferred to a desired location in real time from a continuously connected communication environment. The transferred data is analyzed through the software, a decision to be made and a situation to be done is determined and the action is taken. Sensors are the basis of concepts such as Smart System and Smart Product that we often hear today [3].

The proposed model generally consists of 5 stages. These are;

Stage 1: Development of sensor technologies to generate data

Stage 2: Development of Internet of Things technologies to collect data

Stage 3: Setting up Cloud Computing technologies to store data

Stage 4: Application of Big Data approaches to data analysis

Stage 5: Using Artificial Intelligence technologies for decision making

The objectives of the proposed model in the second part of the study, the development of related software hardware technologies in the third part, and the proposed model in the fourth part were mentioned, and finally the study ended with the results part.

2. OBJECTIVES OF THE PROPOSED MODEL

The purpose of the proposed model is to develop locally and nationally the software and hardware technologies required for the digital transformation needed to make cities end-to-end smart. There is currently no such comprehensive solution in our country. The digital transformation process is given in Figure 1. In the digital transformation process, Data is Produced with Sensor Technologies, Data is Collected with Internet of Things technology, Data is Stored with Cloud Computing technology, Data is Analyzed with Big Data technology, Decision is made with Artificial Intelligence technology, and value is produced at the end of the process.

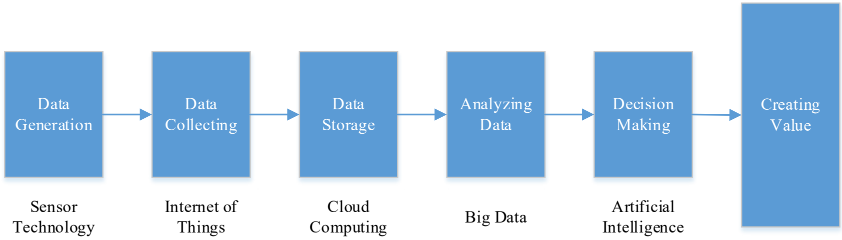

Figure 1. Digital Transformation Process

Generally expected goals are as follows. Local-national development of approximately 40 different products, including low energy consumption and high security sensor node to generate data, close to 10 sensor panels where common sensors can be used together, approximately 20 Wireless interface cards, approximately 10 Industrial protocol cards (Figure 2).

Figure 2. Sensor Technologies

Developing the necessary coordinator node to collect data, Clustering and routing protocol design to collect data and provide scalability, Developing Over-the-Air Programming and Encryption Libraries for Nodes. Setting up Cloud Computing technologies to store data. The expected goals and objectives in the implementation of Big Data-Artificial Intelligence approaches for data analysis and decision making are as follows. Big Data Analytics Platform is a distributed software platform that aims to collect large data stacks of different content and structure and to make analytical inferences over these stacks. This platform allows the collection of real-time or offline data from information systems created for different purposes and sensor resources that make measurements with these systems, on a single interface, to be stored on the Hadoop platform and to make analytical inferences. The data to be collected can be software or hardware sourced, structural or non-structural, binary or text / json format. The collected data is intended to be used for machine learning purposes within the scope of the analytics engine component to be developed within the Hadoop platform. In addition, within this platform, it is aimed to develop a kind of Management dashboard application in order to monitor the results of machine learning and analytical evaluation. All technologies to be used within the scope of the proposed model are open source and scalable, and the system will be able to continue to operate at high performance even if the amount and structure of the data in the model changes. In addition, it will be ensured that the systems to be developed are end-to-end secure.

3. DEVELOPMENT OF SOFTWARE AND HARDWARE TECHNOLOGIES

The issues to be considered in each of the five phases in the proposed model are specified in this section. Stage 1: In most applications, sensor nodes are installed in a remote location. Therefore, situations arise where nodes are extremely difficult to maintain. The lifetime of the node is determined by the life of the battery on it, so that the battery should be used in the most efficient way with minimal energy consumption. Charging large numbers of sensor batteries can be an expensive and time-consuming task [4]. Sensor technologies have low processor capacity, limited memory and radio transmission, and network life is limited by battery life [5]. Since sensor technologies can be used in thousands of applications in some applications (forest fire monitoring, monitoring agricultural lands, etc.), they must be low-cost. In order to ensure low cost, the equipment used is preferred accordingly. Therefore, the capacity of the hardware such as processor and microcontroller on sensor technologies is limited. For maximum benefit, low memory and low processor should be used efficiently. An attacker infiltrating any of the sensor technologies could take over the entire system [6]. Therefore, data privacy, data integrity, authentication, data freshness, data availability security principles must be provided. Sensor technologies are very sensitive to safety. The security mechanisms of the sensor nodes should be designed considering the resource constraints of the sensor nodes and malicious detectors [7]. For all these reasons, sensor technologies should be designed with low energy consumption and high security. An appropriate encryption algorithm and operation mode [8-11] should be used to ensure Data Privacy, Data Integrity, Authentication, Data Freshness in Sensor technologies. In order to meet the usability principle, a new detection-defense unit should be established.

Stage 2: Encryption libraries should be created within the coordinator node using block cipher algorithms in accordance with the philosophy of high security - low energy consumption. The coordinator node receives the data collected with the help of the sensor network cooperation and sends it to the cloud information system. Sensor networks can include thousands of sensor technologies using inexpensive, small sized sensors. Scalability and managing this large number of sensors are a major challenge. Clustering is one solution to this problem. In clustering, neighboring nodes are combined to form a cluster and a cluster head is selected to manage that cluster. Self-organization of the network is indispensable in situations such as placing multiple sensor technologies in difficult-to-access environments. During the life of the network, nodes can collapse and new nodes can join the network. Therefore, the network must be able to reconfigure itself periodically. Thus, it will be able to continue its function. It is also important to protect the connections of the entire network in cases such as individual nodes disconnecting and connecting from the network. Also, in some smart city applications, sensor nodes may need to cover a geographically wide area, and their number in a system can exceed tens of thousands. Due to node redundancy, each event is detected by more than one sensor nodes, and hence the amount of data that needs to be carried in the network increases. In other words, redundancy increases the amount of data sent to the base station and reduces the lifetime of the network. These problems are overcome with data clustering protocols and routing protocols. In the proposed model, a hierarchical routing protocol [12] capable of clustering should be developed, in this protocol, the network should be mapped (without using GPS to increase the cost), Sleep-Wake / Load Balancing, and routing with Data Merge-clustering algorithms.

Stage 3: In the process of setting up the cloud system, the Docker platform should be used in order to use server resources more efficiently. Docker is a set of products that uses virtualization at the operating system level to run software in packages called containers. Containers are isolated from each other and package and install their own software, libraries and configuration files. Linux (Ubuntu) operating system should be preferred as the server operating system. Because the UBUNTU operating system is one of the systems that provides the best performance in cloud server systems. In order to ensure the security of the Cloud System, a security license that will ensure the application and server security as a whole should be preferred. The preferred box security application should have the capacity to perform security audits at all layers of TCP/IP.

Stage 4 and 5: All technologies to be used within the scope of the proposed model should be open source and scalable. With its scalability feature, the system should be able to continue operating at high performance even if the amount and structure of the data in the model changes. Classical relational database management systems (DBMS) such as MySQL, Oracle and Microsoft SQL Server are used for data storage and query. It is not possible to distribute data to multiple servers in these DBMS. In addition, these DBMSs are insufficient in environments where there is an increase in exponential data such as smart city data, twitter, and facebook. NoSQL (Not Only SQL) DBMS can store large data, meet the needs of systems with high traffic and scale horizontally [13]. NoSQL database versions support TLS and Key Management Interoperability protocols. For secure authentication, Kerberos uses the industry standard client / server authentication. It also allows two networks to be connected to the database over an encrypted or limited-access network model with the use of Virtual Private Networks. NoSQL database models contain many security infrastructures provided by relational database models [14]. In order to realize the proposed model, MongoDB, an open source code, NoSQL database application that supports cloud computing and supports indexing on data, can be used to store and query data. The data can be stored as JSON based document. If it is understood that it is necessary, open source MySQL can also be used. In the benchmark test conducted by Yahoo, it is seen that MongoDB is significantly ahead of the basic databases in terms of throughput and latency in a number of configurations.

Apache spark can be used for data analytics studies in the decision support system to be developed within the scope of the proposed model. Apache Spark is an open source library developed with Scala that enables parallel processing on large data sets. With Apache Spark instead of Hadoop, data can be processed more easily and faster. Machine learning applications can be developed thanks to the MLib library included in Apache Spark. Data can be processed instantly with Apache Spark Streaming.

4. PROPOSED MODEL

The model will basically take data from data traps and data from IoT, Web and smart city resources such as electricity and water. The received data will be saved to the Distributed file system via data paths. The system to be developed will continuously communicate with the outside world with the help of Rest APIs. Analytical inferences that will be determined with Apache Spark ML will be realized. Mobile compatible web interfaces will be developed to monitor management dashboard, users, system performance, and display the results obtained from the analytical engine. Node.JS will be used in the development of interfaces. Node.JS is a development environment that enables javascript codes to be run asynchronously. The Node.JS development environment will be used while developing user panels. With Node.JS, HTML5, CSS3, Javascript (jQuery) will be used under the Express web framework. The reason for using NodeJS is its performance and up-to-date technology. Besides, it works as non-blocking. Bower and npm will be used to check and update their packages.

As shown in Figure 3, in the model, separate data acquisition service will be developed for each data set that will be received from IoT sensors, data coming via web stream and IoT devices from home services such as electricity, gas and water.

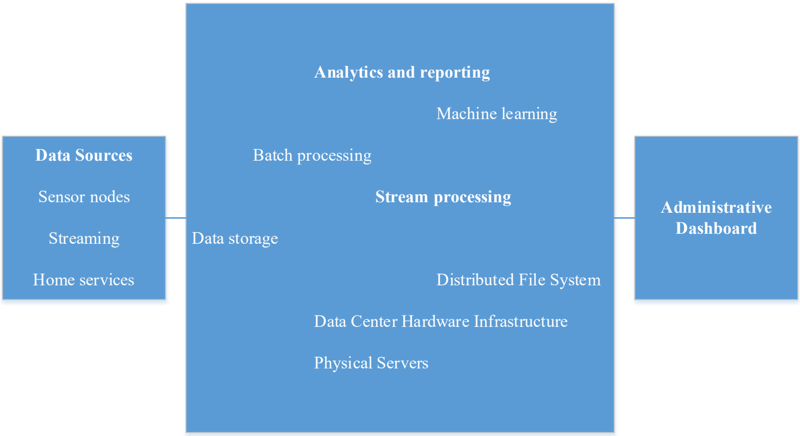

Figure 3. Architecture of the Proposed Model

A repository (SINK) is a class or function designed to receive events from another object or function. Sink (Data pools) will be developed in order for the data to be included in the spark environment. Then the data will be written to MongoDB over the streaming channel JSON based. The data will be processed in Apache Spark ML (Machine Learning) environment and decision support deductions (Classification and prediction) will be made. In the method of the proposed model, it is planned to follow the Cross Industry Standard Process Model steps for Data Mining [15]. The model consists of six steps: "Defining the Problem", "Understanding the Data", "Data Preparation", "Model Building", "Model Evaluation and Selection" and "Implementation of the Model".

Defining the Problem**:** The learning process is expressed by Simon as any change that will enable a system to perform the same task a second time or to perform better in a new task related to the same population. Mitchell [16] stated how a machine would change its behavior for learning, taking into account its performance: "If the performance of a computer program in G tasks as measured by P increases with experience D, then some G tasks of that computer program have classes and a performance measure of P. it is said to have learned from experience D ".

Understanding the Data and Data Preparation: In order to develop a decision support system with high sensitivity for the smart city application that will work most efficiently, it should be planned to examine smart city data containing at least 1 million data. In order to test the operation of the system to be developed at different scales, first of all, open access data, including data obtained from IoT devices in smart cities on hub.packtpub.com, can be used. Data set production for training and testing processes can be provided from IoT devices to be developed later within the scope of the model. The operation and performance of the system should be improved by producing data that is large enough to be considered within the scope of big data from these devices. Finally, the model should start working with sources that provide live data. In the model, a series of pre-processing should be planned before the data collected are analyzed. At this stage, firstly, some descriptive statistics can be obtained by calculating the maximum and minimum values of the numerical features in the data set, the median value and the frequency values of the categorical features. Completion of missing data, boxplot, scatter diagrams and correlation calculations between variables, control of outliers and repeating records, and data normalization should also be performed at this stage.

Model Building: In this step of the proposed model, the decision mechanisms models of the decision support system to be developed, "regression methods", "LSTM (long short-term memory) prediction", "classification with deep neural networks", "decision trees (CART, C4.5, C5.0) , random forest) "," k-Nearest Neighbor Algorithm "," Naive Bayes Classifier ", should be created using machine learning and deep learning techniques. Deep learning is considered within machine learning, which is a sub-branch of artificial intelligence. It includes nonlinear units for feature extraction, feature selection and feature conversion in traditional machine learning algorithms. Thus, artificial intelligence processes, which were done gradually before, started to be carried out under a single deep learning architecture. Deep learning, like other artificial intelligence algorithms, enables inferences from historical data through learning. The most important of these inferences are estimation and classification. In the model proposal, firstly, basic regression methods and prediction operations, and for classification, classification operations with artificial neural networks, Naive Bayes and similar machine learning algorithms should be performed. Then, as the data set increases in size to be evaluated within the scope of big data, classification with Deep Neural Networks and prediction studies with LSTM (Long short term memory) should be performed for classification. Sepp Hochreiter and Juergen Schmidhuber developed LSTM (Figure 4) in 1997 to solve the vanishing gradient problem [17].

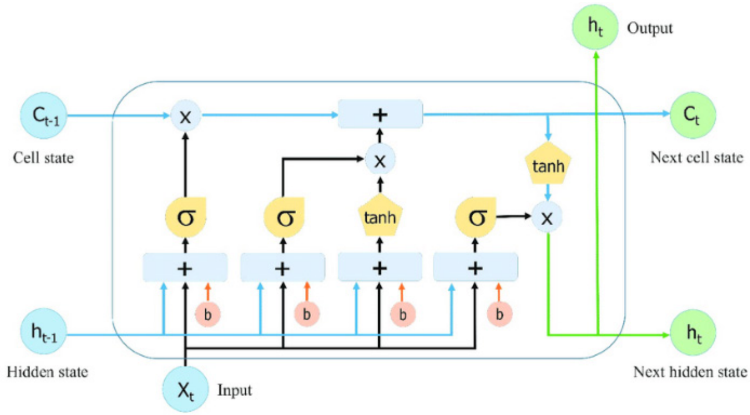

Figure 4. Long short term memory [18]

LSTM (Long short term memory) networks to be used for prediction operations in the decision support system are self-repeating neural network architecture used in deep learning. Unlike standard feed forward neural networks and known feed forward neural networks in LSTMs, there are feedback links. The information received by gates called Xt can be stored, written to the cell and read. Outputs called ht are produced at the output. In the LSTM, the cell decides what to store, when it will allow it to read, write or delete through gates. These gates have a network structure and activation function. Just like neurons, it passes or stops the incoming information according to its weight. These weights are calculated during the learning of the recurrent network. In the model, LSTM networks should be used to make predictions from the data coming in the form of time series.

Model Evaluation and Selection: Different models should be developed by using the algorithms mentioned above; However, the main purpose is to select the model with the highest performance that minimizes the error in the decision to be taken in smart city applications and to integrate it into the decision support system. There are many model performance evaluation methods such as “Hold-out”, “k-Fold Cross-Validation” and “Bootstrapping” in the literature to find the algorithm with the best performance. In order to compare the models with each other, there are many model performance evaluation criteria in the literature. In line with the model goals, the accuracy and error to be obtained from each model should be calculated. Also; Different performance evaluation measures such as Sensitivity, Specificity, F-Criterion, Positive Likelihood Ratio (Precision), Negative Likelihood Ratio should also be used. One of the biggest mistakes in artificial intelligence studies using various algorithms is to look only at the accuracy rate as a success parameter. The accuracy rate does not give us enough information, especially in unstable data sets.

A similar situation can be seen in smart city applications. In such cases, it will be useful to look at other performance analysis results in addition to the accuracy parameter.

Performance parameters to be used in classification processes: In the classification studies using artificial intelligence methods in the field of smart cities, sensitivity, precision and ROC values are mainly used. In order to obtain the classification parameters, it is necessary to obtain the confusion matrix. If the classification result is accepted as positive and negative class, it basically ensures that the results that should be classified in the positive or negative class are correctly classified and not classified. In addition to certainty, sensitivity, accuracy, and AUC values, the ROC curve is widely used to measure the performance of artificial intelligence architectures [19]. The performance of the designed network is determined by evaluating the results generated against the test data that the network has never seen. The performance of the network to be developed in the model will be measured with these parameters. The ROC curve is a two-dimensional graphical representation of the relationship between sensitivity and selectivity values used to evaluate the classification performance of test results. In tests, results are grouped as positive or negative. When creating these groups, the classification charts are grouped as True Positive if the sample is positive, False Negative if the sample is positive but negative, True Negative if the sample is classified as negative and negative, and False Positive if the sample is classified as negative but positive.

Performance parameters to be used in prediction processes: Regression methods for estimating numerical results and LSTM (Long short-term memory) in learning will be used in the analysis of artificial intelligence and mental city data. R2, MAE, MAPE and RMSE performance parameters are frequently used in data estimation with regression analysis. R2 (Accuracy value): It is used to explain how accurate the regression model is. It sees the same value as the accuracy metric in the classification method. The closer the result is to one, the more successful the model is. MAE (Mean absolute Error): The statistical term defined as the mean absolute error. It is a parameter that shows the performance of the model developed for regression methods. The closer this value is to zero, the better the estimation ability of the model [20]. MAPE (Mean Absolute Percantage Error): It is known as the mean absolute error percentage and is one of the main error measurement methods. It is found by averaging the ratio of deviations in a time series to actual values. It is desired to be as close to zero as possible. RMSE (Root Mean Square Error): root of mean square error, root mean square error, root mean square error, etc. It is a statistical term that is translated by definitions and originally stands for root mean squared error. RMSE is a parameter used to evaluate the performance of estimation models made with regression techniques. RMSE is used to find the error value between the obtained value and the designed model. The fact that the RMSE value approaches zero value in the designed model shows that the artificial intelligence design achieves the best result. For detailed performance evaluation of the models to be designed, the error rates of mean square error, peak signal-to-noise ratio, root-mean-square error, normalized root-mean-square error, mean absolute percent error and symmetric mean absolute percent error should be calculated [21].

Implementation of the Model: It should be aimed to develop the Smart City Decision Support System with the best models obtained by data mining and to ensure its use in cities. The Smart City Decision Support System is thought to produce two different outputs. These; Prediction and Classification. Prediction (First, regression, then LSTM algorithm in deep learning, prediction operations should be performed on big data). Classification (First of all, basic classification techniques and then Deep learning based classification algorithms should be used). The following steps should be followed for the workflow of applying Big Data approaches to data analysis. Data Collector Infrastructure: Detection of Data Sources, Installation of Data Traps, Installation of SNMP traps (traps), Development and Installation of Spark Sources (Sources), Installation of Hadoop Cluster (Node Network), Installation of Data Bus (Message Bus), Installation of Spark Sinks. Data Storage Infrastructure: Installation and Configuration of MongoDB NOSQL Database, Installation of HUE Component. Data Processing Infrastructure: Apache Spark Installation, Pyspark Installation. Management Interface Infrastructure: Development of REST-based management interface, writing REST endpoints to integrate Dashboard Screens with the Management Interface. Dashboard Infrastructure: Creating DashBoard screens with Power BI and visualizing analytical results, developing dashboard screens that will provide visual access to the management interface. Decision Support Infrastructure: Examining Data Sources, Cleaning Data and Pre-Processing, Apache Spark ML (Machine Learning) Installation, Integration of NOSQL Database with Apache Spark ML, Prediction and Classification with Basic Machine Learning Algorithms, Prediction and Classification with Deep Learning Algorithms Performance analysis of Machine Learning Algorithms and Deep Learning Algorithms.

5. CONCLUSIONS

All kinds of smart systems can be built with the proposed model. For the first time in the field of smart cities, our country will have domestic-national and original products that can serve end-to-end. The technologies to be developed in the 1st and 2nd stages of the proposed model will be completely local-national and original. These technologies are not readily available in our country and are imported from abroad. Since the sensor and internet of things technologies to be developed will include all of the existing technologies, they will be able to talk to each other in smart systems. Data obtained from smart transportation can also be used in smart environment applications. In this way, there are many systems in a city, but there will be no situations that are negatively criticized as technology dumps, which are made as if they are not connected to each other. Before any smart system is installed, the feasibility of the relevant campus will be done. As a result of the feasibility, which sensor panels, which wireless interface cards etc. will be decided to be used. When making this decision, sensor types, required distances, required topology type will be taken into account. In the third stage of the proposed model, cloud computing technologies will be used. In order to process the data produced in smart city infrastructures, storage server systems that are fast, easy to manage, sufficient capacity and can provide uninterrupted service are needed. The server infrastructure required for the storage and management of big data to be produced in cities will be realized through cloud computing technologies. With the advancing technology and the increase in the amount of data, the administrative and administrative architecture of the cities started to change. Obtaining meaningful data within the scope of instant calculation and offline planning from data in different formats, especially from various sources in smart cities, has been one of the important study topics [22]. In this context, the size of structural, semi-structural and unstructured data from various devices, social media, platforms and systems is increasing day by day. The insufficiency of classical database management systems and methods for data with different formats, types and contents coming from these different sources has revealed the big data concept and technologies [23]. In addition, multiple technologies such as IoT, cloud computing, artificial intelligence, cyber security and similar need to be used and managed simultaneously. Big data is defined as rapidly increasing data in different formats [24]. It includes technologies that enable data storage, analysis and management processes under a single roof. Big data solutions are used in many fields, especially in industry, and have started to be used intensively in the smart city area [25]. In the 4th and 5th stages of the proposed model, it is aimed to instantly manage the data obtained from smart cities with open source platform and software. Paid and ready-made servers such as Amazon AWS, Microsoft Azure, Google Cloud etc. and big data processing services will not be used in the model. The proposed solution is scalable and provides high performance, IoT devices will be processed and displayed instantly with Spark Streaming, used in decision support systems for authorized users for planning studies such as infrastructure renewal in smart cities, vehicle purchase, determination of the location of management and assembly centers of municipal services. Web-based data analytics interfaces will be provided with Node.js technology. In addition, in the proposed solution, decision-making will take place as a result of processing the data with deep learning-based artificial intelligence techniques.

In summary, the software and hardware technologies required for the digital transformation needed to make cities end-to-end smart can be developed domestically and nationally within the model. If the proposed model is realized, an important gap in this area will be closed in our country, and a guiding role will be obtained at the point of domestic-national smart cities.

REFERENCES

1. Elvan, L., Terzi, F., Ocakçı, M., Kayapınar, E., Özdil, S., Tekir, A., Benli, B., Gezer, M., Doğan, M., Yılmaz AZ, Erten, D., Baraçlı, H., Onaygil, S., Büyükkınacı, B., Güler, Ö., Yurtseven, MB, Erken, A., Güler, K. (2017). Smart Cities, *ITU Foundation Magazine*, *77*, 1-129.

2. Söylemez, A. (2018). Waste Management in Smart Cities and Examples on Smart Waste Management from the World, *Journal of Law*, *37*, 87-100.

3. General Directorate of Geographical Information Systems. (2017), Smart Cities, 1-132.

4. Kalaycı, T.E., (2013). Wireless Sensor Networks and Applications, *Academic Informatics*, 1-8.

5. Zhou, H.Y., Luo, D.Y., Gao, Y., Zuo, D.C. (2011). Modeling of Node Energy Consumption for Wireless Sensor Networks, *Wireless Sensor Network*, *3*, 18-23.

6. Meghdadi, M., Özdemir, S., Güler, İ. (2008). Security in Wireless Sensor Networks: Problems and Solutions, *Information Technologies Journal*, *1*, 1-7.

7. Karaboğa D., Ökdem S. (2006). Secure Communication Techniques in Wireless Sensor Networks, National Electronic Signature Symposium, Ankara, Turkey, 1-4.

8. Pauley, J.T., Bhatia, S.J, (1983). American national standard for information systems—Data encryption algorithm—Modes of operation, American National Standards Institute, New York.

9. Rinne, S., Eisenbarth, T., Paar, C. (2007). Performance Analysis of Contemporary Light-Weight Block Ciphers on 8-bit Microcontrollers, ECRYPT Workshop SPEED - Software Performance Enhancement for Encryption and Decryption, Amsterdam.

10. Großshädl, J., Tillich, S., Rechberger, C., Hofmann, M., and Medwed, M. (2007). Energy evaluation of software implementations of block ciphers under memory constraints, DATE '07: Proceedings of the conference on Design, automation and test in Europe, 1110–1115, San Jose, CA, USA.

11. Devesh, C.J., Dhiren, R., Kankar, S.D. (2008). Optimizing the Block Cipher Resource Overhead at the Link Layer Security Framework in the Wireless Sensor Networks, Proceedings of the World Congress on Engineering 2008.

12. Dener, M. (2018). A New Energy Efficient Hierarchical Routing Protocol for Wireless Sensor Networks, *Wireless Personal Communications*, *101*(1), 269–286.

13. Eken, S., Kaya, F., Sayar, A., Kavak, A. (2014). Document Based NoSQL Databases: MongoDB and CouchDB horizontal scalability comparison, Engineering and Technology Symposium, Ankara.

14. Polat, H., Oyucu, S. (2019), A Non-relational Database-Based Approach to Storage of Heterogeneous Medical IoT Data, *Journal of Politeknik*, *22*(4), 989-998.

15. Shearer, C. (2000). The CRISP-DM model: the new blueprint for data mining. *Journal of data warehousing*, *5*(4), 13-22.

16. Mitchell, T. M. (1997), Machine Learning, 1st Edition, McGraw-HillScience/Engineering/Math, ISBN: 0-07-042807-7.

17. Hochreiter, S., Schmidhuber, J. (1997). Long Short-term Memory, *Neural Computation*, *9*(8):1735-80.

18.Yan, S. Understanding LSTM and Its Diagrams. Available online: https://medium.com/mlreview/understanding-lstm-and-its-diagrams-37e2f46f1714 (accessed on 16 August 2020).

19. Tokan, F., Türker, N., Yıldırım, T., (2006) "Determination of the neural network performances in the medical prognosis by ROC analysis", International Conference of IEEE Signal Processing and Communications Applications, Antalya, 1-4.

20. Kök, İ., Şimşek, M. U., & Özdemir, S. (2017). A deep learning model for air quality prediction in smart cities. In 2017 IEEE International Conference on Big Data (Big Data), 1983-1990.

21. Huang, C. J., & Kuo, P. H. (2018). A deep cnn-lstm model for particulate matter (PM2. 5) forecasting in smart cities. *Sensors*, *18*(7), 2220.

22. Oussous, A., Benjelloun, F. Z., Lahcen, A. A., & Belfkih, S. (2018). Big Data technologies: A survey. *Journal of King Saud University-Computer and Information Sciences*, *30*(4), 431-448.

23. Rathore, M. M., Paul, A., Hong, W. H., Seo, H., Awan, I., & Saeed, S. (2018). Exploiting IoT and big data analytics: Defining smart digital city using real-time urban data. *Sustainable cities and society*, *40*, 600-610.

24. Osman, A. M. S. (2019). A novel big data analytics framework for smart cities. *Future Generation Computer Systems*, *91*, 620-633.

25. Malapur, B. S., & Pattanshetti, V. R. (2017). IoT based waste management: An application to smart city. In 2017 International Conference on Energy, Communication, Data Analytics and Soft Computing (ICECDS), 2476-2486.

Chapter 16

DYEING OF WOOL YARNS WITH *PARTHENOCISSUS QUINQUEFOLIA* L. LEAVES EXTRACT[*]

Selime MENTEŞ ÇOLAK[1]

Meruyert KAYGUSUZ[2]

Fatoş Neslihan ARĞUN[3]

[*]This study was presented as an oral presentation at the 3rd Anatolian International Social Sciences Congress held in Diyarbakır on 28-29 December 2019; afterwards it was expanded and turned into a book chapter.

1 Prof. Dr., Pamukkale University, Denizli Vocational School of Technical Sciences, Traditional Handcrafts Department, Denizli, TURKEY, scolak@pau.edu.tr

2 Assoc. Prof., Pamukkale University, Denizli Vocational School of Technical Sciences, Textile, Garment, Footwear and Leather Department, Denizli, TURKEY, meruyertk@pau.edu.tr

3 Lecturer, Pamukkale University, Denizli Vocational School of Technical Sciences, Traditional Handcrafts Department, Denizli, TURKEY, fargun@pau.edu.tr

INTRODUCTION

Natural dyeing, which started and developed with the weaving culture in the history, has been applied by many civilizations in the world and has taken its place among the traditions of these civilizations (Etikan, 2011). Natural dyeing tradition in Turkish culture have been started with the carpet art in Central Asia and then moved to Anatolia. Using the advantage of having rich plant resources in Anatolia, a strong Turkish Natural Dyeing culture was formed by synthesizing the knowledge, traditions and customs of the civilizations that lived here in past (Arlı, 1984).

Continuing as a craft passed from father to son in Anatolia, natural dyeing has been widely applied in dyeing of the wool fibers required for Anatolian carpets. The natural dyeing tradition, which is considered as a whole with our carpets and plain weavings, is very important in terms of ensuring its sustainability and continuity of our culture. It is a fact that the cultural and artistic value of carpets, rugs or woven fabrics using yarns dyed with natural dyes cannot be found in chemically dyed products (Etikan, 2011). Natural dyes have given color to our cultural assets such as carpets, fabrics, felt and tiles.

In natural dyeing, there are animal and vegetable sources that give almost all colors. From past to present colors have many physical and psychological effects on people. This situation can be understood from the clothes that reflect people's thoughts and tastes. Sometimes individuals try to express what they want to say not with sentences, but with the colors they prefer on their clothes, and even on their accessories (Ayhan and Birol, 2016).

Natural dyes were the main source used in the coloring of textile materials until the end of the 19th century and lost their importance with the development of synthetic dyes (Bechtold et al., 2003; Bechtold et al., 2006). However, reasons such as the harm of some chemical dyestuffs, demands for natural products, sustainable processes and environmental sensitivity have significantly caused natural dyestuffs to come back to the agenda.

Recent human awareness and mature demands on eco-preservation, eco-safety and health concerns pressurized the textile industry to use natural colorants that have no negative impact on environment and aquatic ecosystem. Advanced developments for natural bio-resources and bio-sourced colorants and their sustainable use for functional clothing have created a revolution in textile research and development (Yusuf et al., 2017).

Many studies have been performed on natural dyeing of wool carpet yarns with different mordants and dyeing methods (Ölmez, 2005; Kayabaşı and Etikan, 2006; Raja and Thilagavathi, 2008; Win and Swe, 2008), and it was reported that healthier and more environmentally friendly applications have been carried out. Whether it is through contact with human health or because of the dyestuffs contained in waste water and the chemicals used with this dyestuff pollute the environment, textile researchers have led to the search for natural dyes as well as natural fibers. Many researchers have done ecological dyeing with natural dyes that are known or grown in their region and suggested that these studies can be adapted to the industry.

In dyeing process the whole plant can be used as well as the roots, leaves, tubers, bark or branches of some are used. *Parthenocissus quinquefolia* L., known as Virginia creeper, Victoria creeper, five leaved ivy or five finger and American ivy in our country, is a plant species of the Vitaceae family. Etymologically, "parthenocissus" means "virgin ivy" from Greek, "quinquefolia" means "five-leaved" (www.wikipedia.org). *Parthenocissus quinquefolia* is a climbing plant with bright green leaves, usually grown in the summer. It is known for the magnificent red color of its leaves in autumn. This plant is preferred frequently in landscaping and is grown as an ornamental plant due to its pleasant appearance and perfect covering of the fence and garden walls (Fig. 1). *Parthenocissus quinquefolia* contains anthocyanin as a natural dye pigment (Ben Ticha et al., 2017). For this reason, its use in dyeing different textile fabrics has been recently investigated (Benli, 20174; Ben Ticha et al., 2017), but it has not been used in dyeing of wool carpet yarns yet. In this study, ecological phyto-dyeing process of wool carpet yarns with *P. quinquefolia* L. leaves extract and pre-mordanting with different mordants was investigated.

Figure 1. *Parthenocissus quinquefolia* L. (American Ivy)

MATERIALS AND METHOD

Materials

American ivy leaves were collected from the Gerzele region of Denizli in December 2019. The leaves were used fresh for dye preparation. In our study, double twisted wool carpet yarn was used. Three different mordant materials as aluminum sulfate ($KAl(SO_4)_2.12H_2O$, Tekkim), iron sulfate ($FeSO_4.7H_2O$, Tekkim) and copper sulfate ($CuSO_4.5H_2O$, Tekkim) were used in the mordanting process.

Extraction of plant dye

760 g of fresh American ivy leaves were immersed in 22 L of water and boiled for 2 hours. The plant extract was then allowed to cool for 30 minutes. The leaves were removed from the extract solution and the obtained colored dyestuff solution was used in subsequent applications (Fig. 2). pH value of the extract solution was determined to be 4.0.

Figure 2. Dyestuff extraction from *P. quinquefolia* L. leaves

Preparation of wool yarns

Wool yarns were washed in a solution of soda and detergent for 30 minutes at 40^{o}C in order to remove the impurities on them. They were made ready for dyeing by rinsing several times with warm water (Fig. 3).

Figure 3. Wool yarns prepared for dyeing process

Dyeing procedures

The washed wool samples were divided into four groups according to the dyeing method (Fig. 4). The first group (control group) was dyed without mordanting. In the experiments with addition of mordants pre-mordanting and dyeing method were used. Accordingly, in the second group 20% aluminum sulfate ($KAl\ (SO_4)_2.12H_2O$), in the third group 4% copper sulfate ($CuSO_4.5H_2O$), in the fourth group 3% iron sulfate

($FeSO_4.7H_2O$) were used as mordants. The mordanting process of wool yarns was carried out at 70°C for 60 minutes. The ratio of dyeing liquor was adjusted to be 1/30, experiments started at room temperature, then the bath was heated slowly to 98°C and dyeing was carried out for 60 minutes. After the bath was cooled, the wool yarns were pressed, rinsed with water and dried at room temperature. Color evaluations were made for the dried samples. During each application, the pH values of the dyeing baths with different mordants were determined.

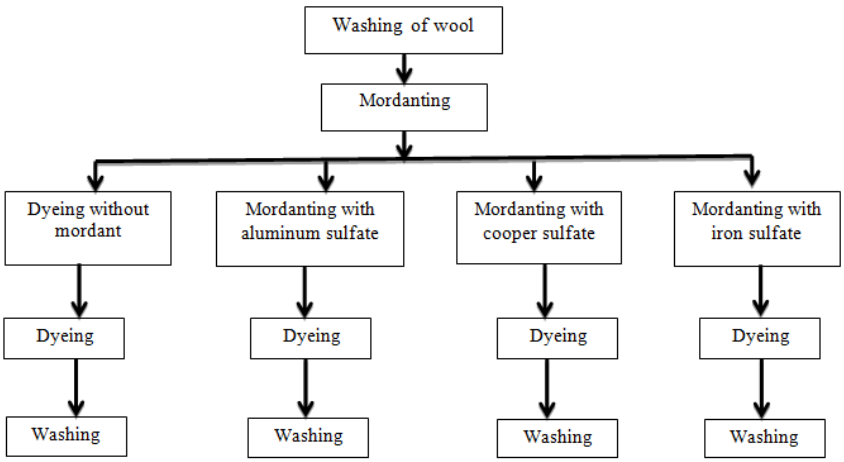

Figure 4. Dyeing procedures of the wool carpet yarns with *P. quinquefolia* extract

RESULTS AND DISCUSSION

It is known that *P. quinquefolia* contains anthocyanin pigment as a natural dye. Anthocyanins are a large group of red-blue plant pigments, occurring in all developed plants, mostly flowers and fruits, but also in leaves, stems and roots (Ben Ticha et al., 2017). Until now, more than 500 anthocyanins have been isolated from plants, and it has been determined that the basic building blocks are the flavylium ion (Fig. 5).

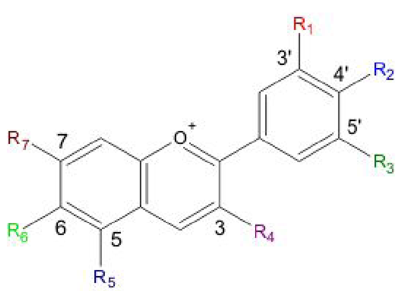

Figure 5. Chemical formula of anthocyanin pigment (http://www.food-info.net/tr/colour/anthocyanin.htm)

Anthocyanins are powerful water-soluble colorants and are responsible for the extraordinary blue, purple, and red colors of fruit and flowers. Due to its water solubility properties, its use depends on pH. Therefore, pH change has an effect not only on the molecular structure of anthocyanins but also on their staining (Ben Ticha et al., 2017). Its color changes to orange-red in acidic environments, purple in a neutral environment, and blue in an alkaline environment (Keleş, 2015).

Mordants are usually metal salts and are used as mediators to bind dyestuffs or to strengthen the dyeing effect. Different color tones can be obtained in natural dyeing process by using dyes obtained from plants in the presence of mordants (Ölmez, 2004; Demir et al., 2010). Mordants create a strong chemical bond between the dye and the fiber, improving the color and fastness properties of the dye, and gaining durability against environmental conditions. In addition, mordants are effective on the pH value of the dye bath, and improve the affinity of fibers towards the dyes.

In the application of the natural dyes, different techniques of mordanting were used to improve color fastness properties (Bechtold et al., 2003). Textile materials treatment with mordants prior to dyeing is called as pre-mordanting, which provides exclusive, sufficient time and sites on textile material to bind to the mordants. A proper layering of dye, mordant and textile material formed in this type of processing of natural colorants on textiles. Metal complexation with textile surface sites from one side and from dye on the other make the color fast to light, washing and rubbing. Chelating complexation of this processing makes the proper energy dissipation of photons of light in the complex and provide better light fastness to dyed materials (Yusuf et al., 2017).

In our study, three different mordants were used and the pH values of both the mordants and the dyeing bath were determined. The determined pH values are shown in Table 1.

Table 1. The pH values of the mordants and the dyeing baths

Mordants	pH of mordants	pH of the dyeing bath
Control (without mordants)	-	4.0
Iron sulfate	6.0	5.0
Copper sulfate	5.0	5.0
Aluminum sulfate	3.0	5.0

The fibers that are most suitable for dyeing with natural dyes are cationic fibers such as wool and polyamide (Yaver, 2015). Wool is the fiber covering the body of animals (sheep, goats, camels, angora, alpaca, etc.) and constitutes the most important and characteristic example of textile fibers (Mauersberger, 1948). The raw material of woven handicraft products is wool. It can be shown that natural dyed products do not adversely affect humans and the environment, unlike synthetic products, and these materials, which are already a part of nature, are evaluated and presented to human use by producing healthy products.

It is known that the first hand-woven carpets and rugs, which have a wide use in Turkish culture, were woven with natural wool yarns. Valuable Turkish carpets and rugs have been woven in many different regions throughout history. Turkish rugs, with their rich colors, warm tones, extraordinary textures and traditional motifs, are perfect works of art that have been known in the world for centuries. The materials used in weaving are dyed or non-dyed yarns. Three types of yarn are used in the production of hand-woven carpets: warp, weft and loop yarn with different characters. The colors of wool carpet yarns after pre-mordanting with three different metal salts and phyto-dyeing with *P. quinquefolia* extract are shown in Figure 6.

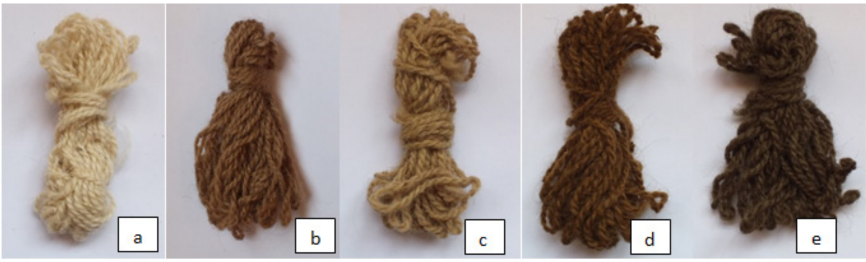

Figure 6. Colors of wool carpet yarns a) undyed, b) dyed without mordant, c) dyed with addition of aluminum sulfate, d) copper sulfate and e) iron sulfate mordants

As seen in Figure 6, different color and tones have emerged as a result of the phyto-dyeing with *P. quinquefolia* extract. While the color of the raw wool yarn was light beige, the color of the yarn dyed with the *P. quinquefolia* extract in the dyeing trial without using any mordant substance was in light brown tone (Fig. 6). The use of mordant causes the color tones to change. The color of the yarn, which was mordanted with aluminum sulfate and dyed with the extract, created a light bright mustard color, while the use of copper sulfate mordant and dyeing with the extract created darker brown tones, and the composition of dye with iron sulfate formed tones ranging from bitter brown to dark gray (Fig. 6). Dark colors such as bitter coffee and tobacco were dominant in the dyeing made using iron salt. In general, the colors obtained were similar to the study of dyeing wool fabric with the dyes obtained from different parts of the American ivy plant (Benli, 2017). In our study, the darkening of the color tones occurred as follows: (from dark to light tones) $FeSO_4$> $CuSO_4$> Mordant free> $KAl(SO_4)_2$> raw wool. Thus, it has been determined that matt colors are obtained from iron and copper salts and bright and vivid colors are obtained from aluminum salt. It was stated that the darker the fabric colors, the higher the light fastness (Benli, 2017). It has been reported that different colors from black to brown, green to yellow and orange can be obtained with different mordant applications (Samanta and Konar, 2011). In our study, this color difference is thought to be caused by both the metal salts and the change of anthocyanin structure (Ben Ticha et al., 2017).

CONCLUSION AND RECOMMENDATIONS

In this study, after the wool carpet yarns were pre-mordanted with three different mordant materials, dyeing process was carried out with a dye solution obtained from the leaves of *P. quinquefolia* plant. When the colors obtained were evaluated, it was seen that the use of different mordants can create different colors and tones in wool yarns. It is understood from the results obtained that matt colors are obtained from iron and copper salts, while light and bright colors are obtained from alum and mordant-free dyeing. Thus, in the light of the data obtained, it was revealed that *P. quinquefolia* leaves can be used as a natural dye source and the dye obtained from this plant can be used for textile dyeing.

One of the ways to regain the importance of natural dyeing in the past and revive it nowadays when it is about to disappear will be realized with the education of students who take courses on natural dyes and natural dyeing. It is very important to reinforce the information that will be given to the students not only theoretically but also by making applications. In this way, thanks to the applications they make with different natural dyes, they will be able to dye with their own means in the future. In this way, they will not only have job opportunities but also keep alive the natural dyeing tradition, which is our very important cultural heritage.

REFERENCES

Arlı, M. (1984). Doğal bitkisel boyalarla boyama yöntemleri üzerinde düşünceler. 2.Ulusal El Sanatları Sempozyumu Bildirileri. Dokuz Eylül Üniversitesi Güzel Sanatlar Fakültesi Yayınları, 19. İzmir.

Ayhan, A., Birol, M. (2016). Düşüncelerin dışavurumu olarak moda dünyası: iletişimsel kodlara yansıyan örnekler üzerinden karşılaştırmalı bir analiz, *Intermedia International e-Journal*, 3(1), 242-261.

Bechtold, T., Turcanu, A., Ganglberger, E., Geissler, S. (2003). Natural dyes in modern textile dyehouses - how to combine experiences of two centuries to meet the demands of the future?, *Journal of Cleaner Production*, 11, 499-509.

Bechtold, T., Mussak, R., Mahmud-Ali, A., Ganglberger, E., Geissler, S. (2006). Extraction of natural dyes for textile dyeing from coloured plant wastes released from the food and beverage industry, *Journal of the Science of Food and Agriculture*, 6, 233-242.

Benli, H. (2019). Amerikan sarmaşığı (*Parthenocissus quinquefolia* L.) bitkisinin yünü boyama özelliklerinin araştırılması, *Tekstil ve Mühendis*, 24(106), 54-61.

Ben Ticha, M., Meksi, N., Attia, H. E., Haddar, W., Guesmi, A., Ben Jannet, H., Mhenn, M. F. (2017). Ultrasonic extraction of *Parthenocissus quinquefolia* colorants: Extract identification by HPLC-MS analysis and cleaner application on the phytodyeing of natural fibres. *Dyes and Pigments* 141, 103-111.

Demir, M., Çelik, S., Noyan, Ö. F. (2010). Türkiye'de yetişen bazı önemli boya bitkilerinin üretim teknikleri ve elde edilen renklerin haslık dereceleri. III. Ulusal Karadeniz Ormancılık Kongresi, 20-22 Mayıs 2010 Cilt: III, 1187-1196.

Etikan, S., (2011). Doğal boya geleneğinin türk halı sanatında yeri ve önemi üzerine bir değerlendirme, *Türk Sanatları Araştırmaları Dergisi*, 1(1), 11-16.

Kayabaşı, N., Etikan, S. (2006). Asma yaprağından (*Vitis vinifera* L.) elde edilen renklerin subjektif ve objektif yöntemlerle değerlendirilmesi. *Tekstil ve Konfeksiyon*, 2, 90-93.

Keleş, Y. (2015). Antosiyanin Pigmentlerin Biyokimyası ve Analizi. *Türk Bilimsel Derlemeler Dergisi,* 8(1), 19-25.

Mauersberger, H.R. (1948). *Matthews' textile fibers*. Sixth edition, 1283 p., London.

Ölmez, F.N. (2004). Yün halı ipliklerinin çeşitli karıştırma metodlarıyla boyanmasından elde edilen renkler ve haslık dereceleri. *SDÜ Fen Bilimleri Enstitüsü Dergisi*, 3, 86-94.

Ölmez, F.N. (2005). Yün halı ipliklerinin fındık (*Corylus avellana* L.) yaprakları ile Boyanmasından elde edilen renkler ve bazı haslık değerleri. Yüzüncü Yıl Üniversitesi, Ziraat Fakültesi, *Tarım Bilimleri Dergisi*, 15/1(2005), 77-84.

Raja, A.S.M., Thilagavathi, G. (2008). Dyes from leaves decidous plants with a high tanin content for wool. *Coloration technology*, 124(5):285-289.

Samanta, A.K., Konar, A. (2011). Dyeing of textiles with natural dyes, in Akçakoca Kumbasar, E. P. (Eds.), *Natural dyes*, InTech, Croatia.

Şanlı, H.S., Çatalkaya Gök, E. (2017). Bitkisel boyacılıkta kökboyanın (*Rubia tinctorum* L.) önemi. *Uluslararası Sosyal Araştırmalar Dergisi*, 10(48), 772-778.

Yaver, Ş. (2015). Tekstil üretiminde temiz teknolojilerin kullanılması çerçevesinde kimyasal modifikasyon yoluyla akrilik liflerinin doğal boyalarla boyanabilirliğinin geliştirilmesi, Yüksek Lisans Tezi, Tekstil Mühendisliği Anabilim Dalı, Fen Bilimleri Enstitüsü, Namık Kemal Üniversitesi, Tekirdağ, 53 s.

Win, Z. M., Swe, M. M. (2008). Purification of the natural dyestuff extracted from mango bark for the application on protein fibres. Proceedings of World Academy of Science, Engineering and Technology 36, 540-544.

Yusuf, M., Shabbir, M., Mohammad, F. (2017). Natural Colorants: Historical, Processing and Sustainable Prospects. *Nat. Prod. Bioprospect*. 7, 123-145.

Internet sources:

http://www.food-info.net/tr/colour/anthocyanin.htm Accessed on 03.12.2019.

www.wikipedia.org, *Parthenocissus quinquefolia* L. Accessed 03.12.2019.

Chapter 17

CHALLENGES IN INVENTORY MANAGEMENT AND A PROPOSED FRAMEWORK

***Fatih YİĞİT*[1]**

***Bahar YALÇIN*[2]**

1 Asst. Prof. Fatih Yiğit, Istanbul Arel University, Industrial Engineering Dept.,

fatihyigit@arel.edu.tr

2 Asst. Prof. Bahar Yalçın, Istanbul Arel University, Industrial Engineering Dept., baharyalcin@arel.edu.tr

1 Introduction

In today's economy, efficient inventory management is vital for all companies. Business environment, which is considered as volatile, uncertain, complex, and ambiguous (VUCA), big savings can be achieved with efficient inventory management. Effective implementation and management of inventory management system is vital for a company's success. The success of such implementation not only affects the profit but also customer satisfaction.

Despite the many challenges are faced by practitioners, most of them are not mentioned in textbooks. Proposed framework aims to investigate these challenges by systematic literature review and propose methods to overcome these problems. The intention is to cover the gap between practice and theory.

Inventory management is becoming more complex due to new challenges. To name a few, product life cycles become shorter, demand becomes more unpredictable, green supply chain and relevant new topics adding complexity to the issue.

The increased financial costs put additional pressure on companies. As a result, companies are focusing on net working capital (NWC) to free additional cash. One of the three pillars of NWC is inventory besides account receivables and payables.

Inventory management is complex in nature due to many stakeholders involved with conflicting goals. These goals and stakeholders may change with the type of inventory. Spare parts are critical for a manufacturing site therefore a plant or maintenance manager is involved with this type of inventory. Similarly finished product inventory level is important for a sales manager as it directly affects the customer service level and logistics manager due to warehouse limitations.

Raw material inventory level is associated with the performance of planning manager and supply manager. Increased inventory levels give the planning manager freedom to switch production or compensate any unpredictable incidents. Additional safety stock also helps supply manager to overcome any supply problems. A purchasing manager wishes to increase the inventory in order to get additional discounts from suppliers.

There are also other departments which have contradicting goals. For logistics or warehousing managers, the higher turnover is desirable. This high turnover gives freedom for the warehousing manager to optimize the inventory. For a finance manager, NWC reduction is a primary goal. Therefore, a decrease in inventory is important as it both frees cash that can be used elsewhere such as investments, and due to reduced financial costs.

On the other hand, high inventory level gives the sales team flexibility to compensate forecast variations. Such additional inventory also allows sales department to approach new customers without sacrificing service level of existing customers.

Inventory management should be a joint effort due to the importance and effects on the overall success of a company. Therefore, all members of an institution should have the responsibility of inventory management. This way, a collaboration among members can be achieved. Besides, the most valuable issue is requirement of better quality of the information flow between partners in supply chain, what needs: close relationships, activities coordination, reliable and accurate information (Czwajda and Kosacka 2017).

The framework suggested is about to overcome the focuses on challenges faced by practitioners working in the field of inventory management. Effective inventory management provides a potential system to improve performance by matching inventory management practices and competitive advantages (Mahyadin et al. 2013). The study first makes an overall explanation of challenges and shares the proposed methods to overcome these challenges.

2 Importance of Inventory Management

Supply chain is a vital part of business. With globalization, many companies prefer to supply goods which fits their strategies regardless of locations. Proper management of supply chain has therefore a strong effect of the performance of a company.

Inventory management typically is considered as a part of supply chain management. The importance of proper inventory management lies mainly on two reasons. The first reason is customer service level and the second one is its effect on the total cost of inventory and eventually NWC.

Customer service level is critical due to its effect on customer retention and sales revenue generated. Modern customer service, if it is based on appropriate standards, makes a great impression on customers. Consequently, they are willing to buy goods or services again (Skowron and Cehaba 2019). Therefore, proper management of inventory management directly affects the revenue generated.

Inventory management has also an effect on financials. Cost effect of inventory is a part of inventory models due to costs associated with inventory decisions. These costs are split into inventory and ordering costs. As a result, proper inventory management lowers the total cost of inventory. On the other hand, another aspect of inventory management is its effect on NWC. NWC is the cash tied for the everyday running of a company. Practically is the amount of cash tied to receivables and inventory vs payables.

NWC is a critical financial ratio used for firm valuation and a critical key performance indicator (KPI) for the assessment of proper financial management. A study by PricewaterhouseCoopers (PwC) (2020) shows that days inventory outstanding (DIO) is one of the two major areas for improvement in NWC. The same study shows that typical DIO is 56.2 days in 2018. In some sectors such as pharmaceuticals and life sciences worldwide, the DIO may reach up to 200 days.

These numbers show the reason behind the proposed framework that has the goal of defining a method for effective inventory management.

3 Challenges

Challenge is defined as "(the situation of being faced with) something that needs great mental or physical effort in order to be done successfully and therefore tests a person's ability" (Cambridge Dictionary 2020).

As can be interpreted from the definition, it covers the many issues that practitioners face who work in business life. As a result, challenges faced is an area where academic studies are made. On the other hand, based on our best knowledge and review, an extensive study and proposed solutions are not available in literature.

Most of the studies covers a specific area where a unique challenge is met. To name a few, challenges in demand modeling for slow moving goods is reviewed by Grange (1998). In this study, the specific but usually undervalued items of slow-moving items is investigated. The study underlines the challenges faced for the demand distribution of slow-moving items and proposes alternative methods to predict slow-moving items demand. The outcome of the study proves that misapplication of a demand distribution will yield unsatisfactory inventory optimization results.

Dhoka and Choudary (2013) investigated the demand uncertainty and eventual classification of XYZ to overcome the challenges faced by uncertainty. According to the study there are different reasons that causes uncertainty. Highly critical parts low in consumption value may be overlooked and periodic updates and review become critical and cannot precisely consider all problems of inventory control like thousands of low value items.

Various MRP tools and techniques address both shortcomings by coordinating the quantities and timing of the deliveries from known target requirement to minimize cost or achieve desired service levels (Stößlein et al. 2013). With realistic lead times and realistic forecasts, the resulting inventories would be optimal for the circumstances. Lack of realism in the areas, however, undermined the operation of MRP systems, yielding less than the desired service and more than desired inventories (Dhoka and Choudary 2013). Also, as periods of planning horizon increases the forecasting errors are affected adversely (Beutel and Minner 2012).

Similarly, perishable products' inventory management is complex in nature and deserves specific focus. Based on extensive research no specific attention is given to the effects of inventory management decisions for perishable products. Typical safety stock calculation neglects the perishability of products. Also, classical methods such as economical-order-quantity (EOQ) doesn't cover the mentioned effects on perishable products. Therefore, perishable products are considered as an additional challenge for practitioners.

New regulations associated with environmental concerns also causes additional challenges for production and inventory managers. Study by Inman (1999) shows that environmental management trends have profound effect on production and inventory managers. Although some methods has been proposed to cope with some of the problems, there are still some others that have no solution. Such challenges can only be solved with proper training and skills. With proper skill and training, the practitioners can adapt to changing needs.

Globalization, shorter product life cycle, rapidly changing demand and increase in the expectations and demands of customers, confirm that world is changing dynamically, what affects increasing requirements for supply chain (Czwajda and Kosacka 2017).

Therefore, skills and trainings are major areas for improvement in inventory management.

Such challenges are not prevalent in only manufacturing industry but also in some other areas such as service. A study by Boone et al. (2008), investigates the critical issues faced by service parts managers and help to gap the bridge between theory and practice.

A study made by Patil and Divekar (2014), investigates the inventory management challenges of B2C E-Commerce retailers. Although the study is sector specific, the outcomes covers the challenges in demand variations, reverse logistics, seasonal fluctuations, and stockless policy. The risks involved associated with underperforming inventory management are lost sales, lost customers, low customer satisfaction. To counter these challenges online retailers adopted strategies such as dropship strategy, classification of inventory, hybrid strategy, pre-purchase stocks and stock less policy that is purchasing stocks after customer orders.

Some the challenges are more specific in nature. In return, more specific studies are made in literature.

A study by Czwajda and Kosacka (2017) investigates the challenges due to multi-echelon inventory management. According to the study, a multi-echelon inventory is more complex in nature compared to single-echelon inventory. The study contributes, the introduction of challenges of multi-level inventory systems. The study shows that multi-echelon systems makes the inventory management more complex compared to single-echelon systems.

With increased level of inventory management, there is an increased level of uncertainty and complexity in inventory management. As a result, additional challenges are prevalent in such environment.

Practitioners face some issues that are not solved by inventory models or such theoretical knowledge in textbooks. Classical models incorporate, deterministic and probabilistic inventory models, with quantity discounts, MRP applications, replenishment policies or such. In literature, inventory management textbook covers the EOQ that aims to minimize the total cost but ignores the additional cost of perishability, waste of stock etc. Besides many constraints prevalent in business life are not adequately presented such as budget, total quantity procured, limitation from one or more type of products procured or stored etc.

Research Gap = What is clear from the foregoing literature, there are many studies existing regarding "inventory models" and proposed methodologies. On the other hand, as far as we investigated, there aren't any studies regarding the challenges faced for inventory management practitioners. Thus, the main objective of this study is;

- To identify the challenges
- To identify the reasons
- To identify the proposals for solutions
- To create a decision support infrastructure to be used for inventory management

As a result, the primary purpose of this chapter is to cover the gap between practice and theory. This can further be achieved by application of artificial intelligence and/or fuzzy systems. In the following subsection, each challenge is given.

3.1 Multi- Echelon

The concept of multi-echelon inventory management has gained importance over the last decade mainly because of increasing complexity of supply chain and dynamic development of information technology what enables integrated control of supply chains consisting of several processing and distribution stages. (Gumus and Guneri 2009) The multi-echelon systems made the already complex inventory management more complex.

Although multi-echelon inventory has many benefits such as shorter replenishment times, proximity to point of consumption, higher customer service level. Low performance in management may cause increased stock due to bull-whip effect, higher waste and scrap due to perishability, increased dead and slow movers due to storage in different locations, increased costs due to increased logistics costs partly because of less-than-truckload (LTL) shipments.

The bullwhip effect refers to increasing swings in inventory in supply chain in response to ineffective information flow, what results in excessive accumulation of stocks in particular supply chain partners. It is also called "misalignment between the demand and order signal" (Costantino et al. 2015a). Inadequate information flow or lack of them between the partners in the supply chain, leads to distortion of information moving along the supply chain. It results in the intensification of demand variability and the bullwhip effect (Lee 2003).

This phenomenon creates serious problems partners in the supply chain, causing errors in demand forecasts, low capacity utilization, excess inventory, and poor customer service.

Study by Costantino et al. (2015b) showed the importance of bull-whip effect on supply chain and in particular inventory management decisions. Also indicated that many studies in literature don't propose solutions that are easy to implement and acceptable when cost-benefit comparison is made. The proposed framework aims to fill this gap by evaluating an ordering policy that can mitigate the bullwhip effect while keeping acceptable inventory performance. The proposed actions to counter this gap is given in Section 4.1.

3.2 Visibility of inventories

Visibility of the inventories is a critical factor for inventory management. Any deviation may cause a deviation between intended target and outcome.

Typically, accuracy of the inventory may change from sector to sector because of the uniqueness of the products and environment. The deviations don't occur only because of the typical losses such as wrong shipments, losses or theft but also due to the nature of the products. Chemicals and food products has a tendency to expire with the limited shelf-life. After the shelf-life the products lose their value significantly or become waste.

Also, a study made by Raman et al. (2001) inaccurate inventory records has reduced profits by ten percent.

Therefore, accuracy of the inventory records is vital for the performance of an inventory management system and necessary actions should be taken accordingly.

3.3 Uncertainty

Uncertainty is an important risk in inventory management. Uncertainty may arise from internal factors or external factors. Lack of accurate data for demand, inventory, costs, lead times, inventory records may undermine the performance of any decision made. These factors are considered as internal factors. Economical or global instability that affects the demand, or new regulations may affect the business.

Davis (1993) pointed out that, the key issue affecting the efficiency of the supply chain is uncertainty. The reason of keeping safety stock is mainly to deal with uncertainty in supply chain. According to Czwajda and Kosacka (2017), globalization, technological change, increasing demands from customer for better service lead to increased requirements from supply chain. In return it may result in a higher level of uncertainty for the organization and thus a higher level of incurred risk.

Consequently, it impedes achieving their objectives (Pluta-Zaremba 2008). Proper risk management and effective collaboration among all responsible parties would help to overcome the negative effects.

In order to counter the disadvantages of uncertainty, proposed measures are given in section 4.3.

3.4 Skills and Training

Lack of skills and proper training of the professionals can be a major issue for the efficiency of inventory management. Most of the necessary skills can be acquired with formal undergraduate or graduate level educations, also specific courses can be taken to acquire required skills when necessary. The main understanding of inventory management principles and methods are vital for an effective management.

The factors, documentation/store records, planning, knowledge of employees/staff skill have shown to significantly influence the effectiveness of inventory management while the funds have shown slightly significant influence on the inventory management in manufacturing small medium enterprises (Chan et al. 2017).

Study conducted by Mahyadin et al. (2013) in the area of inventory management practices revealed that improper management may have been caused by the level of skills that the practitioners have. Although experience in a specific area is important, it may also cause some important areas for improvement to be overlooked.

In section 4.4, a framework for the assessment and training subjects or skills of a practitioner is given accordingly. In return, the suggested framework will provide a guidance to cover a possible gap in this area.

3.5 Product Classification (ABC Analysis)

There are also challenges faced due to product specific characteristics. Some typical characteristics are, short expiry periods, dangerous or extremely valuable goods and substitute products. Generalization of such products may cause their importance or need for special management to be ignored. Some products may be extremely important for production or for a customer. Such classification may cause products to be classified under the lowest class of C. Therefore, the desired customer service level cause them regularly to be out-of-stock and cause the performance of inventory management system to underperform. In Section 4.5, some specific attributes of products are given. By assessing products accordingly or managing products based on these specifications may contribute the performance of the total inventory system.

3.6 Perishability

Products with shelf-life are not taken into consideration by main textbooks in the area of inventory management.

Typical safety stock calculation and economical order quantity (EOQ) models ignore the perishability attribute of products. Therefore, if all other values such as lead time, lead time variability, ordering and stock keeping costs and variability of these values are same, the outcome will be the same for a perishable or non-perishable product.

Although there are research in this area, they may be too complicated for either practitioners or case specific. To overcome these problems, applications implementing proposed models can be used for inventory management decisions.

In literature, there are studies associated with the perishable products, most may be considered too complicated for daily use. The mathematical model proposed in Section 4.6 takes into consideration the perishability of products. of the total cost. perishability of products. The goal is to integrate this attribute into the proposed model with the objective of achieving minimization of cost and satisfying constraints such as budget, total inventory level etc.

3.7 Type of inventories, different strategies.

Especially when the number of products increase, it is important to classify, products based on their importance. Therefore, ABC analysis is a widely used approach for the classification of goods. After 70 years, the need for more complex classifications emerged. Single criterion classification is not enough to assess the importance of inventory and make decisions accordingly. As a result, multiple criteria approaches are realized and implemented. This subsection of inventory classification is called multiple criteria inventory classification (MCIC). Although such application is better to define the inputs for business decisions, such applications also bring additional workload and complexity. To make accurate assessments, relevant criteria should be agreed among the decision makers. Besides decisions about criteria, classification methods should be accurately decided.

Although inventory classification models such as ABC analysis models are used for classifications, some items in inventory are not accurately defined in such classifications. Therefore, some other goods should be classified based on different characteristics. A typical class for such classification is slow moving items and dead items.

The distinction between slow moving items typically has low demand but due to goods in inventory, it may have a significant effect on a company's financials along with dead stock. According to Sugumaran and Sukumaran (2019) dead stock is a major issue in garment industry as it affects business cash flow, takes up valuable warehouse space and freezes earnings that otherwise should be dedicated to the purchase of revenue-generating products. Unsold garments that remain in warehouses, see zero sales in a defined number of months, and retard business growth, can be referred to as "dead stock".

Challenges are about the definition of slow-moving items and definition of goods with very minimal demand close to "0". Such products are called "dead stock" in literature. A definition of slow-movers and dead-stock is given in Section 4.7. Such classificiation and exceptions may be revised based on the specific cases of the practitioners.

In the same section, necessary actions to lower the amount of dead-stock and slow-moving items is given as well.

3.8 General Inventory Models

In typical inventory models namely deterministic or stochastic models, constraints are not considered. In economic order quantity models, based on the demand and costs an optimum quantity is calculated to lower the total cost. On the other hand, such application does not take into consideration the constraints faced in business life.

Typical objective is the total inventory cost which are limited with the budget or financial availability, expiry dates and perishability, special concerns associated with product specific requirements such as food grade, dangerous goods etc. However, in business life, most of the decisions are subject to some constraints. Such constraints can be physical, financial, environmental or such. Warehousing capacity, outsourced warehouse capacity, total value of purchase or inventory value, total amount of inventory or purchase are some examples of such constraints.

In typical textbook models, inventory models don't cover the price fluctuations of goods and/or perishability of products. In deterministic or stochastic models' emphasis is given for safety stocks and economical order quantities. In these models' prices are considered as fixed and products have no shelf-life. As a result, all inventory decisions will be same for products regardless of their shelf-life.

The proposed model in Section 4.6, aims to cover the gap in literature. The proposed model covers not only the total cost structure but also the constraints that are a part of the any inventory decision. When integrated into a software system, applications will fit more to the realities of business life.

4 Model Formulation and Proposed Framework

In Section 4, the details of the approach proposed is given. Methodology of the study consists of exploratory survey of relevant literature and analysis of the experience of the author based on 15+ years of experience in inventory management. Typical measures to overcome each challenge group are discussed separately in the remaining of the section 4.

4.1 Multi-Echelon Systems Management

Due to customer service requirements or logistics networks, multi-echelon inventory systems are widely used in business. A typical comparison between single and multi-echelon distribution systems is given in Fig.1.

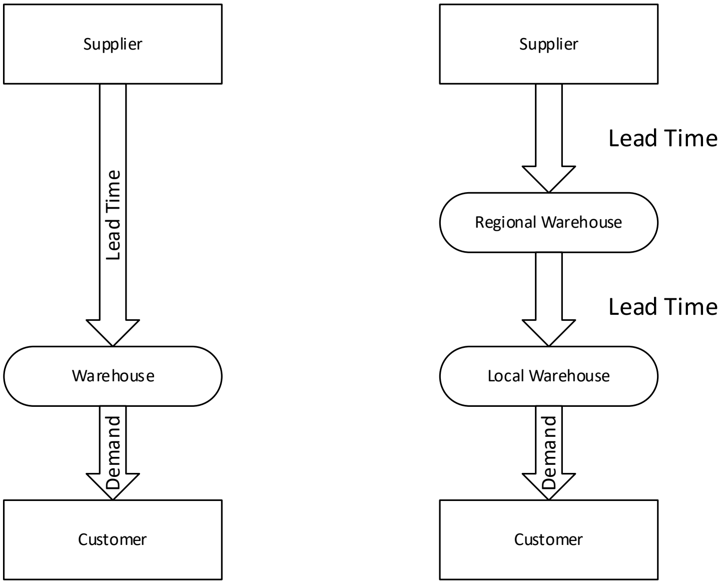

Figure 1 Single and Multi-Echelon Systems

Multi-echelon inventory systems cause bull-whip effects. Bullwhip effect represents the amplification and distortion of demand variability as moving upstream in a supply chain, causing excessive inventories, insufficient capacities, and high operational costs. Bull-whip effect is a typical problem for inventory systems, as additional layers causes complexity and vagueness in inventory systems. Study by Zhu et al. (2020) shows that, multi echelon system can create significant inefficiencies in the supply chain (e.g., excessive inventories, misguided production or capacity planning, poor customer service and lost revenue due to shortages).

A growing body of literature recognizes ordering policies and the lack of coordination as two main causes of the bullwhip effect, suggesting different techniques of intervention (Costantino et al. 2015a).

Excessive inventories and reduced customer service level due to stock outs may undermine the performance of inventory systems. The integration of traditional ordering policies with a collaborative approach proved its success in different configurations as for Information-Enriched Supply Chain, Vendor Managed Inventory, Quick Response and Collaborative Planning, Forecasting and Replenishment (CPFR) (Costantino et al. 2015a).

Therefore, the proposed framework will cover a forecasting system implementation that will be regularly checked about the discrepancies and modified accordingly. Besides, such forecasting system every part of the organization should have the responsibility of such implementation and execution.

The forecast phase in the framework given in Section 5 covers two alternative forecasting techniques and a feedback from relevant departments. The mentioned workflow of the framework also covers the assessment of the accuracy to find the reasons of deviations and to take necessary actions.

4.2 Inventory Visibility

Visibility of inventory is a major concern. In order to make accurate decisions, any decision maker needs the status of inventories. Typical models cover the lead time and/or demand as probabilistic and quantities on hand as deterministic. Unfortunately, due to frequent wastes, wrong shipments, theft etc. it is not always possible to have the accurate figures in the system compared to the actual inventory on hand.

As a result, inventory records in the system may deviate from the actual values that are used for decisions. Therefore, physical inventory procedures should be executed not only due to accounting requirements but also for to ensure that the actual and records are accurate.

The first action is to implement a strategy to make physical inventory procedures, a method to overcome discrepancies. Physical inventory routine should be used both for accuracy and for improving the inventory status. Each physical inventory procedure should be accompanied by meetings with the goal of improvement of the inventory record keeping. Also, physical inventory periods should be relevant with the accuracy. As an example, the physical inventory should be done monthly till the discrepancy is above %3 and so.

Additionally, whenever possible inventory records should be done based on actual values and recorded at the time of consumption or receipt. Address assignment to each lot or use of technologies such as RFID or barcoding systems would contribute the performance of inventory management.

The workflow will cover the actions necessary to assess the situation and take necessary actions to improve the accuracy and hence the visibility of inventory.

4.3 Uncertainty

A factor of uncertainty does not only affect the inventory but also other functions of an organization. Modern applications such as grey systems is used to overcome such problems. In order to overcome this issue in the area of inventory management, safety stock is used.

The sources of uncertainty can be divided into three groups (Simangunsong et al. 2012):

1. Uncertainties from the focal company, e.g. internal organization uncertainty (product characteristics, manufacturing process, control/chaos, decision complexity, organizational/behavioral issues and IT/IS complexity)

2. Internal uncertainty of the supply-chain arising within the realm of control of the focal company or its supply chain partners (end-customer demand, demand amplification, supplier, parallel interaction, order forecast horizon and chain configuration, infrastructure and facilities)

3. External uncertainties, associated with factors outside the supply chain, which are outside a company's direct areas of control (environment, government regulation, competitor behavior and macroeconomic issues, and disasters)

Considering uncertainty will be a part of any business decisions necessary actions should be taken to counter uncertainty. To deal with uncertainty, the data that is used for decision making should be as accurate as possible. By the application of ABC analysis, more focus can be applied on the A class that has a higher effect on the outcomes. Therefore, the proposed framework given in Section 5 will integrate and ABC analysis and use of a traditional safety stock calculation with the goal of achieving customer service level.

4.4 Skills and Training

As stated in chapter 3., skills of inventory management professionals directly affect the performance of the desired system. Typical educational programs aim to improve the educational level of professionals. The proposed model includes the assessment of the training need of the relevant staff in some areas, which are mandatory for professionals. As stated in Chapter 6, the suggested workflow covers the assessment of the skills of the responsible people. After the assessment, proper trainings should be conducted to cover the gap between the desired level and status. Adequately trained practitioners are a key factor for the efficient management of the proposed framework.

A typical inventory management responsible should be well trained in the following areas.

- MRP & DRP Systems
- Economical Order Quantities (EOQ)
- Inventory Models & Inventory Related Costs
- ABC Classification
- Physical Inventory Procedures

- Safety Stocks & Customer Service Level
- Forecasting
- Spreadsheet Experience and Expertise
- Basic Statistics

The proposed model and framework cover the assessment of necessary skills and relevant trainings as well. Accurate assessment of the skills of the inventory management practitioners is although beyond this study, an experienced manager may evaluate the current levels of practitioners with high accuracy.

4.5 Management of Extreme Cases

Generalization of all products to limited classes via ABC analysis may cause products that need special attention to be neglected. Therefore, after the classification of goods, some exceptions may be needed. The proper management of exceptions involves defining some special categories. These categories are managed according to different specifications and needs. To name a few, a product that can only be used with a different material e.g two component glue, or a product that is subject to strict regulations in terms of storage or sales, explosives, or toxic materials. These exceptions should be managed according to specific needs.

The workflow proposed in Chapter 5, covers the typical sub specifications that can't be addressed under ABC classification.

Such classifications are;

- Complementary items
- High perishability items
- Items with extremely high value/quantity ratio
- Products subject to product specific regulations (e.g. food, feed etc.)
- Dangerous Goods (Toxic, Flammable, Oxidizers etc.)

4.6 Management of Perishable Products

Typical inventory policies or models do not make any distinction between perishable or non-perishable products. As a result, proper management of perishable goods is mandatory for the effective management of goods. Our proposed model takes into consideration of goods that has a shelf-life and costs associated with these goods. In the last phase of the model, where the objective function is defined to cover the perishability of products.

Lack of policies that covers the overall global strategy causes significant local decisions to be made. Such decisions are optimal from limited perspective. Such decisions cause local gains and profits from that view but on the other side may generate greater losses.

The behavior of a purchasing agent may be given as an example. In case of a huge price discount, due to lower costs, a typical behavior would be to give orders covering the many months ahead. Alternatively, especially in container shipments, the minimum ordering quantity is considered as the quantity in a container. Whereas accepting some dead freight, total quantity may be negotiable with the supplier. Therefore, to cover the gap between local and global optimum decisions, policies covering inventory decisions should be clearly defined. Such policies are purchasing, warehousing and inventory related investments such as packaging, new warehousing investments etc.

In the proposed framework costs such as deterioration, damage and wear are included in the cost of inventory. If a product remains in stock beyond its expiration date, the product becomes unusable and there is a loss equal to the value of the product. On the other hand, this spoiled product must be disposed of in accordance with the laws. The disposal costs incurred as a result of this process should also be added to the total cost.

In order for a product to become waste or obsolete, the product purchased in a certain period must not be sold within the expiration period. Stocks on hand must be used or sold according to First-In-First-Out (FIFO) principle. Therefore, the demands within the expiry period must first be deducted from the existing stock, and the remaining demand must be deducted from the amount that will come from the newly arrived product.

It is important that the new product is consumed within the expiration period to avoid deterioration, aging and related disposal costs.

The equation for deterioration and aging costs is given in Eq. 5.1. In the said equation, it is formulated that if a product does not receive enough demand within the expiration period, after the product is supplied, the quantity in stock will expire and the associated costs will occur.

$$BY_{xt} = \begin{cases} t < k = 0 \\ t > k \;=\; HaMx(t-k) - \sum_{t=t-k}^{n} Tlpxt \end{cases}$$

$$TWC = \quad \sum_{x=1}^{m} \sum_{t=1}^{n} (BY_{xt} * (BuM_{xt} + UC_x) \qquad \forall x, t$$

$$PI_{xt} = PI_x(t-1) - HaM_{xt} + Tlp_{xt} - BY_{xt} \quad (5.1)$$

$$SC_{xt} = PI_{xt} * (UC_x + WC_x + FC_{xt})$$

$$TSC = \quad \sum_{t=1}^{n} \sum_{x=1}^{m} SC_{xt} \quad \forall x, t$$

$$OC_{xt} = \begin{cases} OC_{xt} & if\ HaM_{xt} > 0 \\ 0 & if\ HaM_{xt} < 0 \end{cases}$$

$$TOC = \quad \sum_{t=1}^{n} \sum_{x=1}^{m} OC_{xt} \quad \forall x, t$$

The following constraints should be taken into consideration.

Customer Service Level

$$CS_x = \frac{PI_{xt}}{Tlp_{xt}} \ \forall x, t$$

Total Purchased Quantity

$$\sum_{x=1}^{m} \sum_{t=1}^{n} HaM_{xt} \leq TP$$

Total Purchased Value

$$\sum_{x=1}^{m} \sum_{t=1}^{n} HaM_{xt} * UC_x \leq TPV$$

Total Waste

$$\sum_{x=1}^{m} \sum_{t=1}^{n} HaM_{xt} * UC_x \leq TPV$$

Total Amount of Procured from Product

$$\sum_{t=1}^{n} HaM_{xt} \leq TAP_x$$

x	= Product number	(x = 1, 2, 3,….m)
t	= Period	(t = 1, 2, 3, ….n)
k_x	= Expiry period for product x	
PI_{xt}	= Inventory on hand per period t per product x	
HaM_{xt}	= Calculated Order Quantity per period t per product x	
Tlp_{xt}	= Demand per period t per product x	

CS_x	= Customer Service Level for the product x
TP	= Total Purchased Quantity Constraint Value
TPV	Total Purchased Value Constraint Value
TWL	= Total Waste Quantity Constraint Value
TAP_x	= Total Procured Quantity Constraint Value for the product x
BY_{xt}	= Perished product quantity per period t per product x
BU_{xt}	= Waste cost per period t per product x
UC_x	= Unit cost per product x
WC_x	= Warehousing cost per product x
FC_{xt}	= Financial cost per period t per product x
SC_x	= Storage cost per period t per product x
OC_{xt}	= Ordering cost per period t per product x
TWC	= Total Waste Cost
TSC	= Total Storage Cost
TOC	= Total Ordering Cost

4.7 Inventory Classification

A typical method to classify goods according to their consumption is to use the inventory turnover or days in inventory (DIO) metrics. As mentioned in chapter 3.7, such methodology is limited. Based on characteristics given is Section 3.7, products need to be classified based on not only value or turnover but also more elaborative approaches. In literature such classifications are given in multi criteria inventory classification (MCIC). In the proposed methodology, a MCIC model proposed by Yiğit and Esnaf (2020) is used for such classification. Dead and slow-moving items are not classified under such model. To solve this problem, assessment of dead and slow mover is executed before MCIC model application. To classify dead and slow-moving items following workflow is used.

As an example, classifying goods with "0" or very low demand as dead stocks, can also classify the newly supplied goods as well. Regular new purchases with new SKU's makes the classification difficult. Especially in sectors with high turnover such as fast fashion low priced alternatives make the traditional use of turnover or days inventory outstanding (DIO) classification of slow-movers or dead stocks difficult.

In the study prepared by Grange (1998) of all dealer's parts that is, these with 20 or more weeks of very low or zero demand in a year. On the other hand, classifying good based on their consumptions is sometimes difficult.

In the flowchart given below, DIO of 1500 days is used for Dead items, DIO between 360 and 1500 days is used for Slow Moving goods. 4 month no consumption is used for defining new products.

Calculate DIO of items

%Define DIO for Dead and Slow-Moving items Classification

for x=1 to m

  If DIOx > 1500 days then ABC_x = Dead (D)

  If 360 > DIOx > 1500 days then ABC_x = Slow Moving (SM)

  If first supply is last 4 months then $ABC_x \neq$ New Product (NP)

  For x ≠ Dead or Slow-Moving or New Product

end

Apply ABC Analysis for ABC_x ≠ D or SM or NP

Figure 2 Dead-Slow Moving or New Product Classification Algorithm

Therefore, the variables may be amended based on changing needs of the practitioner. In the algorithm given below, 4 months is considered as time needed for new products. 4 months can be as less as 1-2 days for new products in retail business or 4 months in chemical business.

4.8 Forecasting

Inventory models proposed in literature do not cover some of the challenges faced by inventory management practitioners.

Forecasting of future demand is an important area for inventory management practitioners. Typical textbook inventory models cover future demand as a probabilistic demand or forecast is covered entirely another area for research. The proposed model covers the forecasting procedure as a part of inventory management decisions. Therefore, when not enough data is available for future decisions, forecasting procedure will help the decision maker for such decisions.

The proposed framework aims to help practitioners to apply a workflow to gain benefits in inventory management. The proposed framework covers a selection of alternatives among alternatives or use of hybrid methodology for an efficient forecasting system. As given in Figure

3, sales department should be a part of forecasting methodology. Also, relevant feedbacks should be given to parties based on the performance feedback of forecasts.

5 Proposed Methodology for Inventory Management

The flowchart given in Figure 3 represents a workflow that covers the proposed methodology for an efficient inventory management.

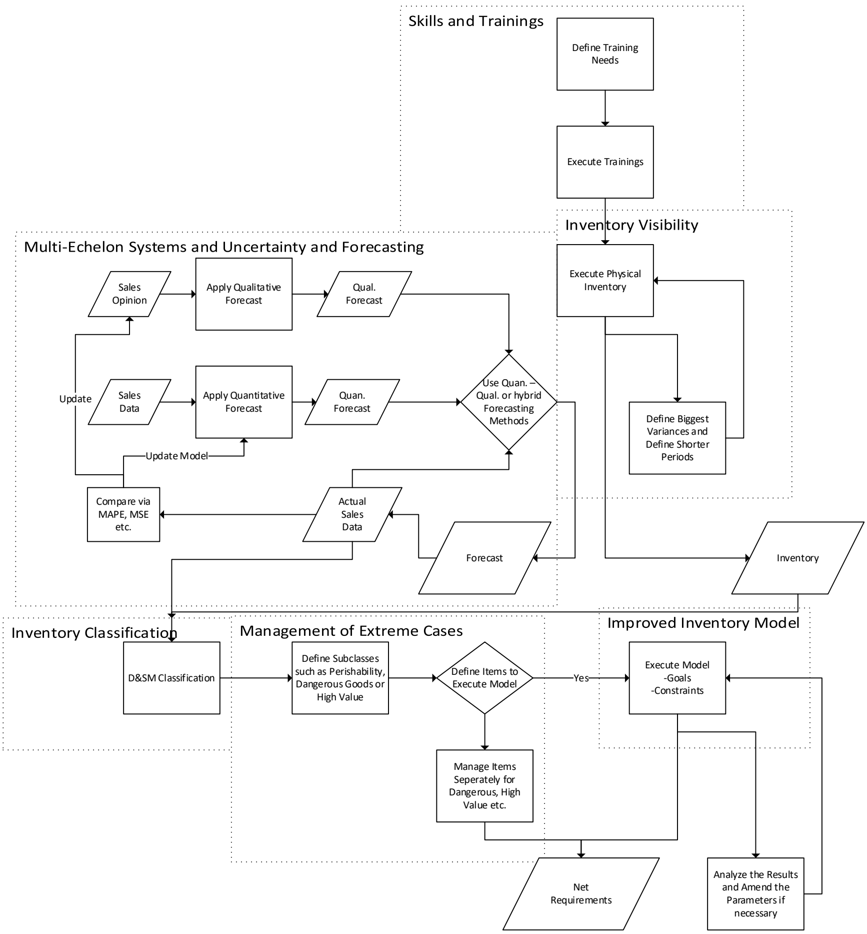

Figure 3Flowchart of the Proposed Framework

6 Conclusion

Inventory practitioners face many challenges, especially in the early stages of learning curve. Normally, inventory management involves decisions based on vague information such as sales demand, lead times and sound information such as inventory level. However, actions such as use of forecasting is as good as the application. Also, information that is expected to be sound is sometimes not enough accurate. Therefore, the proposed framework covers the forecasting phase to solve this issue. Also a skills and training phase is added in order to assess the level of the training of decision-makers to take necessary actions. D&SM and extreme cases identification along with ABC analysis is integrated into the proposed framework to differentiate products. This method allows the decisions maker to focus on the few that has the most value for a business unit. Improved inventory model is given to model a decision that covers both important objectives and constraints. The improved model would help the decision maker to make decision that has the minimum total cost while satisfying the constraints.

Further needs and research in the area may be added to the framework by users who has experience and/or academic background for further improvements.

REFERENCES

Beutel, A. L., & Minner, S. (2012). Safety stock planning under causal demand forecasting. International Journal of Production Economics, 140(2), 637-645.

Boone, C. A., Craighead, C. W., & Hanna, J. B. (2008). Critical challenges of inventory management in service parts supply: A Delphi study. Operations Management Research, 1(1), 31-39.

Cambridge Dictionary, retrieved from https://dictionary.cambridge.org/tr/s%C3%B6zl%C3%BCk/ingilizce/challenge, Date of visit 15.08.2020

Chan, S. W., Tasmin, R., Aziati, A. N., Rasi, R. Z., Ismail, F. B., & Yaw, L. P. (2017). Factors influencing the effectiveness of inventory management in manufacturing SMEs. In IOP Conference Series: Materials Science and Engineering (Vol. 226, No. 1, p. 012024).

Costantino, F., Di Gravio, G., Shaban, A., & Tronci, M. (2015a). The impact of information sharing on ordering policies to improve supply chain performances. Computers & Industrial Engineering, 82, 127-142.

Costantino, F., Di Gravio, G., Shaban, A., & Tronci, M. (2015b). SPC forecasting system to mitigate the bullwhip effect and inventory variance in supply chains. Expert Systems with Applications, 42(3), 1773-1787.

Czwajda, L., & Kosacka, M. (2017). The challenges of concept Multi-Echelon Inventory Management. Research in Logistics & Production, 7.

Davis, T. (1993). Effective supply chain management. *Sloan management review,* 34, 35-35.

Dhoka, D. K., & Choudary, Y. L. (2013). XYZ Inventory Classification & Challenges. IOSR Journal of Economics and Finance, 2(2), 23-26.

Grange, F. (1998). Challenges in modeling demand for inventory optimization of slow-moving items. In 1998 Winter Simulation Conference. Proceedings (Cat. No. 98CH36274) (Vol. 2, pp. 1211-1217). IEEE.

Gumus, A.T. & Guneri, A.F. (2009). A multi-echelon inventory management framework for stochastic and fuzzy supply chains, Expert Systems with Applications, No. 36, pp. 5565–5575.

Inman, R. A. (1999). Environmental management: new challenges for production and inventory managers. Production and Inventory Management Journal, 40(3), 46.

Lee C.B. (2003). Multi-Echelon Inventory Optimization, Evant White Paper Series.

Mahyadin, F. A., Mahidin, R. S., Asaad, M. N. M., & Zien, R. (2013). The influence of inventory management practices towards inventory management performance in Malaysian public hospitals. Medicine.

Patil, H., & Divekar, B. R. (2014). Inventory management challenges for B2C e-commerce retailers. Procedia Economics and Finance, 11, 561-571.

Pluta-Zaremba A. (2008). Proces ograniczenia niepewności popytu w łańcuchu dostaw, Gospodarka Materiałowa & Logistyka, No. 11, pp. 2–8.

Raman, A., DeHoratius, N., & Ton, Z. (2001). Execution: The Missing Link in Retail Operations. Califonia Management Review, 43(3), 136-152.

Simangunsongy E., Hendry L.C. & Stevenson M. (2012). Supply-chain uncertainty: a review and theoretical foundation for future research, International Journal of Production Research, Vol. 50, No. 16, pp. 4493–4523.

Skowron, K., & Cheba, D. (2019). Diagnostic assessment of MZK Tychy's customer service level. Organizacja i Zarządzanie: kwartalnik naukowy.

Stößlein, M., Kanet, J. J., Gorman, M., & Minner, S. (2014). Time-phased safety stocks planning and its financial impacts: Empirical evidence based on European econometric data. International Journal of Production Economics, 149, 47-55.

Sugumaran, P., & Sukumaran, V. (2019). Recommendations to improve dead stock management in garment industry using data analytics. Math. Biosci. Eng, 16, 8121-8133.

Working Capital Report, PWC. (2019). retrieved from https://www.pwc.com/gx/en/services/advisory/deals/business-recovery-restructuring/working-capital-opportunity.html; Date of Visit: 15.08.2020

Yiğit, F., Esnaf, Ş. (2020). A new Fuzzy C-Means and AHP-based three-phased approach for multiple criteria ABC inventory classification. J Intell Manuf (2020). https://doi.org/10.1007/s10845-020-01633-7

Zhu, T., Balakrishnan, J., & da Silveira, G. J. (2020). Bullwhip effect in the oil and gas supply chain: A multiple-case study. International Journal of Production Economics, 224, 107548.

Chapter 18

TAGUCHI BASED MULTIPLE REGRESSION MODELING OF CONCRETE CONTAINING SILICA FUME STRENGTHENED USING POLYMER WITH PHOSPHAZENE EXPOSED TO FREEZE-THAW

Harun TANYILDIZI[1]

1 Prof. Dr., Department of civil engineering, Firat University Elazig/TURKEY, e-mail: htanyildizi@firat.edu.tr, Telephone:+90-424-2370000-4315, https://orcid.org/0000-0002-7585-2609

1. INTRODUCTION

Concrete is one of the most important materials in civil engineering (Vejmelková et al., 2015). It has been used for long years in water structures, roads, dams, bridges and infrastructure work (Pawan et al., 2015). The mineral additives in roller compacted concrete, self-compacting concretes and lightweight concretes are replaced with cement for meliorate the resistance and durability properties of concrete (Mardani-Aghabaglou et al., 2014). The most prevalent additives used in concrete are silica fume, fly ash, slag. Silica fume is known to increase compressive strength, adherence resistance and durability properties of concrete (Lilkov et al. 2014). Silica fume is the byproduct of silicone and ferro-silicone industry. By heating silicone up to 2000 °C, high purity SiO_2 vapors are produced. The content of silica fume depends on the produced alloy (Siddique, 2014).

When a reinforced concrete structure is exposed to freezing, the water within the capillary pores converts to ice and its volume approximately increases by 9% (Chung et al., 2010). In cold climates, the freeze-thaw phenomenon is one of the most important problems in concrete (Molero et al., 2012). The articles have been conducted regarding the resistance of silica fume containing concrete against freeze-thaw. Chung et. al (2010) investigated the effect of freeze-thaw of concrete containing silica fume and fly ash. Silica fume containing concrete samples performed high durability factor and low chlorine ion permeability (Sun et al., 1999). Sabir (1997) examined the effect of freeze-thaw on concrete with silica fume. At the end of his research, he obtained durability factor for control concrete as 92%, while this result was 85% for silica fume containing concrete. Yazıcı (2008) examined the freeze-thaw resistance of concretes with high amount of fly ash and silica fume. At the end of the study, the compressive strengths of concretes containing silica fume and fly ash were higher than compressive strength of control concrete. Zhang and Li (2013) examined the effects of polypropylene fiber on concrete with silica fume and fly ash subjected to freeze-thaw. When freeze-thaw capacities of concrete were compared which does not contain fiber and concrete containing fiber with silica fume, it was determined that freeze-thaw resistance of concretes containing fiber was higher. It was also reported in the literature that silica fume usage increases the drying shrinkage and tension cracks of concrete (Haque, 1996; Bissonnette, 1995; Rao, 1998; Li et al. 1999).

P-N bonded compounds are formed from the reactions of phosphorus compounds and nitrogenous nucleophiles. The compounds containing double bonds between phosphorus (P) and nitrogen (N) are named as phosphazens. Phosphazenes have organic character as they are dissolved in organic solvents but they also have inorganic character due to P=N chain. Phosphazens, depending on the repetition quantity of $-N=PX_2-$ group in their structure, constitute the biggest class of inorganic macromolecules including many compounds varying from small compounds to polymers (Allcock, 1972). The physical and chemical properties of the phosphazene compounds change depending on the group which is bound to the phosphazene main structure. Therefore, the area of usage is wide. According to the data obtained from the literature, some of the application fields are: dielectric property (Koran et al. 2014), gas sensor (Gleria and Jaeger, 2004) and catalyst support material (Song et al., 2005). They are also used in the medical field as well. In some studies performed on animals, it was observed that they demonstrated tumor formation preventive effect (Song et al., 2005). It was also found out that phosphazene derivatives are effective against bacteria and microorganisms causing various illnesses (Tumer et al., 2013; Akbas et al., 2013). It was observed that organo-phosphazenes have anti-microbial effect (Yilmaz et al., 2002; Koran et al., 2013). Some of the phosphazene derivatives are used as the tooth filling material (Gleria and Jaeger, 2004).

Polymer impregnated concrete is produced by impregnating polymer to concrete. Monomer, which penetrates to thinnest capillary gaps of concrete, is polymerized there and therefore impermeable and high-strength concretes are obtained (Piskin, 2010). As a result of reinforcing concrete with polymer, the strength of concrete increases significantly (Monteny et al., 2001;Puy and Dikeou, 1973). Furthermore, the durability resistance of concrete increases because of the reinforcing of polymer to concrete (Allan and Horn, 2006; Yang et al., 2009; Moreira et al., 2006; Chmielewska, 2007; Ogawa et al., 2007; Shirai, 2007; Cheng, 2006).

In this study, the mechanical properties of concrete subjected to freeze-thaw were modelled by the Taguchi based multiple regression.

2. EXPERIMENTAL MATERIALS AND PROCEDURES

2.1. Materials

The cement (CEM I 42.5 R) used in the experiments was provided from the Cement Factory in Elazig. The super plasticizer was used in mixtures. In the experiments, the silica fume at a rate of 0 %, 10 % and 20 % of the cement was used by weight. The properties of the silica fume and cement were provided in Table 1.

Table 1. *The chemical compositions of silica fume and cement*

Chemical compositions	**Cement**	**Silica fume**
CaO, (%)	62.94	0.71
Al_2O_3, (%)	5.62	0.58
SiO_2, (%)	21.12	91
Fe_2O_3 (%)	3.24	0.24
SO_3, (%)	2.30	1.06

MgO, (%)	2.73	0.33
K_2O, (%)	-	4.34
Na_2O, (%)	-	0.38
Cl, (%)	-	0.8-1.0
Specific gravity (g/cm^3)	3.1	2.2
Specific surface area (cm^2/g)	3430	144000

2.2. Design of Tests

Taguchi method was developed Dr. Taguchi (Davim, 2001). The mechanical properties of concrete generally depend on the physical and chemical additives, curing and durability attacks. In the current study, the ultrasonic pulse velocity and compressive strength of concretes strengthened with polymer including phosphazene subjected to the freeze–thaw cycles and their optimum parameters were found with Taguchi analysis. Moreover, it was developed Taguchi based multiple regression model. The experimental variables were used as the percentage of silica fume used in concrete, the percentage of phosphazene in polymer and curing days. According to these variables, L_9 (3^3) orthogonal test plan was selected in this study. Table 2 shown the level of variables used in the experimental study. In Table 2, the phosphazene in polymer, silica fume and curing days was selected three levels. Then, the mixtures in given Table 3 were prepared. According to these mixtures, the 100×100×100 mm cubes were produced. They removed the molds after keeping for 1 day and were cured at 20±2°C for 3, 7 and 28 days.

Table 2. *The variables used in the experimental study*

	Level 1	Level 2	Level 3
The percentage of phosphazene in polymer, P (%)	0	1	2
The percentage of silica fume, S (%)	0	5	10
Curing time, T (day)	3	7	28

Table 3. *The mixture proportions*

	Cement (kg/m^3)	Silica fume (kg/m^3)	W/C	Aggregates, 0-7 mm (kg/m^3)	Aggregates, 7-16 mm (kg/m^3)	Super plasticizer (kg/m^3)
P	400	--	0.55	1038	692	0.6
S	380	20	0.55	1034	689	0.6
T	360	40	0.55	1030	686	0.6

2.3. Polymerization and freeze-thaw test

In order to perform the freeze thaw cycle, the specimens were dried oven of 105 ±5 °C for 24 hours after curing days. The cooled specimens were waited for 24 hours in vinyl acetate monomer in atmospheric conditions. After this, they were kept at 60 °C for 6 hours for the polymerization. Then, they were subjected to freeze–thaw cycles experiment compliant to TS EN 15177 standard (TSE CEN/TR 15177, 2012). According to this standard, samples were placed in the freeze-thaw cabin, which was pre-adjusted to -20±2 °C and was kept in the cabin for 8 hours. After freezing process was finished, the specimens were kept in water for 4 hours at 13± 8 ºC. Totally 56 freeze-thaw cycles were applied to the samples. Then, the ultrasonic pulse velocity and compressive strength experiments of samples were carried out.

3. RESULTS

3.1. Compressive strength

In the current study, the compressive strengths of the concretes strengthened with polymer including phosphazene subjected to freeze–thaw cycles were examined experimentally and then modelled using Taguchi based multiple regression. The rate of phosphazene in polymer was used as 0 %, 1 % and 2 %. The silica fume was used 0 %, 10 % and 20 % of cement weight. Moreover, the specimens were cured at 20±2 ºC for 3, 7 and 28 days. Table 4 shown the compressive strength results of the specimens.

Table 4. *The results of compressive strength of the concretes strengthened with polymer including phosphazene subjected to freeze–thaw cycles*

Phosphazene percentage, (%)	Silica fume percentage, (%)	Curing time, (Day)	Compressive Strength (MPa)
1	1	1	24.03
1	2	2	28.51
1	3	3	23.03
2	1	2	49.15
2	2	3	54.58
2	3	1	52.33
3	1	3	56.79
3	2	1	61.1
3	3	2	65.91

The Taguchi analysis was carried out for the compressive strength of the concretes strengthened with polymer including phosphazene subjected to freeze–thaw cycles. In this study, the loss function was used to find the deviation in between the required and experimental values (Pshadke, 1995; Ross, 1996). In the current study, "higher is better" loss function was selected because the higher compressive strength of the samples is better. The LB loss function (L_{ij}) were given in Equation 1:

$$L_{ij}=\frac{1}{r_a}\sum_{i=1}^{r_a}\frac{1}{y_1^2} \tag{1}$$

Equation 1 is the loss function of performance no i during the test number j. The numbers of tests in a trial are r_a. The value measured for each test is y. The S/N rate (η) for this loss function were given Equation 2 (Pshadke, 1995; Ross, 1996).

$$S/N_{LB} = -10\log(L_{ij}) \tag{2}$$

The S/N rates were calculated using the experimental variables in Table 2.

The S/N rates of the compressive strength of concrete strengthened with polymer including phosphazene subjected to freeze-thaw cycles were shown in Table 5.

Table 5. *S/N rates for the compressive strength of concrete strengthened with polymer including phosphazene subjected to freeze–thaw cycles*

	S/N rates		
	Level 1	**Level 2**	**Level 3**
Percentage of phosphazene in polymer, P (%)	32.54	33.00 [s]	32.28
Percentage of silica fume, S (°C)	32.12	33.10 [s]	32.60
Curing time, T (%)	27.93	34.26	35.64 [s]

[s] Optimum level

Mean S/N rate=32.61.

As Table 5 was examined, the highest compressive strength was obtained from samples that were containing silica fume 5 % at 28 days and used the polymer including phosphazene 1%. To increase the mechanical properties and durability properties of concrete, it must be decreased the gaps and cracks. It is possible to say that the polymer impregnation method is successful in reducing these gaps and cracks. Thus, the mechanical properties and durability properties increase by using of this method (Bal, 1998; Sidney and Young, 1981). The reason for this increase is: it occurs the combination of polymer molecules having polar groups by physical links by the strict adhesion of them to each other (Tanaka et al., 2002; Yalçın, 1998). Furthermore, a continuous polymer phase increases the interfacial transition zone in between the cement paste and aggregate (Satish and Ohama, 1994; Bhutta et al., 2013). This study was found that the use of 1% phosphate in the polymer increased the compressive strength of concrete.

Furthermore, the Taguchi based multiple regression in predicting the compressive strength of concrete strengthened with polymer including phosphazene subjected to the freeze–thaw cycles was in this study. The proposed equation was given bellow.

$$F_c = 46.16 - 20.97 \times P_1 + 5.86 \times P_2 + 15.11 \times P_3 - 2.84 \times S_1 + 1.90 \times S_2 + 0.93 \times S_3 + 0.34 \times T_1 + 1.70 \times T_2 + 1.36 \times T_3 \quad (3)$$

where

F_c= Compressive strength

$P_{1\text{-}3}$= The levels of phosphazene

$S_{1\text{-}3}$= The levels of silica fume

$T_{1\text{-}3}$= The levels of curing days

The estimation results obtained using equation 3 was given in Figure 1.

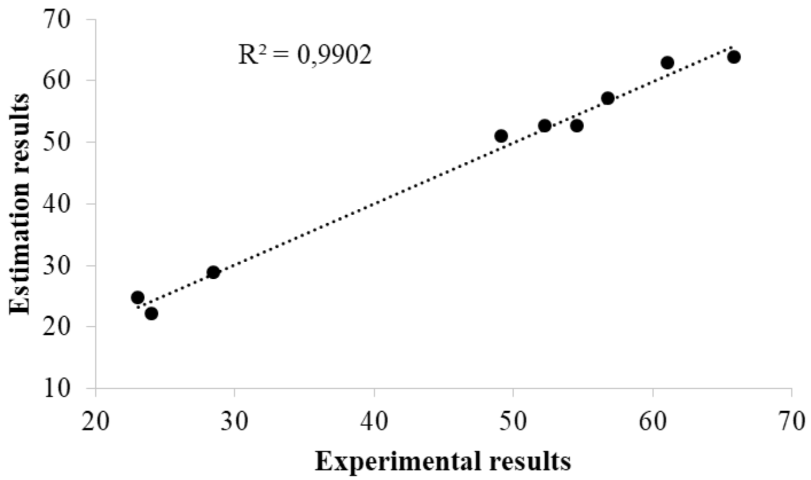

Fig. 1. *The estimation results and experimental results for compressive strength of concrete strengthened with polymer including phosphazene subjected to freeze–thaw cycles*

According to Fig. 1, the proposed equation 3 estimated the compressive strength of concrete strengthened with polymer including phosphazene subjected to the freeze–thaw cycles with 99.02% accuracy. Thus, it was found that this equation can be used to find the compressive strength of concrete containing silica fume strengthened with polymer including phosphazene after subjected to freeze-thaw cycles.

3.2. Ultrasonic pulse velocity

The ultrasonic pulse velocity (UPV) is the determination of the travel time of an ultrasound sent to the concrete (Awal and Shehu, 2015; Lin et al., 2011). If the UPV is large, it thought that the mechanical properties of concrete are good. Furthermore, the UPV is a good method to evaluate the concrete (Al-Rousan, 2015). This method gives an idea the cracks or gaps of the concrete (Güneyisi et al., 2015). The UPV of concrete strengthened with polymer including phosphazene subjected to freeze-thaw cycles were found in the current study. The results were given in Table 6.

Table 6. *The results of UPV of concrete strengthened with polymer including phosphazene subjected to freeze–thaw cycles*

Phosphazene percentage, (%)	Silica fume percent, (%)	Curing time, (Day)	UPV (km/s)
1	1	1	2.58
1	2	2	3.5
1	3	3	3.41
2	1	2	3.98
2	2	3	4.07
2	3	1	4.42
3	1	3	4.24
3	2	1	4.55
3	3	2	4.78

When examined in the table 6, it is understood that the most significant decrease of ultrasonic pulse velocity occurred in samples in which phosphazene was not used. It is understood by this study that impregnation polymer with phosphazene process increases the quality of concrete. Concretes, which are more resistant against freeze-thaw, can be produced by the impregnation of polymer with phospazene.

Taguchi analysis were used to evaluate the effect of each variables on the UPV found in the experimental study. The variables in Table 2 were selected in the calculation of the S/N. The S/N values for the UPV of concrete strengthened with polymer including phosphazene exposed to freeze-thaw cycles were shown in Table 7.

Table 7. *S/N rates of the UPV of concrete strengthened with polymer including phosphazene subjected to freeze–thaw cycles*

	S/N rates		
	Level 1	**Level 2**	**Level 3**
Percentage of phosphazene in polymer, P (%)	10.03	10.38	11.21 [s]
Percentage of silica fume,S (%)	9.20	11.22 [s]	11.21
Curing time, T (day)	8.37	11.21	12.04 [s]

[s] Optimum levels

Mean S/N rate=10.54.

The larger S/N rates must provide the larger ultrasonic pulse velocity. As it can be seen from Table 7, the largest UPV value was obtained from samples that were containing silica fume 5 % at 28 days and used the polymer including phosphazene 2 %. Moreover, Taguchi based multiple regression in predicting the UPV of concrete strengthened with polymer including phosphazene subjected to the freeze–thaw cycles was in the current study. The proposed equation was given bellow.

$$UPV = 3.9478 - 0.784 \times P_1 + 0.209 \times P_2 + 0.576 \times P_3 - 0.348 \times S_1 + 0.092 \times S_2 + 0.256 \times S_3 - 0.098 \times T_1 + 0.139 \times T_2 - 0.041 \times T_3 \quad (4)$$

where

UPV= Ultrasonic pulse velocity

$P_{1\text{-}3}$= The levels of phosphazene

$S_{1\text{-}3}$= The levels of silica fume

$T_{1\text{-}3}$= The levels of curing days

The estimation results obtained using equation 4 was shown in Figure 1.

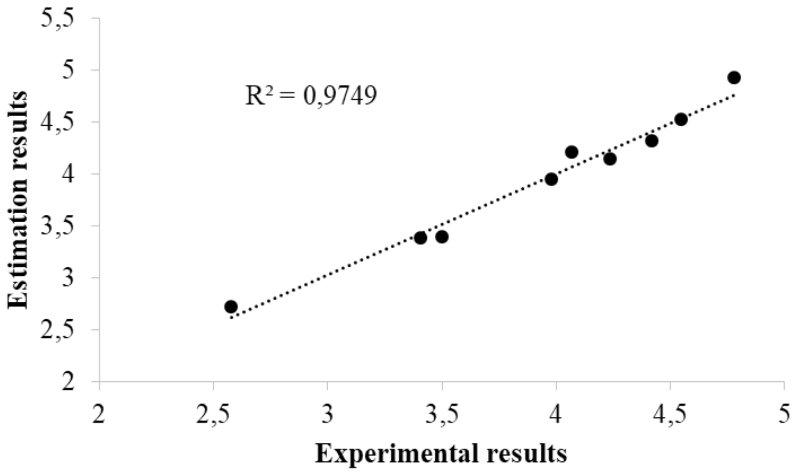

Fig. 2. *The estimation results and experimental results for the UPV*

It can be seen from Fig. 2 that the proposed equation 4 estimated the UPV of concrete strengthened with polymer including phosphazene exposed to the freeze–thaw cycles with 97.49 % accuracy. As a result, it can be said that this equation can be used to find the UPV of concrete the concretes containing silica fume strengthened with polymer including phosphazene after exposed to freeze-thaw cycles.

3.3. The relative dynamic modulus of elasticity

In this study, the relative dynamic modulus of elasticity (RDME) of samples was found using the UPV at the end of 56 freeze-thaw cycle. The equation used in calculating the RDME of samples was given in below (ASTM C666, 2015).

$$RDME = 100 \times \left(\frac{UPV_L}{UPV_F}\right)^2 \quad (5)$$

where

RDME=The relative dynamic modulus of elasticity,

UPV_F= The result of ultrasonic pulse velocity of sample at 0 cycles,

UPV_L= The result of ultrasonic pulse velocity of sample at 56 cycles.

The RDME results of specimens were shown in Fig. 3.

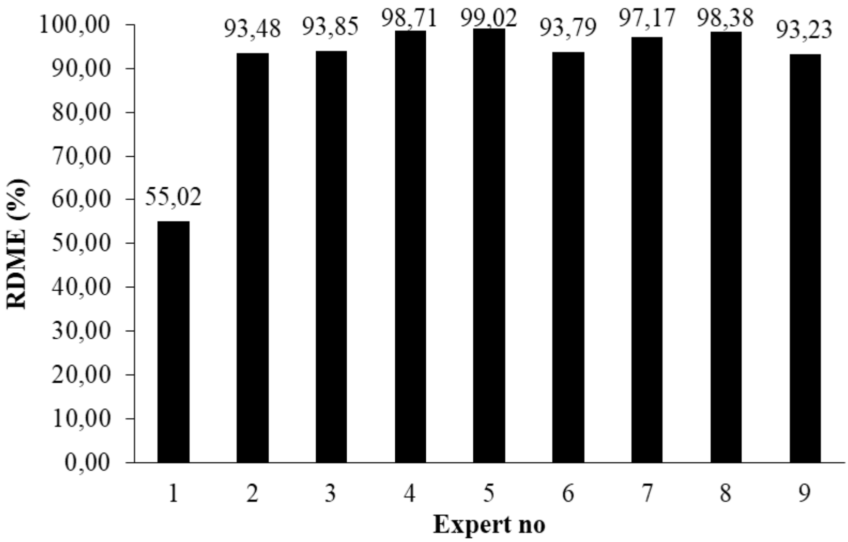

Fig. 3. *RDME results of specimens*

It can be seen from Fig. 3 that the lowest RDME was obtained from specimen in first expert number. The phosphazene level 1 (0%), silica fume level 1 (0%) and curing day level 1 (3 day) were used in this specimen. Moreover, the highest RDME was obtained from specimen in five expert number. The phosphazene level 2 (1%), silica fume level 2 (5%) and curing day level 3 (28 day) were used in this specimen. According to these results, the use of 1% phosphazene and 5 % silica fume in the polymer improved the resistance of concrete against freeze-thaw.

4. CONCLUSIONS

In the current study, the compressive strength and UPV changes of the concretes containing silica fume strengthened with polymer including phosphazene exposed to freeze-thaw cycles were examined and then modelled. In the experimental study to decrease the quantity of experiments and to find the maximum compressive strength and UPV values Taguchi method was used. According to Taguchi analysis, the highest compressive strength was obtained from samples to which cure was applied for 28 days, which contained 5% silica fume and in which polymer containing 1% phosphazene was used. Differently, the highest UPV was obtained in samples to which cure was applied for 28 days, which contained 5% silica fume and in which polymer including 2% phosphazene was used. Besides, the UPV of concretes was deterimed before and after being subjected to freeze-thaw in order to find freeze-thaw damage. The RDME's of samples were calculated. The freeze-thaw damage varied from 0.98% to 44.98 %. It was observed that the polymer impregnation containing phosphazene decreased freeze-thaw damage significantly. In the current study, it was determined that the impregnation of polymer including phosphazene to concrete can be useful in concretes in which freeze-thaw damage may occur. Furthermore, the compressive strength and UPV of concrete exposed to freeze-thaw were modelled using the Taguchi based multiple regression. The proposed equation 3 and 4 estimated the compressive strength and UPV with 99.02 and 97.49% accuracy, respectively.

REFERENCES

Akbas H, Okumus A, Kılıç Z, Hökelek T, Süzen Y, Koç LY, Açık L, Çelik Z B. (2013). Phosphorusenitrogen Compounds Part 27. Syntheses, Structural Characterizations, Antimicrobial and Cytotoxic Activities and Dnainteractions of New Phosphazenes Bearing Secondary Amino and Pendant (4-Fuorobenzyl)Spiro Groups. *European Journal of Medicinal Chemistry*, 70, 294-307.

Al-Rousan, R. Z., Haddad, R. H., & Swesi, A. O. (2015). Repair of shear-deficient normal weight concrete beams damaged by thermal shock using advanced composite materials. *Composites Part B: Engineering*, *70*, 20-34.

Allan, A., & Horn, W. (2006). Some properties of polymer-impregnated cements and concrete. *J Am Ceram Soc*, *54*(6), 282-285.

Allcock, H. (2012). *Phosphorus-nitrogen compounds: cyclic, linear, and high polymeric systems*. Elsevier.

ASTM C666 / C666M-15 (2015). Standard Test Method for Resistance of Concrete to Rapid Freezing and Thawing, ASTM International, West Conshohocken, PA, 2015,

Awal, A. A., & Shehu, I. A. (2015). Performance evaluation of concrete containing high volume palm oil fuel ash exposed to elevated temperature. *Construction and Building Materials*, *76*, 214-220.

BAL H. (1998). Bazı Polimerlerin Harç Ve Betonda Kullanabilirliliğinin Araştırılması. Yüksek Lisans Tezi,.

Bhutta, M. A. R., Maruya, T., & Tsuruta, K. (2013). Use of polymer-impregnated concrete permanent form in marine environment: 10-year outdoor exposure in Saudi Arabia. *Construction and Building Materials*, *43*, 50-57.

Bissonnette, B., & Pigeon, M. (1995). Tensile creep at early ages of ordinary, silica fume and fiber reinforced concretes. *Cement and concrete research*, *25*(5), 1075-1085.

Chen, C. H., Huang, R., Wu, J. K., & Chen, C. H. (2006). Influence of soaking and polymerization conditions on the properties of polymer concrete. *Construction and Building Materials*, *20*(9), 706-712.

Chmielewska, B. (2008). Adhesion strength and other mechanical properties of SBR modified concrete. *International Journal of Concrete Structures and Materials*, *2*(1), 3-8

Chung, C. W., Shon, C. S., & Kim, Y. S. (2010). Chloride ion diffusivity of fly ash and silica fume concretes exposed to freeze–thaw cycles. *Construction and Building Materials*, *24*(9), 1739-1745.

Davim, J. P. (2001). A note on the determination of optimal cutting conditions for surface finish obtained in turning using design of experiments. *Journal of materials processing technology*, *116*(2-3), 305-308.

De Puy GW, Dikeou JT. (1973). Polymer in Concrete. Publication SP- 40, American Concrete Institute, Detroit, Mich.

Gleria M, De Jaeger R. (2004). Phosphazenes: A Worldwide Insight. New York.

Güneyisi, E., Gesoğlu, M., Booya, E., & Mermerdaş, K. (2015). Strength and permeability properties of self-compacting concrete with cold bonded fly ash lightweight aggregate. *Construction and Building Materials*, *74*, 17-24.

Haque, M. N. (1996). Strength development and drying shrinkage of high-strength concretes. *Cement and concrete Composites*, *18*(5), 333-342.

Kalla, P., Rana, A., Chad, Y. B., Misra, A., & Csetenyi, L. (2015). Durability studies on concrete containing wollastonite. *Journal of Cleaner Production*, *87*, 726-734

Koran K, Ozkaya A, Ozen F, Cil E, Arslan M. (2013). Synthesis, Characterization and Biological Evaluation of New Oxime Phosphazenes, *Res Chem Intermed*, 39, 1109-1124.

Koran, K., Özen, F., Torğut, G., Pıhtılı, G., Çil, E., Görgülü, A. O., & Arslan, M. (2014). Synthesis, characterization and dielectric properties of phosphazenes containing chalcones. *Polyhedron*, *79*, 213-220.

Li, Z., Qi, M., Li, Z., & Ma, B. (1999). Crack width of high-performance concrete due to restrained shrinkage. *Journal of materials in civil engineering*, *11*(3), 214-223.

Lilkov, V., Rostovsky, I., Petrov, O., Tzvetanova, Y., & Savov, P. (2014). Long term study of hardened cement pastes containing silica fume and fly ash. *Construction and Building Materials*, *60*, 48-56

Lin, Y., Hsiao, C., Yang, H., & Lin, Y. F. (2011). The effect of post-fire-curing on strength–velocity relationship for nondestructive assessment of fire-damaged concrete strength. *Fire Safety Journal*, *46*(4), 178-185.

Mardani-Aghabaglou, A., Sezer, G. İ., & Ramyar, K. (2014). Comparison of fly ash, silica fume and metakaolin from mechanical properties and durability performance of mortar mixtures view point. *Construction and Building Materials*, *70*, 17-25

Molero, M., Aparicio, S., Al-Assadi, G., Casati, M. J., Hernández, M. G., & Anaya, J. J. (2012). Evaluation of freeze–thaw damage in concrete by ultrasonic imaging. *Ndt & E International*, *52*, 86-94.

Monteny, J., De Belie, N., Yincke, E., Beeldens, A., & Taerwe, L. (2001). Simulation of corrosion in sewer systems by laboratory testing. In *Proceedings-fib-Symposium on Concrete and Environment 2001* (pp. 91-92).

Moreira, P., Aguiar, J. B., & Camões, A. (2006). Systems for superficial protection of concrete. In *ISPIC 2006 international symposium on polymers in concrete. Guimarães, Portugal* (pp. 225-36).

Ogawa, H., Kano, K., Mimura, T., Nagai, K., Shirai, A., & Ohama, Y. (2007). Durability performance of barrier penetrants on concrete surfaces. In *12th International Congress on Polymers In Concrete, Chuncheon-Korea* (pp. 373-82).

Phadke, M. S. (1995). *Quality engineering using robust design*. Prentice Hall PTR.

Pişkin A. Polimer Beton Üretiminde Cam Tozu Kullanılabilirliğinin Araştırılması, (Yüksek Lisans Tezi), Sakarya Üniversitesi Yapı Eğitimi Bölümü, 2010.

Rao, G. A. (1998). Influence of silica fume replacement of cement on expansion and drying shrinkage. *Cement and concrete research*, *28*(10), 1505-1509.

Ross, P. J. (1996) Taquchi Tecniques for Quality Engineering, 2nd edn. New York: McGraw-Hill.

Sabir, B. B. (1997). Mechanical properties and frost resistance of silica fume concrete. *Cement and Concrete Composites*, *19*(4), 285-294.

Satish C, Ohama Y. (1994). Polymers in concrete. Florida: CRC Press.

Shirai, A., Kano, K., Nagai, K., Ide, K., Ogawa, H., & Ohama, Y. (2007). Basic properties of barrier penetrants as polymeric impregnants for concrete surfaces. In *12th International congress on polymers in concrete, Chuncheon, Korea* (pp. 607-615).

Siddique, R. (2011). Utilization of silica fume in concrete: Review of hardened properties. Resources, Conservation and Recycling, 55(11), 923-932

Sidney R, Young JF. (1981). Concrete. Prentice Hall, Inc, Englewood Cliffs. New jersey 07632.

Song, R., Jun, Y. J., Kim, J. I., Jin, C., & Sohn, Y. S. (2005). Synthesis, characterization, and tumor selectivity of a polyphosphazene–platinum (II) conjugate. *Journal of controlled release*, *105*(1-2), 142-150

Sun, W., Zhang, Y. M., Yan, H. D., & Mu, R. (1999). Damage and damage resistance of high strength concrete under the action of load and freeze-thaw cycles. *Cement and Concrete Research*, *29*(9), 1519-1523.

Tanaka, T., Tsuruta, K., & Naitou, T. (2002, October). Development and application of polymer impregnated concrete. In *Proc of the first fib congress* (pp. 347-54).

TSE CEN/TR 15177 (2012). Testing the freeze-thaw resistance of concrete - Internal structural damage.

Tümer, Y., Asmafiliz, N., Kılıç, Z., Hökelek, T., Koç, L. Y., Açık, L., ... & Yavuz, M. (2013). Phosphorus–nitrogen compounds: Part 28. Syntheses, structural characterizations, antimicrobial and cytotoxic activities, and DNA interactions of new phosphazenes bearing vanillinato and pendant ferrocenyl groups. *Journal of Molecular Structure*, *1049*, 112-124.

Vejmelková, E., Koňáková, D., Kulovaná, T., Keppert, M., Žumár, J., Rovnaníková, P., ... & Černý, R. (2015). Engineering properties of concrete containing natural zeolite as supplementary cementitious material: Strength, toughness, durability, and hygrothermal performance. *Cement and Concrete Composites*, *55*, 259-267

Whiting, D., & Kline, D. E. (1976). Theoretical predictions of the elastic moduli of polymer-impregnated hardened cement paste and mortars. *Journal of Applied Polymer Science*, *20*(12), 3353-3363

Yalçın F. (1998). Polimer Emdirilmiş Betonun Bazı Mekanik Özelliklerinin İncelenmesi. Yüksek Lisans Tezi, Sivas.

Yang, Z., Shi, X., Creighton, A. T., & Peterson, M. M. (2009). Effect of styrene–butadiene rubber latex on the chloride permeability and microstructure of Portland cement mortar. *Construction and Building Materials*, *23*(6), 2283-2290.

Yazıcı, H. (2008). The effect of silica fume and high-volume Class C fly ash on mechanical properties, chloride penetration and freeze–thaw resistance of self-compacting concrete. *Construction and Building Materials*, *22*(4), 456-462.

Yilmaz, Ö., Aslan, F., Öztürk, A. İ., Vanli, N. S., Kirbağ, S., & Arslan, M. (2002). Antimicrobial and biological effects of N-diphenylphosphoryl-P-triphenylmonophosphazene-II and di (o-tolyl) phosphoryl-P-tri (o-tolyl) monophosphazene-III on bacterial and yeast cells. *Bioorganic chemistry*, *30*(5), 303-314.

Zhang, P., & Li, Q. F. (2013). Effect of polypropylene fiber on durability of concrete composite containing fly ash and silica fume. *Composites Part B: Engineering*, *45*(1), 1587-1594.

Chapter 19

FREQUENT FAULTS ON THE DC SIDE IN PHOTOVOLTAIC SYSTEMS

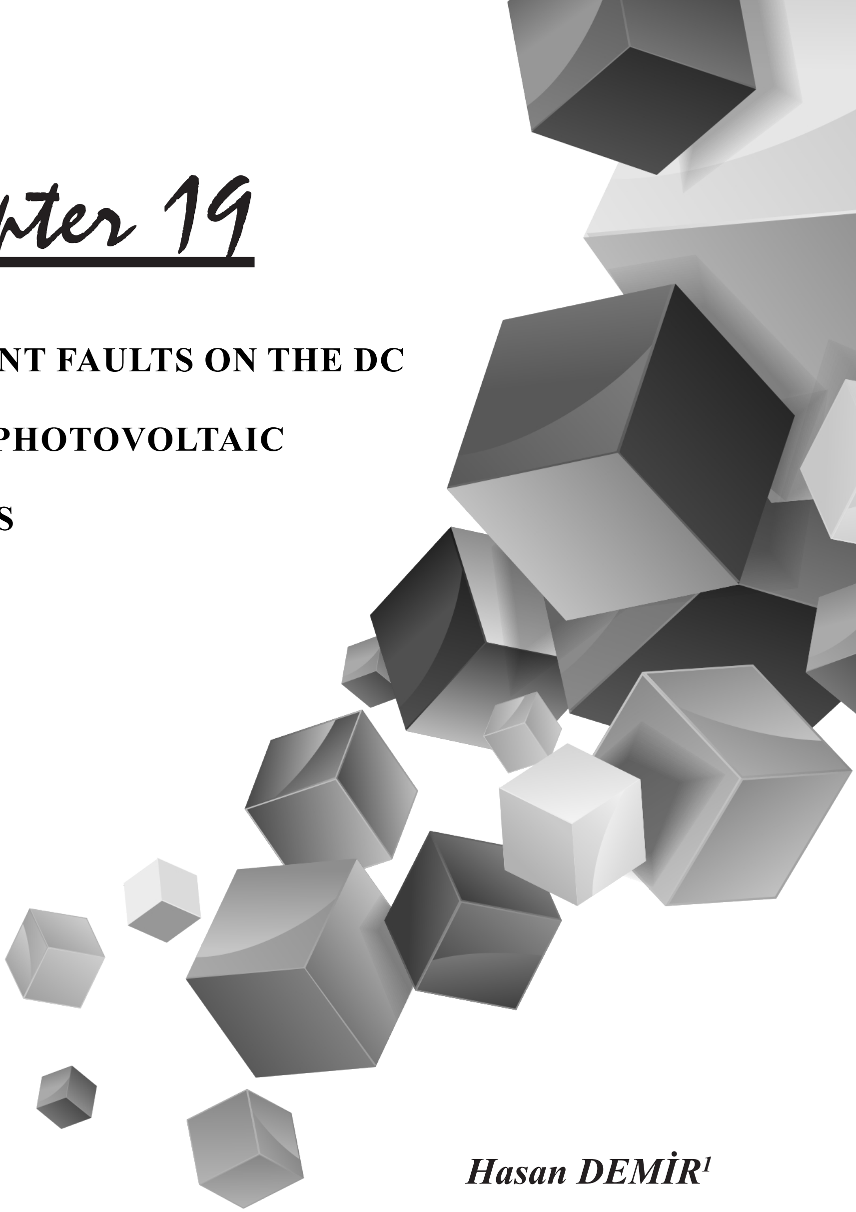

Hasan DEMİR[1]

1 Dr. Hasan Demir, Aksaray University, Department of Mechatronic, Aksaray, Turkey. hasandemir@aksaray.edu.tr

1. Introduction

Depending on the developing industry and modern life in the world, the need for energy is increasing day by day. Traditionally, the energy is provided from hydro carbon sources, nuclear sources, water sources, etc. In order to meet the increasing energy need and to reduce the damage caused by energy production to nature, the tendency towards green power technologies has increased (Alsafasfeh et al. 2018; Despotou et al. 2010; IEA 2007; Surek 2003). Green energy technology consists of renewable energy sources such as solar, wind, hydro, tidal. The best method among renewable energy sources and the method whose number is rapidly increasing is to obtain electricity from the sun. Solar photovoltaic panels (PV) are systems that convert solar energy into electrical energy. Despite the developing technology today, the efficiency of PV is between 15 and 19 percent (Coşgun and Uzun 2017). PVs are installed outdoors and are exposed to environmental factors such as rain and snow. This situation can reduce the performance of PVs depending on both environmental and electrical reasons. Studies have shown that the annual power loss due to faults is 18.9 percent (Firth, Lomas, and Rees 2010). Power losses due to faults increase energy generation costs.

Faults that occur in PVs affect the normal operating performance of the panels. In order to minimize the efficiency losses caused by faults, faults should be detected. In this study, a brief summary about PVs is given and various faults occurring in the DC side of PVs are explained.

2. Overview of Photovoltaic Panel

As a result of a series or parallel connection of many solar cells shown in Figure 1, PV modules are created. Solar cells consist of different semiconductor such as monocrystalline silicon, polycrystalline silicon, amorphous silicon, Cadmium telluride and copper indium selenide / sulphide (Coşgun and Uzun 2020). Bypass diodes are available between the cell lines to prevent the cells overheating by acting as a receiver while generating energy in sunlight.

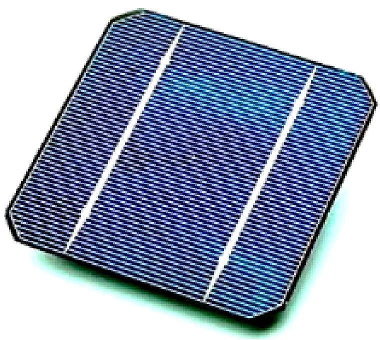

Figure 1. Solar cell (Zhao 2010)

PVs are used in many areas today to meet high energy needs. Besides this, solar cells are used to meet low energy need such as calculators, garden lights. There are many environmental, meteorological and electrical reasons that affect the operation of PVs and cause faults on the DC side.

3. PhotovoltaIc System FaIlures In DC Sıde

We can generally divide the faults that occur in PV into 2 parts: DC side and AC side (Davarifar, Rabhi, and Hajjaji 2013). The basic elements of a solar energy cycle are PV array, DC / AC converter and grid connect inverter. DC / AC converter divides the system into two as DC and AC. The faults on the DC side are explained in this study.

Figure 2. Block Schematic of Solar Energy Conversion System (Madeti and Singh 2017)

3.1. Photovoltaic Ground Fault

PV arrays consist of non-current carrying parts such as modulated frames, metal enclosures, distribution panels and mounting racks. These parts are conductive but do not carry current during normal operation. Contact of electrically carrying parts with these non-electric parts can cause electrical damage. In order to prevent these damages, all these non-electric but conductive parts must be connected together to ground. Figure 3 shows a grounded PV system using Equipment grounding conductor (Bower and Wiles 1994; Zhao et al. 2011, 2013).

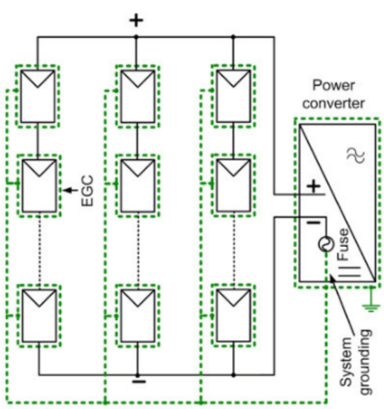

Figure 3. Schematic diagram of grounded PV systems (Bower and Wiles 1994).

3.2. Diodes Fault

While a bypass diode prevents reverse voltage caused by shadowing in the panels, the block diode prevents reverse currents. As a result of over long time exposure to partial shadowing, the diode faults occur in PV panels (Rezgui et al. 2014; Winter, Sizmann, and Vant-Hull 1991). Bypass diode compensates for power losses caused by ghosting. The reverse current is the reason of the hot spot on the panels and it could give seriously damage PV panels. Other reason of diodes faults is the reverse connection or disconnection (Köntges et al. 2014).

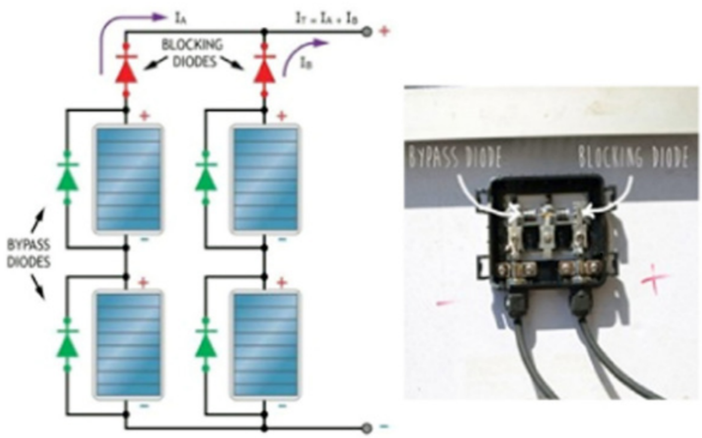

(a) (b)

Figure 4. a) Shematic block of bypass and blocking diodes, b) Junction boxes (Mellit, Tina, and Kalogirou 2018).

3.3. Junction Box Fault

Junction box faults are among the most important issues encountered in the field and during testing. Degradation, especially in hot and humid climates, increases the corrosion contact resistance. As a result of this event, the temperature increases at the contact leads and the junction box may melt and erode. Sparking can occur in junction box failure and the PV arrays can be damaged (Chang et al. 2015; Triki-Lahiani, Bennani-Ben Abdelghani, and Slama-Belkhodja 2018). Figure 5 shows PVs damaged by junction box faults.

Figure 5. Junction box faults (Mellit et al. 2018)

3.4. PV Module Fault

PV module faults are usually physical faults. These faults are caused by corrosion, problems in the grounding line, leakage currents in the module, faults in the production phase, and short circuits in the module. Some of faults cause electrical damage and there is a risk of fire. These faults affect system performance and reduce productivity. Figure 6a shows broken glass on the PV module, Figure 6b shows corrosion, Figure 6c and 6d shows bubbles (Köntges et al. 2014; Munoz et al. 2011; Stellbogen 1993).

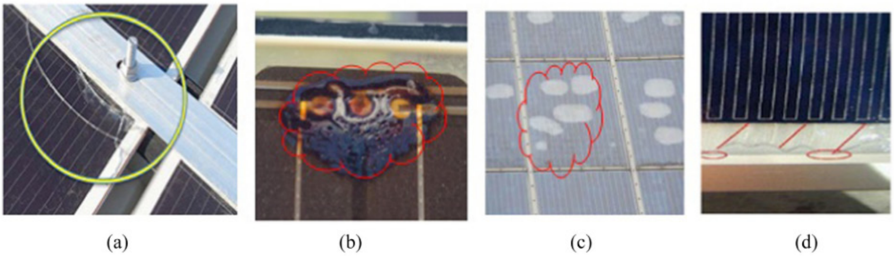

Figure 6. a) Damaged glass, b) corrosion, c) bubbles and d) degradation (Mellit et al. 2018).

3.5. Mismatch Fault

Mismatch faults are caused by changes in electrical parameters between the cell or cells. The main reason for the mismatch fault is that some solar cells cannot generate electricity. Some cells in the PV module cannot produce electricity due to shading, temperature, solar irradiation, while others can. This causes the cell, which cannot generate electricity, to heat up and cause irreversible damage. We can categorize incompatibility faults as temporary and permanent.

3.5.1. Permanent Mismatches

Permanent mismatches is caused by permanent faults in some cells on the panels. Permanent deterioration of some solar cells creates electrical incompatibility with other cells. The most common faults that cause permanent mismatch, such as hot spot, discoloration, delamination, soldering, will be examined under separate headings (Davarifar et al. 2013; Jiang and Maskell 2015).

3.5.2. Temporary Mismatches

Temporary shadowing on PV modules causes mismatch faults. Climatic conditions such as snow, dust and clouds cause shadowing on the panels. In addition, due to the movement of the sun, obstacles such as buildings and trees cause shading on the PV panels.

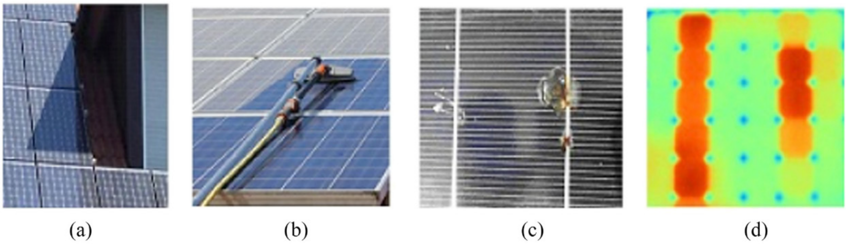

Figure 7. a) shading, b) dusting, c) solar cell damaged by hot spot, d) hot spots detected by the infrared method (Mellit et al. 2018).

3.6. Hot Spot Faults

Hot spot fault may occur because a solar cell in the PV module cannot generate electricity for any reason. The voltage of the cell that cannot produce current drops and the cell starts to work in reverse bias. As a result, performance starts to decline. Hot spot faults are caused by situations such as high resistance, cold solder points, contamination, dust accumulation, insulation, degradation, partial shadow (GREEN et al. 2012; Kalogirou, Agathokleous, and Panayiotou 2013; Massi Pavan, Mellit, and De Pieri 2011; Solórzano and Egido 2013). In addition, hot spots may occur in cells with damaged bypass diodes and solar panels may be damaged if the heated cell is not intervened. Thermal imaging is generally used to detect hot spot cells (Simon and Meyer 2010; Yang et al. 2010). Hot spots in PV is shown in Figure 8.

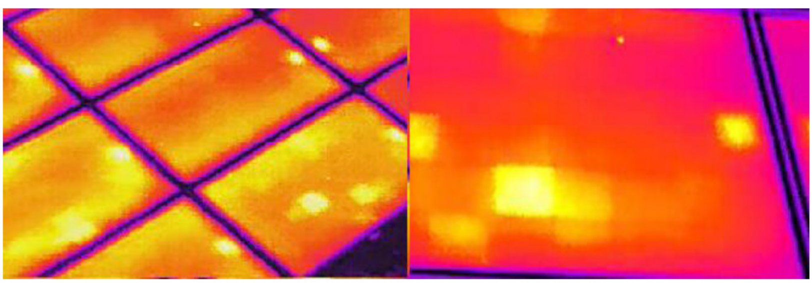

Figure 8. Hot Spots in PV (Alsafasfeh et al. 2018).

3.7. Discoloration and Encapsulant Yellowing

Discoloration occurs by photothermal decomposition of ethyl vinyl acetate (EVA) encapsulant as a result of prolonged exposure to UV rays and high temperatures. Generally, hot and humid environmental conditions are the main cause of discoloration. Visually detectable discoloration causes corrosion, leading to a decrease in series resistance (Park et al. 2013; Sinha et al. 2020; Wohlgemuth, Kempe, and Miller 2013). Examples of discoloration are given in Figure 9.

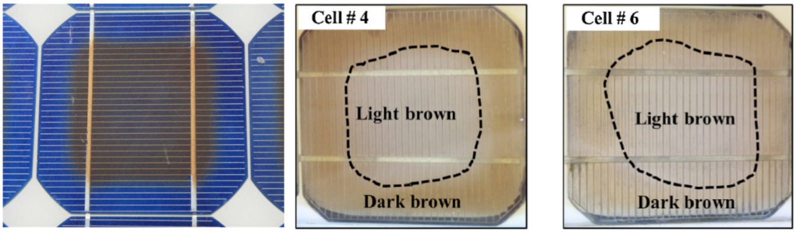

Figure 9. Discolorations (Park et al. 2013; Wohlgemuth et al. 2013).

Yellowing is usually caused by the deterioration of EVA or the deterioration of the adhesive between the solar cell and the glass sheet. The reasons for yellowing are UV rays, humidity and heat. This deterioration causes the solar panel to turn yellow or brown in colour. As a result of the yellowing fault, water penetrates into the solar panel due to the loss of the property of the adhesive between the glass and solar panel in the photovoltaic panel (Munoz et al. 2011; Oreski and Wallner 2009). Yellowing faults in the PV module are shown in Figure 10.

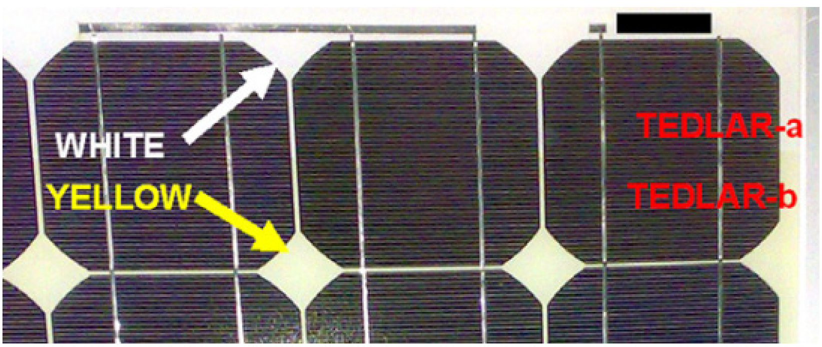

Figure 10. Yellowing area in PV module (Munoz et al. 2011; Oreski and Wallner 2009).

3.8. Thermal Fault

Thermal imaging is based on the principle of detecting infrared radiation caused by the thermal effect. Thermal imaging shows the temperature differences in the environment being displayed. Bubbles can occur behind the PV modules due to adhesive deterioration by the high temperatures. These situations that occur as a result of the high temperature effect can be called thermal faults. Fault detection can be made with thermal imaging due to temperature differences. Figure 11 shows the temperature differences on the PV module due to bubble and fractures by thermal imaging (Munoz et al. 2011).

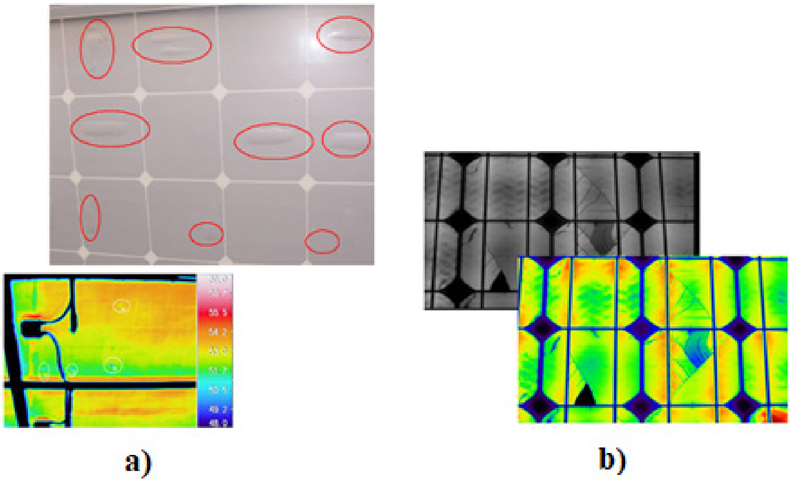

Figure 11. a) Bubbles and thermal image behind the PV module, b) Fractures and thermal image on the PV module (Munoz et al. 2011).

3.9. Delamination

Delamination is the separation between layers on the PV module. There are encapsulant (EVA) and solar cell layers on the PV module. Especially in hot and humid climates, water droplets are formed between EVA and solar cell. Corrosion occurs due to water droplets and decomposition occurs between layers. In addition, corrosion affects the solder connections and cell interconnections, increasing the resistance and causing power loss in the PV module. Figure 12 shows the cross-sectional view of the area where delamination occurred on the PV module (Berman, Biryukov, and Faiman 1995; Gxasheka, Van Dyk, and Meyer 2005; Kempe 2006; Morita et al. 2003; Wenham et al. 2011).

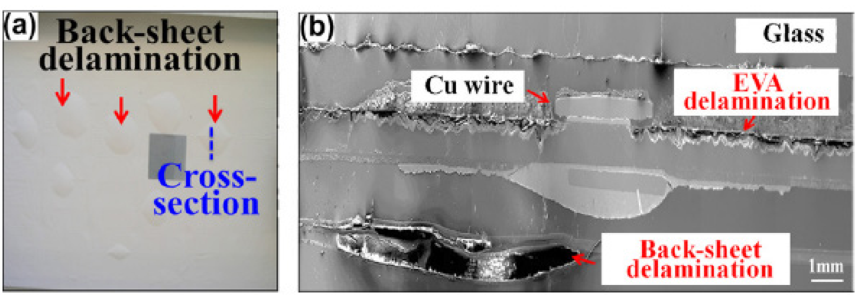

Figure 12. Delaminated area; a)Back-sheet, b) the cross-sectional view of the area (Park et al. 2013).

3.10. Anti-reflective Coating Faults

PV modules are covered with an anti-reflective coating to prevent the reflection of sunlight. This coating allows more sunlight to reach the active area of the solar cells and increases performance. Anti-reflection coating is made using such as silicon dioxide, aluminium nitride and silicon nitride materials. Solar-induced ultraviolet radiation is the main reason for the degradation of the anti-reflection coating. The colour of the reflective coating that started to deteriorate changes and the sunlight reaching the cell starts to decrease (Krugel et al. 2013; Munoz et al. 2011).

Anti-reflection coatings made using different materials increase the performance of PV. While this is an advantage, as a disadvantage, the coating deteriorates over time and reduces the performance. Hot spots may occur on the PV module in the later stages of deterioration.

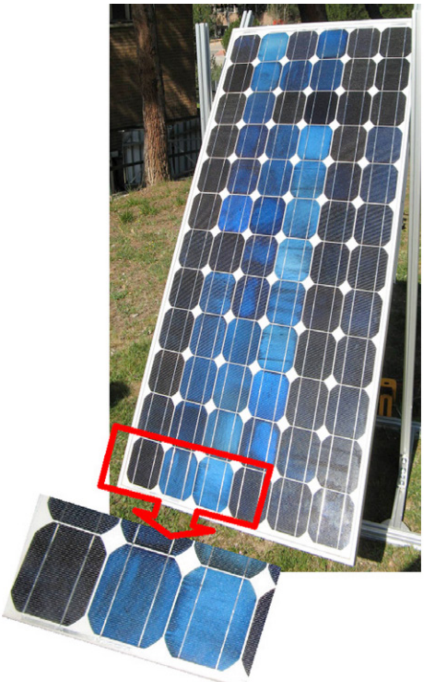

Figure 13. The colour change due to deterioration of the anti-reflective coating in PV module (Munoz et al. 2011).

3.11. PV's Package Degradation

Since PV modules are located in outdoor conditions, they can be exposed to physical or chemical deterioration over time. Glass breakage, dielectric breakdown, and back sheet cracking are examples of these deteriorations. Disturbances that occur cause leakage current faults and ground faults in modules. Hot spots occur on the modules as a result of package degradation. Figure 14 shows the hot spot caused by the crack on the panel (Spagnolo et al. 2012).

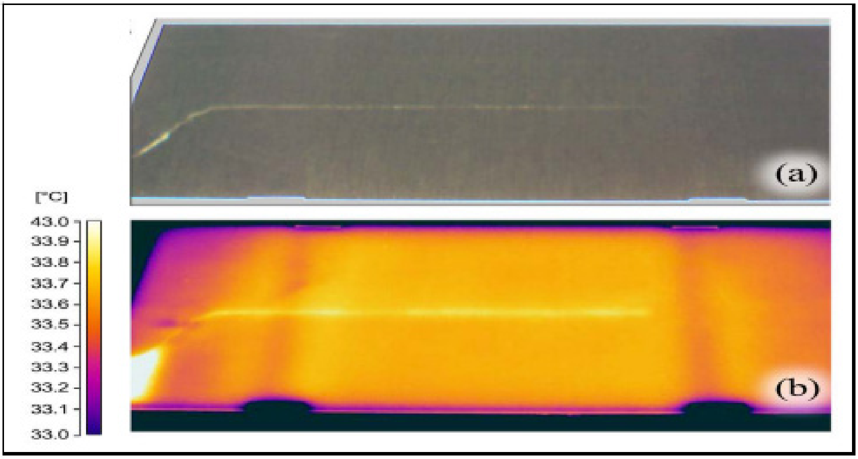

Figure 14. The hot spot caused by the crack on the panel (Spagnolo et al. 2012).

3.12. Soldering Faults

Soldering faults are usually caused by corrosion. Corrosion and cracks may occur in PV modules that work for a long time. The deterioration of solder joint increases the resistance and affects cell- interconnect bus bars, and resistances in junction-box terminations (Park et al. 2013). Figure 15 shows solder joint degradation caused by corrosion.

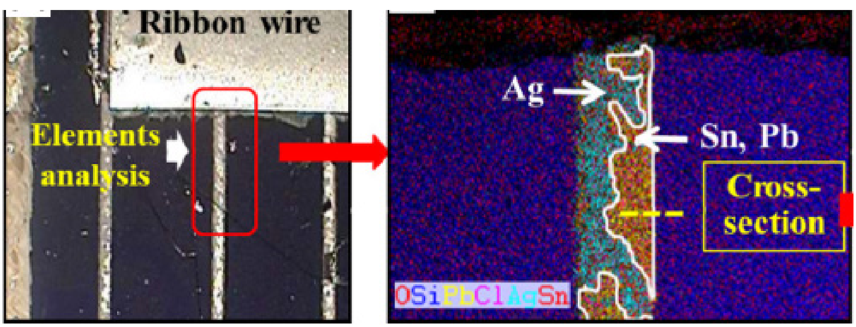

Figure 15. The corrosion of the solder joint (Park et al. 2013).

Since solder joint breakdown increases the resistance, it affects the performance of the PV module and reduces the power. In addition, it causes an increase in temperature and causes a hot point on the modules. Figure 16 shows the hot point formed on the module due to the increasing resistance (Spagnolo et al. 2012).

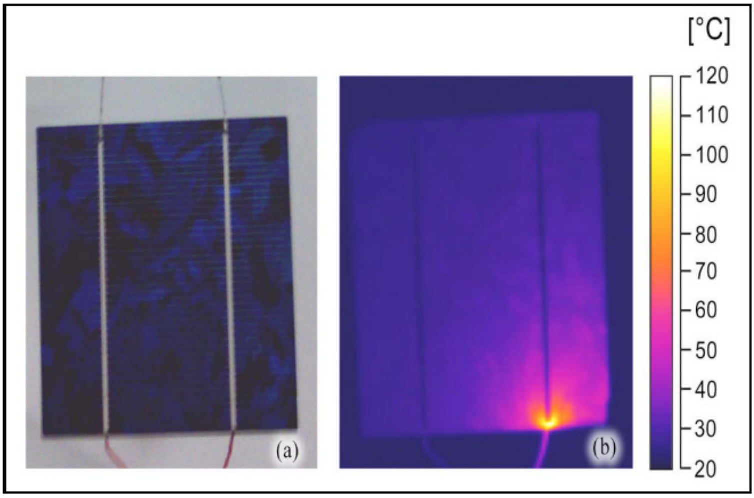

Figure 16. the hot point formed on the module due to the increasing resistance (Spagnolo et al. 2012).

4. Conclusion

Today, PV modules are the key elements of clean and renewable energy production from solar energy. In PV plants, the reliability and profitability of the enterprise is one of the most important issues, and electricity production with PV modules is increasing day by day. This increase has made the faults that cause power losses in PV modules an important issue and the faults have increased the costs of enterprises. Faults in PV modules can occur for a number of reasons. Majority of faults are caused by environmental conditions such as temperature, humidity and the structure of PV modules. Literature researches are helpful resources to understand these faults. In this study, important faults on the DC side of a Solar Energy Conversion System are explained. Causes of faults and situations that may occur as a result are mentioned. This study has been prepared to guide researchers doing research in the scientific field and to explain the faults experienced in small or large-scale PV plants.

REFERENCES

Alsafasfeh, Moath, Ikhlas Abdel-Qader, Bradley Bazuin, Qais Alsafasfeh, and Wencong Su. 2018. "Unsupervised Fault Detection and Analysis for Large Photovoltaic Systems Using Drones and Machine Vision." *Energies* 11(9):1–18.

Berman, David, Sergey Biryukov, and David Faiman. 1995. "EVA Laminate Browning after 5 Years in a Grid-Connected, Mirror-Assisted, Photovoltaic System in the Negev Desert: Effect on Module Efficiency." *Solar Energy Materials and Solar Cells* 36(4):421–32.

Bower, Ward I. and John C. Wiles. 1994. "Analysis of Grounded and Ungrounded Photovoltaic Systems." *Conference Record of the IEEE Photovoltaic Specialists Conference* 1:809–12.

Chang, Maoyi, Chienyu Chen, C. H. Hsueh, W. J. Hsieh, Eva Yen, K. L. Ho, H. P. Chuang, C. Y. Lee, and Haomin Chen. 2015. "The Reliability Investigation of PV Junction Box Based on 1GW Worldwide Field Database." Pp. 1–4 in *2015 IEEE 42nd Photovoltaic Specialist Conference, PVSC 2015*.

Coşgun, Atıl Emre and Yunus Uzun. 2017. "Thermal Fault Detection System for Pv Solar Modules." *Electrical and Electronics Engineering: An International Journal* 06(03):09–15.

Coşgun, Atıl Emre and Yunus Uzun. 2020. "Thermal Monitoring System For a Pv Solar Module." (August 2016).

Davarifar, Mehrdad, Abdelhamid Rabhi, and Ahmed El Hajjaji. 2013. "Comprehensive Modulation and Classification of Faults and Analysis Their Effect in DC Side of Photovoltaic System." *Energy and Power Engineering* 05(04):230–36.

Despotou, Eleni, Adel El Gammal, Benjamin Fontaine, Daniel Fraile Montoro, Marie Latour, Sophie Lenoir, Gaeten Masson, Patricia Philbin, and Pieterjan Van Buggenhout. 2010. "Global Market Outlook for Photovoltaics until 2014." *EPIA*, 28.

Firth, S. K., K. J. Lomas, and S. J. Rees. 2010. "A Simple Model of PV System Performance and Its Use in Fault Detection." *Solar Energy* 84(4):624–35.

GREEN, MA, K. EMERY, Y. HISHIKAWA, W. WARTA, ED DUNLOP, DAR BARKHOUSE, O. GUNAWAN, T. GOKMEN, TK TODOROV, and DB MITZI. 2012. "Solar Cell Efficiency Tables (Version 40)." *Ieee Trans Fuzzy Syst* 20(6):1114–29.

Gxasheka, A. R., E. E. Van Dyk, and E. L. Meyer. 2005. "Evaluation of Performance Parameters of PV Modules Deployed Outdoors." *Renewable Energy* 30(4):611–20.

IEA. 2007. "COST AND PERFORMANCE TRENDS IN GRID-CONNECTED PHOTOVOLTAIC SYSTEMS AND CASE STUDIES."

Jiang, Lian Lian and Douglas L. Maskell. 2015. "Automatic Fault Detection and Diagnosis for Photovoltaic Systems Using Combined Artificial Neural

Network and Analytical Based Methods." *Proceedings of the International Joint Conference on Neural Networks* 2015-Septe:1–8.

Kalogirou, Soteris A., Rafaela Agathokleous, and Gregoris Panayiotou. 2013. "On-Site PV Characterization and the Effect of Soiling on Their Performance." *Energy* 51:439–46.

Kempe, Michael D. 2006. "Modeling of Rates of Moisture Ingress into Photovoltaic Modules." *Solar Energy Materials and Solar Cells* 90(16):2720–38.

Köntges, M., S. Kurtz, C. E. Packard, U. Jahn, K. Berger, K. Kato, T. Friesen, H. Liu, and M. Van Iseghem. 2014. *Review of Failures of Photovoltaic Modules*.

Krugel, Georg, Aashish Sharma, Winfried Wolke, Jochen Rentsch, and Ralf Preu. 2013. "Study of Hydrogenated AlN as an Anti-Reflective Coating and for the Effective Surface Passivation of Silicon." *Physica Status Solidi - Rapid Research Letters* 7(7):457–60.

Madeti, Siva Ramakrishna and S. N. Singh. 2017. "A Comprehensive Study on Different Types of Faults and Detection Techniques for Solar Photovoltaic System." *Solar Energy* 158(August):161–85.

Massi Pavan, A., A. Mellit, and D. De Pieri. 2011. "The Effect of Soiling on Energy Production for Large-Scale Photovoltaic Plants." *Solar Energy* 85(5):1128–36.

Mellit, A., G. M. Tina, and S. A. Kalogirou. 2018. "Fault Detection and Diagnosis Methods for Photovoltaic Systems: A Review." *Renewable and Sustainable Energy Reviews* 91(February):1–17.

Morita, K., T. Inoue, H. Kato, I. Tsuda, and Y. Hishikawa. 2003. "In: Photovoltaic Energy Conversion." Pp. 1948–51 in *In: Photovoltaic Energy Conversion*. OSAKA.

Munoz, M. A., M. C. Alonso-García, Nieves Vela, and F. Chenlo. 2011. "Early Degradation of Silicon PV Modules and Guaranty Conditions." *Solar Energy* 85(9):2264–74.

Oreski, G. and G. M. Wallner. 2009. "Evaluation of the Aging Behavior of Ethylene Copolymer Films for Solar Applications under Accelerated Weathering Conditions." *Solar Energy* 83(7):1040–47.

Park, N. C., J. S. Jeong, B. J. Kang, and D. H. Kim. 2013. "The Effect of Encapsulant Discoloration and Delamination on the Electrical Characteristics of Photovoltaic Module." *Microelectronics Reliability* 53(9–11):1818–22.

Rezgui, W., NK Mouss, LH Mouss, MD Mouss, Y. Amirat, and M. Benbouzid. 2014. "Faults Modeling of the Impedance and Reversed Polarity Types within the PV Generator." Pp. 1–6 in *Proceedings of the 3rd International Symposium on Environmental Friendly Energies and Applications (EFEA)*.

Simon, Michael and Edson L. Meyer. 2010. "Detection and Analysis of Hot-Spot Formation in Solar Cells." *Solar Energy Materials and Solar Cells* 94(2):106–13.

Sinha, Archana, Hamsini Gopalakrishna, Arun Bala Subramaniyan, Deepak Jain, Jaewon Oh, Dirk Jordan, and Govinda Samy Tamizhmani. 2020. “Prediction of Climate-Specific Degradation Rate for Photovoltaic Encapsulant Discoloration.” *IEEE Journal of Photovoltaics* 10(4):1093–1101.

Solórzano, J. and M. A. Egido. 2013. “Automatic Fault Diagnosis in PV Systems with Distributed MPPT.” *Energy Conversion and Management* 76:925–34.

Spagnolo, G. Schirripa, P. Del Vecchio, G. Makary, D. Papalillo, and A. Martocchia. 2012. “A Review of IR Thermography Applied to PV Systems.” *2012 11th International Conference on Environment and Electrical Engineering, EEEIC 2012 - Conference Proceedings* 879–84.

Stellbogen, Dirk. 1993. “Use of PV Circuit Simulation for Fault Detection in PV Array Fields.” *Conference Record of the IEEE Photovoltaic Specialists Conference* 1302–7.

Surek, Thomas. 2003. “Progress in U . S . Photovoltaics :” *3rd World Conference on Photovoaltic Energy Conversion* 2507–12.

Triki-Lahiani, Asma, Afef Bennani-Ben Abdelghani, and Ilhem Slama-Belkhodja. 2018. “Fault Detection and Monitoring Systems for Photovoltaic Installations: A Review.” *Renewable and Sustainable Energy Reviews* 82(March):2680–92.

Wenham, S. R., M. A. Green, M. E. Watt, R. Corkish, and A. Sproul. 2011. *Applied Photovoltaics*. Routledge.

Winter, C. J., Rudolf L. Sizmann, and Lorin L. (Eds. .. Vant-Hull. 1991. *Solar Power Plants*. Springer-Verlag Berlin Heidelberg.

Wohlgemuth, John H., Michael D. Kempe, and David C. Miller. 2013. “Discoloration of PV Encapsulants.” *Conference Record of the IEEE Photovoltaic Specialists Conference* 3260–65.

Yang, Hong, Wenwu Xu, He Wang, and Mohan Narayanan. 2010. “Investigation of Reverse Current for Crystalline Silicon Solar Cells-New Concept for a Test Standard about the Reverse Current.” *Conference Record of the IEEE Photovoltaic Specialists Conference* 2806–10.

Zhao, Ye. 2010. “Fault Analysis in Solar Photovoltaic Arrays.” Northeastern University.

Zhao, Ye, Brad Lehman, Jean François De Palma, Jerry Mosesian, and Robert Lyons. 2011. “Challenges to Overcurrent Protection Devices under Line-Line Faults in Solar Photovoltaic Arrays.” *IEEE Energy Conversion Congress and Exposition: Energy Conversion Innovation for a Clean Energy Future, ECCE 2011, Proceedings* 20–27.

Zhao, Ye, Jean Francois De Palma, Jerry Mosesian, Robert Lyons, and Brad Lehman. 2013. “Line-Line Fault Analysis and Protection Challenges in Solar Photovoltaic Arrays.” *IEEE Transactions on Industrial Electronics* 60(9):3784–95.

Chapter 20

HOT-AIR AND MICROWAVE-ASSISTED FOAM-MAT DRYING OF AVOCADO

Ayşe Nur YÜKSEL[1]

Gülşah ÇALIŞKAN KOÇ[2]

1 Asst. Prof. Dr. Ayşe Nur YÜKSEL, Alanya Hamdullah Emin Paşa University, Faculty of Arts and Design, Department of Gastronomy and Culinary Arts, 07400, Alanya, Antalya, Turkey

2 Dr. Gülşah ÇALIŞKAN KOÇ. Alanya Hamdullah Emin Paşa University, Faculty of Arts and Design, Department of Gastronomy and Culinary Arts, 07400, Alanya, Antalya, Turkey

1. Introduction

Avocado (*Persea americana* Mill.) is an oleaginous fruit which belongs to *Lauraceae* family and grows in tropical regions. It is consumed all over the world. The production of avocado increased in two decades, in 2016 5.5 million of tones of avocado produced in the world. Mexico is the major producer with 1.9 million tones (Colombo & Papetti, 2019). Avocado is very rich in nutrition as vitamins, proteins, carotenoids, lipids, polyphenols, unsaturated fatty acids and fibers (Ali et al., 2008; Araujo, Rodriguez-Jasso, Ruiz, Pintado, & Aguilar, 2018).

Drying is the most common used method to increase the shelf-life of fruits and use of these products in different food formulations. Foam mat drying is a technique where liquid or semi-liquid foods are whipped in order to obtain a stable foam. The air is trapped in foam by the presence of foaming agent and stabilizers, then foam is dried. Drying can be performed by using various methods as hot-air, microwave, vacuum and freeze-drying techniques (Thuwapanichayanan, Prachayawarakorn, & Soponronnarit, 2008). Foam-mat drying provides simple and inexpensive drying, accelerated drying rates at lower temperatures and the powder which is produced is tend to rehydrate instantly in cold water with enhanced product quality (Kadam & Balasubramanian, 2011). As foaming agent, gelatin, egg albumin, carboxymethyl cellulose, glycerol mono stearate (GMS), methyl cellulose, soy protein isolate, whey protein concentrate and xanthan gum can be used. GMS was used in the studies of Chakraborty, Mazumder, and Banerjee (2017) and Zheng et al. (2013) for foam-mat drying of potato and berry puree, respectively. Kadam and Balasubramanian (2011) obtained tomato powder by hot-air foam-mat drying with adding various percentages of egg albumin (0-20 %, w/w). In literature, there are studies about foam-mat drying of different kinds of fruits and vegetables in which drying methods e.g., air, freeze and microwave and foaming agents used were different (Qadri, Srivastava, & Yousuf, 2019; Sangamithra, Venkatachalam, John, & Kuppuswamy, 2015).

There is no investigation in the literature about the foam-mat drying of avocado puree. Therefore, this study aimed to investigate how the change of temperature and power intensity effect the drying rate and time during hot-air and microwave drying processes, respectively, to calculate the activation energy for both drying methods and to find the best fitted thin-layer drying models for microwave and hot-air dryings of avocado-foam by using statistical parameters.

2. Materials and methods

2.1 Materials

The mature avocados and commercial pasteurized liquid egg whites were obtained from upper market in Alanya, Turkey. The mature avocados were peeled and the puree was obtained by using home type kitchen blender (1000W power, SHB 3107, Sinbo, Turkey).

2.2 Methods

2.2.1 Foam Preparation

150g of avocado puree and 30% (by weight) of liquid egg white as a foaming agent were added to the glass beaker (2 liters). In order to obtain avocado foam, the home type kitchen blender (at a maximum speed of 1000W power, SHB 3107, Sinbo, Turkey) was used for 6 minutes. The total amount of avocado foam was 20.00±0.20g for each drying experiment. Samples were placed flat as a slab 10.50 cm x 0.2 cm diameter x thickness so drying occured from one side.

2.2.2 Hot-Air Drying

The avocado foam was dried in a convective oven (Memmert, UF 110, Germany) at 60, 70 and 80°C temperatures and at 20% ventilation rate. The weight loss was measured for every 5 min until the constant weight was reached.

2.2.3 Microwave Drying

The microwave drying process (Arçelik MD574, Turkey) were performed at 120, 460 and 700W microwave powers. Avocado foam was removed periodically (10s intervals) from the microwave oven and weighed. When the change in the mass of the samples dropped to 0.01 (g) between the two measurements, experiments were finished.

2.3 Mathematical modeling of drying data

The moisture ratio (MR) was computed as $(m_t-m_e)/(m_i-m_e)$ where m_t is the moisture content at time t, m_i and m_e are the initial and equilibrium moisture contents (kg/kg dry solid (DS)), respectively. The calculation of drying rate (R) was made as $(-L_s/A)*((X_{t+1}-X_t)/(t_{t+1}-t_t))$, where R is the drying rate (kg/ m^2*h); L_s is the weight of dry solid (kg); A is the drying area (m^2); X_t is the moisture content at specific time (kg/kg DS) and t is time (h).

Moisture ratio as a function of drying time was determined by using five thin-layer drying models as Page (Eq. (1)) (Diamante & Munro, 1993), two-term (Eq. (2)) (Henderson, 1974), Midilli and others (Eq. (3)) (Midilli, Kucuk, & Yapar, 2002), Peleg (Eq. (4)) (da Silva, Rodrigues, Silva, de Castro, & Gomes, 2015) and Silva and others (Eq. (5)) (D. I. Onwude, N. Hashim, R. B. Janius, N. M. Nawi, & K. Abdan, 2016b).

$$MR = \exp(-k * t^n) \quad (1)$$

$$MR = a * \exp(-k_1 * t) + b * \exp(-k_2 * t) \quad (2)$$

$$MR = a * \exp(-k_1 * t^n) + b * t \quad (3)$$

$$MR = 1 - t/(a + b * t) \tag{4}$$

$$MR = \exp(-a * t - b\sqrt{t}) \tag{5}$$

where a, k, n, k_1, k_2 and b are constants in models and *t* is time.

2.4 Effective moisture diffusivity

Fick's second law were used in calculation of the effective moisture diffusivity which is used for long drying times and infinite slab geometry in one dimension. First term of the series could be taken into account (Eq. (6)) when the assumptions were accepted such as a) water removal occurs with diffusion; b) volume of sample during drying was constant; c) the distribution of temperature was uniform and coefficient of diffusion was constant during drying (Chayjan & Kaveh, 2014; Crank, 1975).

$$MR = \frac{8}{\pi} * exp(\frac{-D_{eff} * \pi^2 * t}{4 * L^2}) \tag{6}$$

where D_{eff} is the diffusion coefficient (m^2 s^{-1}); L is the half thickness of sample (m) and t is the drying time (s). D_{eff} can be determined by plotting ln(MR) versus time (s) (Doymaz & Ismail, 2011).

2.5 Estimation of activation energy

Activation energy (E_a) (kJ/mol) of convective drying was computed by an Arrhenius type relationship due to the temperature dependence of the effective diffusivity (Eq. (7)).

$$D_{eff} = D_0 \exp\left(-\frac{Ea}{RT}\right) \tag{7}$$

Where D_0 is the pre-exponential factor (m2/s), R is the universal gas constant (kJ/mol* K) and T is the absolute temperature (K). From the slope of the straight line of lnD_{eff} versus 1/T, the activation energy was computed (Kumar, Sarkar, & Sharma, 2012).

For microwave drying, the ratio of the microwave power intensity to sample amount instead of the temperature was used for calculation of the E_a (Dadali, Demirhan, & Ozbek, 2007). Where P is microwave power intensity (W) and m is the mass of sample (g) (Eq. (8)).

$$D_{eff} = D_0 \exp\left(-\frac{Ea\, m}{P}\right) \tag{8}$$

2.6 Data analysis

The best fitted model to experimental drying data was determined by regression analysis using Sigma Plot software (Erkrath, Germany). To evaluate the goodness of fitted model, correlation coefficient (R^2), residual sum of squares (RSS), the reduced chi-square (χ^2) and root mean square error (RMSE) were computed using equations below (Eq. (9-11)) (McMinn, 2006):

$$\chi^2 = \frac{\sum_{i=1}^{N}(MR_{exp,i} - MR_{pred,i})^2}{N - n_p} \tag{9}$$

$$RMSE = \sqrt{\frac{1}{N}\sum_{i=1}^{N}(MR_{exp,i} - MR_{pred,i})^2} \tag{10}$$

$$RSS = \sum_{i=1}^{N}(MR_{exp,i} - MR_{pred,i})^2 \tag{11}$$

where $MR_{exp,i}$ is the experimental moisture ratio; $MR_{pred,i}$ is the predicted moisture ratio; N is the number of data points and n_p is the number of parameters in model.

3. Results and discussion

3.1 Drying of avocado-foam

Drying curves are given in Figures 1 and 2. Drying times of convectional hot-air drying were reduced to 3.13, 19.35 and 21.88 % when the drying temperature increased from 60 to 70°C, 70 to 80°C and 60 to 80°C, respectively. Drying rates were increased to 5.17, 26.23 and 32.76% for the temperature increase from 60 to 70°C, 70 to 80°C and 60 to 80°C, respectively. On the other hand, drying times were shortened by 81.82, 29.17 and 87.12 % for microwave drying from 120 to 460 W, 460 to 700 W and 120 to 700 W, respectively. Furthermore, the increments of the drying rate were observed as 433.19, 35.74 and 623.77 % for the increasing microwave power intensity from 120 to 460 W, 460 to 700 W and 120 to 700 W, respectively. The drying times of microwave dried avocado- foam were extremely low compared to the convective dried ones. Similarly, drying rates of microwave drying were much higher than convective drying. The reason of this, water molecules absorbs and transmits the microwave energy and provides uniform heat generation with faster boiling of water than the convective drying (Ilter et al., 2018). The experimental results illustrated that the free moisture contents of avocado-foams decreased depending on time. Increase in air temperature and microwave power intensity speeded up the drying process, thus shortened the time. It demonstrated that heat and mass transfer through the avocado-foam were faster at higher temperature and microwave intensity. Similar findings were reported for foam-mat dried tomato juice (Kadam & Balasubramanian, 2011), banana (Sankat & Castaigne, 2004; Thuwapanichayanan et al., 2008) and drying of garlic puree with hot-air and microwave drying (Ilter et al., 2018). For both drying methods, there were three periods: warming-up, constant and falling rates. Similar result was obtained in the study where convective, microwave, microwave-convective and microwave-vacuum drying of lactose powder (McMinn, 2006). However, Demirhan and Ozbek (2010) and Akpinar, Bicer, and Yildiz (2003) observed only the falling rate period during the microwave drying of purslane and hot-air drying of red pepper, respectively.

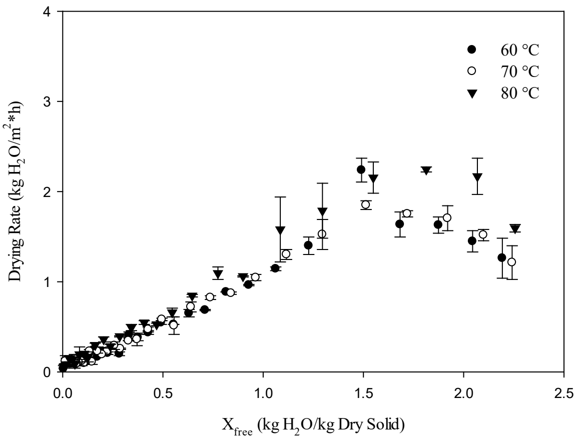

Figure 1. Drying rates for convectional drying

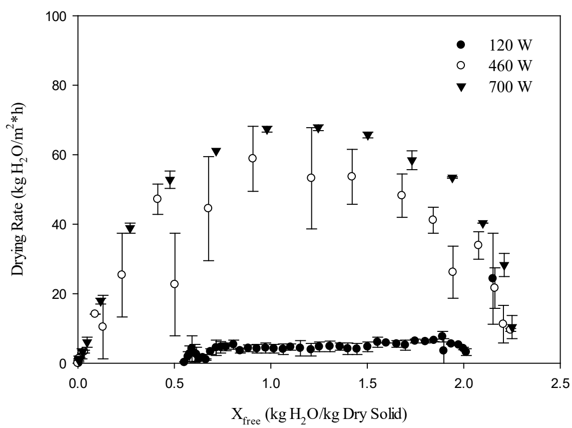

Figure 2. Drying rates for microwave drying

3.2 Drying kinetic of avocado-foam

Five different thin-layer drying models as mentioned in Section 2.3 were used to describe the effect of drying temperature and microwave power intensity on the drying kinetic of avocado-foam. The results of fitting are displayed in Table 1 and 2. Low RMSE, RSS and χ^2, high R^2 values indicate good fitting of the model to the experimental drying data of avocado-foam. Among those models, for convective drying Silva and others model was observed to most appropriate. The correlation coefficients of avocado-foam were obtained between 0.9857-0.9993. The values of R^2 of Silva and others model were more than 0.99 indicating good fit. For microwave drying, Midilli and others model was observed to good fit with R^2 more than 0.99 (Figure 3.). However, even if Page model also gave high R^2 values, low RMSE, RSS and χ^2 values, they were found to be higher than Midilli and others. In the study of foam mat drying at 50, 60, 70 and 80 °C of yellow mombin pulp, de Freitas et al. (2018) found Midilli model as the best mathematical fit at the temperature of 60, 70 and 80 °C, whereas the Wang and Singh model was showed the best fit at 50 °C.

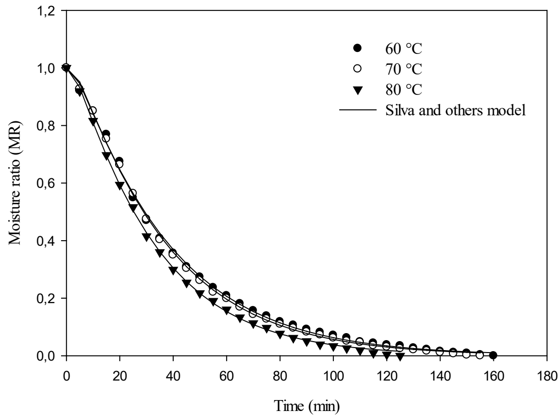

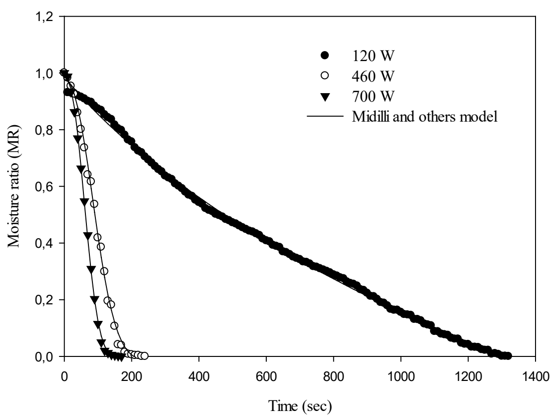

Figure 3. Comparison of experimental hot-air and microwave drying data to predicted values of best fitting models

Table 1. Model parameters and statistical results for hot-air drying

Drying Models	Drying Parameters	60 °C	70 °C	80 °C
Page	R^2	0.9978±0.0001	0.9985±0.0002	0.9988±0.0004
	RMSE	0.0138±0.0005	0.0116±0.0006	0.0104±0.0015
	RSS	0.0062±0.0006	0.0043±0.0005	0.0029±0.0008
	χ^2	0.0002±0.0000	0.0002±0.0001	0.0002±0.0001
	k	0.0135±0.0001	0.0124±0.0000	0.0166±0.0018
	n	1.1500±0.0124	1.1733±0.0193	1.1660±0.0180
Two-term	R^2	0.9960±0.0007	0.9958±0.0007	0.9958±0.0005
	RMSE	0.0184±0.0015	0.0189±0.0016	0.0192±0.0013
	RSS	0.0110±0.0019	0.0115±0.0019	0.0096±0.0012
	χ^2	0.0004±0.0001	0.0004±0.0001	0.0005±0.0001
	a	0.5310±0.0009	0.5337±0.0014	0.5297±0.0017
	k_1	0.0258±0.0010	0.0259±0.0016	0.0322±0.0011
	b	0.5310±0.0009	0.5337±0.0014	0.5297±0.0017
	k_2	0.0258±0.0010	0.0259±0.0016	0.0322±0.0011
Midilli and others	R^2	0.9981±0.0002	0.9988±0.0000	0.9989±0.0003
	RMSE	0.0127±0.0006	0.0104±0.0004	0.0098±0.0014
	RSS	0.0053±0.0006	0.0034±0.0002	0.0025±0.0007
	χ^2	0.0002±0.0000	0.0001±0.0000	0.0001±0.0000
	a	1.0207±0.0035	1.0180±0.0036	1.0160±0.0027
	k	0.0151±0.0008	0.0134±0.0004	0.0189±0.0023
	n	1.1297±0.0235	1.1607±0.0242	1.1345±0.0210
	b	2.69E-05±1.83E-05	4.18E-05±5.42E-07	-3.08E05±3.99E-07
Peleg	R^2	0.9863±0.0024	0.9857±0.0022	0.9884±0.0001
	RMSE	0.0337±0.0029	0.0349±0.0028	0.0318±0.0001
	RSS	0.0374±0.0069	0.0392±0.0061	0.0263±0.0001
	χ^2	0.0012±0.0002	0.0013±0.0002	0.0011±0.0000
	a	36.2478±1.8290	36.8924±2.6920	29.4054±1.7685
	b	0.7372±0.0103	0.7283±0.0098	0.7270±0.0140
Silva and others	R^2	0.9987±0.0003	0.9993±0.0000	0.9992±0.0001
	RMSE	0.0105±0.0009	0.0081±0.0002	0.0083±0.0007
	RSS	0.0037±0.0007	0.0021±0.0001	0.0018±0.0003
	χ^2	0.0001±0.0000	0.0001±0.0000	0.0001±0.0000
	a	0.0309±0.0015	0.0316±0.0025	0.0392±0.0009
	b	-0.0439±0.0036	-0.0486±0.0054	-0.0518±0.0023

Table 2. Model parameters and statistical results for microwave drying

Drying Models	Drying Parameters	120 W	460 W	700 W
Page	R^2	0.9882±0.0040	0.9965±0.0003	0.9984±0.0003
	RMSE	0.0325±0.0027	0.0222±0.0007	0.0151±0.0015
	RSS	0.0998±0.0648	0.0124±0.0009	0.0041±0.0008
	χ^2	0.0011±0.0002	0.0006±0.0001	0.0003±0.0001
	k	1.89E-04±1.73E-04	2.60E-05±9.37E-06	4.28E-05±1.71E-07
	n	1.4884±0.2533	2.2662±0.0708	2.3377±0.0053
Two-term	R^2	0.9559±0.0162	0.9125±0.0051	0.9117±0.0010
	RMSE	0.0644±0.0176	0.1103±0.0040	0.1128±0.0004
	RSS	0.2938±0.0025	0.3046±0.0221	0.2291±0.0018
	χ^2	0.0049±0.0026	0.0146±0.0011	0.0164±0.0002
	a	0.5485±0.0238	0.6056±0.0027	0.6004±0.0012
	k_1	0.0019±0.0002	0.0115±0.0002	0.0168±0.0001
	b	0.5485±0.0238	0.6056±0.0027	0.6004±0.0012
	k_2	0.0019±0.0002	0.0115±0.0002	0.0168±0.0001
Midilli and others	R^2	0.9980±0.0002	0.9975±0.0003	0.9990±0.0001
	RMSE	0.0137±0.0019	0.0186±0.0010	0.0124±0.0008
	RSS	0.0146±0.0039	0.0087±0.0010	0.0028±0.0004
	χ^2	0.0002±0.0001	0.0005±0.0001	0.0002±0.0000
	a	0.9685±0.0235	0.9778±0.0001	0.9827±0.0031
	k	1.05E-03±1.05E-03	1.87E-05±7.13E-06	3.19E-05±1.73E-06
	n	1.3535±0.4707	2.3246±0.0755	2.3964±0.0065
	b	-1.19E-04±8.14E-05	-7.67E-05±8.06E-07	-6.12E-05±8.26E-06
Peleg	R^2	0.9903±0.0073	0.9534±0.0015	0.9459±0.0013
	RMSE	0.0288±0.0147	0.0806±0.0019	0.0884±0.0012
	RSS	0.0549±0.0283	0.1624±0.0074	0.1405±0.0037
	χ^2	0.0011±0.0009	0.0071±0.0004	0.0088±0.0002
	a	758.9982±24.8027	160.0821±7.5613	103.9862±1.4922
	b	0.3749±0.0715	0.2164±0.0345	0.2747±0.0090
Silva and others	R^2	0.9713±0.0064	0.9591±0.0028	0.9641±0.0015
	RMSE	0.0522±0.0104	0.0755±0.0032	0.0720±0.0014
	RSS	0.2023±0.0301	0.1426±0.0120	0.0933±0.0034
	χ^2	0.0030±0.0012	0.0062±0.0005	0.0058±0.0002
	a	0.0026±0.0005	0.0194±0.0002	0.0296±0.0004
	b	-0.0196±0.0093	-0.0999±0.0012	-0.1292±0.0019

3.3 The effective diffusivity and activation energy

The effective diffusivity coefficient is required in design and optimization of processes which are involved internal moisture movement

(Franco, Perussello, Ellendersen, & Masson, 2017). The effective diffusivities increased depending on temperature and microwave power intensity. Similar increments were found in the studies of D. I. Onwude, N. Hashim, R. B. Janius, N. Nawi, and K. Abdan (2016a), Torki-Harchegani, Ghasemi-Varnamkhasti, Ghanbarian, Sadeghi, and Tohidi (2016), Vega, Uribe, Lemus, and Miranda (2007) and Bal, Kar, Satya, and Naik (2010). The effective moisture diffusivities of avocado-foam were between 0.59 x 10^{-8} to 6.78 x 10^{-8} m^2/s (Table 3.). These values are in the range of effective moisture diffusivity of foods (10^{-11} - 10^{-6} m^2/s) (Olanipekun, Tunde-Akintunde, Oyelade, Adebisi, & Adenaya, 2015). Similar D_{eff} values were observed in the hot-air drying of pumpkin slices (Onwude et al., 2016a), foam mat drying of tomato juice (Kadam & Balasubramanian, 2011) and lime juice (Dehghannya, Pourahmad, Ghanbarzadeh, & Ghaffari, 2019), packed bed and microwave drying of enriched couscous (Yüksel, Oner, Bayram, & Oner, 2018).

Activation energy (E_a) values for food and agricultural products were generally lied ranged in 10.7 and 110 kJ/mol (Chayjan, Kaveh, & Khayati, 2015). E_a values of avocado foam were found as 15.97 kJ/mol and 17.56 W/g for hot-air and microwave drying, respectively. Similar values were obtained in the studies of Dadali et al. (2007) for microwave drying of spinach, Azizpour, Mohebbi, Khodaparast, and Varidi (2014) for convective drying of shrimp foam and Salahi, Mohebbi, and Taghizadeh (2015) for foam-mat drying of cantaloupe. High E_a value indicate that water in food material is bounded more strongly and removal of water driven by sample's structure (Chayjan et al., 2015).

Table 3. Effective moisture diffusivities and activation energy of avocado-foam

Dryer	Drying Parameter	Effective Diffusivity (m^2/s)	Activation Energy (E_a)
	60 °C	4.80 x 10^{-8} ±0.23 x 10^{-8}	
Hot-air	70 °C	4.88 x 10^{-8} ±0.49 x 10^{-8}	15.97±4.53 kJ/mol
	80 °C	6.68 x 10^{-8} ±0.31 x 10^{-8}	
	120 W	0.59 x 10^{-8} ±0.12 x 10^{-8}	
Microwave	460 W	4.68 x 10^{-8} ±0.26 x 10^{-8}	17.56±1.30 W/g
	700 W	6.78 x 10^{-8} ±0.05 x 10^{-8}	

4. Conclusions

Avocado foam was prepared by adding 30 % of egg white to avocado puree and dried with hot-air at 60, 70 and 80 °C and microwave dryers at 120, 460 and 700 W. Increment of drying temperature and microwave power intensity resulted in an increase in drying rate and shorten drying time by faster removal of water from avocado-foam. Furthermore, five thin-layer models were used to determine the best fitting model to describe the drying behavior. Midilli and other model and Silva and other model were found as best with higher values of R^2 and lower values of RMSE, RSS and χ^2. Effective moisture diffusivity values were increased while increasing drying temperature and microwave power intensity. On the other hand, activation energy values were found in agreement within the literature.

REFERENCES

Akpinar, E. K., Bicer, Y., & Yildiz, C. (2003). Thin layer drying of red pepper. *Journal of Food Engineering, 59*(1), 99-104. doi:10.1016/S0260-8774(02)00425-9

Ali, S. S., Kasoju, N., Luthra, A., Singh, A., Sharanabasava, H., Sahu, A., & Bora, U. (2008). Indian medicinal herbs as sources of antioxidants. *Food Research International, 41*(1), 1-15. doi:10.1016/j.foodres.2007.10.001

Araujo, R. G., Rodriguez-Jasso, R. M., Ruiz, H. A., Pintado, M. M. E., & Aguilar, C. N. (2018). Avocado by-products: Nutritional and functional properties. *Trends in Food Science & Technology, 80*, 51-60. doi:10.1016/j.tifs.2018.07.027

Azizpour, M., Mohebbi, M., Khodaparast, M. H. H., & Varidi, M. (2014). Optimization of Foaming Parameters and Investigating the Effects of Drying Temperature on the Foam-Mat Drying of Shrimp (Penaeus indicus). *Drying Technology, 32*(4), 374-384. doi:10.1080/07373937.2013.794829

Bal, L. M., Kar, A., Satya, S., & Naik, S. N. (2010). Drying kinetics and effective moisture diffusivity of bamboo shoot slices undergoing microwave drying. *International Journal of Food Science and Technology, 45*(11), 2321-2328. doi:10.1111/j.1365-2621.2010.02402.x

Chakraborty, S., Mazumder, S., & Banerjee, S. (2017). Changes in Thermal Properties and Colour Attributes of Potato (Chandramukhi Variety) during Foam Mat and Thin Layer Drying. *Journal of Microbiology Biotechnology and Food Sciences, 6*(5), 1121-1126. doi:10.15414/jmbfs.2017.6.5.1121-1126

Chayjan, R. A., & Kaveh, M. (2014). Physical Parameters and Kinetic Modeling of Fix and Fluid Bed Drying of Terebinth Seeds. *Journal of Food Processing and Preservation, 38*(3), 1307-1320. doi:10.1111/jfpp.12092

Chayjan, R. A., Kaveh, M., & Khayati, S. (2015). Modeling Drying Characteristics of Hawthorn Fruit under Microwave-Convective Conditions. *Journal of Food Processing and Preservation, 39*(3), 239-253. doi:10.1111/jfpp.12226

Colombo, R., & Papetti, A. (2019). Avocado (Persea americana Mill.) by-products and their impact: from bioactive compounds to biomass energy and sorbent material for removing contaminants. A review. *International Journal of Food Science and Technology, 54*(4), 943-951. doi:10.1111/ijfs.14143

Crank, J. (1975). *Mathematic of Diffusion* (2nd ed.). London: Oxford University Press.

da Silva, W. P., Rodrigues, A. F., Silva, C. M. D. P. S. E., de Castro, D. S., & Gomes, J. P. (2015). Comparison between continuous and intermittent drying of whole bananas using empirical and diffusion models to describe the processes. *Journal of Food Engineering, 166*, 230-236. doi:10.1016/j.jfoodeng.2015.06.018

Dadali, G., Demirhan, E., & Ozbek, B. (2007). Microwave heat treatment of spinach: Drying kinetics and effective moisture diffusivity. *Drying Technology, 25*(10), 1703-1712. doi:10.1080/07373930701590954

de Freitas, B. S. M., Cavalcante, M. D., Cagnin, C., da Silva, R. M., Placido, G. R., & de Oliveira, D. E. C. (2018). Physical-chemical characterization of yellow mombin (Spondias mombin L.) foam-mat drying at different temperatures. *Revista Brasileira De Engenharia Agricola E Ambiental, 22*(6), 430-435. doi:10.1590/1807-1929/agriambi.v22n6p430-435

Dehghannya, J., Pourahmad, M., Ghanbarzadeh, B., & Ghaffari, H. (2019). Heat and mass transfer enhancement during foam-mat drying process of lime juice: Impact of convective hot air temperature. *International Journal of Thermal Sciences, 135*, 30-43. doi:10.1016/j.ijthermalsci.2018.07.023

Demirhan, E., & Ozbek, B. (2010). Drying kinetics and effective moisture diffusivity of purslane undergoing microwave heat treatment. *Korean Journal of Chemical Engineering, 27*(5), 1377-1383. doi:10.1007/s11814-010-0251-2

Diamante, L. M., & Munro, P. A. (1993). Mathematical-Modeling of the Thin-Layer Solar Drying of Sweet-Potato Slices. *Solar Energy, 51*(4), 271-276. doi:Doi 10.1016/0038-092x(93)90122-5

Doymaz, I., & Ismail, O. (2011). Drying characteristics of sweet cherry. *Food and Bioproducts Processing, 89*(C1), 31-38. doi:10.1016/j.fbp.2010.03.006

Franco, T. S., Perussello, C. A., Ellendersen, L. N., & Masson, M. L. (2017). Effect of Process Parameters on Foam Mat Drying Kinetics of Yacon (Smallanthus Sonchifolius) and Thin-Layer Drying Modeling of Experimental Data. *Journal of Food Process Engineering, 40*(1). doi:10.1111/jfpe.12264

Henderson, S. M. (1974). Progress in Developing the Thin Layer Drying Equation. *Transactions of the Asae, 17*(6), 1167-1168. doi:https://doi.org/10.13031/2013.37052

Ilter, I., Akyil, S., Devseren, E., Okut, D., Koc, M., & Ertekin, F. K. (2018). Microwave and hot air drying of garlic puree: drying kinetics and quality characteristics. *Heat and Mass Transfer, 54*(7), 2101-2112. doi:10.1007/s00231-018-2294-6

Kadam, D. M., & Balasubramanian, S. (2011). Foam Mat Drying of Tomato Juice. *Journal of Food Processing and Preservation, 35*(4), 488-495. doi:10.1111/j.1745-4549.2010.00492.x

Kumar, N., Sarkar, B. C., & Sharma, H. K. (2012). Mathematical modelling of thin layer hot air drying of carrot pomace. *Journal of Food Science and Technology-Mysore, 49*(1), 33-41. doi:10.1007/s13197-011-0266-7

McMinn, W. A. M. (2006). Thin-layer modelling of the convective, microwave, microwave-convective and microwave-vacuum drying of lactose powder. *Journal of Food Engineering, 72*(2), 113-123. doi:10.1016/j.jfoodeng.2004.11.025

Midilli, A., Kucuk, H., & Yapar, Z. (2002). A new model for single-layer drying. *Drying Technology, 20*(7), 1503-1513. doi:10.1081/Drt-120005864

Olanipekun, B. F., Tunde-Akintunde, T. Y., Oyelade, O. J., Adebisi, M. G., & Adenaya, T. A. (2015). Mathematical Modeling of Thin-Layer Pineapple Drying. *39*(6), 1431-1441. doi:10.1111/jfpp.12362

Onwude, D. I., Hashim, N., Janius, R. B., Nawi, N., & Abdan, K. (2016a). Modelling Effective Moisture Diffusivity of Pumpkin (Cucurbita moschata) Slices under Convective Hot Air Drying Condition. *International Journal of Food Engineering, 12*(5), 481-489. doi:10.1515/ijfe-2015-0382

Onwude, D. I., Hashim, N., Janius, R. B., Nawi, N. M., & Abdan, K. (2016b). Modeling the Thin-Layer Drying of Fruits and Vegetables: A Review. *Comprehensive Reviews in Food Science and Food Safety, 15*(3), 599-618. doi:10.1111/1541-4337.12196

Qadri, O. S., Srivastava, A. K., & Yousuf, B. (2019). Trends in foam mat drying of foods: Special emphasis on hybrid foam mat drying technology. *Critical Reviews in Food Science and Nutrition*, 1-10. doi:10.1080/10408398.2019.1588221

Salahi, M. R., Mohebbi, M., & Taghizadeh, M. (2015). Foam-Mat Drying of Cantaloupe (Cucumis Melo): Optimization of Foaming Parameters and Investigating Drying Characteristics. *Journal of Food Processing and Preservation, 39*(6), 1798-1808. doi:10.1111/jfpp.12414

Sangamithra, A., Venkatachalam, S., John, S. G., & Kuppuswamy, K. (2015). Foam Mat Drying of Food Materials: A Review. *Journal of Food Processing and Preservation, 39*(6), 3165-3174. doi:10.1111/jfpp.12421

Sankat, C. K., & Castaigne, F. (2004). Foaming and drying behaviour of ripe bananas. *Lebensmittel-Wissenschaft Und-Technologie-Food Science and Technology, 37*(5), 517-525. doi:10.1016/S0023-6438(03)00132-4

Thuwapanichayanan, R., Prachayawarakorn, S., & Soponronnarit, S. (2008). Drying characteristics and quality of banana foam mat. *Journal of Food Engineering, 86*(4), 573-583. doi:10.1016/j.jfoodeng.2007.11.008

Torki-Harchegani, M., Ghasemi-Varnamkhasti, M., Ghanbarian, D., Sadeghi, M., & Tohidi, M. (2016). Dehydration characteristics and mathematical modelling of lemon slices drying undergoing oven treatment. *Heat and Mass Transfer, 52*(2), 281-289. doi:10.1007/s00231-015-1546-y

Vega, A., Uribe, E., Lemus, R., & Miranda, M. (2007). Hot-air drying characteristics of Aloe vera (Aloe barbadensis Miller) and influence of temperature on kinetic parameters. *Lwt-Food Science and Technology, 40*(10), 1698-1707. doi:10.1016/j.lwt.2007.01.001

Yüksel, A. N., Oner, M. D., Bayram, M., & Oner, M. E. (2018). Mathematical modeling of packed bed and microwave drying of enriched couscous. *Journal of Food Measurement and Characterization, 12*, 1723-1733. doi:10.1007/s11694-018-9787-3

Zheng, X. Z., Wang, Y. K., Liu, C. H., Sun, J. K., Liu, B. X., Zhang, B. H., . . . Liu, H. J. (2013). Microwave Energy Absorption Behavior of Foamed Berry Puree Under Microwave Drying Conditions. *Drying Technology, 31*(7), 785-794. doi:10.1080/07373937.2012.761635